School of Earth and Planetary Sciences
Department of Applied Geology

Crustal Evolution of the Capricorn Orogen, Western Australia

Inalee C. Jahn

This thesis is presented for the Degree of
Doctor of Philosophy
of
Curtin University

February 2018

DECLARATION

To the best of my knowledge and belief this thesis contains no material previously published by any other person except where due acknowledgement has been made. This thesis contains no material which has been accepted for the award of any other degree or diploma in any university.

The author acknowledges that copyright of published works contained within this thesis resides with the copyright holder(s) of those works. I warrant that I have obtained, where necessary, permission from the copyright owners to use any of my own published work (e.g. journal articles) in which the copyright is held by another party (e.g. publisher).

08.02.18

Inalee C. Jahn Date

ABSTRACT

The Capricorn Orogen, Western Australia, is a complex orogenic zone that records the convergence and collision of the Archaean Yilgarn and Pilbara Cratons during the formation of the West Australian Craton (WAC) during two major orogenic events; the Ophthalmian and Glenburgh Orogenies. Following assembly of the WAC, the Capricorn Orogen was affected by five episodic intracratonic reworking events spanning over one billion years. Granites associated with these orogenic and reworking events (the Dalgaringa, Bertibubba, Moorarie, Durlacher and Thirty Three Supersuites) are exposed in the eastern part of the Capricorn Orogen, and record the progressive evolution of a craton from generation to assembly and finally to cratonisation. This study focuses on using integrated application of U–Pb geochronology, trace element geochemistry and radiogenic and stable isotope analysis of zircon in order to determine the magmatic sources, in particular, the relative contributions of material from the mantle and the extent of crustal recycling, and the mechanisms of formation of the granites within the Capricorn Orogen. The resulting data provides an insight into the processes of crustal growth and differentiation of a craton through time.

The Archaean inliers and the deformed margins of the Yilgarn Craton record periods of significant crustal growth and rifting events that have influenced later Proterozoic magmatic events. Components of the Capricorn Orogen, collectively termed the Glenburgh Terrane, have previously been considered to be exotic to the adjacent Pilbara and Yilgarn Cratons based on the lack of similarities in tectonomagmatic history and contrasting Lu–Hf isotope signatures. However, new U–Pb zircon geochronology and Lu–Hf isotope compositions indicate that the basement rocks of the Glenburgh Terrane (the Halfway Gneiss) have similarities with both the Youanmi and Kalgoorlie Terrane of the Yilgarn Craton, and are interpreted to represent a reworked portion of the Yilgarn Craton, re-accreted during the Glenburgh Orogeny.

Arc magmatism along the northern margin of the Glenburgh Terrane accompanied its accretion with the Pilbara terrane during the c. 2215–2125 Ma Ophthalmian Orogeny. The Hf–O isotopic systematics of zircon suggest that arc magmatism involved a 10–80% contribution from a crustal component comparable with a Halfway Gneiss composition. The combined Pilbara Craton-Glenburgh Terrane accreted to the passive margin of the Yilgarn Craton during the c. 2005–1950 Ma Glenburgh Orogeny, resulting in a period of crustal growth. The c. 2005–1970 Ma Dalgaringa Supersuite developed on the southern margin of the Glenburgh Terrane, with Hf–O isotope data indicating mixing between 45–90% mantle material and a 10–55% contribution from an evolved crustal component equivalent to the Halfway Gneiss.

Following the assembly of the WAC the granite magmatism in Capricorn Orogen records a significant change from mantle-derived magmatism and crustal growth to one dominated by reworking and increased incorporation of metasedimentary material, essentially reflecting the evolution of the geodynamic setting from suprasubduction to an intracratonic setting. The isotopic characteristics of the c. 1820–1775 Ma Moorarie Supersuite granites indicate three isotopically distinct sources which include: (1) a reworked meta-igneous component with a composition similar to that of the Glenburgh Terrane (Halfway Gneiss and Dalgaringa Supersuite) (2) a metasedimentary component and (3) a mafic, lower crustal component. Moorarie Supersuite emplacement therefore reflects crustal partial melting during the emplacement of mantle-derived melts, possibly generated by the development of plastic gravitational instabilities in an intracratonic setting. The U–Pb, hafnium and oxygen isotopes from the c. 1680–1620 Ma Durlacher Supersuite within the Gascoyne Province indicate derivation from reworking of the Moorarie Supersuite, while those that intruded the northern margin of the Yilgarn Craton indicate mixing between 88–100% Moorarie Supersuite and 0–12% Halfway Gneiss rocks. Isotopic modelling indicates no contribution from juvenile components and do not require an additional metasedimentary source to account for the Hf–O array observed in the Durlacher Supersuite granites. Generation of granitic magma may have occurred as a response to a combination of mechanisms: radiogenic heat production, shear heating and emplacement of small volumes of mafic melts within the crust. The isotopic compositions of the c. 1030 Ma Thirty Three Supersuite pegmatites indicate that they are largely derived from reworking of the Durlacher Supersuite and an additional metasedimentary component (38–62% contribution). The Thirty Three Supersuite pegmatites represent the last of the granitic magmatism associated with intracratonic events within the Capricorn Orogen.

This research has demonstrated the effectiveness of using an integrated multi-isotopic approach in determining the compositions, ages and sources of granites in order to constrain the crustal evolution of an orogen.

ACKNOWLEDGEMENTS

This PhD has definitely been an interesting experience, an appropriate way to sum it up and mis-quote Lennon: 'I've given it everything I've got for a little peace of mind'. There are so many people who have helped me these last four years, this is my attempt at thanking them. Though I'm sure I've forgotten to mention some, I am thankful to them all.

Firstly, I would like to thank my supervisors Chris Clark, Steve Reddy and Rich Taylor for their guidance and support throughout this project, and for trusting me to get it done when I decided to move interstate. I am especially grateful that Chris agreed to take me on as a student back in 2012 and introducing me to geochronology. The third year field trip to Weekeroo was the main reason I really started to enjoy geology, and Shetland was the reason I started to enjoy research. Rich deserves more thanks than is possible to express. He showed me all things zircon, and I don't think I would have managed to pull off all the sample prep, data collection, processing, interpretation or presentation without his help.

Secondly, I would like to thank all the people who provided me with technical and analytical assistance in the collection of the data. At the GSWA, the support of Simon Johnson is acknowledged. At the University of Western Australia, Heejin Joen is thanked. At Santa Barbara I owe thanks to Andrew Kylander-Clark, who enabled me to collect the mountain of data on the split-stream. I also owe a massive thank you to Holly and Sonia, both who ran multiple graveyard shifts at UCSB. Thank you so much for sitting through those nights, and I hope none of us will have to sit through so many consecutive days of listening to a laser fire ever again. Chris Kirkland and PK are thanked for hugely increasing my understanding of the Lu–Hf system. Thanks to Milo for showing me how to make figures look good way back when, and to Dee who always had an open door and replied to all of my emails. I would also like to thank Tim Johnson, who provided constant encouragement and offered to read my first draft babbles and gave me much needed (and appreciated) constructive criticism.

Admittedly, I spent as little time in the HDR room as I could, but I did make one friend — Holly, these last four years would have been a lot less fun without sharing the experience with you.

I would like to thank my Papa for introducing me to geology, and always supporting me (even when I quit the first time round in 2004). I consider myself lucky, I was inspired by the best.

Finally, to Jess(e), you now probably know everything you never wanted to know about rocks. Here's the haiku I promised:

Jesse is the best
For the equation you wrote
I'm very grateful

ADDITIONAL PUBLICATIONS AND CONFERENCE ABSTRACTS RELEVANT TO THIS THESIS

JAHN, I., CLARK, C., REDDY, S., & TAYLOR, R. 2017. Crustal growth and episodic reworking over one billion years in the Capricorn Orogen, Western Australia: evidence from Lu–Hf and O isotope data. EGU 2017 Conference Abstract

JAHN, I, CLARK, C., REDDY, S., TAYLOR, R., & KYLANDER-CLARK, A. 2015. LASS-ICPMS zircon geochronology: comparisons with SHRIMP. Goldschmidt 2015 Conference Abstract.

OLIEROOK, H. K.H., TAYLOR, R. J. M., ERICKSON, T. M., CLARK, C., REDDY, S. M., KIRKLAND, C. L., JAHN, I, & BARHAM, M. 2018. Unravelling complex geologic histories using U–Pb and trace element systematics of titanite. *Chemical Geology*.

TABLE OF CONTENTS

LIST OF FIGURES

LIST OF TABLES

CHAPTER 1

INTRODUCTION

1.1 BACKGROUND AND RATIONALE

Granitic (*senso lato*) rocks constitute a large proportion of the upper continental crust, therefore understanding the processes of granite petrogenesis can provide constraints on the formation and evolution of the continental crust (Rudnick, 1995; Myers, 1997). Generation of granitic magmas generally involves several sources, and can be formed by differentiation of basaltic magmas with (or without) simultaneous crustal assimilation, or by partial melting of older heterogeneous continental crust, including infracrustal and supracrustal components (Chappell and White, 1974; Huppert and Sparks, 1988; Pearce, 1996; Sawyer, 1996, 1998; Petford et al., 2000; Annen et al., 2006; Kemp and Hawkesworth, 2004; Hawkesworth and Kemp, 2006; Kemp et al., 2007; Brown, 1994, 2013; Johnson et al., 2017b). The geochemistry of granites is fundamentally controlled by the source composition and the processes that affect melts from generation to crystallisation (Chappell, 1996). Therefore, the geological processes that have led to the extraction of material from the mantle and its subsequent reworking during tectonic processes will be reflected in their geochemistry, and detailed investigations into their geochemistry can be used to constrain their formation. The geochemical signatures of granitic rocks can be studied by analysis of the major and trace elements, and radiogenic and stable isotope systems present in various minerals contained in its structure.

An effective method to study the geochemistry of granites is to analyse the multiple isotope systems contained within the mineral zircon. Several physical and chemical features of zircon account for its significance in geochemical investigations: its chemical inertness and stability, high blocking temperature for Pb of >900°C, high hardness and its crystal structure (Harley and Kelly, 2007; Hoskin and Schaltegger, 2003; Kinny and Maas, 2003). These features enable zircon to retain the initial isotopic signatures of the melt from which it crystallised through subsequent metamorphic and tectonic events. In addition, imaging of the internal structure of zircon allows discrete zones to be targeted during analyses, and avoid averaging isotopes from different sources. Geochemical analysis of the high concentrations of trace elements incorporated into zircon, including radiogenic isotope systems (U–Pb, Lu–Hf) and stable isotopes ($\delta^{18}O$), provides multiple datasets from a single internal zone. These data provide constraints on geochemical signatures and magmatic sources and the processes that govern them, forming the framework for crustal evolution models.

U–Pb geochronology can establish crystallisation and subsequent deformation ages, as well as identifying older periods of magmatism through the presence of inherited zircon (e.g. Compston et al., 1986; Nutman et al., 1993; Schaltegger et al., 1999). Hafnium isotope ratios can be used to characterise relative contributions from mantle, crustal and recycled reservoirs within magmas. When used in conjunction, they can help unravel complex crystallisation histories of a crustal block, and follow the source composition through its magmatic evolution (e.g. Amelin et al., 1999; Kemp et al., 2007). One of the major limitations of Hf–isotope and U–Pb geochronological analysis is identifying whether rocks with evolved isotopic signatures were derived from mixed juvenile and recycled metasedimentary sources, or from mantle derived sources that have aged in the deep crust. Isotopic partitioning in stable isotope systems occurs as a result of chemical, rather than nuclear, fractionation processes. Mantle magmas have an average $\delta^{18}O$ of 5.3 ± 0.6‰ (2σ; Valley et al., 2005), and deviations from this mantle value reflect the interaction of magma with supracrustal materials. Therefore, oxygen isotope ratios of zircon grains will reflect the $\delta^{18}O$ of magmatic source rocks and contaminants and can be used to detect different source contributions (Bindeman, 2008).

Understanding the processes by which the crust is generated and modified, in particular the relationship between additions of new material from the mantle and the extent of crustal recycling, is fundamental to understanding the evolution of a crustal block, and can help predict the metallogenic potential of a terrane (e.g. Groves and Bierlein, 2007; Mole et al., 2013). The Capricorn Orogen in Western Australia is a major orogenic zone that records the convergence and collision of the Archaean Yilgarn and Pilbara Cratons during the formation of the West Australian Craton, as well as ~1.4 billion years of subsequent intracontinental reworking (Cawood and Tyler, 2004; Sheppard et al., 2010b; Johnson et al., 2013). The orogen comprises Palaeoproterozoic plutonic igneous rocks and medium-to high-grade metamorphosed tectonic units, Palaeoproterozoic sedimentary basins and the deformed margins of the Pilbara and Yilgarn cratons (Cawood and Tyler, 2004). Metallongeny in the Capricorn Orogen is considered to be the result of multistage hydrothermal events associated with the punctuated tectonic and magmatic episodes that have affected the orogen (Pirajno, 2004). However, mineral exploration in the Capricorn Orogen is currently limited. This is largely attributed to the extensive regolith and Proterozoic sedimentary basin cover which restricts exploration, and the limitation of current technologies to directly detect deposits under deeper cover. Effective exploration requires understanding of crustal scale processes that are involved in the development of mineral systems (McCuaig and Hronsky, 2014), and establishing the sources of the crustal components, and determining the geodynamic setting and larger scale tectonic drivers of an area will contribute towards developing the methods to detect and recognise the distal footprints of deep ore deposits.

This thesis will use an integrated analytical study of the isotopic and geochemical systematics in zircon from Capricorn Orogen granites in order to identify the magmatic sources and the fundamental geodynamic processes that have contributed to its crustal evolution.

1.2 WORKFLOW

This section provides an overview of the workflow. Detailed analytical methods are presented in Chapter 3.

In order to maximise the study area, most samples were collated from external sources. Sources included the Geological Survey of Western Australia (GSWA) and Thundelarra Ltd. A total of 88 samples were collected and processed for analysis. Of these, 42 were heavy mineral separates processed and provided by the GSWA, 38 were hand or crushed samples provided by the GSWA, seven were hand samples collected during fieldwork and one hand sample was provided by Thundelarra Ltd (Appendix A).

The project started in February 2014 and samples were collected during fieldwork conducted in April and August 2014. Heavy mineral separates were provided by the GSWA from areas not sampled, with a total of 26 samples prepared for analysis in the first year. Workflow for pilot data consisted of:

1. **Zircon separation** selective electrical fragmentation of hand samples and recovery of zircon grains using the 'SelFrag Lab' contained at the Department of Applied Geology at Curtin University in Perth, Western Australia.
2. **Zircon characterisation** zircon grains were imaged using transmitted and reflected light followed by cathodoluminescence (CL) imaging technique to determine suitable analysis locations.
3. **Laser ablation inductively coupled plasma mass spectrometry (LA–ICPMS) split-stream analysis** samples were analysed at the University of California Santa Barbara LASS (laser ablation split stream) ICPMS facility where U–Pb and trace element abundances were simultaneously measured.
4. **LA–ICPMS analysis** Lu–Hf analyses were conducted on zircon grains previously dated by the split-stream method. Samples were analysed at the University of California, Santa Barbara LASS facility.

In 2015 a total of 62 samples were obtained from the GSWA, and were prepared and analysed following the workflow developed in the first year. Following completion of collection and processing of U–Pb, trace element and Lu–Hf data, zircon grains were selected for oxygen isotope analysis. Oxygen isotope ratios were determined using a Cameca IMS 1280 multi-collector ion microprobe located at the Centre for Microscopy, Characterisation and Analysis (CMCA) at the University of Western Australia during February-October 2016.

1.3 AIMS

The overall aim of this thesis is to provide new constraints on the crustal evolution of the Capricorn Orogen, Western Australia. This will be achieved by an integrated isotopic and geochemical approach, where U–Pb zircon geochronology will be combined with Lu–Hf and oxygen isotopes, and trace element geochemistry of zircon from Capricorn Orogen granites. The data generated from analysis will be combined with previous published studies in order to constrain the age, source and nature of the crustal evolution in the Capricorn Orogen. The specific aims of this study are:

- To determine the timing of emplacement and characterise the sources of the granites within the Capricorn Orogen, and determine the relative contributions of crustal and mantle material in their petrogenesis.
- To develop a model for the crustal evolution of the Capricorn Orogen.
- To develop an isotopic map of the Capricorn Orogen that maps the crustal evolution in space and time.

1.3 THESIS OUTLINE

This thesis is organised in a manner that systematically presents geochronological, geochemical and isotopic data from suites of granites which are grouped by ages of tectonothermal events. Each of the chapters 4–7 presents all of the data associated with a particular event, and repetition of methods and geological background is kept to a minimum. The reader should refer to Chapter 2 for a regional geological context and background information on the study area, and Chapter 3 for detailed methodology.

Chapter two summarises the regional geological framework of the Capricorn Orogen.

Chapter three describes in detail the analytical techniques and methods used throughout this study.

Chapter four presents U–Pb, trace element and Hf and O isotope data from granitoids from Archaean inliers within the Capricorn Orogen and granitoids from adjacent craton margins. The data are used to determine the spatial, temporal and genetic relationships between the Yilgarn Craton and its inlier components.

Chapter five presents U–Pb, trace elements, Hf and O isotope data from granites generated during the c. 2005–1950 Ma Glenburgh Orogeny in order to constrain their emplacement histories and to determine the relationship between additions of new material from the mantle and the extent of crustal recycling.

Chapter six presents U–Pb, trace elements, Hf and O isotope data from granites generated during the c. 1820–1770 Ma Capricorn Orogney. The role of mantle, infracrustal and supracrustal sources in the generation of these granites is discussed.

Chapter seven presents U–Pb, trace elements, Hf and O isotopes, constraints on intracratonic Palaeoproterozoic magmatism and deformation during the c. 1680–1620 Ma Mangaroon Orogeny and the c. 1030–995 Ma Edmundian Orogeny. The origin of these granites and the geodynamic setting is discussed.

Chapter eight presents an overview of the crustal evolution of the Capricorn Orogen which combines previous models with the new data discussed in this thesis. The geodyamic setting and potential drivers for intracratonic reworking are discussed.

Chapter nine summarises the key findings and outcomes of the thesis.

CHAPTER 2

GEOLOGY OF THE CAPRICORN OROGEN, WESTERN AUSTRALIA

2.1 REGIONAL GEOLOGICAL BACKGROUND

The Proterozoic Capricorn Orogen in Western Australia is a 750 km long, 500 km wide region situated between the Archaean Yilgarn and Pilbara Cratons (Tyler and Thorne, 1990; Cawood and Tyler, 2004; Sheppard et al., 2010b; Johnson et al., 2013). The orogen hosts Palaeoproterozoic plutonic igneous rocks and medium-to high-grade metamorphosed tectonic units, Palaeoproterozoic sedimentary basins and the deformed margins of the Pilbara and Yilgarn cratons (Cawood and Tyler, 2004). The tectonic units that comprise the Capricorn Orogen are the western granitic and medium-to-high-grade metasedimentary rocks of the Gascoyne Province, the northern low-grade metasedimentary and metavolcanic Palaeoproterozoic Ashburton and Bresnehan Basins, the Mesoproterozoic Edmund and Collier Basins, and the eastern Palaeoproterozoic Yerrida, Bryah, Padbury and Earaheedy Basins (Cawood and Tyler, 2004; Sheppard et al., 2010b). At the southern margin of the Capricorn Orogen lies the reworked Archean crust of the Yilgarn Craton which forms the Yarlarweelor Gneiss Complex (Occhipinti et al., 2004). At the northern margin lie the deformed continental margin rocks within the Ophthalmia Fold Belt of the Pilbara Craton (Johnson et al., 2013). Archaean inliers within the orogen include the Goodin, Marymia and Sylvania Inliers (Tyler, 1991; Bagas, 1999). Early overviews of the Proterozoic geology and mineralization within Western Australia provided by Tyler et al. (1998) have since been expanded with ongoing geological and geophysical mapping and geochronological analysis of tectonic units (Evans et al., 2003; Occhipinti et al., 2004; Pirajno et al., 2004; Sheppard et al., 2004, 2005, 2007, 2010a; Johnson et al., 2011b, 2011c, 2013, 2017a; Dentith et al., 2014; Aitken et al., 2017).

Early models for the tectonic evolution of the Capricorn Orogen proposed an intracratonic deformation event, with the assumption that the Yilgarn and Pilbara Cratons formed a continuous basement (Gee, 1979; Williams, 1986). The early models were reassessed by later studies that determined that the orogen represented the convergence and collision of the previously discrete Yilgarn and Pilbara Cratons during a single protracted collisional event, the Capricorn Orogeny (Muhling, 1988; Tyler and Thorne, 1990; Myers, 1990; Krapez, 1999; Thorne and Seymour, 1991). Initial Sm–Nd and Rb–Sr age-dating broadly constrained the Capricorn Orogney at

c. 2000–1600 Ma (Libby et al., 1986; Fletcher et al., 1983), later U–Pb zircon geochronology of Evans et al. (2003) constrained the collision and suturing of the Yilgarn and Pilbara Cratons at c. 1830–1800 Ma. However, more recent regional mapping, geochemical and geochronological investigations have revealed a complex multistage history of the Capricorn Orogen, a total of seven distinct tectonothermal events have been recognised (Occhipinti et al., 2004; Sheppard et al., 2010a; Johnson et al., 2010, 2011a, 2011b, 2013). These events include the c. 2215–2145 Ma Ophthalmian Orogoeny (Rasmussen et al., 2005), which is interpreted to record accretion of the Glenburgh Terrane onto the Pilbara Craton (Occhipinti et al., 2004; Johnson et al., 2010, 2011a) and the c. 2005–1950 Ma Glenburgh Orogeny, which records the accretion of the Pilbara Craton-Glenburgh Terrane with the Yilgarn Craton during the formation of the West

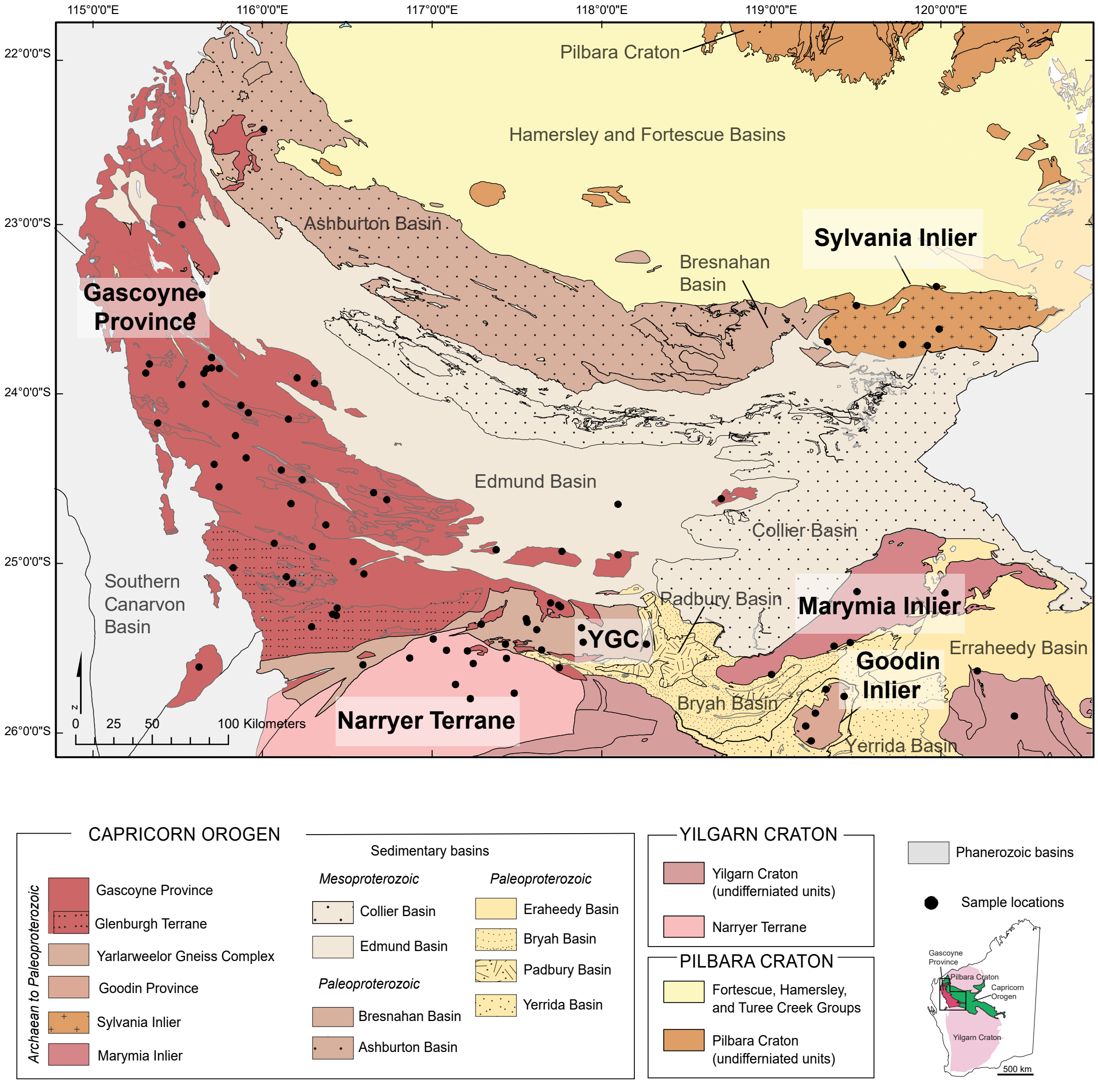

Figure 2.1 Elements of the Capricorn Orogen and surrounding cratons and basins. Lithostraphic and tectonic nomenclature used is the same as currently used by the Geological Society of Western Australia. YGC = Yarlarweelor Gneiss Complex

Australian Craton (Occhipinti et al., 2004; Sheppard et al., 2004, 2005; Johnson et al., 2010). Following the assembly of the West Australian Craton, the Capricorn Orogen is interpreted to have undergone 1.4 billion years of episodic intracontinental reworking during the c. 1820–1770 Ma Capricorn Orogeny (Occhipinti et al., 1998; Cawood and Tyler, 2004; Sheppard et al., 2010a), the c. 1680–1620 Ma Mangaroon Orogeny (Sheppard et al., 1997; 2005), the c. 1320–1170 Ma Mutherbukin Tectonic Event (Korhonen et al., 2015), the c. 1030–955 Ma Edmundian Orogeny (Sheppard et al., 2007) and the c. 570 Ma Mulka Tectonic Event (Johnson et al., 2013).

2.1.1 Yilgarn Craton margin and associated inliers

The Yilgarn Craton lies to the south of the Capricorn Orogen, and consists of several Archaean terranes that amalgamated and cratonised in the Neoarchaean. The craton is divided into the Narryer, Youanmi and South West Terranes, and the Eastern Goldfields Superterrane (Kalgoorlie, Kurnalpi, Burtville and Yamarna Terranes) from west to east (Cassidy et al., 2006; Pawley et al., 2009, 2012). The northern margin of the craton is overlain by numerous basins in which are host to basement inliers of Archaean granite-greenstone, the Marymia and Goodin Inliers (Fig. 2.1).

The Narryer Terrane forms the northwestern part of the Yilgarn Craton, and is the oldest known component of the craton. It consists of the Archean granitic gneissic rocks of the Narryer Gneiss Complex (NGC) with protolith ages between c. 3730 and c. 3300 Ma interleaved with metasedimentary and mafic metaigneous rocks (Kinny et al., 1988; Nutman et al., 1991; Kinny and Nutman, 1996). Rocks of the Narryer Terrane have been repeatedly deformed at high metamorphic grades and intruded by granites between c. 3300 and c. 3050 Ma (Nutman et al., 1991). The rocks were subsequently deformed and metamorphosed and intruded by granites between c. 2750 and c. 2620 Ma , interpreted to represent accretion of the Narryer and Youanmi Terranes (Myers et al., 1990; Nutman et al., 1993). In the north, the boundary between the Narryer Terrane and the Capricorn Orogen is marked by the Errabiddy Shear Zone (Occhipinti et al., 2001). The northeastern part of the Narryer Terrane was extensively deformed and intruded by granites during the c. 1820–1770 Ma Capricorn Orogeny (Johnson et al., 2013). This portion of the Narryer Terrane is termed the Yarlarweelor Gneiss Complex (Sheppard et al., 2003; Fig. 2.1).

The Yarlarweelor Gneiss Complex (YGC) lies to the northeast of the Narryer Terrane, and is considered to be an extension of the terrane that has been reworked during several Palaeoproterozoic orogenic events. The YGC comprises granitic gneisses with protolith ages of c. 3300–2630 Ma that have been repeatedly deformed and intruded by the Bertibubba Supersuite during the c. 2005–1945 Ma Glenburgh Orogeny, and subsequently metamorphosed and deformed and intruded by sheets and veins of granites and pegmatites during the

c. 1820–1770 Ma Capricorn Orogeny (Occhipinti et al., 1998; Sheppard et al., 2003). The Marymia Inlier is a discrete fault bounded Archaean granite–greenstone domain surrounded by Palaeo- to Mesoproterozoic metasedimentary basins. The inlier is widely interpreted to represent a portion of the Yilgarn Craton that was uplifted, rotated and reworked during the Proterozoic (Myers, 1993; Occhipinti et al., 1998; Krapež and Martin, 1999; Pirajno and Occhipinti, 2000; Pirajno et al., 2004). Recent compilations of stratigraphic, geochronological and isotopic data have been used to correlate the Marymia Inlier to the Eastern Goldfields Superterrane of the Yilgarn Craton (Bagas, 1999; Vielreicher and McNaughton, 2002; Vielreicher et al., 2002; Griffin et al., 2004; Gazley, 2011; Gazley et al., 2011; Dentith et al., 2014).

The Goodin Inlier comprises granitic rocks surrounded by, and forms basement to, metasedimentary rocks of the Yerrida Group (Gee, 1987). The granitoids indicate a crystallisation age of c. 2620 Ma (Nelson, 1997b) and are interpreted to represent part of the Younami Terrane that was uplifted during a compressional phase in the Yerrida Basin development (Pirajno and Occhipinti, 2000).

2.1.2 Pilbara Craton margin and associated inliers

The Pilbara Craton comprises volcano-sedimentary greenstone belts, granitic bodies and meta-sedimentary basins (Van Kranendonk et al., 2007). The northern part of the craton is well exposed, the southern 70% is overlain by the volcano-sedimentary rocks of the c. 2770–2630 Ma Fortescue Basin and the c. 2630–2450 Ma Hammersley Basins (Hickman, 2012; Van Kranendonk et al., 2007; Kemp et al., 2015). The rocks of the northern Pilbara Craton are divided into: (1) the c. 3530–3170 Ma East Pilbara Terrane; (2) the c. 3270–3110 Ma West Pilbara Superterrane and (3) the c. 3200–2930 Ma Kurrana Terrane in the southeast (Van Kranendonk et al., 2010). Recent geochronological and isotopic studies have indicated that the Kurrana Terrane and part of the West Pilbara Superterrane (Karratha Terrane) may represent rifted fragments of the East Pilbara Terrane that were re-accreted at c. 3070 Ma (Van Kranendonk et al., 2007; 2010; Hickman, 2012).

The Sylvania Inlier comprises granitoids and minor discontinuous greenstone belts. Early geochemical and isotopic studies interpreted the inlier as part of an allochthonous terrane accreted to the northern Pilbara at c. 3000–2760 Ma (Tyler, 1991; Tyler et al., 1992). Recent compilations of stratigraphic, geochronological and isotopic data have identified the terrane as a rifted fragment of the Pilbara Craton (Van Kranendonk et al., 2010). The Sylvania Inlier is overlain unconformably by the Hammersley Basin in the north, and the Mesoproterozoic Edmund and Collier Basins to the south.

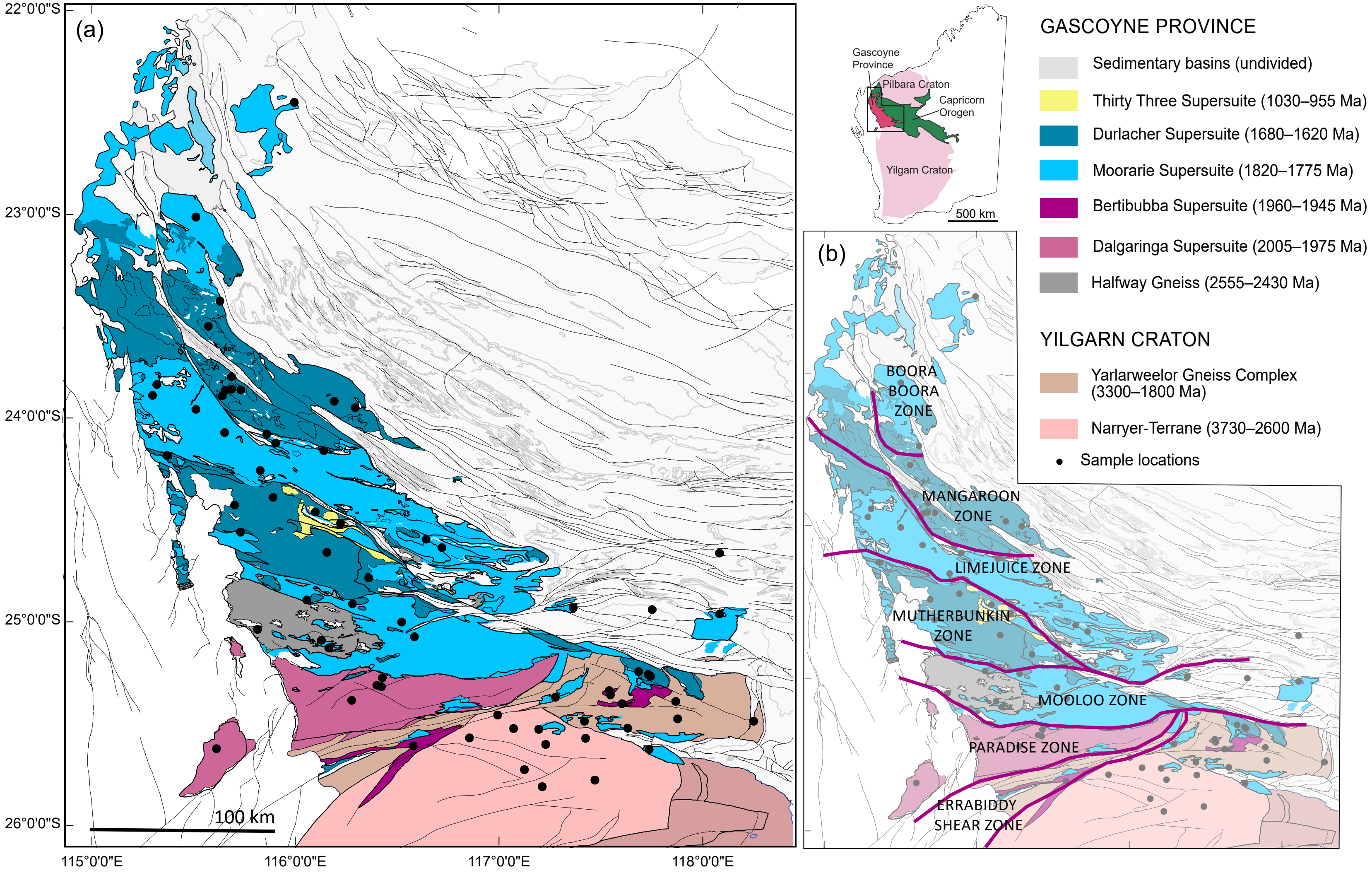

Figure 2.2 Simplified map of the Gascoyne Province showing (a) main magmatic units, and (b) subdivision of the region after structural-metamorphic zones of Sheppard et al. (2010a).

2.2 PALAEOPROTEROZOIC EVENTS AND ASSOCIATED MAGMATISM

The Gascoyne Province has been divided into several east-southeasterly trending structural and metamorphic zones which comprise seven zones, from north to south; the Boora Boora, Mangaroon, Limejuice, Mutherbukin, Mooloo, Paradise and Errabiddy Shear Zone (Fig. 2.2, Sheppard et al., 2010a).

2.2.1 Ophthalmian Orogeny (c. 2215–2145 Ma)

The northern margin of the Capricorn Orogen is located on the southern edge of the Pilbara Craton and comprises the Ophthalmia and Ashburton fold-belts (Tyler and Thorne, 1990; Thorne and Seymour, 1991). The Ophthalmian fold belt has been interpreted as forming in response to continent collision during the Ophthalmian Orogeny (Blake and Barley, 1992; Rasmussen et al., 2005). The Ophthalmian Orogeny is constrained at c. 2215–2145 Ma (Rasmussen et al., 2005) and has been interpreted to record the accretion of the Glenburgh Terrane with the Pilbara Craton (Occhipinti et al., 2004; Sheppard et al., 2010b; Martin and Morris, 2010; Johnson et al., 2011a). The suture is currently unexposed, approximated to be along the Lyons River Fault (Johnson et al., 2013). The polarity of the subduction is unclear, with no evidence of arc magmatism, either on the Pilbara Craton or Glenburgh Terrane, yet established. Protoliths to the 2240–2125 Ma Moogie Metamorphics were deposited during this time, and have been suggested to have been deposited in a foreland basin, or in a large extensional continental back-arc basin, or in a compressional retro-arc basin (Johnson et al., 2010). Based on seismic and Hf–isotope data Johnson et al. (2017a) suggest a southwards dipping subduction zone.

During this time, lithospheric extension along the northern Yilgarn Craton at c. 2200 Ma resulted in the formation of the Yerrida Basin (Pirajno et al., 2004, Occhipinti et al., 2017).

2.2.2 Glenburgh Orogeny (c. 2005–1950 Ma)

The Glenburgh Terrane forms basement to the whole Gascoyne Province and comprises variably deformed and metamorphosed granitic gneisses, Palaeoproterozoic metasedimentary rocks and continental arc related granitoids, the Dalgaringa Supersuite (Sheppard et al., 2004; Selway et al., 2009; Johnson et al., 2010). Basement gneisses of the Glenburgh Terrane indicate protolith ages between c. 2550 and c. 2430 Ma (Johnson et al., 2011b) and are interpreted to represent an exotic microcontinent (Occhipinti et al., 2004; Johnson et al., 2011b). The initial stages of the Glenburgh Orogeny involved the intrusion of the 2005–1970 Ma Dalgaringa Supersuite into the Archaean basement of the Glenburgh Terrane (Sheppard et al., 2004). Parts of interleaved Dalgaringa Supersuite and the Archaean granitic basement were deformed and metamorphosed to form the Halfway Gneiss (Occhipinti and Sheppard 2000; Occhipinti et al., 2001). The Dalgaringa Supersuite is interpreted to have formed on the southern margin of the Glenburgh Terrane above a northwestward dipping subduction zone (Sheppard et al., 1999; 2004). Ocean closure and collision of the Pilbara Craton-Glenburgh Terrane with the passive margin of the Yilgarn Craton took place during the final stages of the Glenburgh Orogeny, and was marked by the intrusion of the 1965–1945 Ma Bertibubba Supersuite across the suture (Sheppard et al., 2004, 2010; Johnson et al., 2010). This event is interpreted as the formation of the West Australian Craton (Johnson et al., 2010). The Errabiddy Shear Zone (Fig. 2.2) defines the boundary of the Glenburgh Terrane and Yilgarn Craton and contains components of the Yilgarn Craton, and metasedimentary and mafic rocks of the Camel Hill Metamorphics, which represent fore-arc and passive margin deposits, with deposition constrained at c. 2610–1955 Ma (Johnson et al., 2010). The suture zone is interpreted to be the Cardilya Fault, seismic reflection and magnetotelluric data indicates a southward directed dip (Johnson et al., 2011c). During this time the Bryah, Padbury and Earaheedy Basins in the eastern Capricorn Orogen were deposited along the rifted northern margin of the Yilgarn Craton in response to thermal, extensional and contractional events associated with the Glenburgh Orogeny (Occhipinti et al., 1998; Pirajno et al., 2004; Pirajno and Occhipinti, 2000). In the northern Capricorn Orogen the Ashburton Formation was deposited in an intracratonic foreland basin between c. 2008 and c. 1796 Ma (Müller et al., 2005).

2.2.3 Capricorn Orogeny (c. **1820–1770 Ma**)

The c. 1820–1770 Ma Capricorn Orogeny is characterised by low- to medium-grade metamorphism, extensive compressional deformation, voluminous granitic magmatism of the 1820–1775 Ma Moorarie Supersuite and metamorphism of the 1840–1810 Ma Leake Spring Metamorphics (Sheppard et al., 2010a). The Moorarie Supersuite comprises stocks, sheets and plutons that intruded across the Gascoyne Province and into the Yarlarweelor Gneiss Complex and Ashburton Basin (Sheppard et al., 2010a). In the centre of the Gascoyne Province (Limejuice Zone) the Moorarie Supersuite forms the 270 km long, 40 km wide Minnie Creek Batholith. Deformation and metamorphism related to the Capricorn Orogeny is observed in the Gascoyne Province, in the Ashburton Basin and Sylvania Inlier the along the southern edge of the Pilbara Craton, the Errabiddy Shear zone and Narryer Terrane in the south, and in the basins along the northern margin of the Yilgarn Craton (Thorne and Seymour, 1991; Krapež and McNaughton, 1999; Martin and Morris, 2010; Occhipinti et al., 1998; Pirajno et al., 2004; Sheppard et al., 2010). Intense deformation and crustal reworking in the northwest margin of the Yilgarn Craton (Narryer Terrane) formed the Yarlarweelor Gneiss Complex (Occhipinti et al., 1998; Sheppard et al., 2003).

2.2.4 Mangaroon Orogeny (c. 1680–1620 Ma)

The c. 1680–1620 Ma Mangaroon Orogeny is associated with medium- to high-grade metamorphism and deformation, coeval granitic magmatism of the 1680–1620 Ma Durlacher Supersuite and metamorphism of the 1760–1680 Ma Pooranoo Metamorphics (Sheppard et al., 2005, 2010b). The Durlacher Supersuite comprises plutons that intruded across the Gascoyne Province and Yarlarweelor Gneiss Complex (Sheppard et al., 2010b). In the Mutherbukin Zone (Fig. 2.2) the Durlacher Supersuite forms the 160 km long, 40 km wide Davey Well Batholith. Deformation and metamorphism associated with the Mangaroon Orogeny is largely restricted to the Mangaroon Zone, however, it is also recorded in the Earaheedy Basin (Fig. 2.2; Sheppard et al., 2005). Like the Capricorn Orogeny, the Mangaroon Orogeny is interpreted to represent an episode of intracontinental reworking (Sheppard et al., 2005, 2010b).

During this time the Bresnahan Group was deposited unconformably on Archaean and Palaeoproterozoic successions in a continental setting along the northeastern margin of the Capricorn Orogen (Thorne and Seymour, 1991). Following the Mangaroon Orogeny, siliciclastic and carbonate sediments of the 1600–1065 Ma Edmund and Collier Groups began deposition over the eastern extent of the Capricorn Orogen. (Fig. 2.1, Sheppard et al., 2010a; Cutten et al., 2016).

2.2.5 Mesoproterozoic and Neoproterozoic events

The c. 1320–1170 Ma Mutherbukin Tectonic Event involved high-grade metamorphism, recorded mainly within the Mutherbukin Zone (Fig. 2.2). Numerical modelling indicates that thickening of crust during the previous reworking events resulted in an increase in radiogenic heat production which provided the heat source for the event (Korhonen et al., 2017). No magmatism or significant sedimentation is associated with the Mutherbukin Tectonic Event (Johnson et al., 2013; Korhonen and Johnson, 2015).

The c. 1030–955 Ma Edmundian Orogeny is interpreted as an intracratonic event that is associated with very low- to low-grade metamorphism and widespread deformation in the Edmund and Collier Groups (Martin and Thorne, 2004; Sheppard et al., 2010a). Within the Gascoyne Province the Edmundian Orogeny is associated with deformation and metamorphism and intrusion of leucocratic granite plutons and rare element pegmatites of the 1030–955 Ma Thirty Three Supersuite (Martin and Thorne, 2004; Sheppard et al., 2007, 2010a; Johnson et al., 2013). Magmatism was limited to the northern edge of the Mutherbukin Zone (Fig. 2.2).

The c. 570 Ma Mulka Tectonic Event is responsible for a series of shear zones across the Gascoyne Province and Edmund and Collier Basins (Johnson et al., 2013).

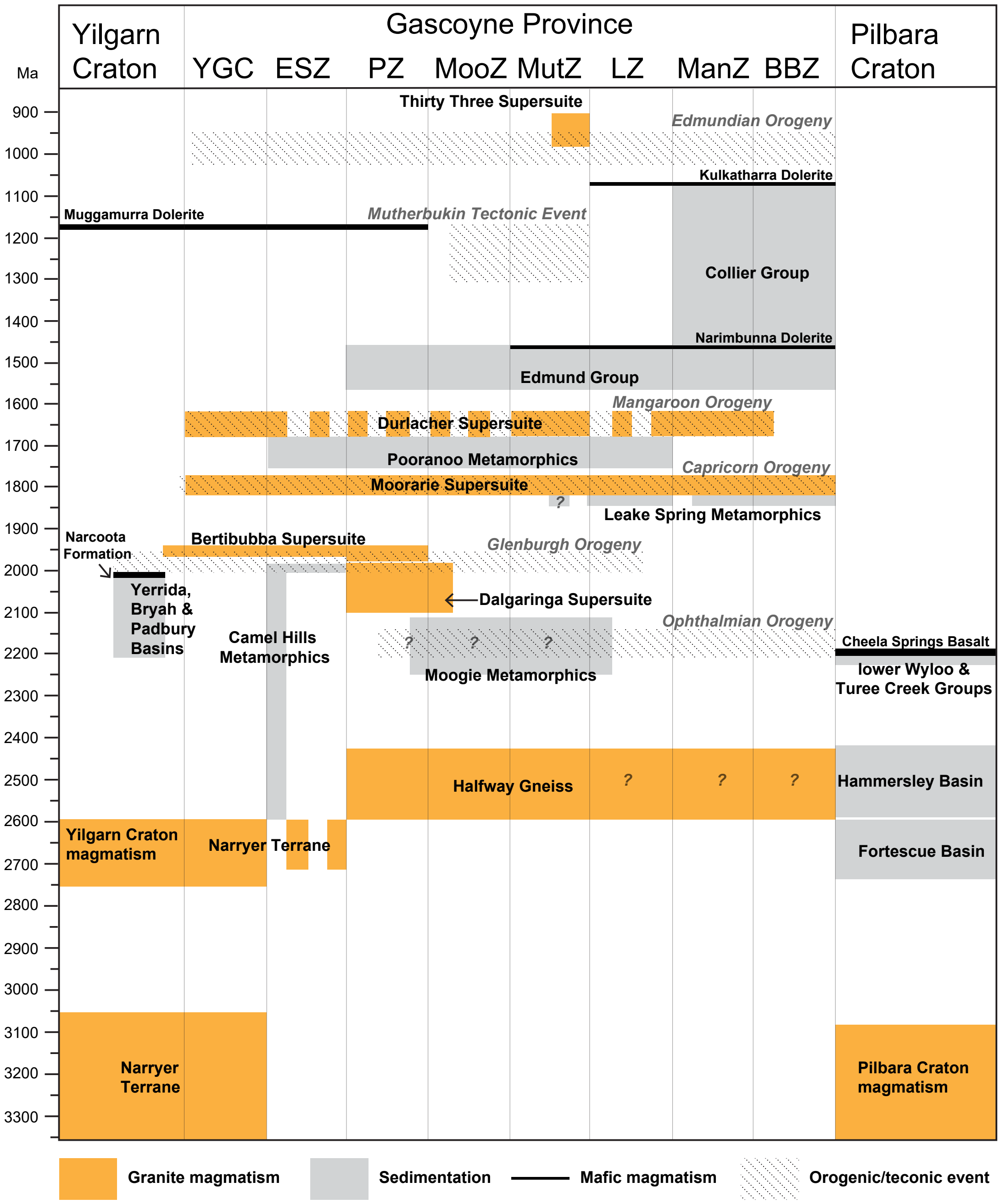

Figure 2.3 Simplified time-space plot for the Capricorn Orogen (modified after Sheppard et al., 2010a, and Johnson et al., 2013). Abbreviations: BBZ, Boora Boora Zone; ESZ, Errabiddy Shear Zone; LZ, Limejuice Zone; ManZ, Mangaroon Zone; MooZ, Mooloo Zone; MutZ, Mutherbukin Zone; YGC, Yarlarweelor Gneiss Complex.

CHAPTER 3

METHODOLOGY

3.1 INTRODUCTION

Geochronological techniques are well established; with the secondary ion mass spectrometry (SIMS) regarded as the industry standard for dating zircon populations due to its high-isotopic precision at an intra-crystalline scale (Ireland and Williams, 2003). Recent technological advances have seen new U–Th–Pb analytical techniques and applications developed (e.g. Johnston et al., 2009; Horstwood et al., 2008; Meinhold, 2010, Schoene et al., 2010; Chew et al., 2011; Cottle et al., 2012; Kylander-Clark et al., 2013; Spencer et al., 2013; Fisher et al., 2014; Schaltegger et al., 2015). Over the last decade studies have shown that the laser ablation inductively coupled plasma mass spectrometry (LA–ICPMS) method produces accurate and precise U–Pb zircon data (e.g. Cocherie and Roberts, 2008; Gehrels et al., 2008; Johnston et al., 2009). A relatively new technique in U–Pb zircon geochronology is the laser-ablation split-stream (LASS) ICPMS method, which provides high-speed, high-spatial resolution, simultaneous isotopic and elemental analysis. LASS was initially described by Yuan et al. (2008), and further adopted by Xie et al. (2008) and Chen et al. (2010), where they split the laser aerosol stream into two streams, with one stream directed into a multicollector (MC)–ICPMS to measure the hafnium isotopic ratio, and the other to a quadrupole (Q)–ICPMS to measure elemental abundances and U–Th–Pb isotopic ratios. The LASS analytical set-up used in this study splits the laser aerosol stream into two, with one stream directed into a Q–ICPMS to measure elemental abundances, and the other aliquot to a MC–ICPMS to measure U–Th–Pb isotopic ratios (e.g. Kylander-Clark et al., 2013). One main advantage of LASS technique is the rapid acquisition of multiple datasets from the same ablation volume from a large number of zircon. Application of this technique to regional studies will enable analysis of a greater number of samples, and thereby enable a more data-rich examination of the crustal evolution of the Capricorn Orogen.

3.2 ANALYTICAL PROCEDURES

3.2.1 Sample preparation

Rock samples were trimmed of weathered surfaces and cut into ~5–8 cm blocks using a rock saw. Samples were then fragmented into their individual mineral components by electric pulse disaggregation (EPD). Unlike traditional crushing techniques, this method is not mechanical and therefore produces a higher yield whilst maintaining the original grain morphology. Electrical fragmentation was performed using the "SelFrag Lab" equipment housed at the School of

Earth and Planetary Sciences at Curtin University in Perth, Western Australia. Approximately 300–600 g of sample was loaded into a portable process vessel filled with de-ionized water. The base of the process vessel was fitted with a mesh, either 360 or 630 µm in size, depending on the sample. As the sample was progressively disaggregated, grains and fragments smaller than 360–630 µm fell through the mesh and into a collection vessel, which is isolated from further electrical pulses. Short pulses of high-voltage electrical fields were applied with a frequency of 2 Hz. Coarse fragmentation was achieved by applying five 160 kV pulses with an electrode gap of 40 mm. The voltage was stepped down to 150 kV for an electrode gap of 30 mm, and to 140 kV for an electrode gap of 20 mm. When the sample had been disaggregated into fragments of 10 mm or less, a voltage of 140 kV was applied for a number of pulses (variable for each sample, ranging from 315–2328), at which point all of the sample had passed through the mesh. Fine and light material fraction are removed and discarded from the <360 or 630 µm fraction by elutriation under controlled flow conditions (~500–800 ml/min).

The remaining fraction was dried overnight in an oven at 50°C before using a Frantz LB-1 Magnetic Barrier Laboratory Separator to separate the non-magnetic fraction. The Frantz was operated at a longitudinal tilt of 14°, a transverse tilt of 12°, and an initial magnet current of a low field setting (0.75A). The non-magnetic fraction from the first cycle was reprocessed at a high field setting (1.7A). The non-magnetic fraction was then treated by heavy liquid separation in di-iodomethane using a separation funnel in order to separate minerals that are denser than a specific gravity of 3.3. Zircon were hand-picked from the final mineral concentrates with the aid of a binocular microscope, and mounted with standard reference material 91500 (Wiendenbeck et al., 1995), GJ-1 (Jackson et al., 2004), OG-1 (Stern et al., 2009), BR266 (Stern, 2001) and Plešovice (Sláma, et al., 2008) in a standard 25 mm diameter epoxy mount. In general, 50–100 representative zircon grains were selected. The mount was cut to a thickness of 5mm and was polished using standard diamond paste. Polishing begins with a 9 µm diamond abrasive to remove the surface layer of epoxy and is then refined through 3 µm to 1 µm.

Each mount was imaged using transmitted and reflected light followed by cathodoluminescence (CL) imaging technique. Transmitted and reflected light images provide internal grain information including zones, cores, rims, inclusions and/or fractures. CL imaging provides internal compositional and textural variations of the zircon grains (Fig. 3.1), and was undertaken using a Tescan Mira3 field emission scanning electron microscope fitted with a KE Developments CL detector using a 12 kV beam current, located in the John de Laeter Centre, Curtin University, Perth, Western Australia. Generated CL images were used to determine analysis locations (e.g. Nasdala et al., 2003; Hanchar and Miller, 1993).

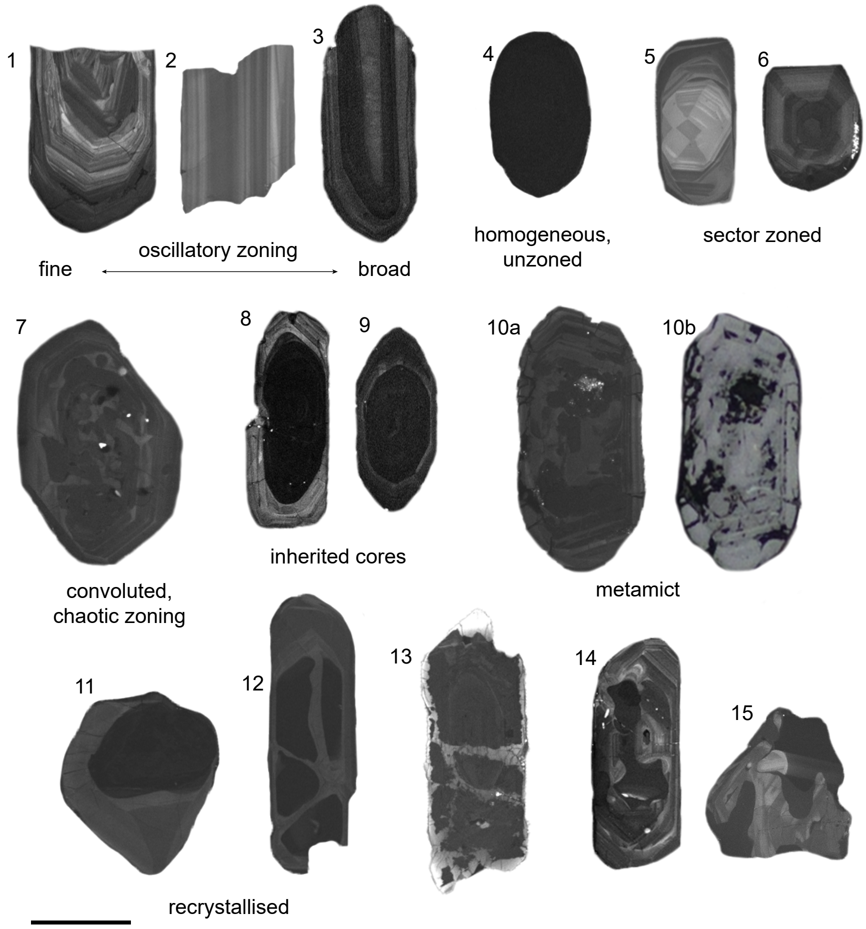

Figure 3.1. Atlas of zircon textures from the Capricorn Orogen granitoids. (**1–3**) oscillatory zoning, showing variation in growth zoning from fine to broad, CL. (**4**) homogeneous unzoned zircon, dark CL response, CL. (**5–6**) sector zoning, CL. (**7**) convoluted, chaotic zoning, CL. (**8–9**) inherited zircon cores, surrounded by oscillatory zoned overgrowths, CL. (**10a**) metamict zircon with fractures radiating out towards rims, CL. (**10b**) metamict zircon with fractures radiating out towards rims, reflected light. (**11–15**) recrystallisation of zircon grains, CL. (**14**) fluid alteration, dissolution embayment, CL. (**15**) fluid alteration, dissolution-reprecipitation, CL. Scale bar is approximately 100 µm.

3.2.2 Laser and ICPMS instrumentation

The LASS–ICPMS system at the University of California, Santa Barbara (UCSB), uses a MC–ICPMS and Q–ICPMS coupled to a 193 nm ArF excimer laser ablation system to rapidly determine simultaneous in situ U–Th–Pb isotopic measurements and trace-element concentrations. Hafnium isotope analyses are carried out by LA–ICPMS using a 193 nm ArF excimer laser ablation system attached to a MC–ICPMS.

3.2.2.1 U–Th–Pb and trace element analyses- Laser ablation split stream (LASS)

Instrumentation consists of a Photon Machines Analyte 193 ArF laser ablation system coupled to an Agilent 7700x quadrupole (Q)–ICP and a Nu Instruments Plasma HR MC–ICPMS (Table 3.1). The Analyte 193 is based on an ATLEX SI ArF 193 nm wavelength excimer laser, equipped with a low-volume HeLeX sample cell (Photon Machines, San Diego, USA) modified from the design of Eggins et al. (1998). Operating conditions for the instrument were routine (e.g. Cottle et al., 2012; Kylander-Clark et al., 2013), with a 25–30 µm ablation spot size, a fluence of ~1–4 J/cm-2, and a repetition rate of 3–4 Hz (for a 30-second total of 120 shots), which ablates at a rate of 0.05–0.15 µm per pulse. Data acquisition consists of (1) two laser pulses at the start of measurement to remove surface contamination, (2) 15-second washout period during which the background signal is collected, (3) 25-seconds of continuous ablation during which data are collected, and (4) ~3 seconds with no laser firing to allow dispersal of all sample material before the next analysis. The ablated material is carried by He from the sample cell and then mixed with Ar to stabilize the aerosol before input to the plasma. Immediately after mixing, the ablation stream is split into approximately half and directed into each mass spectrometer.

U–Th–Pb isotope data were collected using a Nu-Plasma high-resolution multicollector ICPMS (Nu Instruments, Wrexham, UK) which consists of 12 Faraday cups and four electron-transfer polymer (ETP) discrete dynode electron multipliers (Table 2). The detection system on the Nu Plasma at UCSB allows for simultaneous measurement of ^{232}Th and ^{238}U on Faraday cups equipped with 1011 ohm resistors and ^{208}Pb, ^{207}Pb, ^{206}Pb and ^{204}Pb and ^{204}Hg on four ETP discrete dynode electron multipliers. Data were collected over two separate analytical sessions over two years (2014 and 2015). During the second analytical session the detection system

Table. 3.1. Instrumental parameters of laser ablation split-stream ICP-MS used at UCSB.

Laser ablation system		**ICP-MS instruments**		
			MC-ICP-MS	**Q-ICP-MS**
Instrument model	Photon Machines Analyte 193	Instrument model	Nu plasma HR	Agilent 7700x
Laser	ATLEX-SI 193 nm ArF	RF forward power	1300 Wv	1300 W
Repetition rate	3–4 Hz	RF reflected power	<1W	<1W
Excavation rate	~0.07 µm/pulse	Coolant gas	13 L/min	13 L/min
Fluence	1–4 J/cm2	Auxiliary gas	0.8 L/min	0.8 L/min
Delay between analyses	20 s	Make up gas	~1.9 L/min – flow to Agilent	~1.9 L/min – flow to plasma
Ablation duration	25 s	Monitored masses	^{238}U, ^{232}Th, ^{208}Pb,^{207}Pb, ^{206}Pb, ^{204}Pb/^{204}Hg	^{139}La, ^{140}Ce, ^{141}Pr, ^{146}Nd, ^{147}Sm, ^{153}Eu, ^{157}Gd, ^{159}Tb, ^{163}Dy, ^{165}Ho, ^{166}Er, ^{169}Tm, ^{172}Yb, ^{176}Lu, ^{179}Hf
Carrier gas (He) flow	0.25 L/min	^{238}U sensitivity, dry solution	0.7% (290 V/ng)	0.2% (80 V/ng)
		throughput on LASS	0.3% (140 V/ng) ^{238}U	(38 V/ng) ^{179}Hfw
		Dwell time	200 ms	0.3 ms
		Integration	0.2s	0.2s

was set up for measurement of ^{208}Pb, ^{207}Pb, ^{206}Pb, ^{232}Th and ^{238}U on Faraday cups equipped with 1011 ohm resistors and ^{204}Pb + Hg and ^{202}Hg on two ETP discrete dynode electron multipliers. A sample-standard bracket approach was used, with 91500 zircon standard used as the primary reference material to monitor and correct for mass fractionation and instrumental drift. Secondary reference zircon GJ-1 and Plešovice were used to monitor data accuracy and precision. The accuracy of ^{207}Pb/^{206}Pb ratios was verified by comparison with the Archaean OG-1 zircon standard (Stern et al., 2009).

During the 2014 data collection a typical analytical run consisting of approximately 120 unknowns was bracketed by the matrix matched primary and secondary reference material for every 8 unknowns. Total run time per sample was approximately 90 minutes. The entire suite of samples was analysed during a continuous analytical session over a period of approximately 45 hours. Accuracy is within 0.01–1.16% for secondary reference materials GJ-1, Plešovice, OG-1 and BR266 analysed (Fig. 3.1). Precision on individual analyses depend on volume and concentrations of U, Th and Pb. Secondary standards, after normalisation to the primary standard, yielded <3% precision on ^{206}Pb/^{238}U ratios and typically 5–11% precision on ^{207}Pb/^{206}Pb ratios. Secondary reference materials yielded results comparable to published values, with accuracy of ^{206}Pb/^{238}U weighted mean ages within 0.33–0.63% of the reference value: 599.95 ± 0.79 Ma (MSWD = 0.96, 150 of 150) for GJ-1 (601.92 ± 0.7 Ma; Jackson et al., 2004), 339.57 ± 0.55 Ma (MSWD = 0.73, 75 of 78) for Plešovice (337.1 ± 0.37 Ma; Sláma et al., 2008), 564.1 ± 1 Ma (MSWD = 0.77, 73 of 77) for BR266 (559 ± 0.3 Ma; Stern, 2001). The OG-1 reference material (3465.4 ± 1.3 Ma; Stern et al., 2009) yielded a ^{207}Pb/^{206}Pb weighted mean age of 3466.7 ± 2.2 Ma (MSWD = 0.78, 72 of 78).

During the 2015 session a typical analytical run consisting of approximately 175 unknowns was bracketed by the matrix matched primary and secondary reference material for every 8 unknowns. Total run time per sample was approximately 180 minutes, and entire suite of samples were analysed during continuous analytical session over a period of approximately 85 hours. During the analytical sessions Runs 14–17 GJ-1 was used as a primary standard and Plešovice, Temora-2 and OG-1 were used as secondary standards. For all other sessions (Runs 1–13) 91500 was used the primary standard and GJ-1, Plešovice, Temora-2 and OG-1 were used as secondary standards (Fig. 3.1). Isotopic mass fractionation of ^{207}Pb/^{206}Pb ratios during Run 14 were corrected by reference to the OG-1 standard, and measured ratios were decreased by 2.5%. Precision on individual analyses depend on volume and concentrations of U, Th and Pb, with secondary standards, after normalisation to the primary standard, yielding 3–6% precision on ^{206}Pb/^{238}U ratios and typically 5–26% precision on ^{207}Pb/^{206}Pb ratios. Secondary reference materials yielded results comparable to published values, with accuracy of weighted mean ages within 0.04–0.63% of the reference value: 603.6 ± 1.4 Ma (MSWD = 1.04, 110 of 116) for GJ-1 (601.92 ± 0.7 Ma; Jackson et al., 2005), 339.84 ± 0.94 Ma (MSWD = 1.2, 101 of 107) for Plešovice (337.1 ± 0.37 Ma; Sláma et al., 2008), 416.6 ± 1.3 Ma (MSWD = 1.3, 91 of 97) for Temora-2 (416.78 ± 0.33 Ma; Black et al., 2004). The OG-1 reference material (3465.4 ± 1.3 Ma; Stern et al., 2009) yielded a ^{207}Pb/^{206}Pb weighted mean age of 3460.5 ± 7.4 Ma (MSWD = 4.7, 83 of 91). Details of U–Pb zircon standard analyses are given in Appendix A.

Trace element concentrations were measured simultaneously on the Agilent 7700x Q–ICPMS, instrument parameters are given in Table 3.1. GJ-1 zircon was used as a calibration standard to monitor and correct for mass fractionation and instrumental drift. Data were collected using time resolved data acquisition and processed using the Iolite software package (Paton et al., 2010; 2011), and any zircon analyses that sampled inclusions were removed (e.g. Lu et al., 2016). Where appropriate REE values were normalized to chondritic values (Anders and Grevesse, 1989), given as X_N values (X = relevant element). GJ-1 was run every 8-10 unknowns per sample, with 3 analyses at the beginning and end of each run. Stoichiometric Zr was used as the internal standardisation element for zircon (43.14 wt%). Measured trace elements comprise, ^{28}Si, ^{90}Zr, ^{31}P, ^{49}Ti, ^{89}Y, ^{93}Nb, ^{139}La, ^{140}Ce, ^{141}Pr, ^{146}Nd, ^{147}Sm, ^{153}Eu, ^{157}Gd, ^{159}Tb, ^{163}Dy, ^{165}Ho, ^{166}Er, ^{169}Tm, ^{172}Yb, ^{176}Lu, and ^{179}Hf. Uncertainties on individual spot measurements are cited at 2σ level and include the internal uncertainties associated with counting statistics only. Details of trace element concentrations for zircon standard analyses are given in Appendix A.

3.2.2.2 Lu–Hf isotope analyses

Lu–Hf isotope data were collected using a Nu-Plasma high resolution MC–ICPMS (Nu Instruments, Wrexham, UK), at UCSB coupled with the same laser and ablation cell as described above. Hf measurements were performed on ten Faraday cups (also with 1011 ohm resistors) in a central array at 1 atomic mass unit (amu) spacing (Table 3.2). Instrument settings were

Table. 3.2 Mass position configuration for Nu Plasma at UCSB

	Faraday detectors												**discrete dynode ion counters**			
con-figura-tion	ExH	H2	H1	Ax	L1	L2	L3	L4	L5	L6	L7	L8	IC0	IC1	IC2	IC3
1	238	232											208	207	206	204
2	238	232								208	207	206			202	200
3			180	179	178	177		175	174	173	172	171				

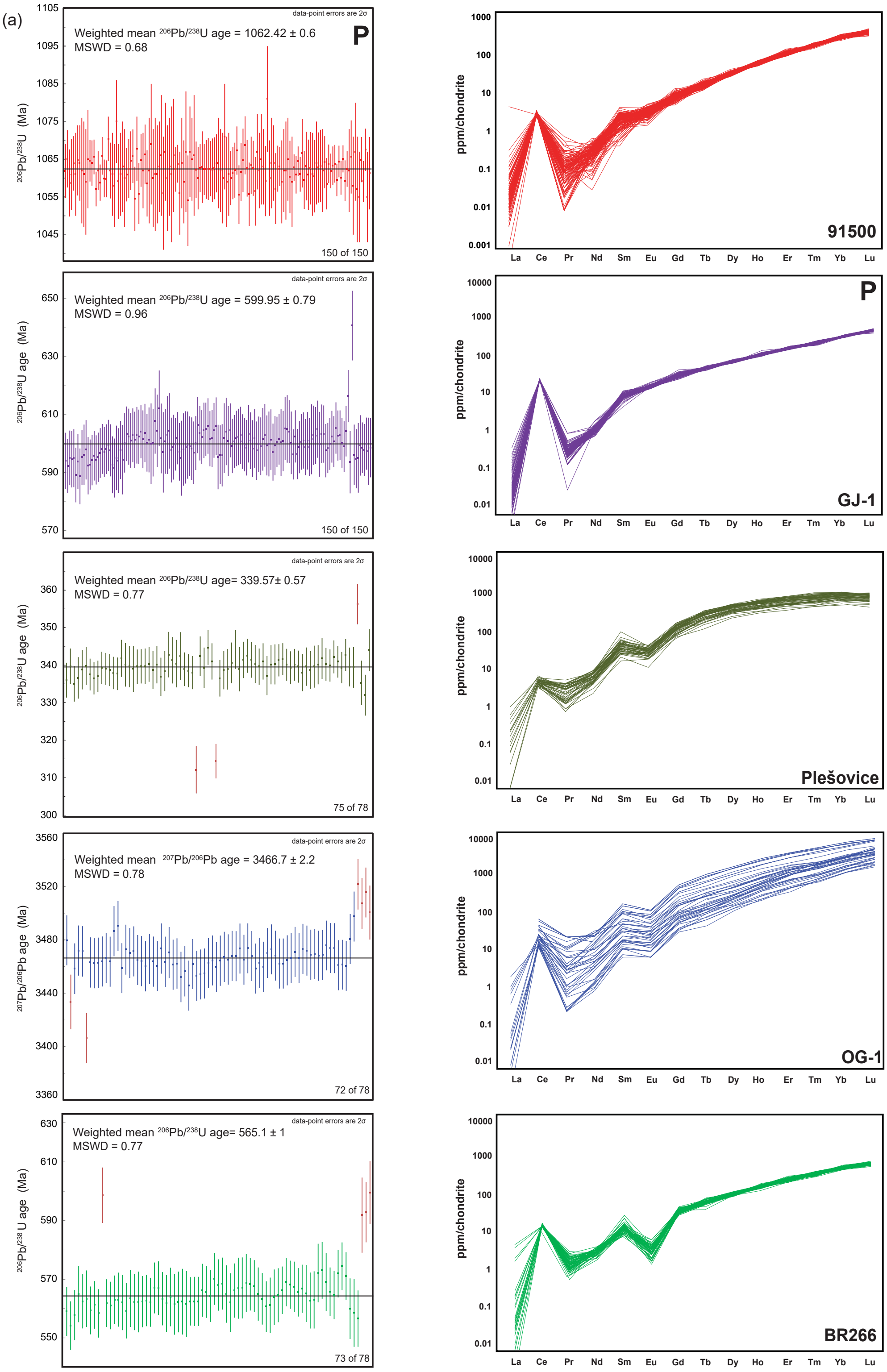

Figure 3.2 LASS (U–Pb and trace elements) data for zircon reference materials for: (a) **2014 session** Primary standard: 91500, and secondary standards GJ-1, Plešovice, OG-1 and BR266, and (b) **2015 session** Primary standard: 91500, and secondary standards GJ-1, Plešovice OG-1, and Temora-2. For comparison the horizontal grey lines are TIMS solution data from Widenbeck et al., 1995, Jackson et al., 2004, Stern et al., 2009 and Sláma et al., 2008, and Stern (2001), respectively, and (b) 2015 session– Primary standard: 91500, and secondary standards GJ-1, OG-1, Plešovice and Temora-2.

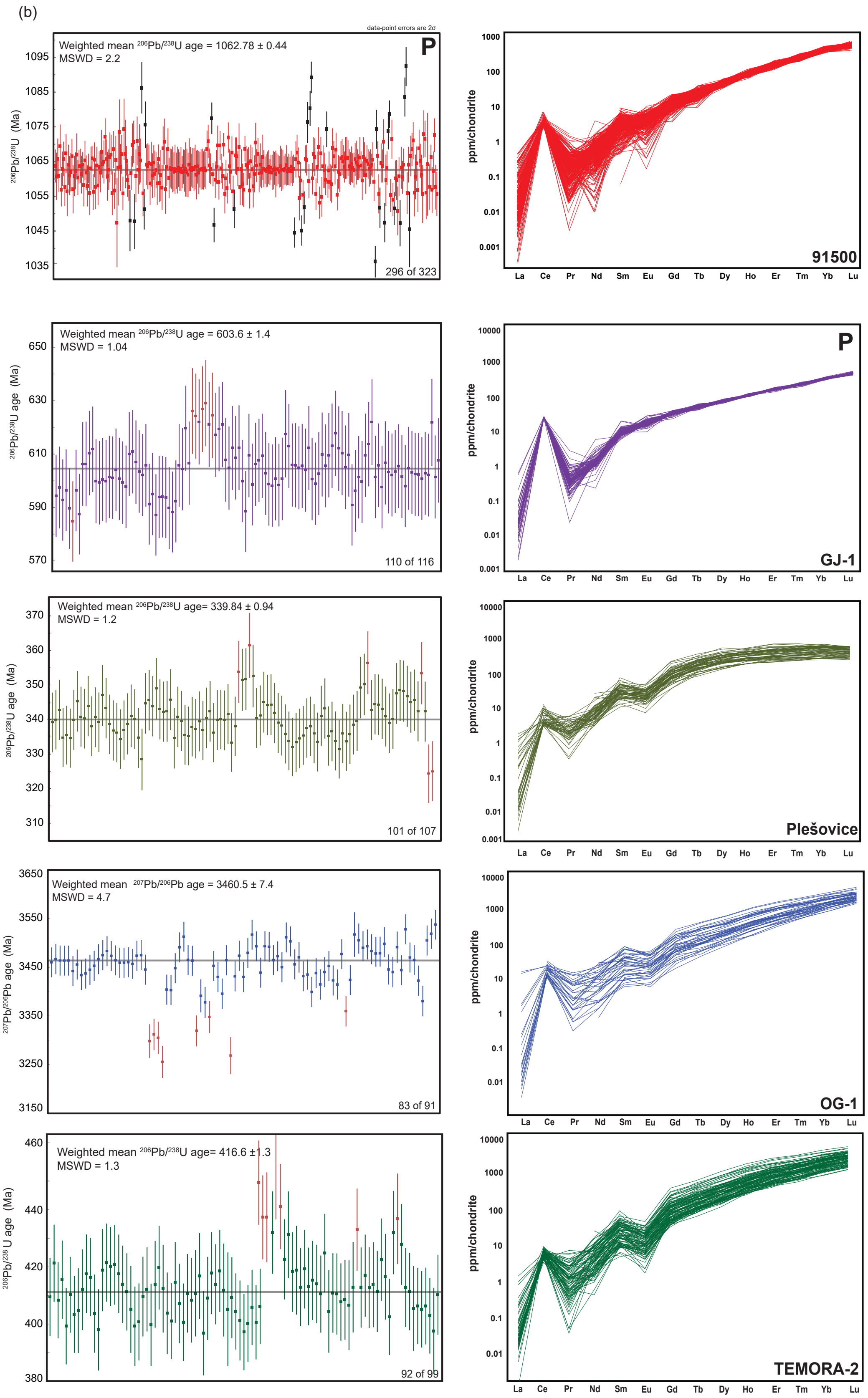

Figure 3.2 continued

established first by analysis of 10 ppb solutions of JMC475 and a Spex Hf solution, and then by analysis of 10 ppb solutions containing Spex Hf, Yb, and Lu. Instrument settings were then optimized for laser ablation analyses and 5 different reference materials (Mud Tank, 91500, Plešovice, and GJ-1) are analysed. When precision and accuracy were acceptable, unknowns were analysed using the same acquisition parameters. Laser ablation analyses were conducted with a laser beam diameter of ~50 µm; yielding approximately 0.8 volts/ppm Hf. Ablation pits were located on top of the LASS analysis pits. Data acquisition consists of (1) two laser pulses at the

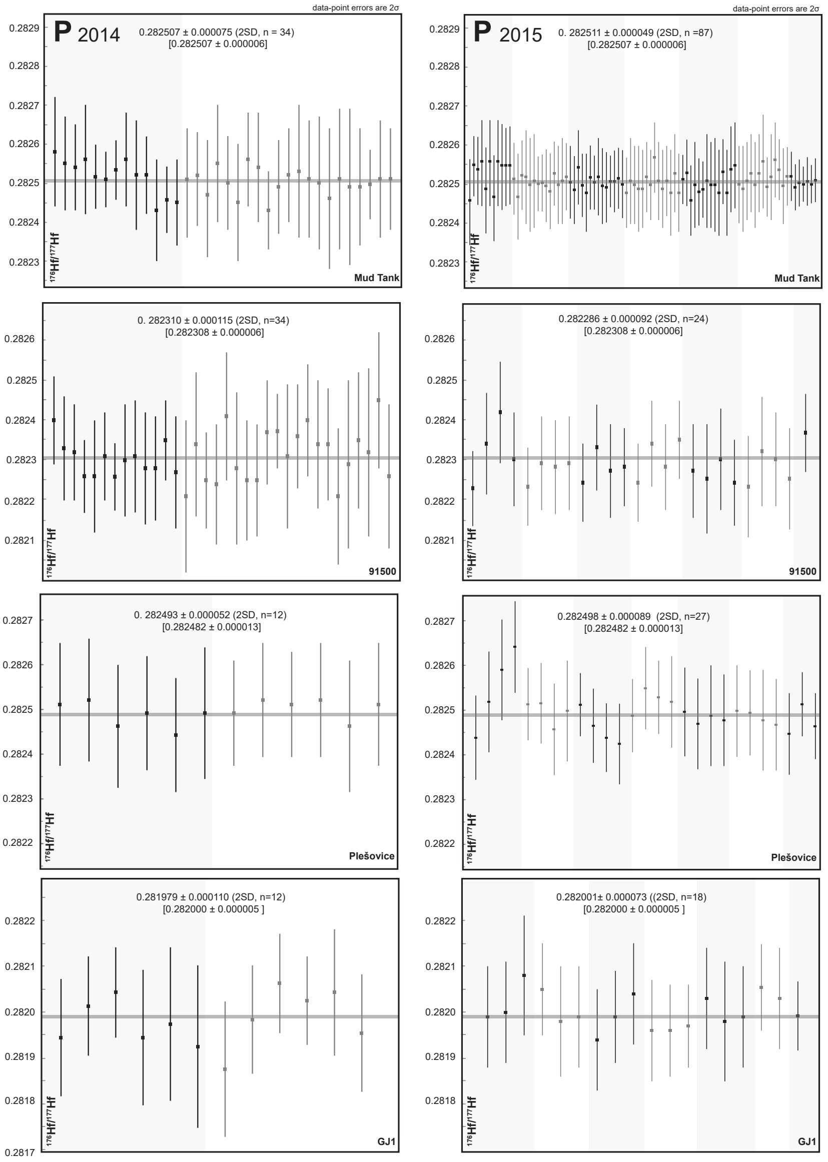

Figure 3.3 Reproducibility of ^{176}Hf/^{177}Hf ratios Hf isotope data for zircon reference materials –Mud Tank (primary), 91500, Plešovice and GJ-1. Left, 2014 and right, 2015. Within each plot, the data are ordered chronologically and separate runs/sessoins indicated by vertical sections. For comparison the horizontal grey lines are TIMS solution data from Woodhead and Hergt, 2005, Blichert-Toft, 2008, Sláma et al., 2008 and Morel et al., 2008, respectively, with average and uncertainties presented in brackets.

start of measurement to remove surface contamination, (2) 40-second of baseline acquisition by the on-peak-zero method, (3) 30-seconds of continuous ablation during which data are collected (laser frequency, 10 Hz; spot size, 44 µm), and (4) ~3 seconds with no laser firing to allow decay of the previous signal before the next analysis. During the first session (2014) the total run time was approximately 125 minutes per run. The entire suite of samples were analysed during continuous analytical session over a period of approximately 7 hours. During the second session (2015) the total run time was approximately 180 minutes per run. The entire suite of samples were analysed in approximately 23 hours over a period of three days. The best estimate of analytical uncertainty (external precision and accuracy) is best represented by the total deviation of ^{176}Hf/^{177}Hf from values determined by ID-TIMS dissolution methods. Mud Tank zircon was used as the primary reference material. A combination of 91500, Plešovice and GJ-1were used as secondary standards to monitor the precision and accuracy of each analytical session (Fig. 3.2).

The average measured ^{176}Hf/^{177}Hf ratios of the primary standard Mud Tank during 2014 (0.282507 ± 0.000075 2SD, n=34) and 2015 (0.282511 ± 0.000049 2SD, n=87) are within uncertainty of the recommended value (0.282507 ± 0.000006 2SD; Woodhead and Hergt, 2005). Analyses of secondary standards yield ^{176}Hf/^{177}Hf within uncertainty of published values; 0.282310 ± 0.000115 (n=34, 2014) and 0.282286 ± 0.000092 (n=24, 2015) for 91500 (0.282308 ± 0.000006, Blichert and Toft, 2008); 0.282493 ± 0.000052 (n=12, 2014) and 0.282498 ± 0.000089 (n=27, 2015) for Plešovice (0.282482 ± 0.000013, Sláma et al., 2008); 0.281979 ± 0.000110 (n =12, 2014) and 0.282001 ± 0.000073 (n=18, 2015) for GJ-1 (0.282000 ± 0.000005, Morel et al., 2008). Details of Lu–Hf zircon standard analyses are given in Appendix A.

3.2.2.3 ^{18}O/^{16}O isotope analyses

Oxygen isotope ratios (^{18}O/^{16}O) were determined using a Cameca IMS 1280 multi-collector ion microprobe located at the Centre for Microscopy, Characterisation and Analysis (CMCA) at the University of Western Australia. Analytical conditions were similar to those outlined in detail by Kita et al. (2009). A static ~3 nA Cs+ beam with an impact energy of 20 keV was focused to a 15 µm spot on the sample surface. Analyses were performed within the same CL zones on grains used for U–Pb and Lu–Hf analyses.

Oxygen secondary ions are sputtered from the sample by bombarding its surface with a 10 kV, Gaussian Cs+ beam with intensity of 3 nA and total impact energy of 20 keV. This primary beam is rastered over a 10 × 10 µm area at the surface of the sample. Secondary ions are admitted in the double focusing mass spectrometer within a 110 µm entrance slit and are focused in the centre of a 4000 µm field aperture (×130 magnification). They are energy filtered using a 40 eV band pass with a 5 eV gap toward the high-energy side. ^{16}O and ^{18}O are collected simultaneously in Faraday cup detectors fitted with 1010 Ω (L'2) and 1011 Ω (H'2) resistors, respectively, and operating at a mass resolution of ~2430. The magnetic field was regulated using NMR control.

Each analysis includes a pre-sputtering over a 15 × 15 μm area during 30 s and the automatic centering of the secondary ions in the field aperture, contrast aperture and entrance slit. Each analysis then consists of 20 four-second cycles. Penglai zircon (5.31‰, Li et al., 2010) was used as the primary reference material to monitor and correct for mass fractionation and instrumental drift. Secondary reference zircon Temora-2 (8.2‰; Black et al., 2004) was used to monitor data accuracy and precision (Fig. 3.3). Analyses of secondary standards yield average δ^{18}O values of 8.32 ± 0.54‰ (2 SD), in good agreement to the published value (8.2 ± 0.1‰, Black et al., 2004). During session 11 zircon 91500 was run as a secondary standard and returned a δ^{18}O value of 10.07 ± 0.26 (2SD), identical to the published value (δ^{18}O = 10.07 ± 0.03‰; Valley et al., 2005). The external precision based on analyses of the standard was 0.52‰ (2SD) across the total of 13 analytical sessions (Fig. 3.3; Appendix A). Data are presented as raw ^{18}O/^{16}O ratios and corrected δ^{18}O quoted with respect to Vienna standard mean ocean water (VSMOW). All oxygen isotope values reported here are in per mil (‰) and relative to VSMOW. Details of each oxygen zircon standard analyses are given in Appendix A.

3.3 DATA REDUCTION

3.3.1 U–Th–Pb and trace element analyses

Data reduction, including calculation of U–Th–Pb ratios and their uncertainties, were carried out using Iolite version 2.5 (Paton et al., 2010; 2011; Cottle et al., 2012) and includes corrections for baseline, instrumental drift, mass bias, and down-hole fractionation. Uncertainties are quoted at the 2σ level and include errors from counting statistics, and the U–Pb calibration errors based on reproducibility of U–Pb measurements of the primary standard.

U–Th–Pb isotope ratios were calculated on an integration-by-integration basis to enable calculation of ^{207}Pb/^{206}Pb, ^{206}Pb/^{238}U, and ^{208}Pb/^{232}U ratios. All ages in this study were calculated using the U decay constants of Jaffey et al. (1971) and the Th decay constant of Amelin and Zaitsev (2002). Elemental U, Th and Pb concentrations are calculated by applying a correction factor obtained by dividing the total counts of U, Th and Pb measured in the matrix matched primary reference material (91500) by the known value. Dates are based on ^{206}Pb/^{238}U ratios where they are less than ~1.5 Ga and on ^{207}Pb/^{206}Pb ratios for dates older than ~1.5 Ga (Spencer et al., 2016). For the purpose of calculating crystallisation ages, single populations (where multiple analyses are considered together to define the age of a geological event) were identified using

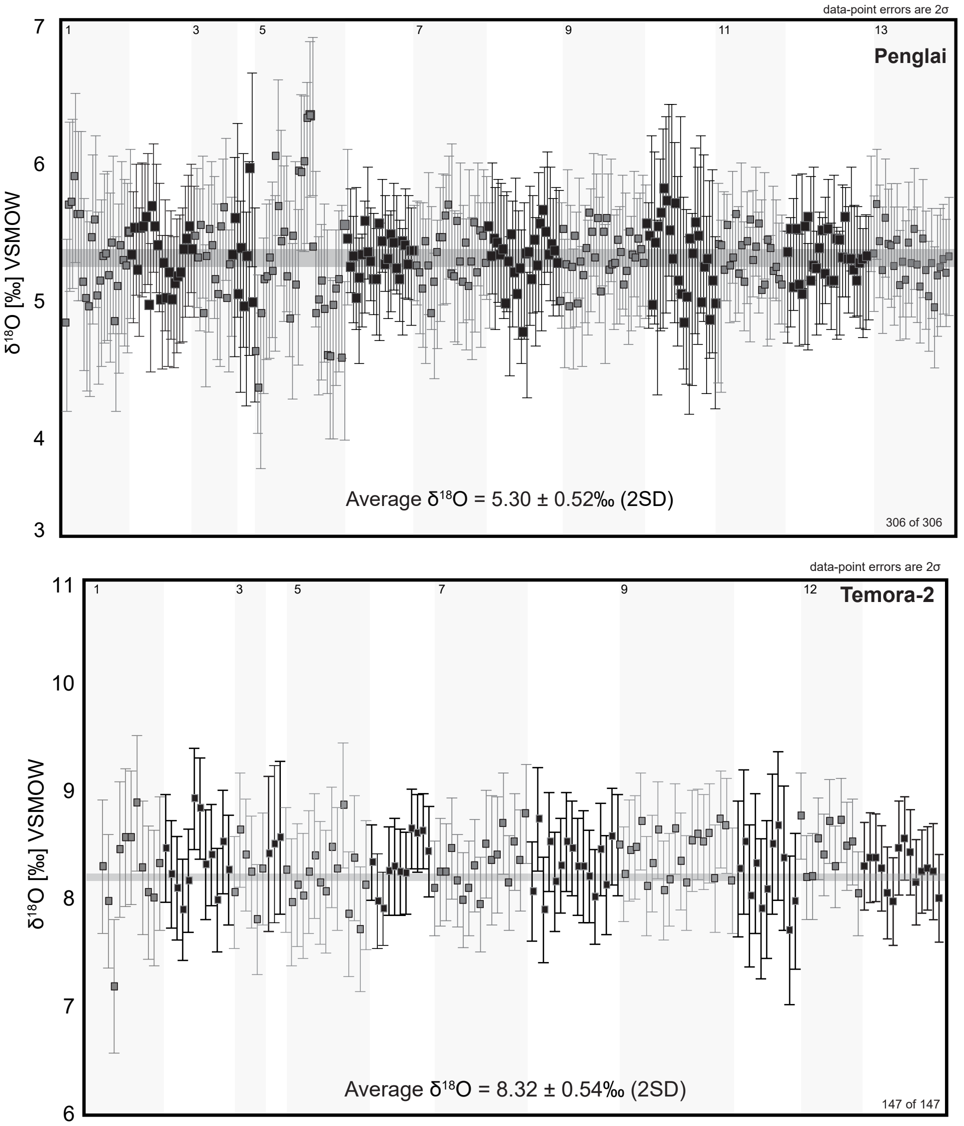

Figure. 3.4 Oxygen isotope data for zircon reference materials – Penglai (primary) and Temora-2. Within each plot, the data are ordered chronologically and separate sessions indicated by vertical sections. For comparison the horizontal grey lines are from published values Li et al., 2010 and Black et al., 2004, respectively. Individual analytical sessions are indicated by shaded vertical spaces and associated session number.

the reduced chi-squared statistic (Wendt and Carl, 1991) following the procedures outlined in Spencer et al. (2016). Uncertainties of weighted mean values for pooled analyses and concordia ages are at the 95% confidence level. Error ellipses on concordia diagrams are at the 2σ level. Data >10% discordance are excluded from Concordia diagrams. Concordia diagrams were constructed using Isoplot 3.75 (Ludwig, 2012). When a sample has few concordant analyses, the age obtained from the youngest analysis is generally interpreted as a minimum crystallisation age. Zircon analyses that have younger ages than the crystallisation age could represent part of the main group of zircons which underwent early Pb loss, or new grains or rims that crystallised at younger ages. The term 'inherited zircon' will be used to define any zircon that is interpreted not to have newly crystallised from the melt in the rock of interest (i.e. is older that the crystallisation of the magmatic rock). Time-resolved analysis signals allow for identification of isotope heterogeneity, examples of which include inclusions, inherited cores, zones of Pb loss and zones of common Pb. If multiple zones are identified, the largest clear portion of the signal was used. No common Pb correction has been applied, and the relatively small uncertainty in age due to common Pb contents is incorporated in the external reproducibility of the secondary reference materials (e.g. Kylander-Clark et al., 2013). Measurement of ^{204}Pb in ICPMS is hampered by an isobaric interference from Hg, however, it can be used to monitor for very high counts for when common lead is high. Analyses that that recorded a total ^{204}amu signal of >200 cps and ^{206}Pb/^{204}Pb ratios <1500 were assessed for possible common-Pb contributions and rejected where required. Data quality for each analysis was evaluated and analyses were rejected based on (1) >10% uncertainty in ^{207}Pb/^{206}Pb and ^{206}Pb/^{238}U isotopic ratios (3) discordance (normal or reverse) is >5%, (4) ^{206}Pb/^{204}Pb ratios <1000. In some cases over 80% of the data were removed so that only representative analyses were used in age determinations.

3.3.2 Lu–Hf analyses

Lu–Hf isotope data collected on the multicollector were reduced using a data reduction scheme developed by the lab at UCSB using Iolite version 2.5 (Paton et al., 2010). Interference corrections for the overlap of ^{176}Yb and ^{176}Lu on ^{176}Hf are similar to the ones described by Horstwood (2008) and Fisher et al. (2014) so that βHf is determined from the measured ^{177}Hf/^{179}Hf, βYb is determined from the measured ^{171}Yb/^{173}Yb during the run, and the ^{176}Yb/^{177}Hf is calculated using the natural ^{176}Yb/^{171}Yb ratio following Woodhead et al. (2004). βLu is assumed to be the same as βYb, and an exponential formula is used for fractionation correction. Yb and Lu interferences are corrected by measurement of ^{173}Yb/^{176}Yb and ^{175}Lu/^{176}Lu (respectively). All corrections have been done line-by-line. For very low Yb signals, βHf is used for fractionation of Yb isotopes. The corrected ^{176}Hf/^{177}Hf values are filtered for outliers (2-sigma filter), and the average and standard error are calculated from the resulting integrations. To determine the present day ^{176}Hf/^{177}Hf the ^{176}Lu interference on the ^{176}Hf peak was subtracted using an accepted ^{176}Lu/^{175}Lu ratio of 0.02656 (Vervoort et al., 2004).

Initial Hf-isotope ratios (^{176}Hf/^{177}Hf$_i$) were calculated for each zircon using the ^{176}Lu decay constant of 1.867 x 10^{-11}/y (Scherer et al., 2001), measured ^{176}Hf/^{177}Hf ratios and ^{207}Pb/^{206}Pb or ^{206}Pb/^{238}U ages, using the 1.5 Ga threshold (Spencer et al., 2016). The chondritic (CHUR) ratios of ^{176}Hf/^{177}Hf = 0.0332 and ^{176}Lu/^{177}Hf = 0.282772 (Blichert-Toft and Albarede, 1997), depleted mantle (DM) ratios of ^{176}Hf/^{177}Hf = 0.0384 (Griffin et al., 2004) and ^{176}Lu/^{177}Hf = 0.283251

(Nowell et al., 1998), and average crustal ratio of ^{176}Lu/^{177}Hf = 0.015 (Griffin et al., 2002) were used to calculate initial epsilon Hf (εHf$_t$), Hf model ages (T$_{DM}$) and crustal model ages (T$_{DM}{}^{C}$). εHf$_t$ indicates parts per 10 000 derivation of the ^{176}Hf/^{177}Hf ratio of the sample from the ratio of CHUR. The composition of the mantle is highly heterogeneous, and therefore DM lines used in figures are based on ^{176}Lu/^{177}Hf of 0.283251 (Nowell et al., 1998) and 0.283164 (lower line; Chauvel et al., 2008) to show a range of possible mantle compositions. Hf data are presented on Hf-evolution diagrams that show εHf$_t$ (t) and ^{176}Hf/^{177}Hf$_i$ values at the time of crystallization. To increase confidence that the U–Pb and Hf data are linked, samples that show a significant change in ratio during the acquisition are rejected.

Where no reliable age data is available (i.e. >10% discordance) to calculate initial ^{176}Hf/^{177}Hf and εHf$_t$ the following method is used: (1) the range of measured ^{176}Hf/^{177}Hf ratios with corresponding magmatic ages is determined, (2) if the measured ^{176}Hf/^{177}Hf ratio of the analysis with no reliable age data is within this range, the magmatic U–Pb crystallisation age of the sample is used.

3.3.3 Oxygen isotope analyses

Data obtained from the Cameca IMS 1270 ion microprobe has been corrected and reduced externally using an in-house sheet developed by L. Martin and H. Jeon at The Australian Microscopy and Microanalysis Research Facility (AMMRF) at the University of Western Australia.

3.3.4 Propagation of uncertainties

3.3.4.1 U–Pb analyses

The secondary reference materials were used to assess the uncertainty propagation procedure. GJ-1 zircon was used as a secondary reference material, and data have been corrected with uncertainty propagated by quadratic addition for the precision of the analysis and reproducibility of the 91500 primary reference material. The data reduction methodology is outlined in Paton et al. (2010) and Hortswood et al. (2016); in brief, the excess uncertainty generated for each analytical session is combined with internal precision for each spot analysis. The excess error can be estimated by calculating the additional uncertainty required to produce an MSWD of 1 on the secondary standard (GJ-1). By combining this excess uncertainty in quadrature with the internal error of the individual spot analyses, a total error for each analysis is generated. For the first session (2014; n=150) these are 1.4% and 1.2% for ^{206}Pb/^{238}U and ^{207}Pb/^{206}Pb, respectively (n=148), and for the second session (2015; n=116) these are 2.5% and 2% for ^{206}Pb/^{238}U and ^{207}Pb/^{206}Pb, respectively.

CHAPTER 4

U–Pb, HAFNIUM AND OXYGEN ISOTOPE CONSTRAINTS ON ARCHAEAN MAGMATISM (c. 3400–2500 Ma)

4.1 INTRODUCTION

The Capricorn Orogen is a Proterozoic orogenic belt comprising sedimentary basins with variable amounts of volcanic rock that overly the Palaeoproterozoic Gascoyne Complex and the deformed margins of the Archaean Pilbara and Yilgarn Cratons (Johnson et al., 2013). Along the margins of the orogen, numerous basins overlie basement inliers of Archean granite-greenstone: the Marymia and Goodin Inlier of the Yilgarn Craton, and the Sylvania Inlier of the Pilbara Craton (Dentith et al., 2014).

The northwestern edge of the Yilgarn Craton margin was reworked and modified during collision with the Glenburgh Terrane during the c. 2005–1945 Ma Glenburgh Orogeny. This area was subjected to further deformation and metamorphism during the Capricorn Orogeny to form the Yarlarweelor Gneiss Complex (YGC). In the east the northern margin of the Yilgarn Craton is obscured by sedimentary basins, along which lie two Archaean inliers, the Goodin and Marymia Inlier. Current geological and geochronological data indicate that Marymia and Goodin Inliers are part of the Yilgarn Craton (Bagas, 1999; Vielreicher and McNaughton, 2002; Vielreicher et al., 2002; Gazley et al., 2011). North of the YGC lies the Halfway Gneiss of the Glenburgh Terrane which records igneous protolith ages between c. 2555 and c. 2430 Ma. Previously, based on dissimilarities in the magmatic history and isotopic characteristics of the Halfway Gneiss to the Yilgarn and Pilbara Craton, the Glenburgh Terrane has been interpreted to represent an element exotic to both these cratons (Johnson et al., 2011b). Sylvania Inlier lies in the northeastern part of the orogen, and is thought to represent the granite-greenstone Pilbara Craton. The Sylvania Inlier of the southern Pilbara Craton extends eastward under the eastern Ashburton Basin (Hackney, 2004). Field relationships in the granite-greenstone of the Sylvania Inlier resemble those of the northern Pilbara. However, differences in isotope and rare-earth-element patterns, suggest separate evolution of the Sylvania Inlier prior to 3.0 Ga (Tyler, 1991; Tyler et al., 1992).

The provenance, age and nature of the rocks of the inliers are not yet fully resolved. The geochronological, geochemical and isotopic data presented in this chapter are used to identify regions with a shared history of granite emplacement corresponding to a common geological and crustal evolution, and are used to constrain the relationships between the basement inliers and the Yilgarn and Pilbara Cratons. These data will provide constraints on the timing of granitoid formation and the source of magmatic material.

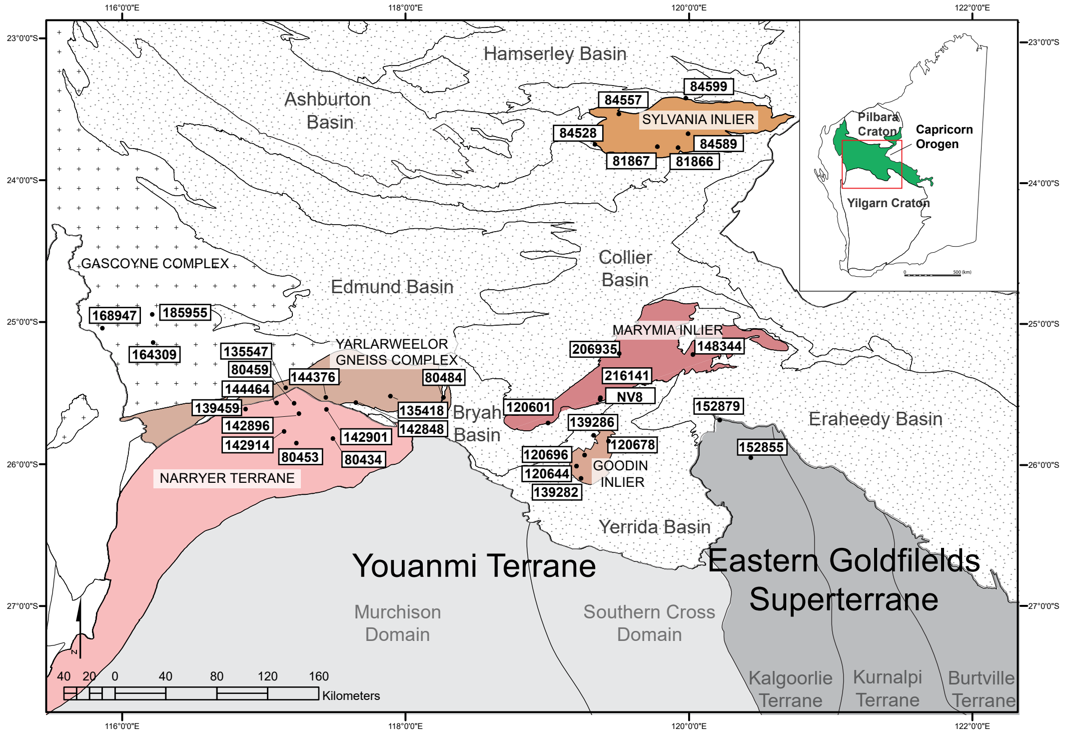

Figure 4.1 Simplified geological map of part of the Capricorn Orogen detailing the Archaean inliers and Yilgarn Craton margin, showing sample locations mentioned in the text.

4.2 REGIONAL GEOLOGICAL SETTING

This study area covers the northern edge of the Yilgarn Craton, specifically the Narryer Terrane and the northern extent of the Youanmi Terrane and EGST (Fig. 4.1). The Narryer Terrane, Yarlarweelor Gneiss Complex, basement inliers and Halfway Gneiss are discussed in detail in Chapter 2, this section briefly discusses the tectonic elements that make up the northern Yilgarn Craton and Pilbara Craton.

4.2.1 Yilgarn Craton

The Yilgarn Craton is an extensive region of Archean continental crust dominated by several terranes with distinct crustal histories that amalgamated at different times during the Neoarchean (Cassidy et al., 2005). The Narryer, South West and Youanmi Terranes form the western Yilgarn, which is separated from the Eastern Goldfields Superterrane (EGST) by the crustal-scale Ida Fault

(Drummond et al., 2000; Cassidy et al., 2006). The Youanmi Terrane comprises the Murchison and Southern Cross Domain, and the EGST is subdivided, from west to east, into the Kalgoorlie, Kurnalpi, Burtville and Yamarna Terranes (Fig. 4.1, Cassidy et al., 2006; Pawley et al., 2009, 2012). These terranes were juxtaposed, intruded by sheets of granite, intensely deformed and metamorphosed at c. 2700–2600 Ma.

4.2.2 Narryer Terrane and Yarlarweelor Gneiss Complex

Outlined in Chapter 2.

4.2.3 Youanmi Terrane

The Youanmi Terrane is divided into the Murchison and Southern Cross Domains (Fig. 1), and comprise of c. 3010–2630 Ma granitic rocks, greenstones and mafic-ultramafic intrusions (Van Kranendonk et al., 2013). The Youanmi Terrane is isotopically distinct from the other terranes, and possibly represents the nucleus, or protocraton, onto which younger terranes were accreted (Cassidy et al., 2006; Czarnota et al., 2010; Wyche et al., 2012).

Recent studies have suggested autochthonous crustal development from 2820 to 2600 Ma within the Murchison Domain (Champion and Cassidy, 2002; Van Kranendonk and Ivanic, 2009, Ivanic et al., 2012, Van Kranendonk et al., 2013), with significant mantle input between c. 2820 and c. 2720 Ma. The oldest known component of the Murchison Domain formed at c. 3050–2935 Ma (Pidgeon and Wilde, 1990; Yeats et al., 1996; Wang et al., 1998), with major periods of volcanism recorded at c. 2825–2740 Ma and c. 2735–2600 Ma (Van Kranendonk et al., 2013). Much of the late Archean history of the Murchison Domain, from 2720 to 2630 Ma, is similar to, and broadly contemporaneous with, events within the EGST. The Southern Cross Domain comprises granite-greenstone successions, and is bounded by the Ida Fault to the east. Existing geochronological constraints for the Southern Cross Domain is limited by the lack of suitable rocks, with ages of greenstone belts ranging between c. 3130 and c. 2730 Ma (Wang et al., 1996; Chen et al., 2003). Two major periods of granite magmatism is recorded at c. 3000–2830 and c. 2800–2600 Ma, with major magmatic pulses at c. 2780–2720 Ma, and continuous granite activity between c. 2700–2610 Ma (Archibald et al., 1978, 1981; Cassidy et al., 2002; Mole et al., 2012).

4.2.4 Eastern Goldfields Superterrane

The EGST consists of four tectonostratigraphic terranes, the Kalgoorlie, Kurnalpi, Burtville and Yamarna Terranes, which are thought to represent accreted crustal and arc elements (Cassidy et al., 2006; Pawley et al 2012). The terranes are bounded by interconnected systems of NNWtrending faults (Swager et al., 1997). The EGST is characterised by a younger history than the Youanmi Terrane, with ages of volcanic activity and greenstone development ranging from c. 2960–2660 Ma and the majority of granite magmatism occurred after c. 2720 Ma (Wyche, 2008; Wyche et al., 2012). Czarnota et al. (2010) suggested the formation of the EGST was an autochthonous rift setting, driven by subduction roll back.

4.2.4.1 Pilbara Craton

The c. 3720–2830 Ma Pilbara Craton comprises low grade volcano-sedimentary greenstone belts, granitic bodies and meta-sedimentary basins (Van Kranendonk et al., 2007). The southern margin of the craton is unconformably overlain by volcanics and sediments of the Fortescue (c. 2770–2630 Ma) and Hammersley (c. 2630–2450 Ma) Basins (Hickman, 2012; Van Kranendonk et al., 2007; Kemp et al., 2015). The craton is composed of several geologically distinct terranes, the c. 3530–3220 Ma East Pilbara Terrane, the c. 3280–3070 Ma West Pilbara Superterrane which out crops in the northwest of the craton and the c. 3200–2930 Ma Kurrana Terrane in the southeast, interpreted as a rifted fragment of the East Pilbara Terrane (Van Kranendonk et al., 2007, 2010).

4.2.4.2 Archean Inliers

Outlined in Chapter 2.

4.3 U–Pb GEOCHRONOLOGY

This chapter presents U–Pb results from thirty-four samples, which cover the Glenburgh Terrane, Narryer Terrane, the Yarlarweelor Gneiss Complex, and the Archaean inliers (Fig. 4.3). Samples are discussed in accordance to their geographical sub-divisions. A summary of zircon data is presented in Table 4.1. Details of each U–Pb and REE, O and Hf sample analysis are given in Appendix B. Zircon grains obtained from heavy mineral separates provided for by the GSWA are indicated in text. All other zircon grains are obtained through EMP as described in Chapter 3. Analytical methods are outlined in detail in Chapter 3. Rock samples were petrographically characterised by GSWA prior to analysis. The majority of weighted mean $^{207}Pb/^{206}Pb$ ages obtained during this study are in agreement with previously established ages. For 2 samples (142914 and 142896) ages were obtained that differ from those obtained during previous studies (<1.7% age difference; Table 4.1). Details of U–Pb sample analyses are given in Appendix B.

4.3.1 Narryer Terrane

The dataset from the Narryer Terrane consists of nine samples, and the analysed zircon cover a period of 1209 Myr, with ages between c. 3766 and c. 2557 Ma. Most of the granites were generated during magmatic episodes at c. 3350 Ma, c. 2720 Ma and c. 2620 Ma. The zircon geochronology of these samples is dominated by >50% inherited material, and although granites and gneisses older than c. 3400 Ma are not preserved, the inherited zircon record granite magmatism of this age and older.

4.3.1.1 GSWA 80434

GSWA 80434 is a granodiorite. Zircon grains from this sample are light brown to black in colour, typically 80–250 µm in length, and subrounded, subhedral to prismatic in shape. Cathodoluminescence (CL) images reveal poorly luminescent oscillatory zoned cores, surrounded by thin structureless rims. Rims were too small to target, only cores were analysed. Inclusions are common. Forty-seven analyses were obtained from 47 grains. Twenty-one analyses are >10% discordant (Group D) and have been rejected. Individual ^{207}Pb/^{206}Pb ages range from c. 3766 Ma to c. 2840 Ma. Twenty analyses plot in a discordant array with the upper intercept at 3355 ± 44 Ma (MSWD = 6.8), the lower limit (1570 ± 140 Ma) is not constrained by any concordant grains, and does not necessarily have any geological significance. Five analyses of zircon cores (Group 1) plot close to Concordia (<5 % discordant) at the upper end of the array, and yield a weighted ^{207}Pb/^{206}Pb age of 3365 ± 30 Ma (MSWD = 2.2). This value is our best estimate of the age of magmatic crystallization. Six analyses (Group X) returned ^{207}Pb/^{206}Pb ages ranging between c. 3766 and c. 3529 Ma, and are interpreted as inherited material.

4.3.1.2 GSWA 80453

GSWA 80453 is a metamonzogranite. Zircon grains are generally 80–120 µm in length, brown, anhedral to subhedral fragmented stubby grains. CL images display homogenous to oscillatory zoned grains, mantled by homogenous or oscillatory zoned rims of variable thickness. Thirty-seven analyses were obtained from 35 grains. Twenty-eight analyses (Group D) are >5% discordant or indicate a high common Pb component, and are not considered further. Four analyses (Group 1) yield a weighted mean ^{207}Pb/^{206}Pb date of 2708 ± 36 Ma (MSWD = 1.8), interpreted as the age of magmatic crystallization. Five analyses zircon cores and one rim (Group X) yield ^{207}Pb/^{206}Pb dates between c. 3400 and c. 2752 Ma, interpreted to reflect the ages of inherited material.

4.3.1.3 GSWA 139459

GSWA 139459 is a metamonzogranite. Zircon grains were hand-picked from heavy mineral concentrates provided by the GSWA. The zircon are dark brown in colour, typically 100–300 µm in length, and subrounded, subhedral to prismatic in shape. CL images display oscillatory zoned cores, which in places is convoluted, surrounded by thin structureless rims of brighter

Table 4.1 Summary of sample descriptions and U–Pb LASS data.

Sample	Unit[1]	Lithology[2]	Pb–Pb age (Ma)[3]	Inheritance (Ma)	Pb–Pb age (Ma)[4]	T_{Ti} (°C)	Lat	Long
80434	NT	granodiorite	3365 ± 30	3766–3529	-	832	-25.773	117.484
80453	NT	metamonzo-granite	2708 ± 36	3400–2752	-	739	-25.806	117.226
139459	NT	monzogranite	2729 ± 8	2785	2738 ± 5	765	-25.567	116.867
142914	NT	monzogranite	2662 ± 9	2779–2719	2615 ± 2	724	-25.723	117.139
133547	NT	granitic gneiss	2645 ± 15	2916–2702	-	816	-25.455	117.007
144464	NT	metgranite	(2618 ± 37)	3233–3078	-	-	-25.522	117.086
80459	NT	felsic gneiss	2643 ± 11	3027–2678	-	739	-25.525	117.21
142901	NT	monzogranite	2615 ± 18	3249–2678	-	726	-25.567	117.438
142896	NT	gneiss	2631 ± 15	3378–2685	2576 ± 11	744	-25.599	117.243
135418	YGC	granitic gneiss	*3506 ± 10*	-		760	-25.474	177.889
144376	YGC	metagranite	3187 ± 12	3351–3227	-	-	-25.484	117.434
142848	YGC	monzogranite	2675 ± 30	2654–2648	-	676	-25.521	117.645
80484	YGC	metagranite	2643 ± 43	2790–2702	-	808	-25.621	115.626
JC15	MI	granitic rock	3332 ± 8	-	-	724	-25.476	119.465
216141	MI	granitic rock	3336 ± 16	3406–3400		735	-25.496	119.37
148344	MI	metagranite	2698 ± 11	-	-	698	-25.181	120.024
206935	MI	granitic gneiss	2699 ± 29	-	-	762	-25.175	119.505
120601	MI	metasediment	2641 ± 12	2936–2655	-	756	-25.664	119.002
139286	GI	granitic rock	[2658 ±17]	-	-	814	-25.752	119.323
139282	GI	granitic rock	2642 ± 12	-	-	787	-26.056	119.236
120644	GI	granitic rock	2650 ± 10	2905	-	827	-25.968	119.203
120678	GI	granitic rock	-	-	-	850	-25.793	119.429
120696	GI	granitic rock	2623 ± 8	2720	-	815	-25.891	119.26
152855	EGST	granitic rock	2668 ± 31	2778–2726	-	639	-25.908	120.433
152879	EGST	granitic rock	(2594 ± 30)	2892–2531	-	-	-25.643	120.215
81886	SI	granitic rock	[3296 ± 24]	-	-	-	-23.723	119.92
81867	SI	monzogranite	3196 ± 9	3299–3288	-	-	-23.716	119.773
84528	SI	granitic rock	(3261 ± 32)	3405–2710	-	-	-23.7	119.333
84557	SI	granitic rock	2879 ± 16	-	-	-	-23.486	119.502
84589	SI	granodiorite	3188 ± 41	3259–3230	-	773	-23.625	119.991
84599	SI	monzogranite	2924 ± 14	3296–3133	-	751	-23.375	119.973
185955	HG	granitic gneiss	-	2788–2341	2527 ± 9	689–871	-24.909	116.294
164309	HG	granodiorite gneiss	2539 ± 6	3521	2548 ± 8	-	-25.086	116.142
168947	HG	monzogranite gneiss	2042 ± 59	2574–2188	2006 ± 6	600–631	-25.033	115.828

[1] NT= Narryer Terrane, YGC= Yarlarweelor Gneiss Complex, MI= Marymia Inlier, GI= Goodin Inlier, EGST = Eastern Goldfields Superterrane, SI= Slyvania Inlier, HG= Halfway Gneiss

[2] Petrographically characterised (GSWA)

[3] Crystallisation age ($^{207}Pb/^{206}Pb$) established by LASS, ages in brackets indicate () minimum or [] maximum crystallisation age.

[4] Crystallisation age ($^{207}Pb/^{206}Pb$) established by SHRIMP (GSWA) (-) indicates no value obtained

luminescence. Forty-four analyses were obtained from 40 grains. Twenty-one analyses (Group D) are >5% discordant, or are core-rim mixtures, and are not considered further. Five rims were analysed, returning ^{207}Pb/^{206}P ages between c. 2718 and c. 2696 Ma, indistinguishable from ages obtained from cores. Twenty-two analyses (Group 1), including both cores and rims identified in CL, yield a weighted mean ^{207}Pb/^{206}Pb date of 2729 ± 8 Ma (MSWD = 1.2), interpreted as the crystallization age of the monzogranite. One core analysis (Group X) yields a ^{207}Pb/^{206}Pb date of c. 2785 Ma, interpreted as the age of an inherited component. The crystallisation age of 2729 ± 8 Ma is in agreement with the SHRIMP U–Pb age previously established by the GSWA (2738 ± 5 Ma; Nelson, 2000a).

4.3.1.4 GSWA 142914

GSWA 142914 is a foliated porphyritic monzogranite. Zircon grains were hand-picked from heavy mineral concentrates provided by the GSWA. The zircon grains are light brown to dark brown in colour, 150–400 µm in length and subrounded, prismatic to stubby in shape. CL imaging reveals CL-intermediate cores with faint oscillatory zoning, which in places is convoluted, mantled by CL-darker rims of varying thicknesses and commonly overprinted by recrystallization zones. Twenty analyses are >5% discordant and Four analyses of recrystallised zones returned ^{207}Pb/^{206}Pb dates between c. 2683 and c. 2665 Ma, indistinguishable from dates obtained from cores. Twelve analyses (Group 1), including both cores and rims identified in CL, yield a weighted mean ^{207}Pb/^{206}Pb date of 2662 ± 9 Ma (MSWD = 0.93), interpreted as the age of magmatic crystallization. Six analyses of 6 cores (Group X) yield ^{207}Pb/^{206}Pb dates between c. 2779 and 2719 Ma, which are interpreted as the age of an inherited component. One analysis of a core (Group P) with a ^{207}Pb/^{206}Pb date of 2620 ± 33 Ma and is interpreted to have lost radiogenic Pb. The crystallisation age of 2662 ± 9 Ma is older than the SHRIMP U–Pb age previously established by the GSWA (2615 ± 2 Ma; Nelson, 1999d).

4.3.1.5 GSWA 135547

GSWA 135547 is a granitic gneiss. Zircon grains from this sample are light brown to black in colour, typically 80–200 µm in length, and subrounded, subhedral to prismatic in shape. CL images reveal poorly luminescent homogenous to weak oscillatory zoning. Forty-six analyses were obtained from 46 grains. Five analyses indicated a high common Pb component and have been rejected (Group D). Thirty-one analyses are >5% discordant, but appear to have only been affected by recent radiogenic-Pb loss. Nine analyses (Group 1) yield an intercept age of 2634 ± 23 Ma (MSWD 1.4, lower intercept at 192 ± 390 Ma) and a weighted mean ^{207}Pb/^{206}Pb age of 2645 ± 15 Ma (MSWD = 1.3). Thirty analyses of cores (Group X) yield ^{207}Pb/^{206}Pb dates between c. 3069 and 2780 Ma. Group X includes twenty-two analyses (Group X2) that yield a weighted mean $^{207}Pb/^{206}Pb$ age of 2745 ± 10 Ma (MSWD 1.7). Two analyses of cores (Group P) yield $^{207}Pb/^{206}Pb$ dates between c. 2570 and c. 2557 Ma and are interpreted to have lost radiogenic Pb. The weighted mean age of 2645 ± 15 Ma indicated by Group 1 is interpreted as the age of magmatic crystallization of the granitic protolith to the gneiss, analyses from Groups X are interpreted as the age of inherited components, and the age of 2745 ± 10 Ma of Group X2 is interpreted as the age of the dominant source of inherited material.

4.3.1.6 GSWA 144464

GSWA 144464 is a metagranitic rock. Zircon grains are light-brown to dark brown in colour, 80–200 µm in length, and subrounded to rounded, subhedral and stubby in shape. CL images reveal structureless and poorly luminescent zircon surrounded by thin oscillatory zoned rims of brighter luminescence. Some grains are locally overprinted by zones of recrystallization. Forty-three analyses were obtained from 38 grains. Seventeen analyses are >5% discordant (Group D) and are not considered further. Three analyses of zircon cores (Group 1) yield $^{207}Pb/^{206}Pb$ ages between c. 2708 and c. 2618 Ma. Twenty-three analyses of cores yield $^{207}Pb/^{206}Pb$ dates between c. 3248 and c. 3078 Ma and are interpreted as the age of inherited components. The age of 2618 ± 37 Ma indicated by the youngest analyses in Group 1 is interpreted to be the minimum age of crystallisation of the granite.

4.3.1.7 GSWA 80459

GSWA 80459 is a felsic gneiss. Zircon grains isolated from this sample are light brown to dark brown, 80–200 µm in length, and subrounded to rounded, subhedral and stubby in shape. CL images reveal a range of textures including oscillatory zoning and homogenous domains of low luminescence. Forty-six analyses were obtained from 43 grains. Twenty-one analyses are >5% discordant or indicate a high common Pb component (Group D) and are not considered further. Nine analyses of cores and one rim (Group 1) yield a weighted mean $^{207}Pb/^{206}Pb$ age of 2643 ± 11 Ma (MSWD = 1.05). Eleven analyses of cores (Group X) yield $^{207}Pb/^{206}Pb$ dates between c. 3027 and c. 2678 Ma. Five analyses (Group P) yield $^{207}Pb/^{206}Pb$ dates between c. 2596 and c. 2520 Ma and are interpreted to have lost radiogenic Pb. The age of 2643 ± 11 Ma indicated by Group 1 is interpreted as the age of magmatic crystallization. The remaining analyses from Group X interpreted as the age of inherited material.

4.3.1.8 GSWA 142901

GSWA 142901 is a foliated, heterogeneous monzogranite. Zircon grains were hand-picked from heavy mineral concentrates provided by the GSWA. Zircon grains are subrounded, subhedral and elongate in shape, colourless to brown in colour, and are typically 100–250 µm in length.

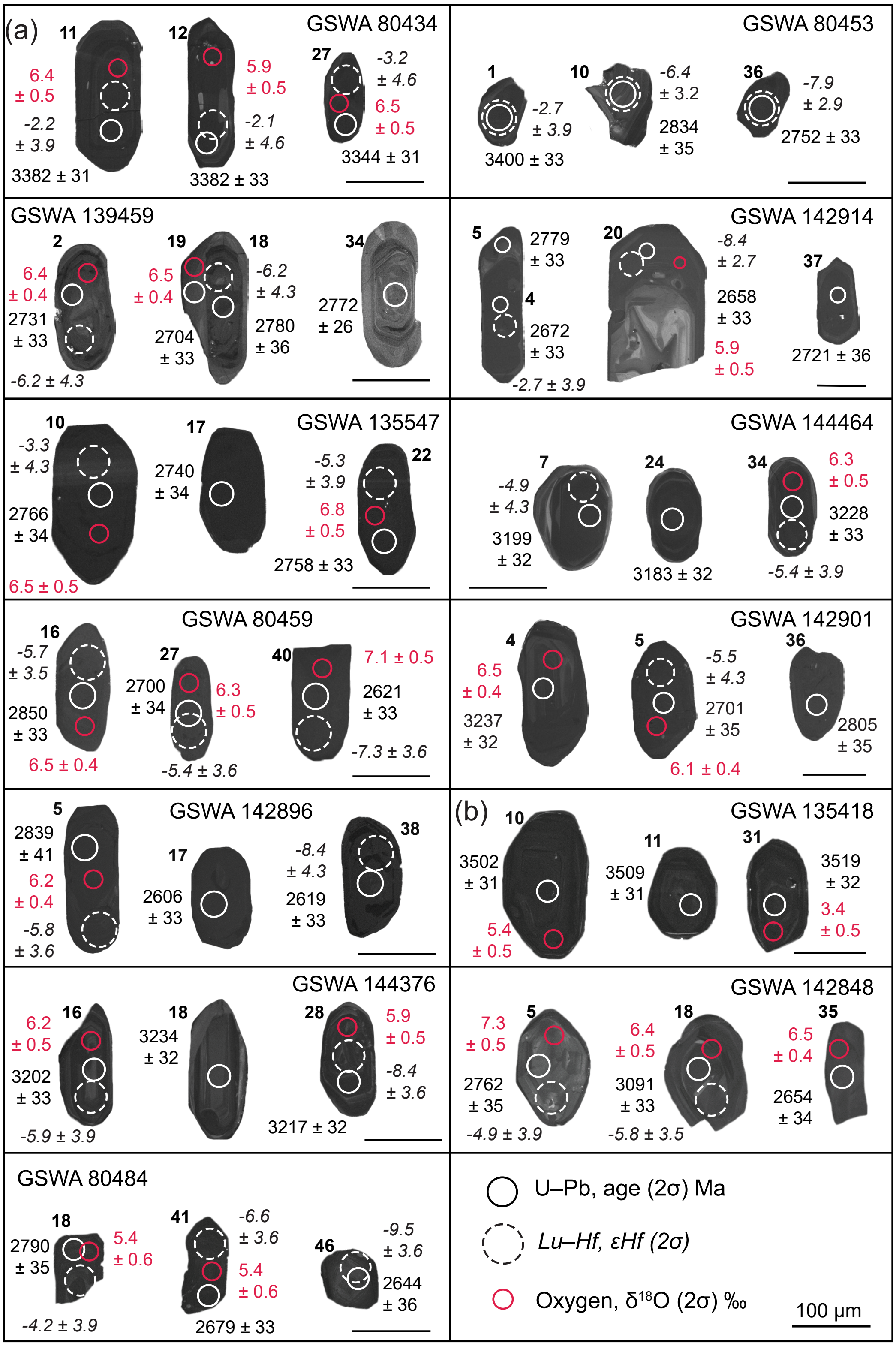

Figure 4.2 continues with caption overleaf

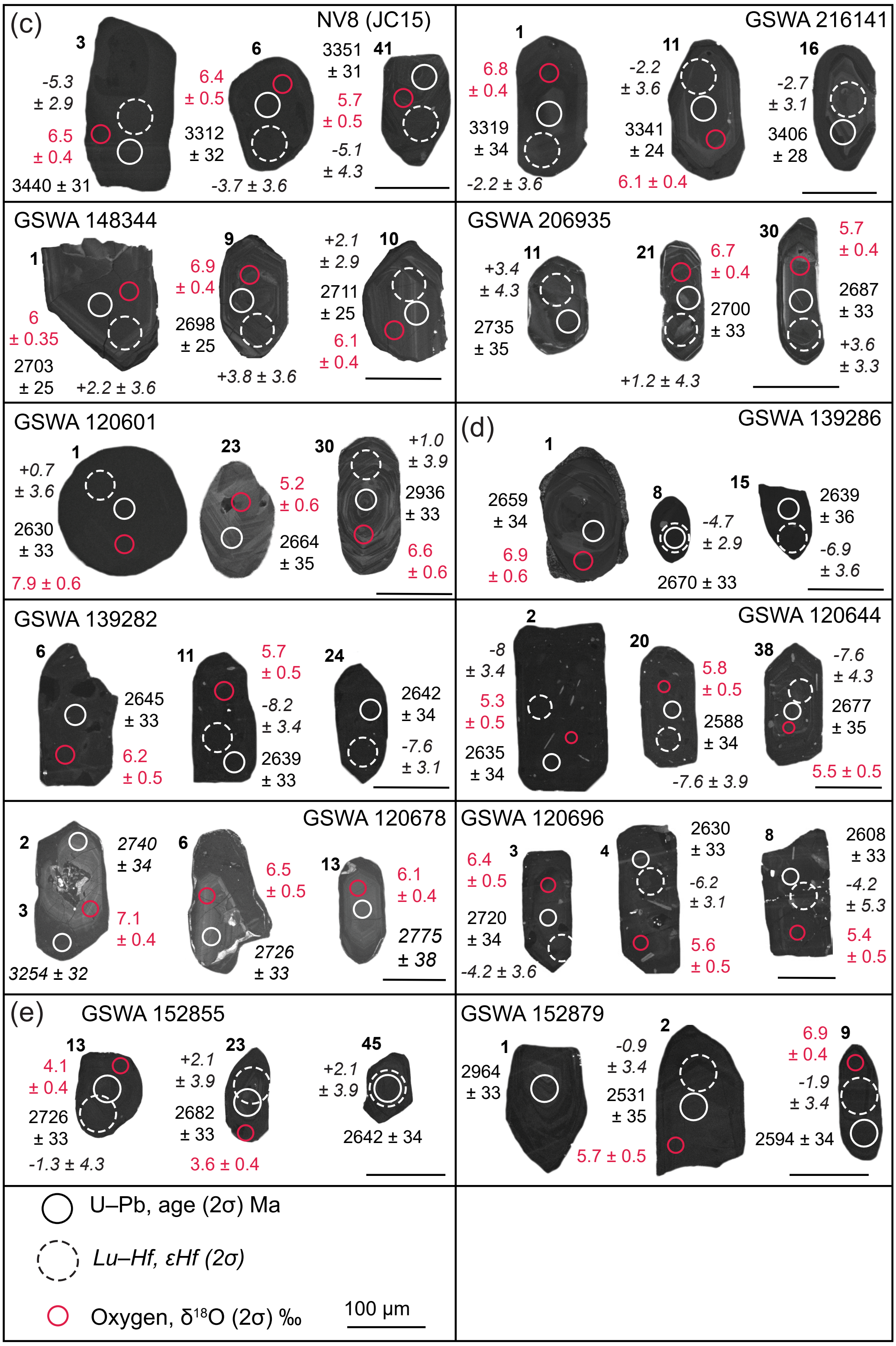

Figure 4.2 continues with caption overleaf

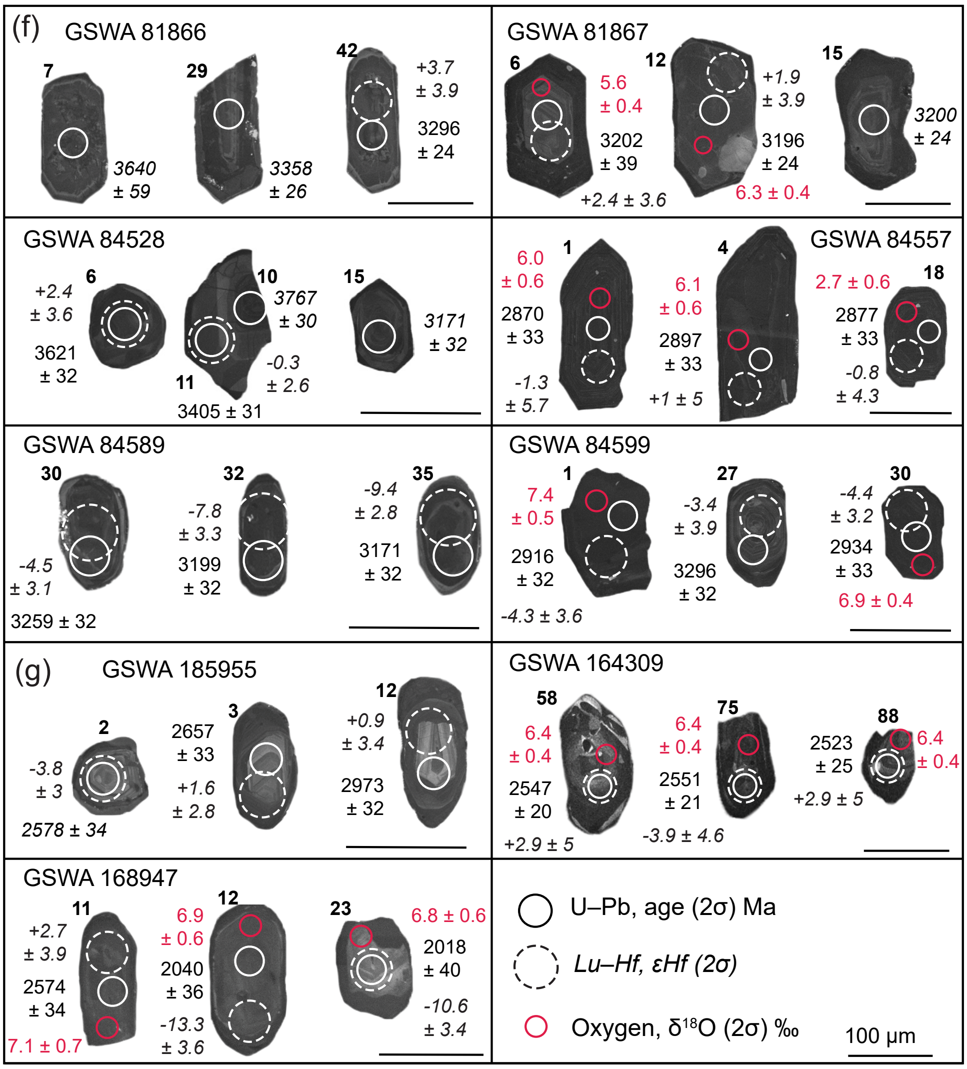

Figure 4.2 Representative CL images of zircon from (a) Narryer Terrane, (b) Yarlarweelor Gneiss Complex, (c) Marymia Inlier, (d) Goodin Inlier, (e) Eastern Goldfields Superterrane, (f) Sylvania Inlier and (g) Halfway Gneiss samples. Ages in italics indicates discordance >10%.

CL images reveal structureless and poorly luminescent, high uranium zircon. Weak oscillatory zoning is visible in some grains. Metamict patches and inclusions are common. Fifteen analyses (Group D) are >5% discordant and have been rejected. Seven analyses of cores (Group 1) yield a weighted mean ^{207}Pb/^{206}Pb age of 2615 ± 18 Ma (MSWD = 1.3). Twenty-four analyses of cores (Group X) yield ^{207}Pb/^{206}Pb dates ranging from c. 3249 to c. 2678 Ma. The age of 2615 ± 18 Ma indicated by Group 1 is interpreted as the crystallisation age of the granite, with the remaining analyses from Group X are interpreted as the ages of inherited material.

4.3.1.9 GSWA 142896

GSWA 142896 is a leucocratic gneiss. Zircon grains were hand-picked from heavy mineral concentrates provided by the GSWA. Zircon grains are subhedral and subrounded and elongate in shape, light brown to dark brown in colour, and 100–250 µm in length. CL images reveal poorly luminescent grains which show a range of textures including oscillatory zoning and homogenous domains, surrounded by structureless rims of varying thickness. Forty-five analyses were obtained from 43 grains. Twenty-one analyses are >5% discordant and have been rejected. Twelve analyses of cores (Group 1) yield a weighted mean ^{207}Pb/^{206}Pb age of 2631 ± 15 Ma (MSWD = 1.8). Eight analyses of cores (Group X) yield ^{207}Pb/^{206}Pb dates of c. 3378–2685 Ma. Four analyses (Group P) yield ^{207}Pb/^{206}Pb dates between 2584 and 2444 Ma and are interpreted to have lost radiogenic Pb. The age of 2631 ± 15 Ma indicated by Group 1 is interpreted as the crystallisation age of the granite protolith, with the remaining analyses Group X interpreted as the ages of inherited material.

The SHRIMP U–Pb age previously established by the GSWA of 2576 ± 11 Ma (Nelson, 1998c) was interpreted as providing either: the maximum time of deposition of a sedimentary component within the gneiss, metamorphism of the gneiss or formation of the gneiss

4.3.2 Yarlarweelor Gneiss Complex

The dataset from the Yarlarweelor Gneiss Complex consists of three samples, and the analysed zircon cover a period of 1190 Myr, with ages between c. 3582 and c. 2390 Ma. Granites were generated during magmatic episodes at c. 3500 Ma, c. 3190 Ma and c. 2690 Ma.

4.3.2.1 GSWA 135418

GSWA 135418 is a granitic gneiss. Zircon grains are light brown to brown in colour, subrounded elongate to rounded in shape, and 80–220 µm in length. CL images display oscillatory zoning. Older cores are present within some grains, and thin homogeneous overgrowths mantle some crystals. Forty-five analyses were obtained from 45 grains. Thirty-four analyses are >5% discordant and are not considered further. Ten analyses (Group 1) of cores yield a weighted mean ^{207}Pb/^{206}Pb age of 3506 ± 10 Ma (MSWD = 0.85), interpreted as the crystallization age of the granite protolith. One analysis (Group P) located on an oscillatory zoned zircon core yields a ^{207}Pb/^{206}Pb date of 3443 Ma. This crystal is interpreted to have been subject to ancient radiogenic-Pb loss. The hafnium isotope data indicate that there is some problems associated with this sample, and it is possible that the U–Pb data are erroneous (see section 4.7.3).

4.3.2.2 GSWA 144376

GSWA 144376 is a metagranitic rock. Zircon grains are light brown to brown in colour, 80–200 µm in length, and subrounded to rounded, subhedral and stubby in shape. CL images reveals CL-intermediate cores with faint oscillatory zoning, some have convoluted zoning, mantled by

CL-darker rims of varying thicknesses and commonly overprinted by recrystallization zones. Forty-eight analyses were obtained from 45 grains. Thirteen analyses (Group D) that are >5% discordance or core-rim mixtures have been rejected. A further eight analyses are characterised by >5% discordance, but appear to have only been affected by recent radiogenic Pb-loss. Seven analyses of cores (Group 1) yield a weighted mean $^{207}Pb/^{206}Pb$ age of 3187 ± 12 Ma (MSWD = 0.51). Nineteen analyses of cores and one rim (Group X2) yield a weighted mean $^{207}Pb/^{206}Pb$ age of 3240 ± 7 Ma (MSWD = 0.87). One analysis (Group X) yields a $^{207}Pb/^{206}Pb$ date of c. 3351 Ma. Eight analyses (Group P) yield $^{207}Pb/^{206}Pb$ dates ranging between c. 3139 and c. 2761 Ma and are interpreted to have undergone ancient radiogenic-Pb loss. The age of 3187 ± 12 Ma indicated by Group 1 is interpreted as the age of magmatic crystallisation, with the remaining analyses from Groups X2 and X interpreted as the ages of inherited material.

4.3.2.3 GSWA 142848

GSWA 142848 is a metamonzogranite dyke. Zircon grains were hand-picked from heavy mineral concentrates provided by the GSWA. Zircon grains are subrounded, subhedral and elongate in shape, colourless to yellow in colour, and are typically 80–250 µm in length. CL images display homogeneous to oscillatory zoned interiors, which in places is contorted. Inclusions are common. Forty-two analyses were obtained from 41 grains. Thirty analyses (Group D) are >5% discordant and are not considered further. Five analyses of cores and one rim (Group 1) yield a weighted mean $^{207}Pb/^{206}Pb$ age of 2675 ± 30 Ma (MSWD = 2.1). Seven analyses of cores (Group X) yield $^{207}Pb/^{206}Pb$ dates of c. 3368–2762 Ma, The age of 2675 ± 30 Ma indicated by Group 1 is interpreted as the age of magmatic crystallization, with the analyses from Groups X interpreted as the ages of inherited material. The crystallisation age of 2675 ± 30 Ma is in agreement with the SHRIMP U–Pb age previously established by the GSWA (2656 ± 5 Ma; Nelson, 1999a).

4.3.2.4 GSWA 80484

GSWA 80484 is a metagranite. Zircon grains are subhedral to euhedral, colourless to pale brown, and are typically 50–150 µm in length, some are up to 300 µm. CL images display oscillatory zoning, which in places is contorted. Inclusions are common. Forty-eight analyses were obtained from 48 grains. Forty-one analyses (Group D) are >5% discordant and are not considered further. Four analyses of cores (Group 1) yield a weighted mean $^{207}Pb/^{206}Pb$ age of 2643 ± 43 Ma (MSWD = 2.5), and is interpreted as the best estimation of the age of magmatic crystallization. Two analyses of oscillatory zoned cores (Group X) yield $^{207}Pb/^{206}Pb$ dates of c. 2790 Ma and c. 2702 Ma and are interpreted as the age of an inherited component. One analysis of an oscillatory zoned rim returned $^{207}Pb/^{206}Pb$ date of 1674 ± 38 Ma. The hafnium and oxygen isotope data associated with the c. 1674 Ma grain indicates it is a contaminant, incorporated into the sample from adjacent sample (GSWA 195819) during the mounting process.

4.3.3 Marymia Inlier

The dataset from the Marymia Inlier consists of five samples, and the analysed zircon cover a period of 820 Myr, with ages between c. 3406 and c. 2620 Ma. Granites were generated during magmatic episodes at c. 3300 Ma and c. 2700 Ma.

4.3.3.1 JCO15 (NV8)

JCO15 is a granitic rock. The zircon grains are light brown to brown, 80–220 µm in length and subhedral, subrounded elongate to stubby in shape. CL images display homogenous to oscillatory zoning, which in places is contorted. Older cores are present within some grains, and homogeneous overgrowths mantle many crystals. Fifty analyses were obtained from 47 grains. Thirty-five analyses (Group D) are >5% discordant and are not considered further. Fourteen analyses of cores and one rim (Group 1) yield a ^{207}Pb/^{206}Pb age of 3332 ± 8 Ma (MSWD = 0.72), interpreted as the timing of magmatic crystallization of the granite. One analysis (Group P) yields a younger ^{207}Pb/^{206}Pb date of c. 3276 Ma and is interpreted to have lost radiogenic Pb.

4.3.3.2 GSWA 216141

GSWA 216141 is a granitic rock. Zircon grains are subrounded, subhedral, elongate to stubby in shape, brown to dark brown in colour, and are typically 80–240 µm in length. CL images reveal poorly luminescent grains which show a range of textures including oscillatory zoning and homogenous domains. Grains are commonly metamict. Forty-five analyses were obtained from 44 grains. Thirty-nine analyses (Group D) are >5% discordant and are not considered further. Four analyses (Group 1) yield a ^{207}Pb/^{206}Pb age of 3336 ± 16 Ma (MSWD = 1.10), interpreted as the timing of magmatic crystallization of the granite. Two analyses of oscillatory zoned cores (Group X) yield ^{207}Pb/^{206}Pb dates of c. 3406 Ma and c. 3400 Ma and are interpreted as ages of an inherited material incorporated into the granite.

4.3.3.3 GSWA 148344

GSWA 148344 is a metagranitic rock. Zircon grains are light brown to brown, 50–100 µm in length and subhedral, subrounded elongate to stubby in shape. CL images reveal poorly luminescent grains which show a range of textures including oscillatory zoning and homogenous domains. Rounded cores are present within some grains, and thin homogeneous overgrowths mantle many crystals. Forty-six analyses were obtained from 45 grains. Forty-one analyses (Group D) are >5% discordant and are not considered further. Five analyses zircon cores (Group 1) yield a ^{207}Pb/^{206}Pb age of 2698 ± 11 Ma (MSWD = 1.02), interpreted as the timing of magmatic crystallization. One analysis (Group P) yields a younger ^{207}Pb/^{206}Pb date of c. 2618 Ma and is interpreted to have lost radiogenic Pb.

4.3.3.34 GSWA 206935

GSWA 206935 is a granitic gneiss. The zircon grains extracted from this sample are subhedral, subrounded and elongate in shape, 100–180 µm in length, and light brown to brown in colour. CL images display cores with oscillatory zoning which are overgrown by high-CL response, homogeneous overgrowths which are typically <5 µm thick. Forty-eight analyses were obtained from 48 grains. Forty-four analyses (Group D) are >5% discordant and are not considered further. Five analyses of zircon cores (Group 1) yield a ^{207}Pb/^{206}Pb age of 2699 ± 29 Ma (MSWD = 2), interpreted as the age of magmatic crystallization of the granitic protolith.

4.3.3.3 GSWA 120601

GSWA 120601 is a leucocratic rock. The zircon grains extracted from this sample are colourless to brown, subrounded and elongate to equant in shape, and 80–200 µm in length. CL images display CL-dark homogenous grains, some grains display oscillatory zoning that is truncated at grain edges, consistent with features with abrasion during sedimentary transport. Forty analyses were obtained from 40 grains. Two analyses are >5% (Group D) and are not considered further. The remaining 38 analyses yield ^{207}Pb/^{206}Pb age of c. 2936–2609 Ma. The youngest 16 analyses (Group Y) yield a ^{207}Pb/^{206}Pb age of 2641 ± 12 (MSWD = 1.7). The remaining 22 analyses (Group S) yield ^{207}Pb/^{206}Pb dates of c. 2936–2675 Ma. The age of 2641 ± 12 indicated by Group Y is interpreted as the maximum age of deposition. The data for combined Groups Y and S indicate significant age components at c. 2929 Ma, 2835 Ma, 2720 Ma, and 2680 Ma and based on approximately 2, 3, 15 and 8 analyses, respectively. These dates are interpreted as the ages of zircon-crystallising rocks in the detrital source region(s), or the ages of detrital components within sediments which have been reworked.

4.3.4 Goodin Inlier

The dataset from the Goodin Inlier consists of five samples, and the analysed zircon cover a period of 315 Myr, with individual ^{207}Pb/^{206}Pb ages between c. 2905 and c. 2592 Ma. Granites were generated during one major magmatic episode at c. 2630 Ma.

4.3.4.1 GSWA 139286

GSWA 139286 is a granitic rock. Zircon grains are colourless to dark brown, 80–100 µm in length and subhedral, subrounded elongate to stubby in shape. CL images display extensive alteration, with only a few grains retaining original texture. Grains have homogenous to oscillatory zoned interiors. Extensive alteration has affected both rims and cores of grains. Fifteen analyses were obtained from 15 grains. Nine analyses are >10% discordant and are not considered further. Six analyses of cores yield $^{207}Pb/^{206}Pb$ dates ranging between c. 2670 and c. 2109 Ma. Four analyses of discordant cores yield a yield a $^{207}Pb/^{206}Pb$ age of 2658 ± 17 Ma (MSWD = 0.55), this age is interpreted as the maximum age of magmatic crystallization of the granite. The remaining two analyses of homogenous grains yield younger $^{207}Pb/^{206}Pb$ dates of c. 2450 Ma–2109 Ma and are interpreted to have lost radiogenic Pb.

4.3.4.2 GSWA 139282

GSWA 139282 is a granitic rock. Zircon grains are colourless to pinky-brown, 80–200 µm in length and subhedral, subrounded elongate to stubby in shape. CL images display oscillatory zoning, which in some places is contorted. Grains are commonly metamict. Forty-five analyses were obtained from 45 grains Thirty-five analyses (Group D) are >5% discordant and are not considered further. Six analyses are >5% discordant, but appear to have only been affected by recent radiogenic-Pb loss. Eight concordant oscillatory zoned cores yield a $^{207}Pb/^{206}Pb$ age of 2642 ± 12 Ma (MSWD = 0.64), interpreted as the timing of magmatic crystallization of the granite. Two analyses of cores (Group P) yields a younger $^{207}Pb/^{206}Pb$ date of c. 2590 Ma and c. 2588 Ma and are interpreted to have lost radiogenic Pb.

4.3.4.3 GSWA 120644

GSWA 120644 is a granitic rock. Zircon grains are brown to dark brown, 100–300 µm in length and subhedral, elongate to stubby in shape. CL images display homogenous to weakly oscillatory zoned cores. Rounded cores are present within some grains, and oscillatory zoned overgrowths mantle many crystals. Inclusions are common. Forty-eight analyses were obtained from 48 grains. Thirty-four analyses (Group D) are >5% discordant and are not considered further. Eleven analyses of cores (Group 1) yield a $^{207}Pb/^{206}Pb$ age of 2650 ± 10 Ma (MSWD = 0.93), interpreted as the timing of magmatic crystallization of the granite. One analysis (Group X) yields a $^{207}Pb/^{206}Pb$ date of c. 2905 Ma, and is interpreted as the age of an inherited component. Two analyses (Group P) yield $^{207}Pb/^{206}Pb$ dates between c. 2603 Ma and c. 2588 Ma and are interpreted to have undergone ancient radiogenic-Pb loss.

4.3.4.4 GSWA 120678

GSWA 120678 is a granitic rock. Zircon grains are brown to dark brown, 80–100 µm in length and subhedral, subrounded elongate to stubby in shape. CL images display cores with oscillatory zoning which are overgrown by homogenous high-CL-response rims. The bright overgrowths are rimmed by homogenous low-CL-response rims. Both the bright and dark rims are typically

<10 µm thick. Forty-eight analyses were obtained from 47 grains. All analyses are between 21 and 90 % discordant, and yield a strong correlation between $^{206}Pb/^{204}Pb$ ratios and discordance, indicating a high common lead component.

4.3.4.5 GSWA 120696

GSWA 120696 is a granitic rock. The zircon grains are brown to dark brown, 100–300 µm in length and subhedral, elongate to stubby in shape. CL images display homogenous cores and oscillatory zoned overgrowths mantle many crystals. Inclusions are common. Forty-eight analyses were obtained from 48 grains. Twenty-eight analyses (Group D) are >5% discordant or indicate a high common Pb component, and are not considered further. Eighteen analyses of cores (Group 1) yield a $^{207}Pb/^{206}Pb$ age of 2623 ± 8 Ma (MSWD = 0.96), interpreted as the timing of magmatic crystallization of the granite. One analysis of oscillatory zoned core (Group X) yields a $^{207}Pb/^{206}Pb$ date of 2720 Ma and is interpreted as the age of an inherited component. One analysis of a core (Group P) yields a younger $^{207}Pb/^{206}Pb$ date of c. 2502 Ma and is interpreted to have lost radiogenic Pb.

4.3.5 Kalgoorlie Terrane, Eastern Goldfields Superterrane

The dataset from the Kalgoorlie Terrane consists of two samples, with individual $^{207}Pb/^{206}Pb$ ages ranging between c. 2778 and c. 2513 Ma.

4.3.5.1 GSWA 152855

GSWA 152855 is a granitic rock. Zircon grains are yellow to dark brown in colour, 100–200 µm in length and subhedral, subrounded and elongate to stubby in shape. CL images reveal ubiquitous oscillatory zoning. Many grains are metamict, inclusions are common. Forty-seven analyses were obtained from 46 zircon. Forty-one analyses (Group D) are >5% discordant and are not considered further. Four analyses of cores yield a $^{207}Pb/^{206}Pb$ age of 2668 ± 31 Ma (MSWD = 1.3), interpreted as the timing of magmatic crystallization of the granite. Two analyses of cores (Group X) yield $^{207}Pb/^{206}Pb$ dates of c. 2778 Ma and c. 2726 Ma and are interpreted as the ages of an inherited component.

4.3.5.2 GSWA 152879

GSWA 152879 is a granitic rock. Zircon grains are colourless to dark brown in colour, 50–200 µm in length and subhedral, subrounded and elongate to equant in shape. CL images reveal ubiquitous oscillatory zoning. Many grains are metamict. Thirty-four analyses were obtained from 34 zircon. Thirty-one analyses (Group D) are >5% discordant or indicate a high common Pb component, and are not considered further. Three analyses of cores (Group X) yield $^{207}Pb/^{206}Pb$ dates between

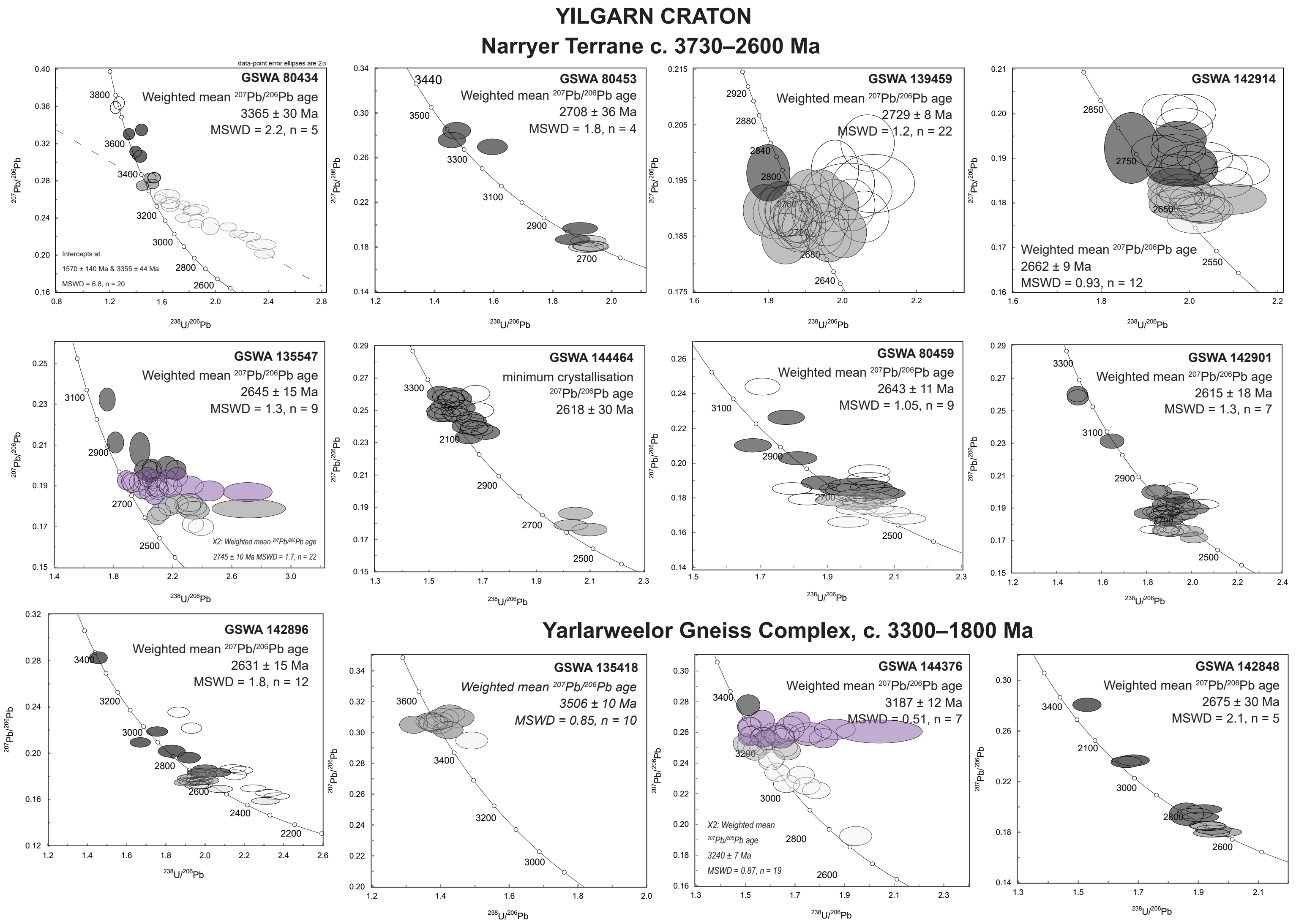

Figure 4.3 continues with caption overleaf

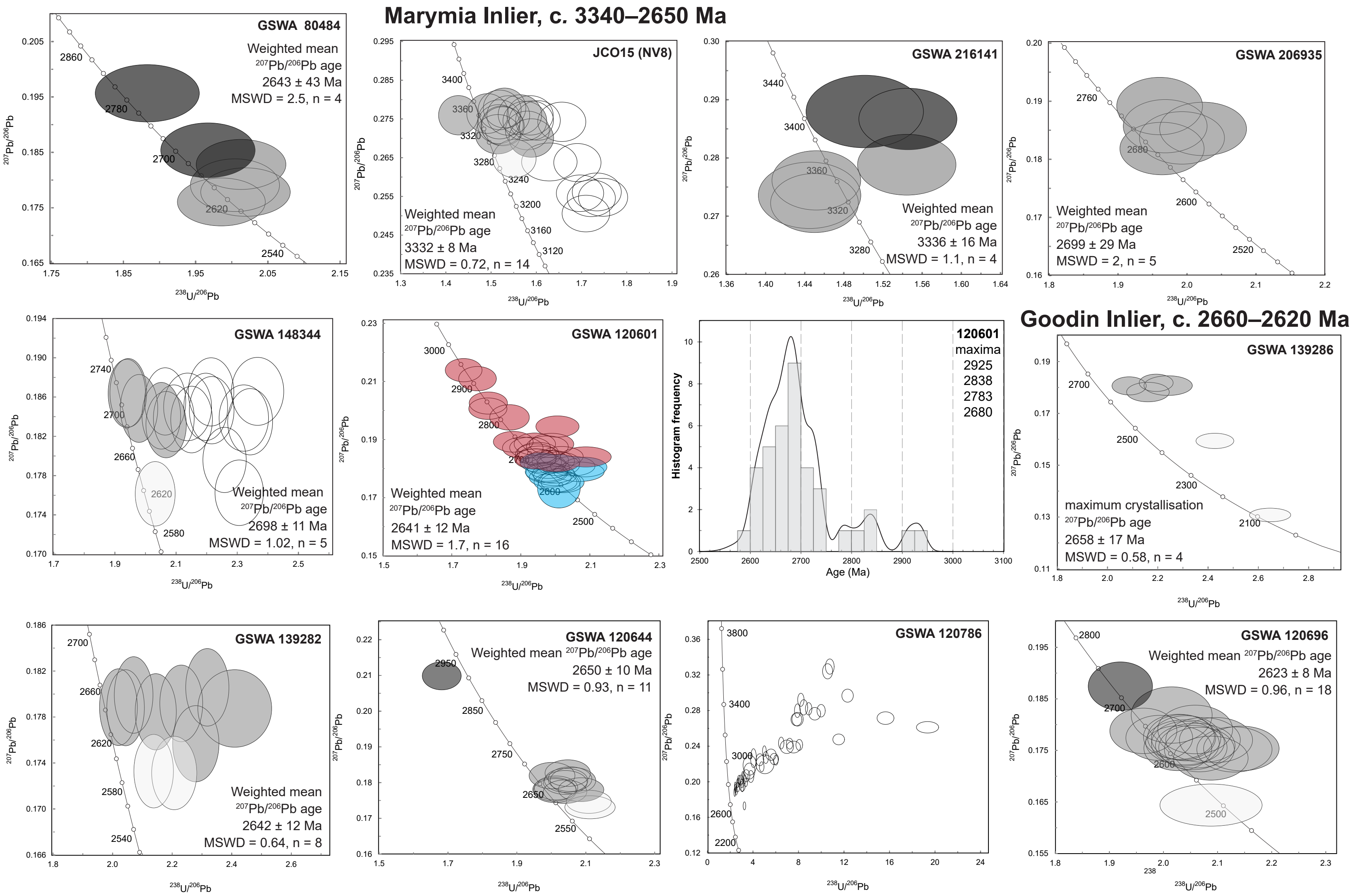

Figure 4.3 continues with caption overleaf

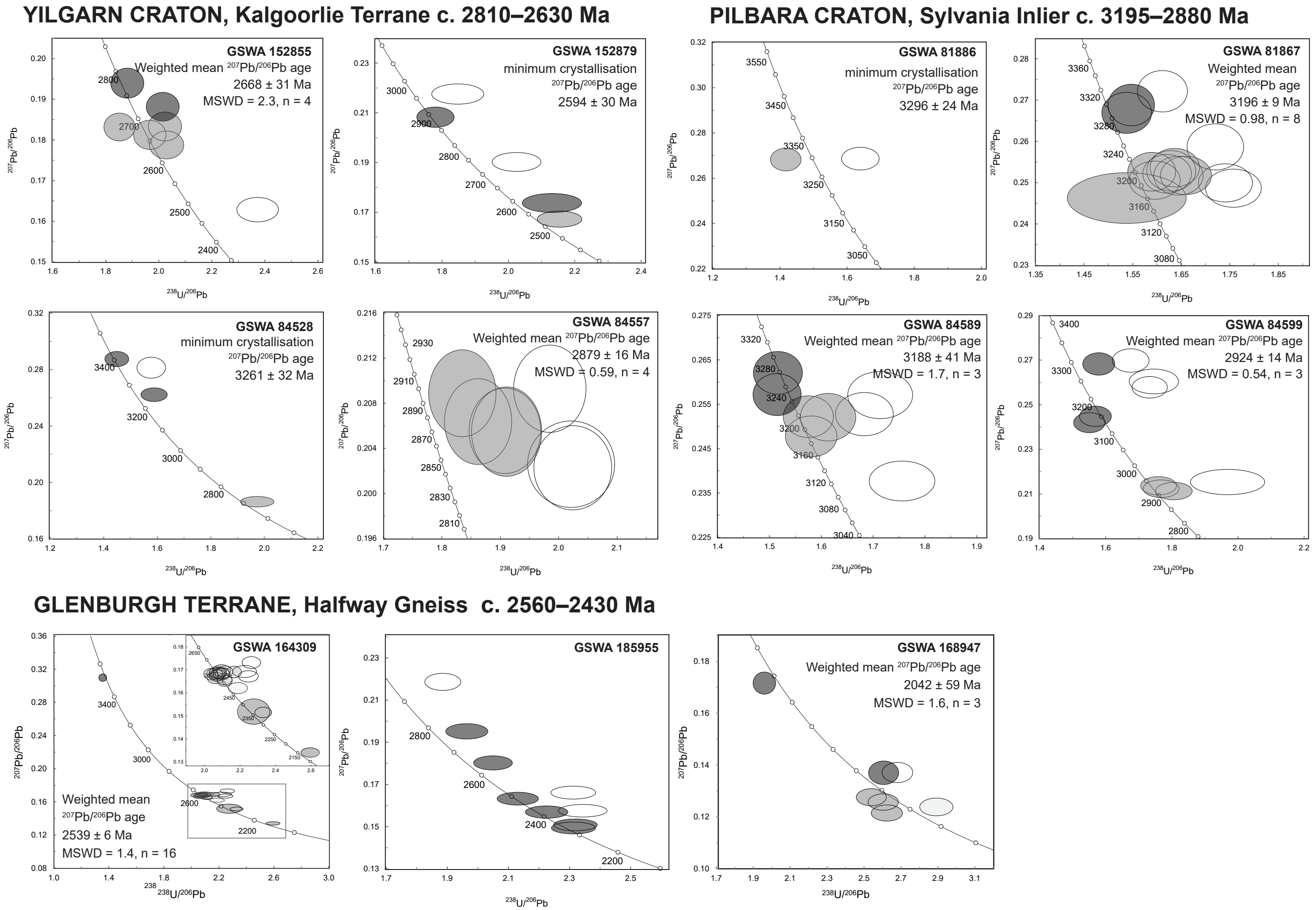

Figure 4.3 Concordia diagram showing the subset of results of zircon with <10% discordance. Grey ellipses indicate analyses used to calculate Group 1 (crystallisation age). Black ellipses indicate inherited zircon (Group X). Purple ellipses indicate analyses used to calculate Group 2 (inherited zircon group). Light grey ellipses indicate radiogenic Pb-loss (Group P). Hollow ellipses indicate outside discordance threshold (Group D). Blue ellipses indicate Group Y (youngest detrital zircon). Red ellipses indicate Group S (older detrital zircon).

c. 2892 and c. 2531 Ma. The date of c. 2531 Ma is younger than the magmatic ages expected for the Kalgoorlie Terrane (c. 2760–2600 Ma; Mole et al., 2012), and is interpreted to have undergone ancient radiogenic-Pb loss. The date of the second youngest concordant analyses at 2594 ± 30 Ma is therefore interpreted as the best estimation of the minimum age of crystallisation of the granite.

4.3.6 Sylvania Inlier

The dataset from the Sylvania Inlier consists of six samples, and the analysed zircon cover a period of 695 Myr, with individual $^{207}Pb/^{206}Pb$ ages between c. 3405 and c. 2710 Ma.

4.3.6.1 GSWA 81866

GSWA 81866 is a granitic rock. Zircon grains are brown to dark brown, 80–250 µm in length and subhedral, subrounded elongate to stubby in shape. CL images display extensively metamict grains, with only a few grains retained original texture. Some grains show oscillatory zoning or homogenous domains. Forty-nine analyses were obtained from 48 grains. Forty-eight analyses (Group D) are >5% discordant or indicate a high common Pb component, and are not considered further. One analysis of a homogenous grain yields a $^{207}Pb/^{206}Pb$ date of c. 3296 Ma, interpreted as the best estimation of the maximum age of crystallisation of the granite.

4.3.6.2 GSWA 81867

GSWA 81867 is a monzogranite. Zircon grains are colourless to dark brown, 100–200 µm in length and subhedral, subrounded elongate to stubby in shape. CL images display CL-intermediate homogenous to oscillatory zoned interiors, mantled by CL-dark rims. Forty-eight analyses were obtained from 47 grains. Thirty-eight analyses (Group D) are >5% discordant and are not considered further. Six analyses of oscillatory zoned cores (Group 1) yield a $^{207}Pb/^{206}Pb$ age of 3196 ± 9 Ma (MSWD = 0.98), interpreted as the timing of magmatic crystallization of the granite. Two analyses of cores (Group X) yield $^{207}Pb/^{206}Pb$ dates of c. 3299 and c. 3288 Ma and are interpreted as the ages of an inherited component.

4.3.6.3 GSWA 84528

GSWA 84528 is a granitic rock. Zircon grains are colourless to dark brown, 80–150 µm in length and subhedral, subrounded elongate to equant in shape. CL images display oscillatory zoning which in some places is contorted. CL-dark rims mantle some grains. Twenty-four analyses were obtained from 23 zircon grains. Twenty-one analyses (Group D) are >5% discordant and are not considered further. Three analyses yield $^{207}Pb/^{206}Pb$ dates ranging from c. 3405 to c. 2710 Ma. The date of c. 2710 Ma is younger than the magmatic ages expected for the Pilbara Craton (c.3800–2830 Ma, Hickman et al., 2008), and is interpreted to have undergone ancient radiogenic-Pb loss. The date of the second youngest concordant analyses at 3261 ± 32 Ma is therefore interpreted as the best estimation of the minimum age of crystallisation of the granite.

4.3.6.4 GSWA 84577

GSWA 84577 is a granitic rock. Zircon grains are light- to dark-brown in colour, 100–280 µm in length and euhedral to subhedral and stubby in shape. CL images display ubiquitous oscillatory zoning, which in some places is contorted. Metamict grains are common. Forty-five analyses were obtained from 45 grains. Forty-one analyses (Group D) are >5% discordant and are not considered further. Four analyses (Group 1) yield $^{207}Pb/^{206}Pb$ age of 2879 ± 16 Ma (MSWD = 0.59), interpreted as the timing of magmatic crystallization of the granite.

4.3.6.5 GSWA 84589

GSWA 84589 is a granodiorite. Zircon grains are colourless to light brown in colour, 80–250 µm in size and subhedral, subrounded and stubby in shape. CL images display oscillatory zoning, which in some places is contorted. Rounded cores are present within some grains, and thin homogeneous overgrowths mantle many crystals. Twenty analyses were obtained from 20 grains. Fifteen analyses are >5% discordant (Group D) and are not considered further. Three analyses of cores (Group 1) yield a $^{207}Pb/^{206}Pb$ age of 3188 ± 41 Ma (MSWD = 1.7), interpreted as the timing of magmatic crystallization of the granite. Two analyses of cores (Group X) yield $^{207}Pb/^{206}Pb$ dates of c. 3259 Ma and c. 3230 Ma and are interpreted as the ages of an inherited component.

4.3.6.6 GSWA 84599

GSWA 84599 is a monzogranite. Zircon grains are light yellow to dark brown in colour, 50–200 µm in length and subhedral, subrounded and elongate to stubby in shape. CL images reveal homogenous cores and oscillatory zoning, some grains are metamict. Inclusions are common. Forty-four analyses were obtained from 44 grains. Thirty-nine analyses (Group D) are >5% discordant and are not considered further. Three analyses of cores (Group 1) yield a $^{207}Pb/^{206}Pb$ age of 2924 ± 19 Ma (MSWD = 0.31), interpreted as the timing of magmatic crystallization of the granite. Three analyses of cores (Group X) yield $^{207}Pb/^{206}Pb$ dates between c. 3296 and c. 3133 Ma and are interpreted as the ages of an inherited component.

4.3.7 Halfway Gneiss, Glenburgh Terrane

The dataset from the Glenburgh Terrane consists of three samples, and the analysed zircon cover a period of 1209 Myr, with individual $^{207}Pb/^{206}Pb$ ages between c. 3766 and c. 2557 Ma. The Halfway Gneiss consists of several interlayered rock types heterogeneously deformed and metamorphosed to at least amphibolite facies (Johnson et al., 2011b).

4.3.7.1 GSWA 164309

GSWA 164309 is a granodiorite gneiss. Zircon grains were hand-picked from heavy mineral concentrates provided by the GSWA. Zircon grains range between 100 and 450 µm in length. They are typically pinkish, yellowish to dark brown in colour, and equant to stubby in shape. CL images display low luminescence cores that are generally structureless, some show weak oscillatory zoning and are commonly surrounded by strongly zoned rims. Some cores appear metamict. Mineral inclusions are common. Thirty-three analyses were obtained from 30 zircon grains. Ten analyses (Group D) are >5% discordant and are not considered further. Sixteen analyses of cores (Group 1) yield a weighted mean ^{207}Pb/^{206}Pb date of 2539 ± 6 Ma (MSWD = 1.4), interpreted as the age of magmatic crystallization. Five analyses zircon cores and one rim (Group X) yield ^{207}Pb/^{206}Pb dates between c. 3400 and 2752 Ma, interpreted to reflect the ages of inherited material. Three analyses (Group 2) indicate ^{207}Pb/^{206}Pb dates of 2363–2153 Ma. Group X consists of one analysis with a ^{207}Pb/^{206}Pb date of c. 3521. The remaining analysis from a core has a ^{207}Pb/^{206}Pb date of c. 2478 Ma (Group P).

The date of 2539 ± 6 Ma for Group 1 is interpreted as the age of crystallisation. The three analyses with younger ages of 2363–2153 Ma analysis may have been derived from the pegmatite intrusions as reported by Nelson (2000b). The older date of c. 3521 in Group X is interpreted as the age of an inherited component. The c. 2478 Ma analysis in Group P is interpreted to reflect ancient loss of radiogenic Pb. The crystallisation age of 2539 ± 8 Ma is in agreement with the previously established SHRIMP U–Pb age (2548 ± 8 Ma; Johnson et al., 2011b).

4.3.7.2 GSWA 185955

Sample GSWA 185955 is a granitic gneiss. Zircon grains were hand-picked from heavy mineral concentrates provided by the GSWA. Zircon grains are subhedral, subrounded, equant to stubby in shape, generally light brown to dark brown in colour and range between 80 to 200 µm in length. CL images reveal oscillatory zoning and homogenous domains, mantled by CL-dark rims of varying thicknesses. Some grains are metamict. Forty-four analyses were obtained from 41 grains. Thirty-eight analyses (Group D) are >5% discordant and are not considered further. Six analyses (Group X) of oscillatory zoned cores yield ^{207}Pb/^{206}Pb ages that range between c. 2788 and 2341 Ma. The two youngest analyses yield a weighted mean ^{207}Pb/^{206}Pb date of 2349 ± 24 Ma (MSWD = 0.47).

A geochronological dataset for this sample has previously been described by Wingate et al. (2010). Seven analyses yielded a weighted mean ^{207}Pb*/^{206}Pb* date of 2527 ± 9 Ma (MSWD = 1.7), interpreted as the crystallisation age of the protolith to the gneiss. Four analyses indicate

^{207}Pb*/^{206}Pb* dates between c. 2829 and c. 2560 Ma, interpreted as the ages of inherited zircon grains, and three analyses yield a weighted mean ^{207}Pb*/^{206}Pb* age of 2342 ± 28 Ma (MSWD = 1.9), interpreted as the age of crystallisation of thin leucocratic veins within the gneiss (Wingate et al., 2010g).

4.3.7.3 GSWA 168947

GSWA 168947 is a gneissic rock. Zircon grains were hand-picked from heavy mineral concentrates provided by the GSWA. Zircon grains are subhedral, subrounded, elongate to stubby in shape, generally light brown to dark brown in colour and range between 80 to 200 µm in length. CL imaging reveals CL-intermediate cores with faint oscillatory zoning, sometimes convoluted, mantled by CL-darker rims of varying thicknesses and commonly overprinted by recrystallization zones. Forty-seven analyses were obtained from 46 zircon grains. Forty-one analysis (Group D) are >5% discordant or indicate a high common Pb component, and are not considered further. Three analyses of cores (Group 1) yield a weighted mean ^{207}Pb/^{206}Pb date of 2042 ± 59 Ma (MSWD = 1.6), interpreted as the age of igneous crystallization of a granitic precursor phase to the gneiss. Two analyses of zircon cores (Group X) yield ^{207}Pb/^{206}Pb dates of c. 2574 Ma and c. 2188 Ma, interpreted as inherited material incorporated into the granite precursor. One analyses (Group P) yield ^{207}Pb/^{206}Pb dates of c. 1978 Ma, and is interpreted to have undergone ancient radiogenic-Pb loss. The crystallisation age of the granite protolith 2042 ± 59 Ma is in broad agreement with the SHRIMP U–Pb age previously established by the GSWA (2006 ± 6 Ma; Nelson, 2001c).

4.4 ZIRCON TRACE ELEMENT COMPOSITION

Grimes et al. (2015) demonstrated that U/Yb ratios in zircon reflect the U/Yb ratio of the parental melt composition. Thus, plotting Hf versus U/Yb, and Y versus U/Yb highlights relative crustal contributions in the parental magmas. Zircon grains from the Narryer Terrane, YGC, Marymia, Goodin and Sylvania Inlier samples have trace-element compositions typical of continental zircon, with both magmatic and inherited populations plotting within continental arc-type zircon fields. The Marymia and Sylvania Inlier zircon show some compositions that overlap the field of oceanic crust zircon (OI-type, Fig. 4.4). Chondrite-normalised REE element patterns of magmatic zircons from the Archaean granitoids are characterised by positive Ce and moderate negative Eu anomalies and a positive heavy REE (HREE) slope, consistent with growth of zircon in a magmatic environment (Rubatto and Hermann, 2007; Hoskin and Black, 2000; Hoskin and Ireland, 2000). Minor variation in the overall REE abundances and in the degree of Eu/Eu* occurs between and within samples; however no systematic change was recognised.

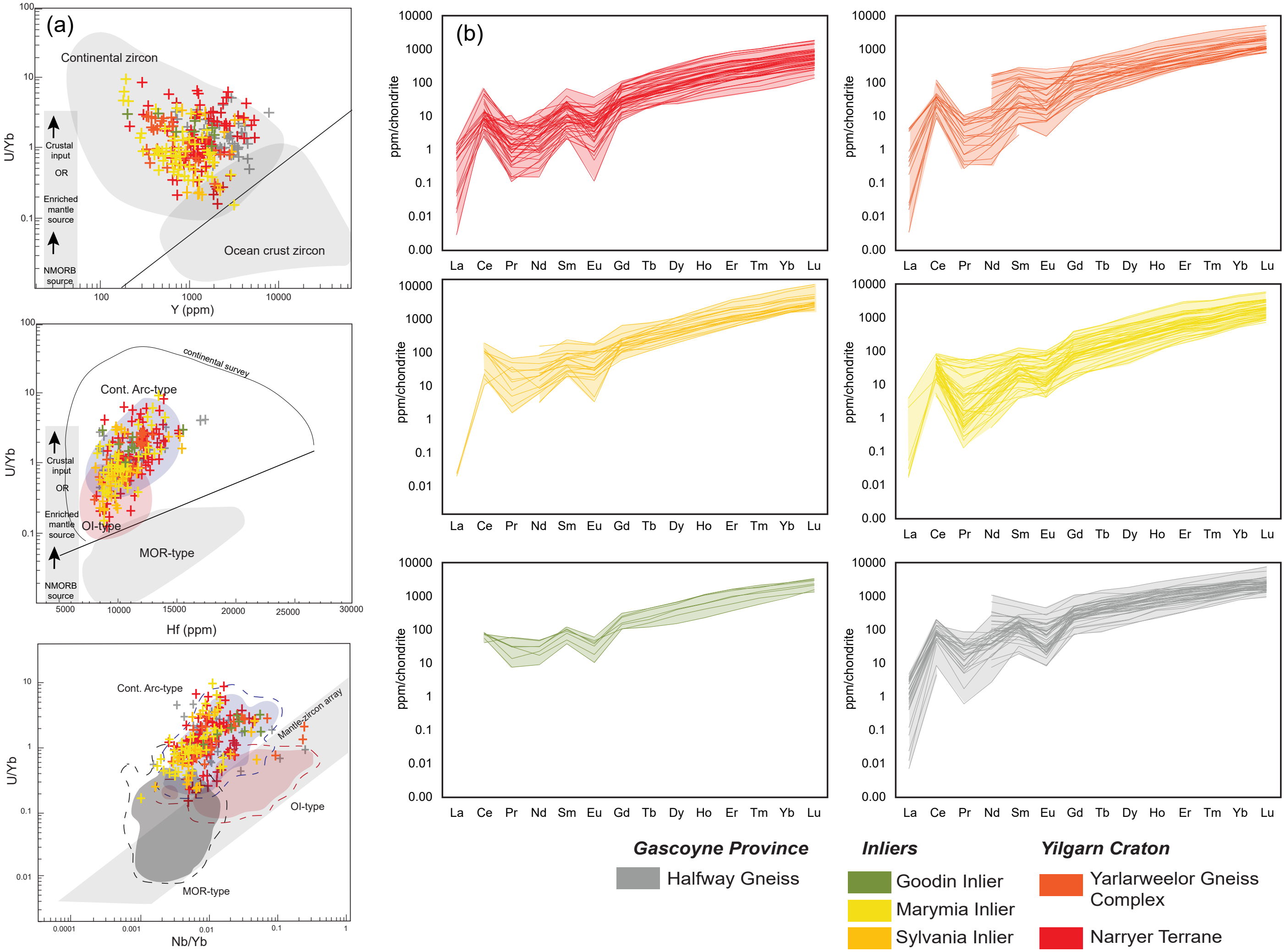

Figure 4.4 (a) Discrimination diagrams for trace elements, after Grimes et al. (2007, 2015), (b) chondrite-normalised trace element plots

Incorporation of rare earth elements (REE) into magmatic zircon is controlled by the pressure, temperature, parental melt composition and the other minerals present in the melt residue (Hanchar and van Westrenen, 2007; Rubatto and Hermann, 2007). Zircon that crystallised in garnet-absent rocks is typically enriched in heavy rare earth elements (HREE) compared to zircon that grew in the presence of garnet (Rubatto, 2002; Hoskin and Schaltegger, 2003). Identification of a 'garnet signature' (i.e. depletion in HREE) in zircon is commonly assumed to indicate melting at a pressure greater than 0.7–1.0 GPa which equates to greater than approximately 20–30 km of crust (Johnson et al., 2017b; Nebel et al., 2018). However, identifying concurrent growth of garnet and zircon in source regions based on REE composition alone is not always implicit, and depletion of HREE in zircon does not necessarily correlate to formation in the lower crust. Partial melting of a garnet-bearing source (i.e. metamafic/ultramafic rocks with residual garnet) can produce melts with high La/Yb ratios without a requirement that they resided in the deep crust (Hanchar and van Westrenen, 2007; Nebel et al., 2018). Magmatic zircon trace element signatures indicate no evidence of co-crystallisation with garnet (i.e. flat HREE pattern with Lu/Gd <3 paired with no negative Eu anomaly, Eu/Eu* >0.75; Rubatto and Hermann, 2007). The zircon record a range of Yb_N/Gd_N of 3–59 and Eu/Eu* of 0.01–1.16, indicating formation in lower pressures than eclogitic minerals (<1.2 GPa, <45 km depth; Rubatto and Hermann, 2007).

Zircon Ti thermometry enables the crystallisation temperatures of magmas to be estimated, and has been used to predict whether magmas should contain inherited zircon (Watson and Harrison, 1983; Miller at al., 2003). Magmas with temperatures >800°C (Watson, 1996) are sufficient to dissolve any zircon <90 µm radius within a few thousand years. As there are uncertainties associated with the interpretation of zircon thermometry (e.g. Nutman 2006; Fu et al., 2008; Kemp et al., 2005, Harrison et al., 2007) they will be used to primarily to compare the crystallisation temperatures between samples in this study. Miller et al (2003) identified two distinct classes of granitoids, low-T inheritance-rich granitoids with T_{Zr} <800°C and high-T inheritance-poor granitoids with T_{Zr} >800°C. They suggested generation of the low-T granites occurs in tectonic settings that do not reach high temperatures, such as regions of crustal thickening. With the exception of the Goodin Inlier, all samples record zircon Ti temperatures with averages between 698 and 832°C. These temperatures are comparable with the low-T inheritance-rich granitoids with T_{Zr} <800°C of Miller et al (2003) that are interpreted as forming in regions of crustal thickening. Goodin Inlier samples record zircon saturation temperatures with slightly higher averages between 787 and 850°C comparable with high-T inheritance-poor granitoids (Miller et al., 2003). These temperatures are comparable with the high-T inheritance-rich granitoids with T_{Zr} >800°C of Miller et al (2003) that are interpreted as typical of felsic magma generation processes in the crust, i.e. dehydration melting,

Table 4.2 Summary of zircon hafnium and oxygen isotope data

Sample	Unit[1]	Pb-Pb age (Ma)	εHf[2]	εHf range	TDMC[3]	$\delta^{18}O$[4] (‰)	$\delta^{18}O$ range (‰)
80434	NT	3365 ± 30	-1.4 ± 3.4 (4)	-4.7 to -0.6	3964–3712	6.49 ± 1.24 (7)	5.90–7.92
80453	NT	2708 ± 36	-10.4 ± 2.7 (7)	-12.3 to -7.9	3959–3861	6.4 ± 0.24 (2)	6.28–6.43
139459	NT	2729 ± 8	-6.9 ± 4.5 (16)	-10.9 to -2.6	3903–3378	6.19 ± 0.77 (13)	5.71–7.12
142914	NT	2662 ± 9	-7.5 ± 1.4 (10)	-8.4 to -6.8	3680–3531	5.93 ± 1.13 (10)	5.09–6.23
133547	NT	2645 ± 15	-9 ± 0.1 (2)	-9 to -8.9	3665–3328	6.81 (1)	5.42–7.77
80459	NT	(2618 ± 37)	-7.3 ± 1.6 (9)	-8.1 to -5.2	-	6.90 ± 0.44 (7)	6.71–7.36
144464	NT	2643 ± 11	-	-7.6 to -4.5	4023–3873	6.39 (1)	5.96–6.74
142896	NT	2615 ± 18	10.4 ± 3 (8)	-13.3 to -8.4	3964–3653	6.23 ± 0.44 (3)	5.93–6.43
142901	NT	2631 ± 15	-	-10.2 to +0.5	4106–3147	-	5.86–7.59
135418	YGC	3506 ± 10	-	-	-	6.05 ± 1.48 (8)	5.21–7.81
144376	YGC	3187 ± 12	-6.8 ± 3.4 (7)	-10.7 to -5.3	3966–3940	6.52 ± 1.55 (7)	6.2–8.13
142848	YGC	2675 ± 30	-6.7 ± 4.3 (4)	-8.8 to -2.9	3716–3361	6.19 ± 1.06 (5)	5.16–6.45
80484	YGC	2643 ± 43	-7.2 ± 2.8 (4)	-9.5 to -6.6	3587–3572	5.64 ± 0.94 (3)	5.23–6.3
Jc15	MI	3332 ± 8	-4.7 ± 2.6 (13)	-7.1 to -2.9	4113–3830	6.41 ± 0.91 (10)	5.65–7.20
216141	MI	3336 ± 16	-2.2 ± 2.6 (4)	-5.2 to -2.1	3812	6.28 ± 0.76 (3)	5.93–6.81
148344	MI	2698 ± 11	+1.8 ± 3.8 (10)	-2.7 to +3.8	3076–3042	6.35 ± 0.55 (9)	6.0–6.94
206935	MI	2699 ± 29	+3.4 ± 2.6 (5)	+1.1 to +4.4	3087–2925	5.94 ± 0.93 (4)	5.6–6.73
120601	MI	2641 ± 12	-0.3 ± 3.1 (12)	-3.9 to +1.5	3216–3137	-	4.75–7.9
139286	GI	[2658 ±17]	-6.4 ± 2.4 (3)	-7.4 to -4.7	-	-	6.4–7.02
139282	GI	2642 ± 12	-6.9 ± 5.5 (6)	-10 to -1.1	3653–3516	5.73 ± 1.55 (5)	4.73–6.89
120644	GI	2650 ± 10	-6.5 ± 3.4 (13)	-8 to -2	3638–3276	5.34 ± 0.83 (13)	4.52–5.76
120678	GI	-	-	-	-	-	5.99–7.12
120696	GI	2623 ± 8	-6.3 ± 3.4 (14)	-8.4 to -2.9	3632–3378	6.15 ± 1.01 (11)	5.42–6.94
152855	EGST	2668 ± 31	+2.7 ± 1.2 (2)	+2.1 to +3.3	2955	5.04 ± 2.92 (2)	3.58–6.93
152879	EGST	(2594 ± 30)	-	-1.9 to +0.0	3107–2809	6.93 (1)	5.84–6.93
81866	SI	[3296 ± 24]	-	+3.7	3401	-	5.04–6.76
81867	SI	3196 ± 9	+1.2 ± 3.2 (6)	-2.3 to +2.4	3716–3414	5.50 ± 1.55 (10)	4.17–6.83
84528	SI	(3261 ± 32)	-	-9.9 to -0.3	-	-	6.31–6.79
84557	SI	2879 ± 16	-0.8 ± 2.5 (5)	-1.3 to +1.3	3393–3269	4.86 ± 2.54 (6)	2.72–6.06
84589	SI	3188 ± 41	-6.9 ± 4.3 (4)	-9.4 to -3.6	-	-	-
84599	SI	2924 ± 14	-4.3± 2.4 (3)	-4.4 to -3.9	-	7.14 ± 0.56 (2)	6.86–7.42
185955	HG	2788-2341	-	-3.9 to +1.6	-	-	5.11–6.43
164309	HG	2539 ± 6	-1.3 ± 5.3 (13)	-4.2 to +4.3	3312–2771	6.24 ± 0.82 (12)	5.76–7.12
168947	HG	2042 ± 59	-10.3 ± 3.9 (3)	-13.3 to -8.6	-	6.88 ± 0.19 (3)	7.07

[1] NT= Narryer Terrane, YGC= Yarlarweelor Gneiss Complex, MI= Marymia Inlier, GI= Goodin Inlier, EGST = Eastern Goldfields Superterrane, SI= Slyvania Inlier, HG= Halfway Gneiss

[2] εHf values of magmatic zircon are expressed as median values in, ±2SD. Number of analyses donated in brackets.

[3] TDMC will only be quoted where $\delta^{18}O$ are within mantle (5.3 ± 0.6 ‰, 2σ) values

[4] $\delta^{18}O$ values of magmatic zircon are expressed as averages, ±2SD. Number of analyses donated in brackets

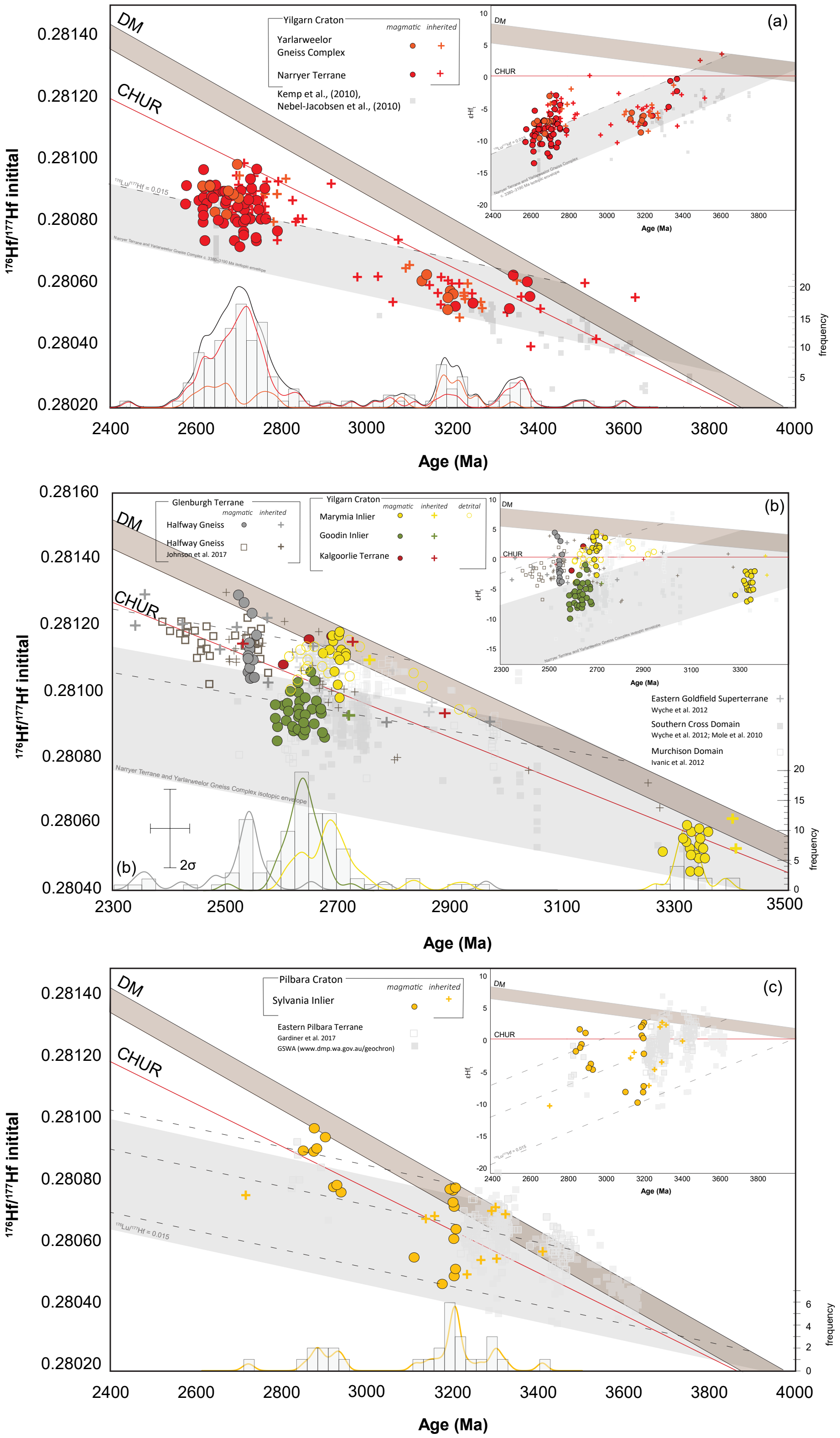

Figure 4.5 Evolution diagram of $^{176}Hf/^{177}Hf$ initial ratios and εHf$_t$ versus age for zircon (n=314) from samples from (a) Narryer Terrane and Yarlarweelor Gneiss Complex, (b) Marymia Inlier, Goodin Inlier and Halfway Gneiss and (c) Sylvania Inlier. The dashed line is a reference evolution line corresponding to a Lu/Hf ratio of 0.015. Inset figures show Hf evolution diagram for zircon grains from the Moorarie Supersuite, deviations of Hf ($^{176}Hf/^{177}Hf$) isotopic composition from the chondrite uniform reservoir (CHUR) standard are expressed in epsilon units, εHf$_t$.

decompression melting or mafic underplating induced melting (Thompson and Connolly, 1995).

4.5 Lu-Hf ISOTOPE DATA

A total of 363 analyses were obtained from 30 samples and include analyses of groups that are interpreted to date crystallisation and inherited zircon. Sixty-five analyses have been rejected due to either poor U–Pb age data (high discordance) or the ablated area consisted of core-rim mixtures or cracks (see Appendix B).

4.5.1 Narryer Terrane

A total of 110 Magmatic and inherited zircon grains were analysed from nine samples. Initial $^{176}Hf/^{177}Hf$ ratios of all analysed zircon grains range between 0.280399 and 0.280978, corresponding to εHf_t values of -13.3 and +3.6. Magmatic grains (n=56) yield a range of initial $^{176}Hf/^{177}Hf$ ratios between 0.280511 and 0.280963 (εHf_t -13.3 and -0.4), with median εHf_t values from each sample ranging between -11.7 ± 4.6 and -2.4 ± 2.9, 2SD. Inherited zircon grains (n=54) with $^{207}Pb/^{206}Pb$ ages ranging between 3619 to 2634 Ma yield a range of εHf_t values between -10.4 and +3.6.

4.5.2 Yarlarweelor Gneiss Complex

A total of 29 zircon grains were analysed from three samples. Initial $^{176}Hf/^{177}Hf$ ratios of all analysed zircon grains range between 0.280484 and 0.280979, corresponding to εHf_t values of -9.5 and -1.2. Magmatic grains (n=15) yield a range of initial $^{176}Hf/^{177}Hf$ ratios between 0.280506 and 0.280979 (εHf_t -9.5 and -2.9). Median values (magmatic) range between -7.2 ± 2.8 and -6.3 ± 4.3 (2SD). Inherited zircon grains (n=14) with $^{207}Pb/^{206}Pb$ ages ranging between 3351 to 2702 Ma yield a range of εHf_t values between -8.4 and -1.2.

4.5.3 Marymia Inlier

Data from the Marymia Inlier consist of 57 analyses of magmatic, inherited and detrital zircon grains from five samples. Initial $^{176}Hf/^{177}Hf$ ratios of all analysed zircon grains range between 0.280447 and 0.281168, corresponding to εHf_t values of -7.1 and +5.7. Magmatic grains (n=31) yield a range of initial $^{176}Hf/^{177}Hf$ ratios between 0.280447 and 0.281181 (εHf_t -7.1 and +4.4). Median values (magmatic) range between -4.7 ± 2.6 and +2.3 ± 2.6 (2SD). Inherited zircon grains (n=3) with $^{207}Pb/^{206}Pb$ ages ranging between 3406 and 2753 Ma yield a range of εHf_t values between -2.7 and +5.7. Detrital zircon (n=22) with $^{207}Pb/^{206}Pb$ ages ranging between 2936 to 2610 Ma yield a range of εHf_t values between -3.9 and +3.4. One analyses with $^{207}Pb/^{206}Pb$ age of c. 3276 Ma, interpreted as having undergone ancient radiogenic-Pb loss, returned εHf_t values of -6.1.

4.5.4 Goodin Inlier

Thirty-seven zircon grains were analysed from four samples. Magmatic grains (n=32) yield a range of initial $^{176}Hf/^{177}Hf$ ratios between 0.280859 and 0.281238 (εHf_t -7.6 and -1.1). Median values for each sample range between -6.5 ± 3.4 and -6.4 ± 1.7 (2SD). One inherited zircon grain with a $^{207}Pb/^{206}Pb$ age of c. 2720 Ma returned a εHf_t value of -4.2. Four analyses with $^{207}Pb/^{206}Pb$ ages between c. 2603 and 2588 Ma, interpreted as having undergone ancient radiogenic-Pb loss, returned εHf_t values between -10 and -5.9.

4.5.5 Kalgoorlie Terrane

A total of six zircon grains were analysed from two samples. Magmatic grains (n=3) yield a range of initial $^{176}Hf/^{177}Hf$ ratios between 0.281074 and 0.281162 (εHf_t -1.9 and +3.3, median εHf_t +2.7 ± 1.2, 2SD). Inherited zircon grains (n=2) with $^{207}Pb/^{206}Pb$ ages of c. 2892 and 2726 Ma returned εHf_t values ranging from 0 to +3.8. One analysis with $^{207}Pb/^{206}Pb$ age of c. 2531 Ma, interpreted as having undergone ancient radiogenic-Pb loss, returned εHf_t values of -0.9.

4.5.6 Sylvania Inlier

A total of 28 zircon grains were analysed from five samples. Magmatic grains (n=19) yield a range of initial $^{176}Hf/^{177}Hf$ ratios between 0.280487and 0.280984 (εHf_t -9.4 and +3.7). Median values (magmatic) range between -7.4 ± 4.9 and +1.2 ± 3.2 (2SD). Inherited zircon grains (n=9) with $^{207}Pb/^{206}Pb$ ages ranging between c. 3405 and 3152 Ma returned a εHf_t value ranging from -6.9 to +2.5. One analysis with $^{207}Pb/^{206}Pb$ age of c. 3133 Ma, interpreted as having undergone ancient radiogenic-Pb loss, returned εHf_t values of -7.9.

5.5.7 Halfway Gneiss

Thirty-one zircon grains were analysed from three samples. Magmatic grains (Archaean protoliths, n=13) yield a range of initial $^{176}Hf/^{177}Hf$ ratios between 0.281042 and 0.281293 (εHf_t -4.2 and +4.3, median εHf_t -1.5 ± 5.7, 2SD). Two grains from pegmatite intrusions dated at c. 2363 and 2153 have εHf_t of -12.2 and -6.1. Neoproterozoic protoliths (n=3) yield a range of initial $^{176}Hf/^{177}Hf$ ratios between 0.281110 and 0.281227 (εHf_t -13.3 and -8.6, median εHf_t-10.6 ± 3.9, 2SD). Inherited zircon grains (n=12) with $^{207}Pb/^{206}Pb$ ages between c. 2973 and 2188 Ma yield a range of εHf_t values between -4.8 and +2.7. Two analysis with $^{207}Pb/^{206}Pb$ age of c. 1979 Ma, interpreted as having undergone ancient radiogenic-Pb loss, returned εHf_t values of -8.6.

4.6 OXYGEN ISOTOPE DATA

A total of 332 zircon grains were analysed from 33 samples (Fig. 4.6) and include analyses of

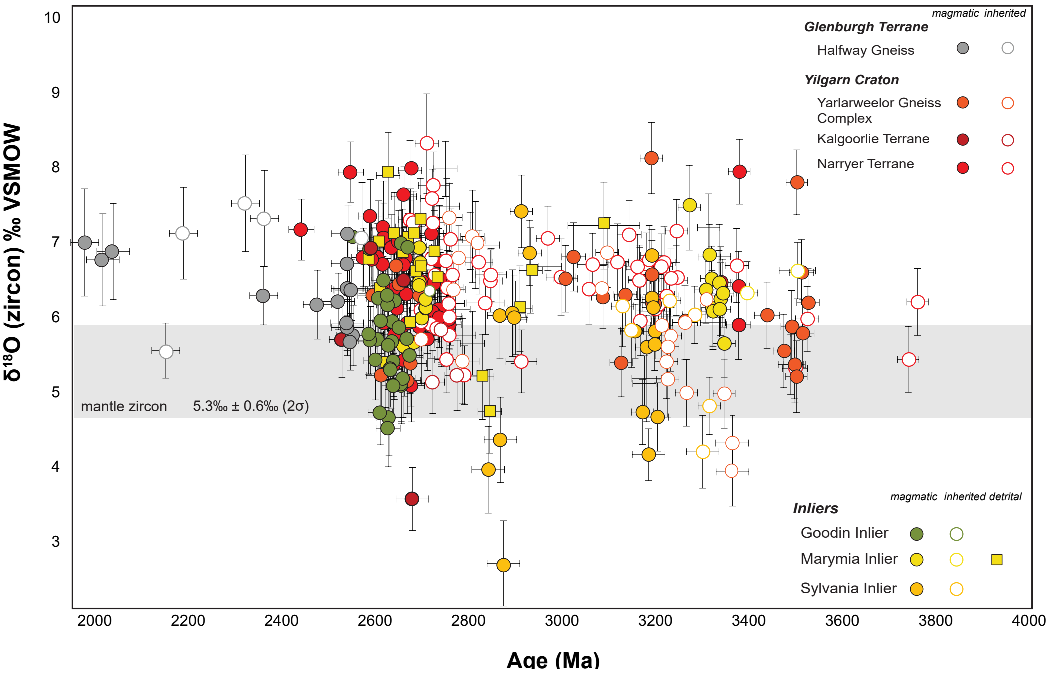

Figure 4.6 $\delta^{18}O$ versus age (n = 273). The compositional field for zircon in equilibrium with mantle-derived melts has a $\delta^{18}O$ VSMOW value of 5.3 ± 0.6‰ (2σ; Valley et al., 2005)

groups that are interpreted to date crystallisation and inherited zircon. Twenty-five analyses were rejected due to ablated area consisting of core-rim mixtures, metamict patches, inclusions, cracks or edges (see Appendix B).

4.6.1 Narryer Terrane

Data from the Narryer Terrane consist of 105 individual analyses from 9 samples. $\delta^{18}O$ values of all analysed samples range between 5.09 and 8.32‰. Magmatic grains (n=50) yield a range of $\delta^{18}O$ values between 5.09 to 7.94‰, with the average $\delta^{18}O$ of magmatic zircon from each sample varying from +5.93 ± 1.13 to 6.94 ± 0.44‰, 2SD. Inherited zircon grains (n=50) with $^{207}Pb/^{206}Pb$ ages ranging between 3766 to 2678 Ma yield a range of $\delta^{18}O$ values between 5.23 to 8.32‰. Analyses with no reliable corresponding age data (n=5) have $\delta^{18}O$ values between 5.89 and 6.74‰.

4.6.2 Yarlarweelor Gneiss Complex

A total of 48 magmatic, metamorphic and inherited zircon grains were analysed from three samples. $\delta^{18}O$ values of all analysed samples range between 3.95 and 8.96‰. Magmatic grains (n=24) yield a range of $\delta^{18}O$ values between 5.16 to 8.13‰, with the average $\delta^{18}O$ of magmatic zircon from each sample ranging between 6.05 ± 1.48 to 6.52 ± 1.55‰, 2SD. Inherited zircon grains (n=18) with $^{207}Pb/^{206}Pb$ ages ranging between 3368 to 2702 Ma yield a range of $\delta^{18}O$ values between 3.95 to 7.34‰. Analyses with no reliable corresponding age data (n=6) have $\delta^{18}O$ values between 5.19 and 6.97‰.

4.6.3 Marymia Inlier

A total of 50 magmatic, inherited and detrital zircon grains were analysed from five samples. $\delta^{18}O$ values of all analysed samples range between 4.75 and 7.9‰. Magmatic grains (n=25) yield a range of $\delta^{18}O$ values between 5.6 to 7.47‰, with the average $\delta^{18}O$ of magmatic zircon from each sample varying from 5.94 ± 0.93 to 6.4 ± 0.9‰, 2SD. Inherited zircon grains (n=3) with $^{207}Pb/^{206}Pb$ ages between c. 3508 and 2744 Ma yield a range of $\delta^{18}O$ values between 5.76 and 6.63‰. Detrital zircon grains (n=22) with $^{207}Pb/^{206}Pb$ ages ranging between 3093 to 2610 Ma yield a range of $\delta^{18}O$ values between 4.75 to 7. 9‰.

4.6.4 Goodin Inlier

Thirty-seven zircon grains were analysed from five samples. $\delta^{18}O$ values of all analysed samples range between 4.52 and 8.5‰. Magmatic grains (n=29) yield a range of $\delta^{18}O$ values between 4.52 and 7.05‰, with the average $\delta^{18}O$ of magmatic zircon from each sample varying from 5.34 ± 0.83 to 6.15 ± 1.01‰, 2SD. One inherited zircon grain with a $^{207}Pb/^{206}Pb$ age of c. 2720 Ma returned a $\delta^{18}O$ value of 6.36‰. Seven analyses with no reliable U–Pb ages associated with them yield $\delta^{18}O$ values between 5.99 and 7.12‰.

4.6.5 Kalgoorlie Terrane

Nine magmatic and inherited zircon grains from two samples were analysed. $\delta^{18}O$ values of all analysed samples range between 2.85 and 6.93‰. Magmatic grains (n=5) yield a range of $\delta^{18}O$values between 3.58 and 6.93‰. Inherited zircon grains (n=2) with $^{207}Pb/^{206}Pb$ ages of 2778 and 2726 Ma return $\delta^{18}O$ values of 5.14 and 5.23‰.Two analyses with no reliable age data yield $\delta^{18}O$ values of 2.85 and 6‰.

4.6.6 Sylvania Inlier

Thirty-four zircon grains were analysed from six samples. $\delta^{18}O$ values of all analysed samples range between 2.72 and 7.42‰ . Magmatic grains (n=18) yield a range of $\delta^{18}O$ values between 2.72 and 7.42‰, with the average $\delta^{18}O$ of magmatic zircon from each sample varying from 5.03 ± 2.64 to 7.1 ± 0.6‰, 2SD. Inherited zircon grains (n=5) with $^{207}Pb/^{206}Pb$ ages ranging between 3319 and 3133 Ma yield a range of $\delta^{18}O$ values between 4.21 to 6.23‰. Analyses no reliable U–Pb ages associated with them (n=11) yield a range of $\delta^{18}O$ values between 4.21 to 6.79‰.

4.6.7 Halfway Gneiss

A total of 21 zircon grains were analysed from three samples. $\delta^{18}O$ values of all analysed samples range between 5.11 and 7.12‰. Magmatic grains (Archaean protoliths, n=12) yield a range of $\delta^{18}O$ values between 5.76 and 7.12‰, average $\delta^{18}O$ of magmatic zircon 6.24 ± 0.82‰, 2SD. Two zircon grains from younger pegmatite intrusions with $^{207}Pb/^{206}Pb$ ages of c. 2360 and 2150 Ma yield $\delta^{18}O$ values of 5.56 and 6.45‰. One inherited zircon grain with a $^{207}Pb/^{206}Pb$ age of 2574 Ma yields a of $\delta^{18}O$ value of 7.07‰. Inherited zircon grains (Neoproterozoic protoliths, n=3) are discussed in Chapter 5. Sample 185955 (n=3) has no concurrent U–Pb ages, yields a range of $\delta^{18}O$ values between 5.11 and 6.43‰.

4.7 DISCUSSION

4.7.1 Timing of magmatism and temporal variations

The oldest magmatic ages are recorded in a gneiss from the Yarlarweelor Gneiss Complex (GSWA 135418; 3506 ± 10 Ma). The Eurada Gneisses with protolith ages of c. 3490–3440 Ma have been identified in the southern part of the Narryer Terrane; however, none have been identified within the Yarlarweelor Gneiss Complex. The hafnium-isotope analyses indicates initial $^{176}Hf/^{177}Hf$ ratios that are more radiogenic than the depleted mantle at c. 3500 Ma, i.e. the data plot above the DM-line. This may be attributed to a common Pb component, whereby discordant analyses have been shifted upwards towards the Concordia curve, resulting in seemingly ‘concordant’ older $^{207}Pb/^{206}Pb$ ages that would produce spurious positive εHf_t values. However, the data show ^{206}Pb cps that suggests the common Pb content has not recognisably effected the calculated ages. There is also no clear correlation between the initial $^{176}Hf/^{177}Hf$ ratios that plot outside of the DM-line and common Pb component. It is suggested that the age and Hf isotope data of this sample should be treated with caution, and as such it will not be included. The analysed zircon from the inliers and Yilgarn Craton margin samples cover a period of 1260 Myr, with individual $^{207}Pb/^{206}Pb$ ages ranging from c. 3766 to c. 2550 Ma and crystallisation ages ranging between c. 3365 Ma and c. 2539 Ma. Major periods of granitic magmatism are observed at c. 3330, 3200–3190, 2925–2875, 2730–2630 and 2540 Ma (Fig. 4.7). The c. 2730–2630 Ma group is the most common, and this magmatism is distributed widely across the Yilgarn Craton and associated inliers. However, it is not observed in the Sylvania Inlier or in the Glenburgh Terrane. Inheritance is common, with a total of 45% of concordant analyses consisting of inherited material with $^{207}Pb/^{206}Pb$ ages ranging between c. 3766 Ma and c. 2153 Ma. Inherited material older than c. 3500 Ma is preserved only in the Narryer Terrane and Halfway Gneiss. Although a lack of inherited zircon grains does not necessarily indicate the absence of older crust, the lack of inheritance >3500 Ma elsewhere in the Yilgarn Craton and surrounding inliers suggests that these early Archaean crustal components have either not been sampled, granite magmatism was more limited in volume and extent, or grains of this age were extensively recycled and not preserved.

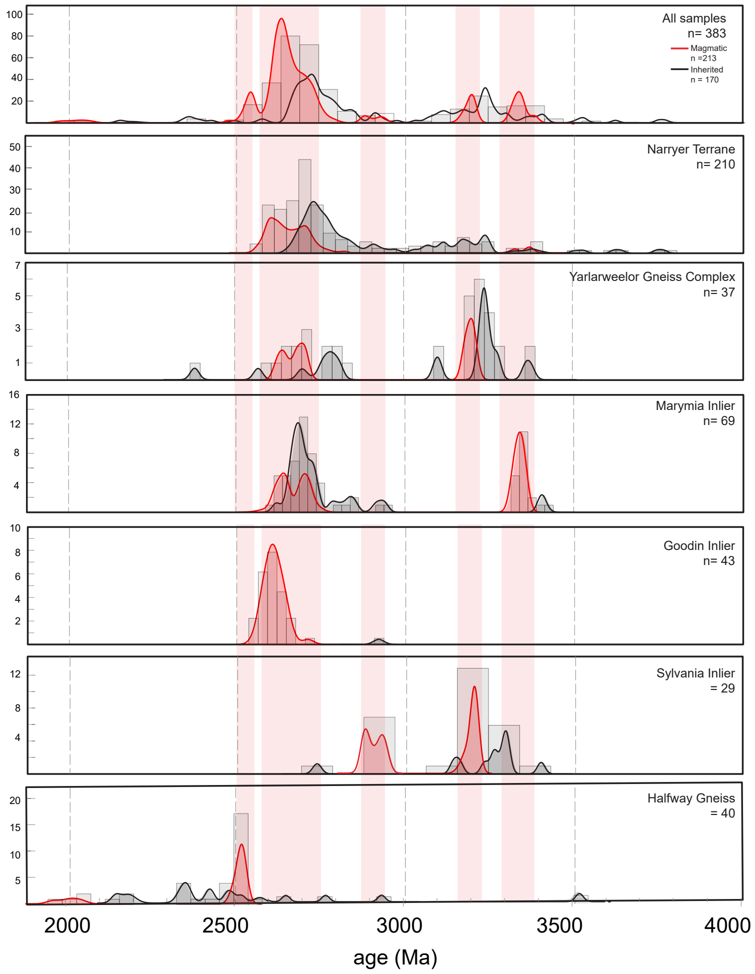

Figure 4.7 Probability plot of magmatic and inherited zircon U–Pb data

The oldest major period of granite magmatism is recorded at c. 3330 Ma in the Narryer Terrane and Marymia Inlier. These samples record crystallisation ages between c. 3365 and c. 3332 Ma. Crystallisation ages of 3332 ± 8 Ma and 3336 ± 27 Ma from the Marymia Inlier are the first to date magmatism of this age. Previous geochronology has dated magmatism in the Marymia Inlier at c. 2720–2690 Ma (Vielreicher and McNaughton, 2002) and inherited material at c. 3802–2930 Ma (Vielreicher and McNaughton, 2002; Lu et al., 2017). This distinguishes these rocks of the Marymia Inlier from the surrounding Yilgarn Craton margin and Goodin Inlier to the south, where the oldest granitoid magmatism is recorded at c. 3010 Ma in the Younamni Terrane. Additionally, no evidence of granitoid magmatism older than c. 2810 Ma in the EGST (Cassidy et al., 2006). The zircon with ages >c. 3000 Ma are restricted to an area south of the Marymia Inlier Plutonic Well greenstone belt. Elsewhere in the Marymia Inlier granitoids record

zircon U–Pb ages between c. 2720 and c. 2698 (Vielreicher and McNaughton, 2002). The c. 3330 Ma U–Pb ages of the granitoids from south of the greenstone belt are similar to the 3365 ± 30 Ma age of a granodiorite from the northeastern part of the Narryer Terrane, indicating essentially coeval granitic magmatism. Inherited zircons with comparable ages (c. 3350 Ma) are found in samples from the Narryer Terrane and Yarlarweelor Gneiss Complex (Nelson, 1998a; this study). The Marymia Inlier has been interpreted to consist of two components separated by the Jenkins Fault: an eastern or northern extension of the Narryer, Murchison or Southern Cross Province, and a northwestern extension of the Eastern Goldfields Province (Bagas, 1999). The c. 3330 Ma zircon U–Pb ages presented in this study indicates a Narryer Terrane association.
Magmatic activity at c. 3190 Ma occurs in the Sylvania Inlier and the Yarlarweelor Gneiss Complex. Inherited components of similar age are observed in the Narryer Terrane. However, given the spatial location of the Sylvania Inlier and its association with the Pilbara Craton, the magmatism is not assumed to be directly related. Granites comparable ages with the c. 3190 Ma Sylvania Inlier samples are recorded in the Pilbara Craton (Nelson, 2004c). There is a distinct period of quiescence observed in the Marymia Inlier, the Goodin Inlier and the Halfway Gneiss (Fig. 4.7). Following this, there is a period of granite emplacement at c. 2925–2875 Ma, restricted to the Sylvania Inlier. Relatively few inherited zircon of this age are observed elsewhere in the region, with minor inherited material identified in the Goodin and Marymia Inlier, Halfway Gneiss and Narryer Terrane. Magmatic activity of this age is noticeably absent from the Yarlarweelor Gneiss Complex. Both the spatial location and U–Pb ages of the Sylvania Inlier indicates separate development from the Yilgarn Craton and southern inliers, and supports interpretations that the inlier is associated with the Pilbara Craton (Tyler, 1991).

The main period of granitoid magmatism at c. 2730–2630 Ma group is the most common, and this magmatism is distributed widely across the Yilgarn Craton and the Marymia and Goodin Inliers. However, it is not observed in the Sylvania Inlier or in the Glenburgh Terrane. Ages of granite emplacement in the Narryer Terrane from c. 2728 Ma to c. 2622 Ma are comparable to zircon ages of c. 2658–2622 Ma in the Goodin Inlier, the c. 2700 Ma ages from the Marymia Inlier and the c. 2668 Ma zircon ages from the EGST. The c. 2730–2630 Ma group was broadly synchronous with the widespread c. 2760–2620 Ma granitoid emplacement associated with terrane assembly and cratonization of the Yilgarn Craton (Myers, 1993; Barley et al., 2003; Cassidy et al., 2006). The c. 2540 Ma period of granite activity is limited to the Halfway Gneiss, and no magmatic grains younger than c. 2590 Ma are recorded elsewhere in the study area. This suggests separate development of these terranes before assemblage by continental collision in the Palaeoproterozoic. Given the close spatial and age relationship between the Yilgarn Craton and the Marymia and Goodin Inliers, it is reasonable to suggest that they are related, i.e. the inliers are the northern extent of the Yilgarn Craton. However, although >c. 2960 Ma contemporaneous granitic events affected all terranes, isotopic data (Sm–Nd and Lu–Hf) indicates that the magmas tapped significantly different sources (Cassidy et al., 2002; 2006; Ivanic et al., 2012; Wyche et al., 2012; Mole, 2012; Mole et al., 2014). Therefore, given that there is a fundamental difference in isotopic signatures of the various terranes of the Yilgarn Craton, it is necessary to establish the isotopic characteristics of the Marymia and Goodin Inlier in order to further constrain their crustal evolution.

4.7.2 Hf Model ages

Zircon Hf isotope compositions can be used to estimate the timing of the extraction of the source reservoir from which the zircon crystallised from a specific mantle reservoir; this is known as the zircon Hf model age (Hawkesworth and Kemp, 2006a). Model ages are assumed to represent the approximate time of addition of juvenile, mantle-derived material to the crust (Vervoot and Kemp, 2016), and have been used to constrain periods of crustal growth (e.g. Hawkesworth and Kemp, 2006a; Belousova et al., 2010; Condie et al., 2011; Dhuime et al., 2012). However, it should be noted that model ages are not quantifiable ages, rather estimates based on a number of assumptions, specifically: (1) the isotope composition of the mantle reservoir; (2) the Lu/Hf ratio of the zircon host-rock and (3) the magma source reflects a single component that has not been modified since extraction, i.e. mixing/contamination by sedimentary source component (Vervoot and Kemp, 2016). Continental crust derived from mantle-derived melts is assumed to have an isotopic composition similar to that of the depleted mantle (DM) (Dhuime et al., 2011). As the DM is not directly measureable, its composition is based on measurement of present-day mid-ocean ridge basalts (eg. Nowell et al., 1998; Griffin et al., 2000). However, as the DM is unlikely to be a compositionally homogenous reservoir, there are uncertainties associated with the use of appropriate mantle compositions (e.g. Dhuime et al., 2011; Payne et al., 2016; Vervoot and Kemp, 2016). The choice of mantle reservoir and Lu/Hf crustal composition values will result in significant variation in calculated model ages, in range of a few hundred million years (Payne et al., 2016). DM lines used in figures within this thesis are based on ^{176}Lu/^{177}Hf of 0.283251 (Nowell et al., 1998) and 0.283164 (lower line; Chauvel et al., 2008) to show a range of possible mantle compositions. The caveat here is that the estimates of the composition of the depleted mantle cannot adequately describe the diversity of isotopic heterogeneities observed in the present-day mantle.

Oxygen isotope ratios of zircon grains ($\delta^{18}O > 5.3 \pm 0.6‰$; 2σ; Valley et al., 2005) have previously been used to discriminate between mantle-derived sources and hybrid/crustal contaminated sources (Kemp et al., 2007; Dhuime et al., 2012; Hawkesworth et al., 2010), this method has been applied in this study and calculated model ages are reported, with the assumption that any Hf model ages are not considered to exclusively represent an age of crustal generation, and that any interpretation of Hf model ages is also supported by the geological data. While the use of oxygen isotope data as a filter for validating Hf model ages in determining rates of continental growth have its limitations (e.g. Roberts and Spencer, 2015; Payne et al., 2016), the combined use/interpretation of Lu–Hf and O isotope systematics in zircon still offer a means of identifying crustal recycling. Considering all uncertainties associated with the calculation and application of model ages, they can still provide insight of crustal evolution as long as they are used with an understanding of their limitations

4.7.3 Nature of the Yilgarn Craton (Narryer Terrane and Yarlarweelor Gneiss Complex)

U–Pb data reveals three main periods of granite emplacement at c. 3380, c. 3190, and a prominent, younger main c. 2740–2625 Ma event. Magmatic zircon from these sample yield initial ^{176}Hf/^{177}Hf ratios between 0.280511 and 0.280963 (εHf$_t$ -13.3 to -0.4). The preponderance of evolved εHf$_t$ values in the Narryer Terrane and YGC samples suggests that these granites were formed mainly from the reworking of isotopically evolved pre-existing crustal components with little to no significant mantle input.

The c. 3380 Ma zircon indicate a large range in εHf$_t$ values (-7.6 to -0.4) which correspond to T_{DM}^{C} ages of 4186 Ma and 3712 Ma, respectively. The δ^{18}O values indicate average δ^{18}O of 6.49 ± 1.24‰ (2SD), with the most radiogenic εHf$_t$ value (-0.4) corresponding with a near mantle δ^{18}O value (6.47 ± 0.47). This suggests the c. 3380 Ma granite was generated by a c. 3700 Ma juvenile component undergoing variable mixing with older early Archaean material, resulting in the large Hf array. The c. 3190 Ma group appear to be reworking of this source, and the c. 2740–2625 Ma granites are the result of further reworking of this source. Zircons from the middle Archaean granites display mainly unradiogenic ^{176}Hf/^{177}Hf ratios between 0.280711 and 0.280963 (εHf$_t$ -8.4 to -4.3). The c. 2740–2625 Ma granites have median εHf$_t$ values (-10.4 to -6.7) that are more evolved than the c. 3380 Ma and the c. 3190 Ma granites (median εHf$_t$ -1.4 to -6.8). Evolution lines defined by a source a ^{176}Lu/^{177}Hf value of 0.015, show that the younger granites lie within the older granites isotopic envelope. Therefore, these isotopic arrays indicate that the melts were formed by reworking of an infracrustal source possessing broadly similar ^{176}Lu/^{177}Hf ratios, such as the c. 3380 Ma granites. However, these data also indicate values that lie above the isotopic evolution line of the c. 3380 Ma granites, indicating that the Hf composition of the c. 2740–2625 Ma granites requires an input of material with a more radiogenic Hf signature. Inherited zircon grains have compositions which plot along this evolution line, and are consistent the interpretation that the c. 2700–2600 Ma granites were sourced from reworking of the c.

3380 Ma granites. This conclusion is supported by the occurrence of c. 3400–3320 Ma inherited zircon with model ages of 4110–3830 Ma in the younger granites.

The c. 2740–2625 Ma zircon from the Narryer Terrane and YGC indicate a relatively narrow distribution of average $\delta^{18}O$ values (5.93 ± 1.13‰ to 6.90 ± 0.44‰) coupled with variably evolved εHf_t compositions (median εHf_t -10.3 to -6.7). Zircon with mantle $\delta^{18}O$ values indicate $T_{DM}{}^{C}$ ages of 3964–3384 Ma. The oxygen isotope data suggest the involvement of ^{18}O-enriched crustal protoliths (supracrustal material or altered igneous rocks) in their generation, either through partial melting of high-$\delta^{18}O$ material, or by assimilation or mixing of enriched $\delta^{18}O$ material with primary magmas. Assuming an average Archaean sediment value of ~10–12‰ (Appleby et al., 2010), and a maximum value of 7.2‰, and is based on the maximum δ18O value measured, this would imply an in input of ~28–40% high-$\delta^{18}O$ material in the Narryer Terrane/YGC magmas relative to an average mantle value (5.3‰, Valley et al., 2005). However, it is not clear whether the range in $\delta^{18}O$ values reflects either (1) melting and mixing of a low $\delta^{18}O$ infracrustal source component with supracrustal (metasedimentary) material, (2) melting of crustal components with enriched $\delta^{18}O$ signature or (3) assimilation of high-$\delta^{18}O$ material into the melt from surrounding crust during magma ascent and/or emplacement within the mid- to low-crust. The preponderance of evolved (unradiogenic) εHf_t values suggests that the magmas that these zircon crystallised from were formed from the partial melting of isotopically evolved pre-existing crustal components with little/no significant juvenile input, rather than mixing of enriched $\delta^{18}O$ material with primative magmas. In addition, a substantial amount of zircon (43%) indicate higher than mantle $\delta^{18}O$ values (>5.9‰), and as oxygen isotope composition of zircon is insensitive to differentiation (Valley et al., 2005) magma generation by differentiation from primary melts can be ruled out. Therefore the c. 2740–2625 Ma granitoids are the result of the reworking of Archaean granites, with melting occurring in the lower to middle crust (<45 km, constrained by the absence of a garnet signature in the zircon).

Crustal evolution lines defined using a source $^{176}Lu/^{177}Hf$ value of 0.015 (Griffin et al., 2002) are plotted from analyses of Narryer Terrane and YGC granites (Fig. 4.5a). The evolution lines show that c. 2740–2625 Ma and c. 3190 Ma granites lie within the isotopic envelope of the c. 3380 Ma granites, consistent with the interpretation that the zircon crystallised from melts derived from the progressive reworking of an older crustal material. Kemp et al. (2010) analysed zircon from c. 3650–2650 Ma meta-igneous rocks from the Jack Hills belt. The zircon from this study returned dominantly unradiogenic εHf_t values (-14.9 to -1.4), interpreted as formation from melts sourced from reworking of older crustal material, rather than differentiation from juvenile magmas. They suggested a >4.4 Ga intermediate to mafic crustal component that was reworked and incorporated into younger magmas. εHf_t values of zircon from Kemp et al. (2010) fall within the isotopic envelope defined by the zircon from this study, and show that the melts that these zircon crystallised from was extracted from a source with a broadly similar Lu/Hf ratio. The Hf isotope compositions zircons measured during this study are in agreement with Lu–Hf data from other meta-igneous rocks of the Narryer Terrane (Fig. 4.5a; Kemp et al., 2010; Nebel-Jacobsen et al., 2010).

4.7.4 Nature and origin of the Goodin Inlier

The U–Pb data reveals one main period of granite emplacement at c. 2660–2620 Ma, contemporaneous with the c. 2760–2620 Ma voluminous granite emplacement observed in the Narryer Terrane, Marymia Inlier and Yilgarn Craton. Previous zircon geochronology has dated magmatism in the Goodin Inlier at 2624 ± 8 Ma (Nelson, 1997b). Although the granitic rocks across the Yilgarn Craton share similar crystallisation ages, there is a distinct temporal evolution in the nature and style of granite intrusion (Cassidy et al., 2002). Extensive Sm–Nd and Lu–Hf studies have established that there is significant difference in the isotopic characteristics between the various terranes across the Yilgarn Craton (McCulloch and Compston, 1981; McCulloch et al., 1983; Fletcher et al., 1984; Champion and Sheraton, 1997; Cassidy et al., 2002; Barley et al., 2003; Griffin et al., 2004; Cassidy and Champion, 2004; Champion and Cassidy, 2007; Ivanic et al., 2012; Wyche et al., 2012; Mole et al., 2010; 2013; 2014). The Lu–Hf isotope data from Wyche et al (2012) and Mole et al (2010; 2014) confirmed that there is a clear distinction in the εHf_t data between zircon from the Youanmi Terrane and the EGST. Those from the Youanmi Terrane are characterised by older model ages and dominantly unradiogenic εHf_t values, whereas those from the EGST are more characterised by younger model ages and dominantly radiogenic εHf_t values. This association highlights the different processes involved in the crustal evolution in the Yilgarn Craton, with granite formation in the EGST comprising a significant juvenile input, while granite formation in the Youanmi Terrane was dominated by crustal reworking.

The Goodin Inlier samples indicate evolved Hf-isotope signatures, with median εHf_t values between -6.9 ± 5.5 and -6.3 ± 3.4 (2SD). εHf_t values from individual magmatic zircon ranging between of -10 and -1.1 (median -6.4), and indicate $T_{DM}{}^{C}$ ages between 3638 and 3276 Ma (median 3514 Ma). The unradiogenic εHf_t values indicate that the melts were sourced from reworked crust with a mean model age of c. 3500 Ma. Oxygen isotope data for the individual magmatic zircon range from 4.52 to 7.12‰, (average $\delta^{18}O$ 5.34 ± 0.83 to 6.15 ± 1.01‰, 2SD). These oxygen values are consistent with the interpretation that the zircons crystallised from a magma generated by melting of pre-existing igneous rocks mixed with evolved sources at lower- to mid- crustal levels. The U–Pb age and Lu–Hf isotope composition of the zircon from the Goodin Inlier zircon and the Youanmi Terrane are similar (Fig. 4.5b). The c. 2680–2580 Ma Youanmi Terrane granites are dominated by unradiogenic zircon (εHf$_t$ -14 to +2.4, median -5.5) and $T_{DM}{}^C$ ages 4191–2880 Ma (median 3527 Ma) (Wyche et al., 2012; Ivanic et al., 2012; Mole et al., 2010). The similarities in U–Pb and Hf-isotopic composition suggest that the Goodin Inlier closely resembles, and is therefore interpreted to be part of, the Youanmi Terrane. However, there is some overlap in the isotopic signature of the zircon from the Murchison and Southern Cross Domains, which precludes further correlation to either domain.

4.7.5 Nature and origin of the Marymia Inlier

The samples from the Marymia Inlier have U–Pb ages of c. 3330–2700 Ma, with two well-defined events at c. 3330 Ma and c. 2700 Ma. Previous geochronology have dated magmatism at c. 2720–2690 Ma (Vielreicher and McNaughton, 2002). The c. 3330 Ma samples are the first to date magmatism of this age in the Marymia Inlier. U–Pb ages older than c. 3300 Ma are rare in the Yilgarn Craton, however, c. 3730–3300 Magmatism is recorded in the Narryer Terrane (Kinny et al., 1988; Nutman et al., 1991; 1993), suggesting a correlation between the two regions. Analyses of magmatic zircon with $^{207}Pb/^{206}Pb$ ages between c. 3360–3320 Ma indicate εHf$_t$ values between -7.1 and -2.1, corresponding to $T_{DM}{}^C$ ages between 4113 and 3812 Ma. The predominance of evolved (unradiogenic) εHf$_t$ values in the c. 3330 Ma samples suggests that these granites were formed mainly from the reworking of isotopically evolved crustal components with little/no significant juvenile input. The magmatic zircon form homogenous oxygen isotope populations with $\delta^{18}O$ values between 5.6 and 6.8‰, and inherited zircon show $\delta^{18}O$ values ranging from 5.93 to 8.09‰. This Hf–O array (unradiogenic εHf$_t$ coupled with mantle to slightly enriched $\delta^{18}O$ values) indicates that the magmas that the zircon crystallised from contained both significant low-$\delta^{18}O$ material representing an infracrustal source component (i.e. a meta-igneous crustal component that has not interacted significantly with shallow crustal material), and negligible amounts of high-$\delta^{18}O$ supracrustal (metasedimentary or volcanic-igneous) material. Both crustal assimilation and melting of older high-$\delta^{18}O$ crust are concluded to be possible processes to produce this array. This is consistent with derivation from reworking of crustal components with Eo- to Palaeoarchaean $T_{DM}{}^C$ ages. The Hf–O isotope data from these samples are comparable to that of the Narryer Terrane and Yarlarweelor Gneiss granites of equivalent age (εHf$_t$ values -7.6 to -0.4, $T_{DM}{}^C$ ages 4186–3712 Ma, and average $\delta^{18}O$ values 5.93 ± 1.13‰ to 6.94 ± 0.44‰). It is not clear whether the c. 3330 Ma crust now part of the Marymia Inlier is a rifted fragment or extension of the Narryer Terrane. If the Narryer-Marymia Inlier Terrane crust is continuous, the same isotopic characteristics would be expected in the granites that crop out in the southwest Marymia Inlier. U–Pb zircon geochronology constrains granites in this region at c. 2670–2660 Ma (Nelson, 1997a; Wingate et al., 2014a), however, isotopic data only exists for a metasedimentary sample (120601) which displays Hf-isotopic signature that overlaps with Youanmi and Kalgoorlie Terrane Hf–U–Pb space.

In contrast to the c. 3330 Ma granites, the Hf isotope data for the c. 2700 Ma granites shows a change to much more radiogenic $^{176}Hf/^{177}Hf$ ratios between 0.280982 and 0.281181 (εHf_t -2.7 to +4.4) corresponding to younger $T_{DM}{}^{C}$ ages between 3087 and 2935 Ma (median c. 3050 Ma). The predominance of positive εHf_t values indicates a indicate that crustal growth occurred largely through the input of juvenile mantle-derived magmatic components. The Hf–isotope array extends to negative εHf_t values, suggesting variable degrees of mixing with more evolved crustal components. These U–Pb ages and Hf–isotope data are similar in age and Hf–isotope signature to those from the EGST (Fig. 4.5b), which show evidence of significant juvenile input variably mixing with a crustal component with a mean model age of c. 3100 Ma (Wyche et al., 2012). Additionally, these isotopic data are distinct from the more evolved signatures and older model ages of the Southern Cross Domain and Narryer Terrane/YGC (Wyche et al., 2012; Mole et al., 2013, 2014). Although there is some overlap with the isotopic signature of zircon from the Murchison Domain at c. 2800–2680 Ma, the model ages are older 3858–3018 Ma, average 3250 Ma (Ivanic et al., 2012). This suggests that the c. 2700 Ma granite magmatism in the Marymia Inlier and Narryer Terrane/YGC were sourced from isotopically distinct crustal components, and that the eastern extent of the Marymia Inlier is correlative with the EGST. However, there is some overlap in the isotopic signature of the zircon from the Kalgoorlie and Kurnalpi Terranes (Wyche et al., 2012), which precludes further correlation to either terrane.

The c. 2700 Ma granites show a range of $\delta^{18}O$ values between 5.6 and 6.94‰, with average $\delta^{18}O$ values of 6.35 ± 0.55 and 5.94 ± 0.93‰ (2SD). This suggests that the melts that these zircon crystallised from were sourced from an infracrustal source component with mantle-like $\delta^{18}O$, and negligible amounts of supracrustal (metasedimentary) material. The melt from which the zircon crystallised from involved mixing of a significant juvenile addition of mantle-derived material at c. 2700 Ma with additional crustal components in the lower to middle crust. The juvenile input at c. 2700 Ma observed in the Marymia Inlier and EGST is contemporaneous with komatiite volcanism recorded in the Kalgoorlie and Kurnalpi Terrane (Barley et al., 2003; Kositicin et al., 2008). The greenstone event is attributed to plume activity, resulting in intrusion of mafic magma into the deep crust which may have been the likely heat source for initiating extensive crustal anatexis that lead to granite magmatism (Campbell and Hill, 1988). The Hf and O isotope data supports previous interpretations that the eastern part of the Marymia Inlier is a northwestern extension of the EGST (Vielreicher et al., 2002; Griffin et al., 2004; Gazley, 2011; Gazley et al., 2011; Dentith et al., 2014).

The isotopic data clearly record the presence of Palaeoarchaean crust in the south-eastern region of the Marymia Inlier. The U–Pb and Hf isotopic data suggests a Narryer Terrane/YGC association, with part of the Marymia Inlier and the Narryer Terrane contiguous for a part of their history. It is possible that the western region of the Marymia Inlier represents an extension of the Narryer Terrane. While no crystallisation ages >c. 2670 Ma are recorded east of the c. 3330 Ma granitoids, inherited zircon from a granite gneiss located 40 km to the west returned ^{207}Pb/^{206}Pb ages between c. 3800 and 2980 Ma (Lu et al., 2017) indicates the presence of Narryer Terrane aged crust in the area. However, U–Pb ages of inherited zircons cannot be considered clear evidence of underlying basement, as the inherited zircon may represent some sediment derived from the Narryer Terrane.

4.7.6 Nature and origin of the Sylvania Inlier

Zircon U–Pb geochronology has identified two main episodes of granite formation at c. 3190 and c. 2900 Ma. The c. 3190 Ma granites have εHf_t values (-9.4 to +3.7), those with mantle like $\delta^{18}O$ values return $T_{DM}{}^{C}$ ages between 3716 and 3440 Ma. This pattern suggests melt production from mixed sources: an older crustal component and an additional juvenile component extracted from the mantle at c. 3400 Ma (Fig. 4.5c). The c. 2900 Ma granites also show a large range in εHf_t values (-4.3 to +1.3) and those with mantle like $\delta^{18}O$ values return $T_{DM}{}^{C}$ ages between 3406 and 3393 Ma. Inherited zircon with ages ranging between c. 3405 and c. 3133 Ma show a large range in εHf_t values (-6.9 to +2.5), those with mantle like $\delta^{18}O$ values return $T_{DM}{}^{C}$ ages between c. 3692 and c. 3522 Ma. The Hf isotope data from the inherited component are comparable to that of the East Pilbara Terrane granites (EPT) of similar age (εHf_t values -9.3 to +3.7; Gardiner et al., 2017). The majority of analyses indicate values that lie within the isotopic evolution line of the EPT, indicating that the rocks of the Sylvania Inlier may have formed from the reworking of crustal material with Hf-isotopic signature similar to that of the EPT. However, these data also indicate radiogenic values that lie above the isotopic evolution line of the EPT, indicating that the Hf composition of the Sylvania Inlier requires an input of material with more radiogenic Hf signature. Similarly, the c. 2900 Ma granites indicate a more radiogenic Hf isotope signature, with values plotting above the Hf evolution line of c. 3190 Ma granites, and therefore requiring an input of additional juvenile material to produce these arrays.

U–Pb ages indicate the main period of granitic magmatism in the Sylvania Inlier occurred c. 3190 Ma, granites of similar ages are not found in the EPT, however, the $T_{DM}{}^{C}$ ages of the magmatic zircon from the Sylvania Inlier (4136–3269 Ma) are comparable to the EPT (4272–

3232 Ma; GSWA, 2016). Inherited components indicate EPT-like ages (c. 3400–3200 Ma), with similar Hf–isotope compositions. The overlap in the isotopic signatures of the Sylvania Inlier and the EPT suggests a shared crustal source. U–Pb ages and Hf–isotope compositions of Sylvania Inlier granites suggests a separate evolution to the EPT after c. 3200 Ma. Similar ages are recorded in the Kurrana Terrane in the southeastern part of the craton (c. 3178 Ma, Nelson, 2004c), interpreted as a rifted fragment of the East Pilbara Terrane separated between 3200 and 3150 Ma, and subsequently re-accreted at c. 2905 Ma (Van Kranendonk et al., 2010). Based on gravity data from Blewett et al. (2000), Hickman (2004) suggested that the southern part of the Kurrana Terrane included the Sylvania Inlier, however, a limited U–Pb geochronology prevented further correlation. The new U–Pb ages and Hf–isotope data are consistent with the interpretation that Sylvania Inlier is a part of the Kurrana Terrane, and represents a rifted portion of the EPT.

4.7.6 Nature and origin of the Glenburgh Terrane

The c. 2550–2430 Ma Halfway Gneiss is considered to be exotic to the adjacent Pilbara and Yilgarn Cratons based on the absence of late Palaeoprotoerozoic magmatism within the Yilgarn Craton, lack of similarities in tectonomagmatic history with the Yilgarn Craton, and contrasting Hf-isotope signatures (Occhipinti et al., 2004; Sheppard et al., 2004; Johnson et al., 2011b). The major, trace and REE compositions of the the younger c. 2600–2430 Ma rocks of the Halfway Gneiss was interpreted by Johnson et al. (2011b) as reflecting recycling of older c. 2730–2600 Ma gneissic components, rather than formation in a subduction-zone tectonic setting. Published Hf isotope data for Halfway Gneiss Archaean protoliths (Johnson et al., 2017a) indicate that the rocks are characterised by εHf_t values that range between -6.8 and +1.9, with $T_{DM}{}^{C}$ ages ranging between 3434 to 2934 Ma. Johnson et al (2017a) suggested that the Hf isotopic data indicate a progressive evolved trend, and they proposed a model for crustal generation in which the magmas were predominantly derived by the reworking of pre-existing crust without the addition of significant juvenile mantle-derived material. Whole-rock geochemistry of the Halfway Gneiss samples (GSWA, 2016) are peraluminous and plot in the 'volcanic arc' field on tectonic discrimination diagram (Pearce et al., 1984) and indicates a calc-alkalic to alkali-calcic trend. The whole-rock geochemistry which indicates selective enrichment in LILE such as Rb, Ba, Th and depletion in HFSE such as Ta, Nb, Zr, Hf, Sm, Y and Yb, are characteristic of suprasubduction zone granitic magmas (Pearce et al., 1984). The VAG affinity enriched LREE-LILE and HFSE depletion, as well as the calc-alkalic to alkali-calcic nature suggests subduction-related magmatism.

The zircon from Archaean protoliths of the Halfway Gneiss samples have εHf_t values ranging from -4.2 to+4.3, those with mantle like $\delta^{18}O$ values return $T_{DM}{}^{C}$ ages between 3312 and 2771 Ma. Palaeoproterozoic protoliths (c. 2045 Ma) of the Halfway Gneiss are discussed in Chapter 5. The magmatic zircons form a homogeneous oxygen isotope population with $\delta^{18}O$ values between 5.56 and 7.12‰ (av. 6.24 ± 0.82‰, 2SD). The range in εHf_t values reflects a heterogeneous magma at the time of crystallisation, and suggests melt production from mixed sources: an older crustal component with $T_{DM}{}^{C}$ ages of > 3320 Ma and an additional juvenile component extracted from the mantle at c. 2770 Ma. Analyses that indicate εHf_t values that are more radiogenic than CHUR have mantle-like $\delta^{18}O$ values, consistent with derivation from juvenile, mantle-derived magmas mixing with additional crustal sources.

The inherited zircon grains with $^{207}Pb/^{206}Pb$ ages between c. 2971 and c. 2492 Ma have εHf_t values ranging from -3.5 to +2.7. The $T_{DM}{}^{C}$ ages of the inherited zircon range between 3473 and 2910 Ma, similar to the c. 2550 Ma protoliths ($T_{DM}{}^{C}$ 3312–2771 Ma), suggesting they were sourced from reworking of a crustal component with the same model age. One inherited zircon grain (c. 2574 Ma) yielded a slightly elevated $\delta^{18}O$ value of 7.07 ± 0.71‰, indicating that the older crustal component had interacted with supracrustal sources, possibly during its path to emplacement. The $T_{DM}{}^{C}$ ages of the most radiogenic Halfway Gneiss analyses are <300 Ma older than the crystallisation ages, indicating a short crustal residence time. Contamination with older crustal material reduces the $^{176}Hf/^{177}Hf$ of mantle-derived magmas, and the short crustal residence times combined with the strongly juvenile signatures (εHf_t +2.9 to +4.3) suggests that the magma source was closely related to mantle material, i.e. extraction to crystallisation was a short process. The range in $\delta^{18}O$ values and εHf_t values requires: (1) input of material into the source that was previously affected by low-temperature alteration at or near Earth's surface, (2) input of an old infracrustal material into the source and (3) input of juvenile mantle-derived material. Taking into account the zircon trace element geochemisty and whole-rock geochemistry, possible tectonic settings for these criteria includes suprasubduction zones, likely to be continental-margin arc environment.

Although analyses of inherited zircon from this study are limited, they show Lu–Hf compositions that overlap Yilgarn Craton compositions from the Murchison and Kalgoorlie Terrane at c. 2970 and c. 2660 Ma (Fig. 4.5b) This is consistent with data from Johnson et al (2017a) that indicate a significant proportion of inherited zircon with ages between c. 2730–2620 Ma have εHf_t values between -4.4 and +3.8 (Johnson et al., 2011b; 2017a). Previously, Johnson et al. (2011b) compared Lu–Hf and Sm–Nd data for the Narryer Terrane, Murchison Domain, Southern Cross Domain and EGST on an event signature plot. They proposed that the c. 2730–2600 Ma period of magmatism in the Halfway Gneiss was dominated by juvenile processes and was significantly different to the reworking trend observed in the Yilgarn Craton. More recent studies have extended this database considerably (e.g. Ivanic et al., 2012; Wyche et al., 2012; Mole, 2012). Although the Hf–isotope data from the present-day adjacent Narryer Terrane indicate unradiogenic εHf_t values (-13.3 to -2.8) during the c. 2730–2600 period, crustal evolution lines show that there is overlap in the most unradiogenic components of the Halfway Gneiss and the most juvenile values of the Narryer Terrane/YGC (Fig. 4.5b). The Hf–composition of the c. 2730–2620 Ma Halfway Gneiss zircon overlaps with those from the Youanmi Terrane, and provide further indication of a shared crustal source (Ivanic et al., 2012; Wyche et al., 2012; Mole, 2012; 2014). This interpretation is supported by c. 2550 Ma zircon grains that lie on a crustal evolution line from the Youanmi Terrane components. In addition, zircon from the EGST (Kalgoorlie Terrane) show evidence of significant juvenile input at c. 2700–2640 Ma, with values for εHf_t between -4.9 to +2.2 (Wyche et al., 2012), which overlap the U–Pb and Hf–isotope compositions of inherited zircon from this study and Johnson et al (2017a). Consequently, as the Halfway Gneiss and the Yilgarn Craton have some degree of isotopic similarity, the Yilgarn Craton should not be ruled out as a possible crustal source.

The Hf–isotope data from the Halfway Gneiss indicate that it is not exotic to the Yilgarn Craton margin. It is possible that the Halfway Gneiss is a rifted fragment of the Yilgarn Craton which separated from the craton during plume-related magmatism initiated at c. 2830 Ma and c. 2720 Ma. Subsequent magmatism at c. 2550 Ma involved the addition of a juvenile component, which resulted in the 'dilution' of the isotopic signature of the unradiogenic Archaean crustal components.

4.8 SUMMARY

- The Narryer Terrane and Yarlarweelor Gneiss Complex are characterised by evolved εHf_t (-13.3 to -0.4) and mantle-derived to slightly elevated mean $\delta^{18}O$ compositions (5.64 ± 0.94 to 6.94 ± 0.44‰, 2SD) and indicate derivation from the progessive reworking of Palaeoarchaean granites.
- The U–Pb data from the Marymia Inlier indicate two periods of granite generation, at c. 3330 Ma and c. 2700 Ma. The U–Pb and Hf–O isotope data of the c. 3330 Ma granites are comparable to granitoids from the Narryer Terrane, suggesting that the eastern portion of the Marymia Inlier is an extension of the Narryer Terrane. The Hf–O isotope data of c. 2700 Ma Marymia Inlier granitoids indicate correlation with the western part of the ESGT (Kalgoorlie Terrane).

- The Goodin Inlier samples indicate evolved Hf–isotope signatures coupled with mantle-derived $\delta^{18}O$ compositions, with melts sourced from the reworking of isotopically evolved pre-existing crustal components with little/no significant mantle input. Hf–isotope data shows that the Goodin Inlier closely resembles, and is interpreted to be part of, the Youanmi Terrane.

- U–Pb zircon geochronology from the Sylvania Inlier date magmatism between 3196 ± 9 Ma and 2879 ± 16 Ma. U–Pb ages and Hf–isotopic data indicate that it is part of the Kurrana Terrane, which represents a rifted portion of the Eastern Pilbara Terrane.

- Hf–O isotope data from the Halfway Gneiss indicate a component with a Yilgarn Craton Hf-isotopic composition made a contribution to the c. 2550 Ma magmatism, and it is therefore not an exotic micro-continent.

CHAPTER 5

U–Pb, HAFNIUM AND OXYGEN ISOTOPE CONSTRAINTS ON EARLY PALAEOPROTEROZOIC MAGMATISM (c. 2005–1950 Ma)

5.1 INTRODUCTION

Fundamental to understanding the generation and evolution of a crustal block is knowledge of the relationship between additions of new material from the mantle, and the extent of crustal recycling. Mechanisms of crustal recycling involve two distinct processes: (1) intracrustal recycling, whereby crustal materials are melted or contaminate mafic magma that intrudes continental crust and (2) mantle recycling, whereby crustal material is returned to the mantle by either subduction or delamination (Mclennan, 1988). Variations in the extent of differentiation, composition of mantle, crustal and recycled sources, and the degree of partial melting all contribute to the variety of geochemical signatures of granitoids (Ardnt, 2013). Analysis of the geochemistry of crustal rocks can be used to determine the relative contributions from mantle, crustal and subducting (recycled) reservoirs. Determining the relative proportions of these various contributions can constrain the generation, evolution and reworking of the continental crust over time.

The southern Gascoyne Province in the Capricorn Orogen comprises Archaean to Palaeoproterozoic rocks that includes variably deformed gneisses, metasedimentary rocks and continental arc related granitoids (Sheppard et al., 2004). These rocks record the convergence and collision of three Archaean crustal components (the Pilbara Craton, the Yilgarn Craton, and the Glenburgh Terrane) during the formation of the West Australian Craton during the c. 2005–1950 Ma Glenburgh Orogeny. Magmatism was generated in a continental arc setting along the southern margin of the Glenburgh Terrane (Johnson et al., 2011b) during the accretion of the southern Gascoyne Complex onto the passive northwestern margin of the Yilgarn Craton (Sheppard et al., 2004).

This chapter presents U–Pb, trace element, hafnium and oxygen isotope data from granitoids associated with the Glenburgh Orogeny in order to constrain the temporal evolution of the Palaeoproterozoic crust, and identify relative contributions of crust and mantle during their petrogenesis.

5.2 GEOLOGICAL SETTING

The samples in this study are from the southern part of the Gascoyne Province (Glenburgh Terrane) and the Yarlarweelor Gneiss Complex (Fig. 5.1). The Glenburgh Terrane comprises variably deformed and metamorphosed granitic rocks with c. 2660–1970 Ma protolith ages interleaved with metasedimentary rocks (Occhipinti et al., 2001; Johnson et al., 2011b). Basement gneisses of the Glenburgh Terrane indicate igneous crystallisation ages between c. 2555 and c. 2430 Ma (Johnson et al., 2011b). In the southern Glenburgh Terrane the majority of granites, the Dalgaringa Supersuite, were emplaced between 2005–1970 Ma, and record two episodes of high-grade metamorphism at c. 1985 Ma and c. 1945 Ma during the Glenburgh Orogeny (Occhipinti et al., 1999; Sheppard et al., 2004). Parts of interleaved Dalgaringa Supersuite and the Archaean granitic basement were deformed and metamorphosed to form the Halfway Gneiss (Occhipiniti et al., 2001). Sheppard et al. (1999) reported similarities between the geochemical characteristics of c. 1975 Ma granites of the Dalgaringa Supersuite and Phanerozoic subduction-related granites, and suggested that the Dalgaringa Supersuite formed in an Andean-type setting along the margin of an early Palaeoproterozoic crust prior to accretion to the Yilgarn Craton during the Glenburgh Orogeny. Johnson et al. (2011b, 2017a) provides Lu–Hf zircon isotopic data of the Dalgaringa Supersuite that supports the interpretation that they formed in

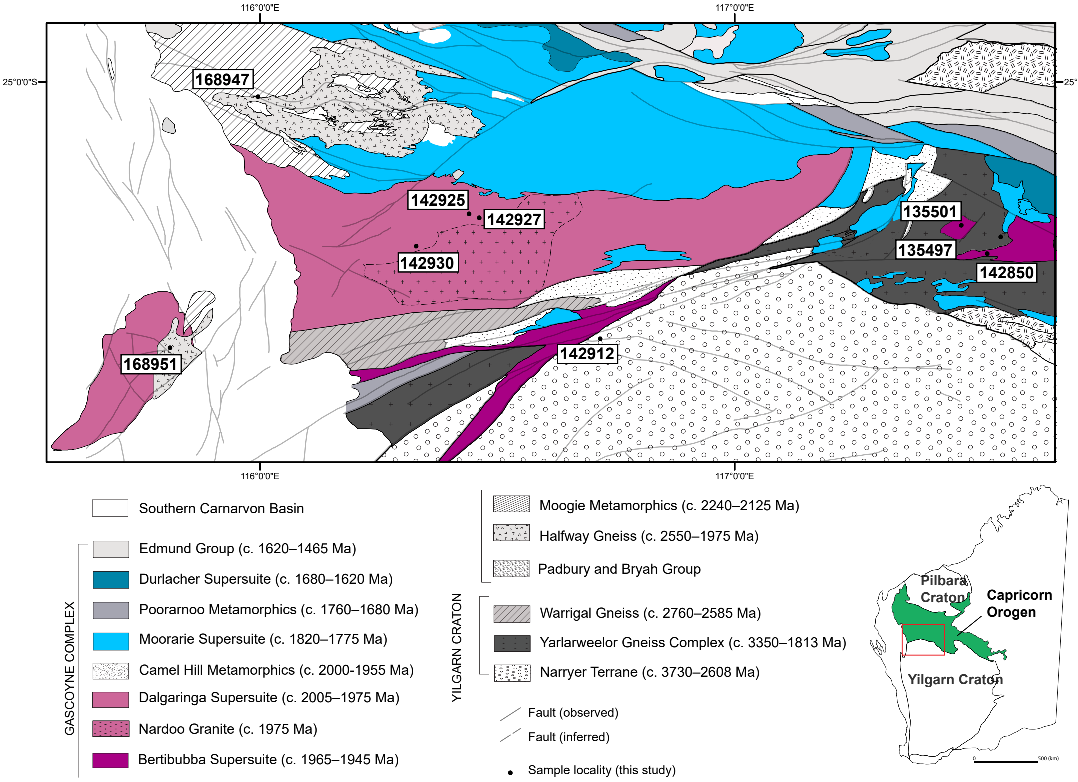

Figure 5.1 Simplified geological map of the southern part of the Capricorn Orogen, showing the principal tectonic units and sample locations mentioned in the text.

a continental margin arc, the Dalgaringa Arc, which reflects the subduction under the southern edge of the Glenburgh Terrane, prior to the amalgamation with the passive margin of the Yilgarn Craton. Parts of the Dalgaringa Supersuite were intruded by younger granites at c. 1975 Ma (Nardoo Granite, Fig. 5.1).

Metamorphic zircon and monazite U–Pb ages from metasedimentary units within the Glenburgh Terrane indicate that collision of the Glenburgh Terrane with the Yilgarn Craton occurred between c. 1960 Ma and c. 1950 Ma (Johnson et al., 2010). This event was accompanied by the intrusion of the c. 1965–1945 Ma Bertibubba Supersuite across the Glenburgh Terrane and the northwestern margin of the Yilgarn Craton (Johnson et al. 2010). The Bertibubba Supersuite is the first common magmatic component to the Glenburgh Terrane and Yilgarn Craton, and has been interpreted to mark the end of the Glenburgh Orogeny, indicating that ocean basin closure and formation of the West Australian Craton occurred prior to c. 1960 (Occhipinti et al., 2001; 2004). The Yarlarweelor Gneiss Complex (Fig. 5.1) comprises c. 3300–2600 Ma granites (Nelson, 1998a; 1999i), granitic gneisses and supracrustal rocks of the Narryer Terrane that were intruded by the c. 1965–1945 Ma Bertibubba Supersuite, and locally deformed and metamorphosed during the c. 1820–1770 Ma Capricorn Orogeny (Occhipinti et al., 2004; Johnson et al., 2013).

5.3 U–Pb GEOCHRONOLOGY

This chapter presents U–Pb results from nine samples of granitoids and granitic gneisses representing the Dalgaringa and Bertibubba Supersuites and the Halfway Gneiss. They cover an area that includes the Glenburgh Terrane and the Yarlarweelor Gneiss Complex (Fig. 5.1). A summary of zircon data is presented in Table 5.1. Details of each U–Pb, REE, O-isotope and Hf-isotope sample analysis are given in Appendix 3. Zircon grains obtained from heavy mineral separates provided for by the GSWA are indicated in text. All other zircon grains are obtained through EMP as described in Chapter 3. Analytical methods are outlined in detail in Chapter 3. For all samples except GSWA 135501 and GSWA 135497 the crystallisation age has already been established as part of previous geochronological studies (Nelson, 1999b, 1999c, 1999f, 1999g, 1999h, 2000d, 2000c, 2001d). The majority of weighted mean $^{207}Pb/^{206}Pb$ ages obtained during this study are in agreement with previously established ages. One sample (GSWA 142925) yielded an age that differs from those obtained during previous studies (<1.1% age difference; Table 5.1).

5.3.1 Halfway Gneiss

The Halfway Gneiss consists of several interlayered rock types heterogeneously deformed and metamorphosed to at least amphibolite facies (Johnson et al., 2011b). The dataset from the Halfway Gneiss consists of one sample with $^{207}Pb/^{206}Pb$ ages between c. 2574 and c. 2018 Ma.

5.3.1.1 GSWA 168947

GSWA 168947 is a gneissic rock showing a weighted mean $^{207}Pb/^{206}Pb$ date of 2042 ± 59 Ma (MSWD = 1.6), interpreted as the age of igneous crystallisation of a granitic precursor phase to the gneiss. (See section 4.3.7.3).

Table 5.1 Summary of sample descriptions and U–Pb LASS data.

sample	Unit[1]	Lithology[2]	Pb–Pb age (Ma)[3]	Inheritance (Ma)	Pb–Pb age (Ma)[4]	T_{Ti} (°C)	Lat	Long
168947	HG	monzogranite gneiss	2042 ± 59	2574–2188	2006 ± 6	-	-25.03388	115.82858
142925	DS	monzogranite	2024 ± 12	2093–2068	2002 ± 3	680	-25.3077	116.4132
142927	DS	granodiorite	-	2539–2102	1999 ± 5	-	-25.3165	116.4369
142930	DS	pegmatite	1995 ± 7	2128–2104	1994 ± 52	773	-25.38185	116.29083
168951	DS	monzogranite	(1976 ± 20)	2353–2023	2007 ± 3	691	-25.62111	115.62623
135501	BS	granodiorite	1967 ± 7	-	-	800	-25.3343	117.55646
142850	BS	monzogranite	(1956 ± 27)	-	1958 ± 4	698–781	-25.39979	117.61641
142912	BS	monzogranite	(1944 ± 66)	3025–2066	1961 ± 3	710	-25.607644	116.59326
135497	BS	metagranite	2015 ± 16, 1905 ± 15	2574–2390	-	698,627	-25.35544	117.56132

[1] HG = Halfway Gneiss, DS = Dalgaringa Supersuite, BS = Bertibubba Supersuite

[2] Petrographically characterised (GSWA)

[3] Crystallisation age ($^{207}Pb/^{206}Pb$) established by LASS, ages in brackets indicate () minimum crystallisation age.

5.3.2 Dalgaringa Supersuite

The dataset from the Dalgaringa Supersuite consists of four samples, and the analysed zircon cover a period of 580 Myr, with individual $^{207}Pb/^{206}Pb$ ages ages between c. 2539 Ma and c. 1959 Ma.

5.3.2.1 GSWA 142925

GSWA 142925 is a metamonzogranite. Zircon grains were hand-picked from heavy mineral concentrates provided by the GSWA. Grains are elongate, colourless, pale yellowish-brown to dark brown, typically 200–450 µm in size. CL imaging reveals CL-dark oscillatory zoned and homogenous interiors, commonly surrounded by CL-intermediate structureless rims of variable thickness. Some grains are equant. Metamict grains are common. A total of 17 analyses were performed on 14 zircon grains. Three analyses are >5% discordant (Group D) and have been rejected. Eight analyses of cores and rims (Group 1) yield a weighted mean $^{207}Pb/^{206}Pb$ date of 2018 ± 11 Ma (MSWD = 1.4), interpreted as the timing of magmatic crystallisation. Three analyses (Group X) returned ^{207}Pb/^{206}Pb ages ranging between c. 2093 Ma and c. 2044 Ma, interpreted as representing inherited material. One analysis of a CL bright recrystallised core returned a ^{207}Pb/^{206}Pb date of 1664 ± 14 Ma. The younger date of 1664 ± 28 Ma could possibly represent a younger disturbance event, but is more likely to represent a contaminant introduced during sample preparation. The crystallisation age of 2018 ± 11 Ma is older than the SHRIMP U–Pb age previously established (2002 ± 3 Ma; Nelson, 1999f).

5.3.2.2 GSWA 142927

GSWA 142927 is a metagranodiorite. Zircon grains were hand-picked from heavy mineral concentrates provided by the GSWA. Grains are pale yellow to dark brown in colour, typically 60–100 µm in length, and subhedral to prismatic in shape. Many zircons contain convolute or oscillatory zoned centres mantled by weakly oscillatory zoned rims of variable thickness. Thirty-eight analyses were performed on 37 grains. Thirty-six analyses are >5% discordant (Group D) and are not considered further. The remaining two analyses returned ^{207}Pb/^{206}Pb ages of c. 2539 Ma and c. 2102 Ma. The discordant plotted data points do not define a meaningful discordance line. These analyses have apparent ^{207}Pb/^{206}Pb ages ranging from c. 4790 Ma to c. 2139 Ma.

A geochronological dataset for this sample has previously been described by Nelson (1999g). Eight analyses yielded a weighted mean ^{207}Pb*/^{206}Pb* date of 1999 ± 5 Ma (MSWD = 1.01), interpreted as the crystallisation age.

5.3.2.3 GSWA 142930

GSWA 142930 is a pegmatite that has intruded tonalite gneiss and fine-grained monzogranite of the Dalgaringa Supersuite (Nelson, 1999). Zircon grains were hand-picked from heavy mineral concentrates provided by the GSWA. Grains are light brown to black in colour, prismatic to subhedral in shape, and 100–200 µm in length. CL imaging revealed structureless and poorly luminescent, high uranium zircon. Weak oscillatory zoning is visible in some. Metamict patches are common. Forty-three analyses were obtained from 43 zircon grains. Twenty-one analyses are >5% discordant (Group D) and are not considered further. Thirteen analyses yield a weighted mean ^{207}Pb/^{206}Pb date of 1995 ± 7 Ma (MSWD = 0.5), interpreted as the timing of magmatic crystallisation. Four analyses (Group X) returned ^{207}Pb/^{206}Pb ages ranging between c. 2128 Ma and c. 2104 Ma, interpreted as representing inherited material. Five analyses (Group P) yield ^{207}Pb/^{206}Pb dates ranging between c. 1948 Ma and 1868 Ma and are interpreted to have undergone ancient radiogenic-Pb loss. The crystallisation age of 1995 ± 7 Ma is within error of the 1994 ± 2 Ma SHRIMP U–Pb age reported by Nelson (1999h).

5.3.2.4 GSWA 168951

GSWA 168951 is a metamonzogranite. Zircon grains were hand-picked from heavy mineral concentrates provided by the GSWA. Grains are dark brown to yellow-brown in colour, generally 120–250 µm in length and subrounded to prismatic in shape. Most have complex internal structures, with many grains displaying subheadral cores, many are metamict. Some have few or no visible growth zones, and some grains are rounded. Rims were generally too small to target, only cores were analysed. Inclusions are common. Forty-six analyses were carried out on forty-two grains. Twenty-nine analyses are >5% discordant (Group D) and are not considered further. Three analyses of the youngest cores return a weighted $^{207}Pb/^{206}Pb$ age of 1976 ± 20 Ma (MSWD = 0.78), interpreted as representing the minimum age of magmatic crystallisation. Fourteen analyses of (Group X) yield $^{207}Pb/^{206}Pb$ dates between c. 2523 Ma and 2023 Ma, interpreted as the ages of inherited material. The minimum crystallisation age of 1976 ± 20 Ma is younger than the maximum crystallisation SHRIMP U–Pb age previously established (2008 ± 3 Ma; Nelson, 2001d).

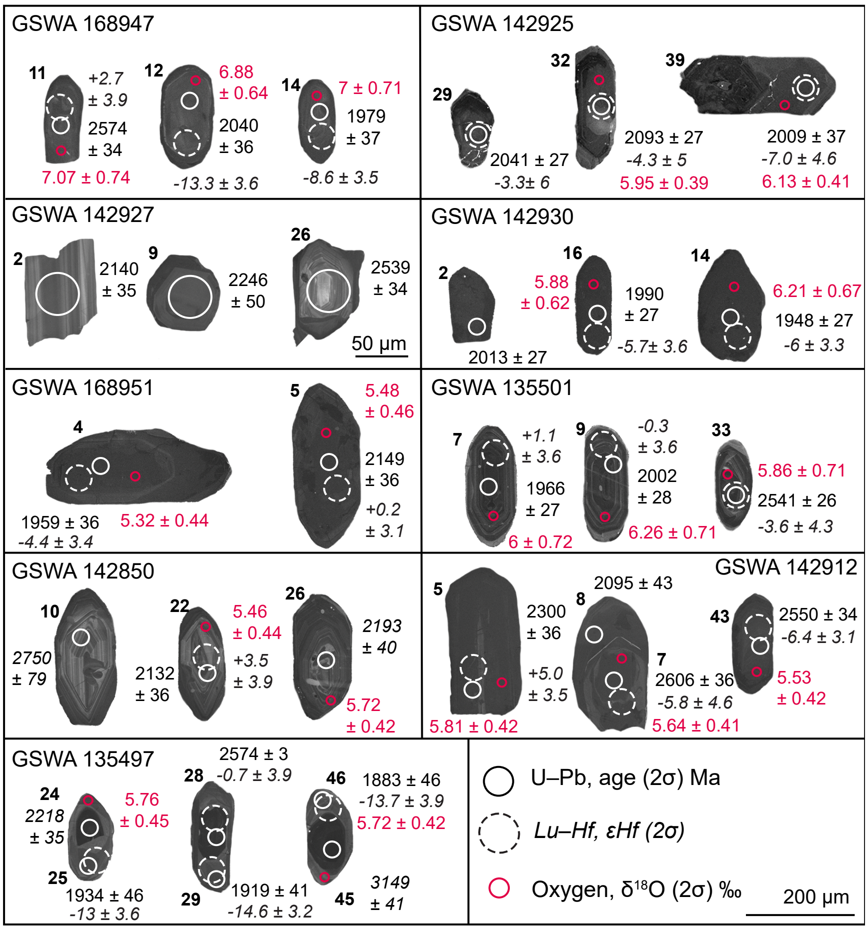

Figure 5.2 Representative CL images of zircon from Glenburgh Terrane samples. Ages in italics indicates discordance >10%.

5.3.3 Bertibubba Supersuite

The dataset from the Bertibubba Supersuite consists of four samples, and the analysed zircon cover a period of 1137 Myr, with individual ^{207}Pb/^{206}Pb ages between c. 3025 Ma and c. 1888 Ma. Granites were generated during a main magmatic episode at c. 1960 Ma.

5.3.3.1 GSWA 135501

GSWA 135501 is granodiorite. Zircon grains are light to dark brown in colour, 80–250 µm in length and subhedral, subrounded and prismatic in shape. CL imaging revealed oscillatory zoned cores surrounded by thin structureless rims of brighter luminescence. Forty-eight analyses were performed on forty-five grains, including both cores and rims identified by CL-imaging. Eighteen analyses (Group D) are >5% discordant and have been rejected. Two rims were analysed, returning ^{207}Pb/^{206}Pb dates of c. 1949 Ma and c. 1945 Ma, indistinguishable from ages obtained from cores. Thirty analyses of 28 cores and 2 rims (Group 1) yield a weighted mean ^{207}Pb/^{206}Pb age of 1967 ± 7 Ma (MSWD = 0.67), interpreted as the age of magmatic crystallization.

5.3.3.2 GSWA 142850

GSWA 142850 is a metagranite. Zircon grains were hand-picked from heavy mineral concentrates provided by the GSWA. Grains are subrounded to prismatic, colourless to pale pink in colour, and generally 120–250 µm in length. Grains generally display oscillatory zoned centres, and in some case, this zoning has become convoluted. A few zircon grains show recrystallised zones, crosscutting the original zoning. Forty-seven analyses were conducted on 47 grains. Forty-five analyses are >5% discordant (Group D) and are not considered further. Two analyses (Group 1) yield a weighted mean ^{207}Pb/^{206}Pb age of 1956 ± 27 Ma (MSWD = 0.96), interpreted as representing the maximum age of crystallisation. The maximum crystallisation age of 1956 ±27 Ma is in agreement with the SHRIMP U–Pb age previously established by the GSWA (1958 ± 4 Ma; Nelson, 1999b).

5.3.3.3 GSWA 142912

GSWA is a metamonzogranite. Zircon grains were hand-picked from heavy mineral concentrates provided by the GSWA. Grains are subrounded to prismatic, light- to dark-brown in colour and 80–250 µm in length. Grains generally display oscillatory zoned centres, and in some cases this zoning has become convoluted. Thin (<20 µm) CL-dark rims mantle some grains. Inclusions are common. Forty-five analyses were conducted on 42 zircon grains. Twenty-seven analyses are >5% discordant or indicate a high common Pb component (Group D) and are not considered further. Three analyses of cores (Group 1) yield a weighted mean ^{207}Pb/^{206}Pb age of 1944 ± 66 Ma (MSWD = 2), interpreted as representing the minimum age of crystallisation. Fifteen analyses

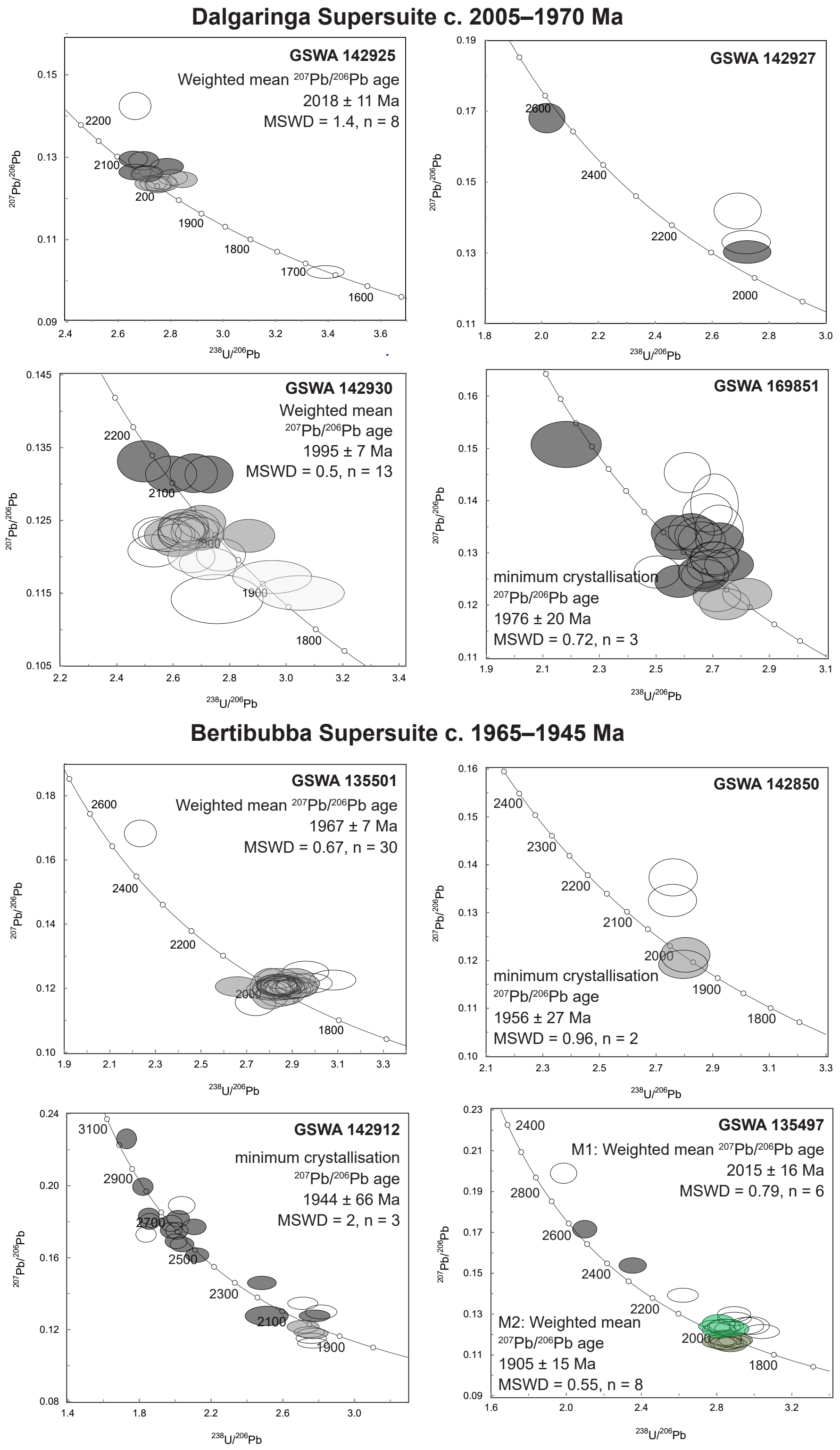

Figure 5.3 Concordia diagram showing the subset of results of zircon with <10% discordance. Grey ellipses indicate analyses used to calculate Group 1 (crystallisation age). Black ellipses indicate inherited zircon (Group X). Green ellipses indicate younger (metamorphic) zircon (Group M). Dark green ellipses indicate younger (metamorphic) zircon (Group M2) Light grey ellipses indicate radiogenic Pb-loss (Group P). Hollow ellipses indicate outside discordance threshold (Group D).

of cores yield (Group X) yield $^{207}Pb/^{206}Pb$ dates ranging from c. 3025 to 2066 Ma, interpreted as the ages of inherited material. The minimum crystallisation age of 1944 ± 66 Ma is in broad agreement with the SHRIMP U–Pb age previously established by the GSWA (1961 ± 3 Ma; Nelson, 1999c).

5.3.3.4 GSWA 135497

GSWA 135497 is a metagranite recovered near an outcrop of the Bertibubba Supersuite within the Yarlarweelor Gneiss Complex. Zircon grains extracted from this sample are 100–380 µm in length, pale pink to brown in colour and subrounded and prismatic to stubby in shape. CL images display homogenous cores which are mantled by high-CL-response, oscillatory zoned overgrowths ("light rims"). Weak oscillatory zoning is visible in some cores. The "light rims" have low U concentrations (70–196 ppm). Fifty-four analyses were conducted on 34 zircon grains. Thirty-eight analyses (Group D) that are >5% discordant or core-rim mixtures have been rejected. Six analyses of "light rims" and one core (Group M) yield a $^{207}Pb/^{206}Pb$ age of 2015 ± 16 (MSWD = 0.79). A total of eight analyses of three "light rims" and five sector zoned or recrystallised grains (Group M2) yield a $^{207}Pb/^{206}Pb$ age of 1905 ± 15 (MSWD = 0.55). Two analyses of cores (Group X) yield $^{207}Pb/^{206}Pb$ dates of c. 2574 and c. 2390 Ma, and are interpreted as inherited material. The age of 2015 ± 16 Ma indicated by Group M is interpreted to date zircon growth during metamorphism. The 1905 ± 15 Ma age indicated by Group M2 is interpreted to reflect the timing of zircon growth during a later deformation event.

5.4 ZIRCON TRACE-ELEMENT COMPOSITION

Zircon grains from the Halfway Gneiss, Dalgaringa and Bertibubba Supersuites have trace-element compositions that are typical of continental zircon, with both magmatic and inherited populations plotting within continental arc-type zircon fields. Chondrite-normalised REE element patterns of magmatic zircons from all samples are characterised by positive Ce and moderate negative Eu anomalies and a positive heavy REE (HREE) slope, consistent with growth of zircon in a magmatic environment (Fig. 5.4; Rubatto and Hermann, 2007; Hoskin and Black, 2000; Hoskin and Ireland, 2000). There is no significant difference in the REE composition of zircon in overgrowths and/or recrystallised zones versus that in oscillatory-zoned cores.

Minor variation in the overall REE abundances and in the degree of Eu/Eu*occurs between and within samples; however no systematic change was recognised. Magmatic zircon trace element signatures indicate no evidence of co-crystallisation with garnet (i.e. flat HREE pattern with Lu/Gd <3 paired with no negative Eu anomaly, Eu/Eu* >0.75; Rubatto and Hermann, 2007), indicating formation in lower pressures than eclogitic minerals (<1.2 GPa, <45 km depth;

Rubatto and Hermann, 2007). All samples record zircon Ti temperatures with averages between 680°C and 800°C.

5.4.1 Halfway Gneiss

Zircon in the Halfway Gneiss show a near flat M-HREE slope (Yb_N/Gd_N = 7–8) and a small Eu anomaly (Eu/Eu*= 0.10–0.15).

5.4.2 Dalgaringa Supersuite

Magmatic zircon have a steep positive M-HREE slope (Yb_N/Gd_N = 12–113) and highly negative

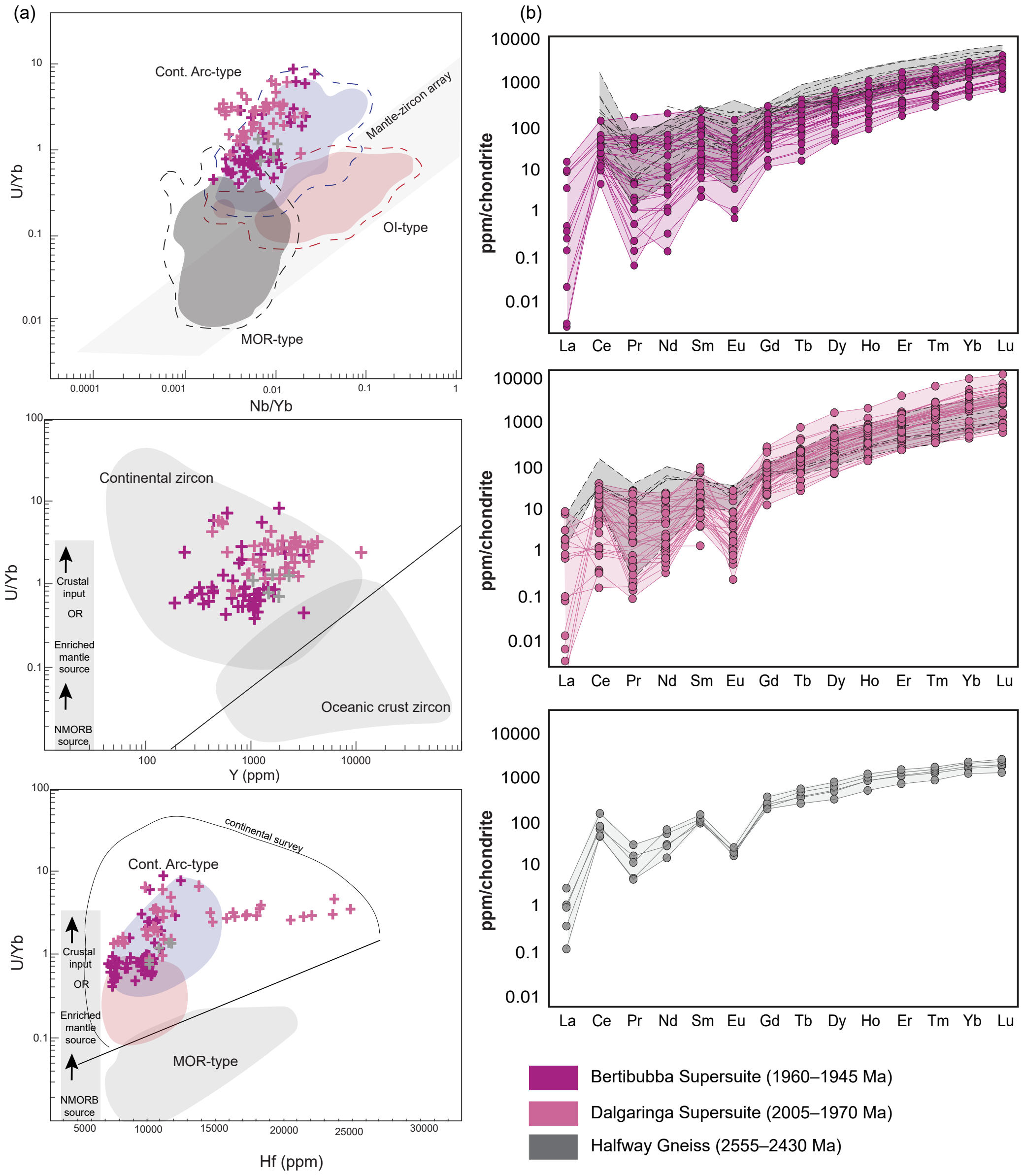

Figure 5.4 (a) Discrimination diagrams for trace elements in Glenburgh Terrane samples, after Grimes et al. (2007, 2015), (b) chondrite-normalised trace element plots

Eu anomaly (Eu/Eu*= 0.01–0.52). Inherited zircon have a slightly flatter M–HREE slope (Yb_N/Gd_N = 7–26) and small Eu anomalies (Eu/Eu* = 0.27–0.52).

5.4.3 Bertibubba Supersuite

Magmatic zircon have a steep positive M-HREE slope (Yb_N/Gd_N = 13–38) and small negative Eu anomaly (Eu/Eu*= 0.13–0.80). Inherited zircon display a similar M–HREE slope and Eu anomaly (Yb_N/Gd_N = 6–36; Eu/Eu* = 0.31–0.76). Zircon rims display a similar M–HREE slope and Eu anomaly (Yb_N/Gd_N = 6–23; Eu/Eu* = 0.38–0.63).

5.5 Lu–Hf ISOTOPE DATA

A total of 92 analyses were obtained from 8 samples and include analyses of groups that are interpreted to date crystallisation, inherited and metamorphic zircon. Twelve analyses have been rejected due to either poor U–Pb age data (high discordance), no available U–Pb data or the ablated area consisted of core-rim mixtures or cracks (see Appendix C).

Table 5.2 Summary of zircon hafnium and oxygen isotope data

Sample	**Unit**[1]	**Pb-Pb age (Ma)**	**εHf**[2]	**εHf range**	**TDMC**[3]	**$\delta^{18}O$**[4] **(‰)**	**$\delta^{18}O$ range (‰)**
168947	HG	2042 ± 59	-10.6 ± 3.9 (3)	-13.3 to -8.6	-	6.9 ± 0.2 (3)	6.77–7.0
142925	DS	2024 ± 12	-3.9 ± 3.0 (6)	-6.8 to -3.3	3077–2895	5.99 ± 0.36 (10)	5.73–6.3
142927	DS	-	-	-	-	-	-
142930	DS	1995 ± 7	-3.5 ± 4.5 (11)	-7.2 to 0	3093–2668	6.44 ± 1.1 (11)	5.88–7.55
168951	DS	(1976 ± 20)	-6.1 ± 2.0 (3)	-6.8 to -4.4	3063–2890	4.93 ± 1.05 (3)	4.31–5.32
135501	BS	1967 ± 7	-1.3 ± 2.5 (16)	-3.2 to +1.1	2807–2598	5.81 ± 0.85 (14)	4.86–6.37
142850	BS	(1956 ± 27)	-0.2 ± 6.1 (2)	-3.3 to +2.8	2440	5.79 ± 0.39 (1)	-
142912	BS	(1944 ± 66)	-6.5 ± 4.6 (2)	-8.8 to -4.4	3142	5.8 ± 0.49 (2)	5.55–6.04
135497	BS	2015 ± 16, 1905 ± 15	-7.5 (1), -13.7 ± 3.7(7)	-7.5, -16 to -11.1	3127, 3582–3127	5.93, 5.84 ± 0.83(6)	5.17–6.52

[1] HG = Halfway Gneiss, DS = Dalgaringa Supersuite, BS = Bertibubba Supersuite

[2] εHf values of magmatic zircon are expressed as median values in, ±2SD. Number of analyses donated in brackets.

[3] TDMC will only be quoted where $\delta^{18}O$ are within mantle (5.3 ± 0.6 ‰, 2σ) values

[4] $\delta^{18}O$ values of magmatic zircon are expressed as averages, ±2SD. Number of analyses donated in brackets. (-) indicates no value obtained. Where no value is obtained for magmatic zircon, the range reflects values from inherited zircon.

5.5.1 Halfway Gneiss

Magmatic zircon grains (n=3) yield a range of initial $^{176}Hf/^{177}Hf$ ratios between 0.281110 and 0.281227 (εHf_t -13.3 and -8.6, median εHf_t -10.6 ± 3.9, 2SD). Inherited zircon grains (n=3) with $^{207}Pb/^{206}Pb$ ages between c. 2574 and c. 2188 Ma yield a range of εHf_t values between -4.8 and +2.7. One analyses with $^{207}Pb/^{206}Pb$ age of c. 1979 Ma, interpreted as having undergone ancient radiogenic-Pb loss, returned εHf_t values of -8.6.

5.5.2 Dalgaringa Supersuite

A total of 33 Magmatic and inherited zircon grains were analysed from three samples. Magmatic grains (n=19) yield a range of initial ^{176}Hf/^{177}Hf ratios between 0.281307 and 0.281511 (εHf$_t$ -7.2 and 0). T$_{DM}^{C}$ values range between 3094 Ma and 2668 Ma. Median values (magmatic) range between -6.1 ± 2 and -3.3 ± 4.5 (2SD). Inherited zircon grains (n=13) with ^{207}Pb/^{206}Pb ages ranging between c. 2511and 2064 Ma returned a εHf$_t$ value ranging from -7 to +4.5, corresponding to T$_{DM}^{C}$ values between 3122 and 2616 Ma. One analyses with ^{207}Pb/^{206}Pb age of c. 1930 Ma, interpreted as having undergone ancient radiogenic-Pb loss, returned εHf$_t$ values of –4.7.

5.5.3 Bertibubba Supersuite

A total of 40 Magmatic, metamorphic and inherited zircon grains were analysed from four samples. Magmatic grains (n=20) yield a range of initial ^{176}Hf/^{177}Hf ratios between 0.281304 and 0.281607 (εHf$_t$ -8.8 and +2.8). T$_{DM}^{C}$ values range between 3148 and 2440 Ma. Median εHf$_t$ values (magmatic) range between -6.5 ± 4.6 and -0.2 ± 6.1 (2SD). Inherited zircon grains (n=12) with ^{207}Pb/^{206}Pb ages ranging between c. 2823 and 2066 Ma returned a εHf$_t$ value ranging from -8.4 to +6.5, corresponding to T$_{DM}^{C}$ values between 3569 and 2520 Ma. Metamorphic zircon grains (n=8) with ^{207}Pb/^{206}Pb ages ranging between c. 2015 and 1934 Ma returned a εHf$_t$ value ranging between -14.7 and -7.5.

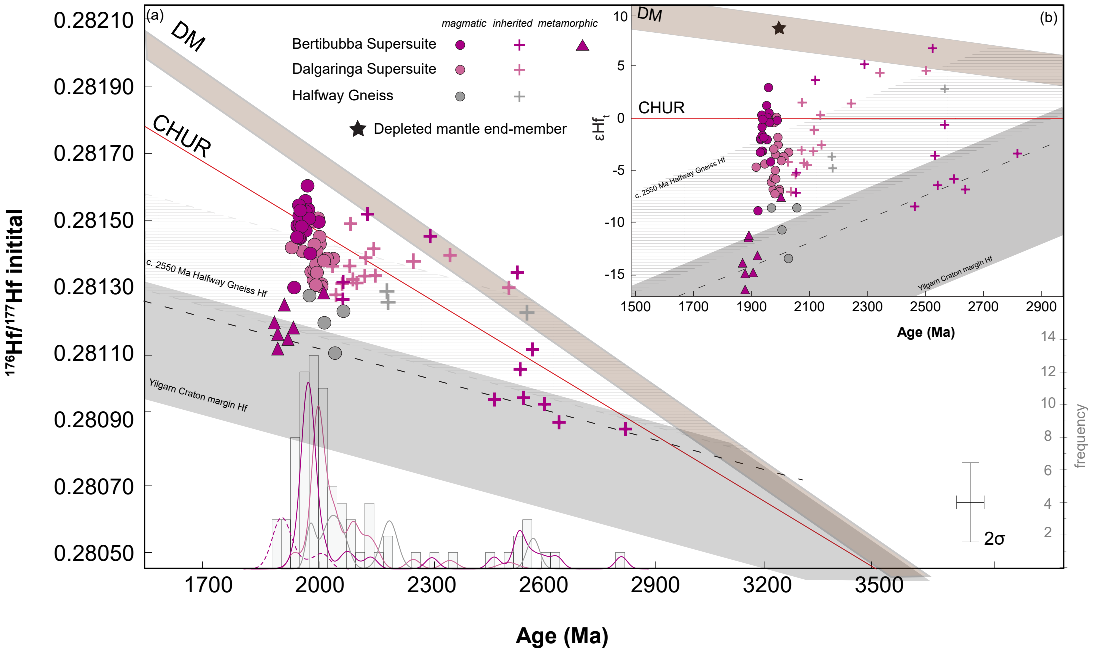

Figure 5.5 Lu–Hf isotope results from the Glenburgh Orogeny samples. Grey shaded area: isotopic envelope for the Yilgarn Craton margin Hf (magmatic), and striped area: isotopic envelope for the Halfway Gneiss Hf (Chapter 4). The dashed line is a reference evolution line corresponding to a Lu/Hf ratio of 0.015. (a) ^{176}Hf/^{177}Hf initial ratios versus age (n = 82), and (b) εHf$_t$ versus age for zircon from samples from the Glenburgh Terrane.

5.6 OXYGEN ISOTOPE DATA

A total of 94 zircon grains were analysed from 8 samples (Fig. 5.6) and include analyses of groups that are interpreted to date crystallisation, inherited and metamorphic zircon. Three analyses were rejected due to ablated area consisting of metamict patches, cracks or edges (see Appendix C).

5.6.1 Halfway Gneiss

A total of seven zircon grains were analysed from one sample. $\delta^{18}O$ values range between 6.77 and 7.53‰. Magmatic grains (n=3) yield a range of $\delta^{18}O$ values between 6.77 and 7‰, with an average $\delta^{18}O$ of magmatic zircon of 6.88 ± 0.19‰, 2SD. Inherited zircon grains (n=3) with $^{207}Pb/^{206}Pb$ ages ranging between 2574 Ma to 2191 Ma yield a range of $\delta^{18}O$ values between 7.07 to 7.53‰. One analysis with no reliable U–Pb data yielded a $\delta^{18}O$ values of 7.32‰.

5.6.2 Dalgaringa Supersuite

Forty zircon grains were analysed from three samples. $\delta^{18}O$ values of all analysed samples range between 3.93 and 7.55‰. Magmatic grains (n=21) yield a range of $\delta^{18}O$ values between 4.31 and 7.55‰, with the average $\delta^{18}O$ of magmatic zircon from each sample varying from 4.93 ±

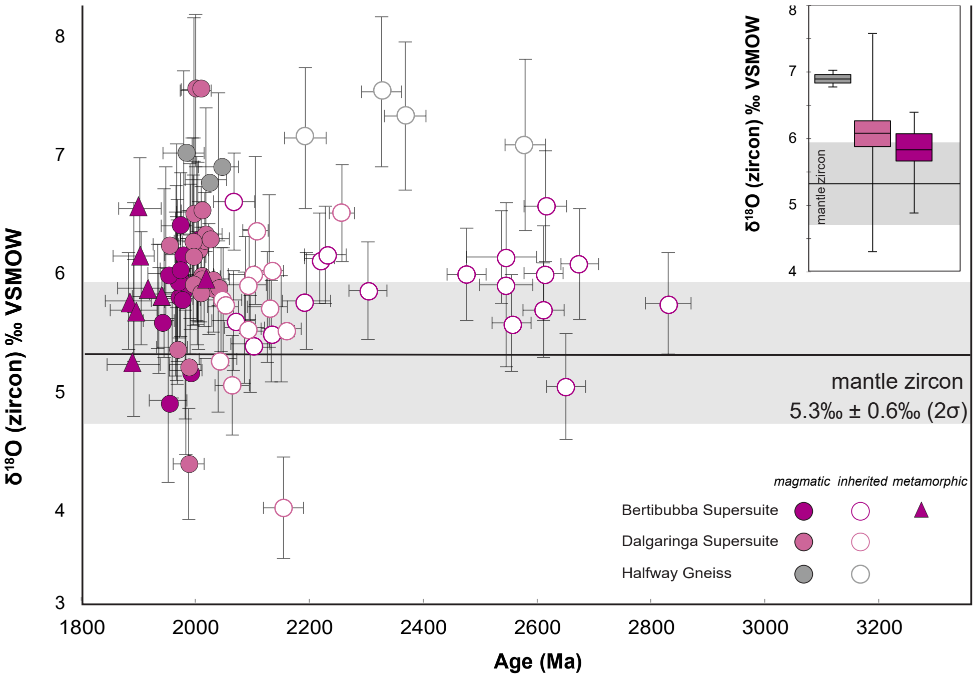

Figure 5.6 (a) $\delta^{18}O$ versus age (n = 86). The compositional field for zircon in equilibrium with mantle-derived melts has a $\delta^{18}O$ VSMOW value of 5.3 ± 0.6‰ (2σ; Valley et al., 2005), (b) Box-and-whisker plots showing the range and median values of $\delta^{18}O$ VSMOW compositions.

1.05 to 6.44 ± 1.1‰, 2SD. Inherited zircon grains (n=12) with $^{207}Pb/^{206}Pb$ ages ranging between 2255 and 2039 Ma yield a range of $\delta^{18}O$ values between 3.93 to 6.48‰. Analyses of zircon cores with no reliable U–Pb data associated with them (n=6) yield a range of $\delta^{18}O$ values between 5.29 and 6.85‰.

5.6.3 Bertibubba Supersuite

Forty-four zircon grains were analysed from four samples. $\delta^{18}O$ values of all analysed samples range between 4.86 and 6.58‰ . Magmatic grains (n=13) yield a range of $\delta^{18}O$ values between 4.86 and 6.37‰, with one sample yielding an average $\delta^{18}O$ of 5.80 ± 0.87‰, 2SD. Inherited zircon grains (n=18) with $^{207}Pb/^{206}Pb$ ages ranging between 2823 and 2066 Ma yield a range of $\delta^{18}O$ values between 4.98 and 6.58‰. Metamorphic zircon (n=8) yield a range of $\delta^{18}O$ values between 5.17 and 6.52‰ (average 5.82 ± 0.77‰, n=7). Analyses of zircon cores with no reliable U–Pb ages associated with them (n=5) yield a range of $\delta^{18}O$ values between 5.15 and 6.30‰.

5.7 DISCUSSION

5.7.1 Previous isotopic constraints

Whole-rock chemistry exists for the Dalgaringa and Bertibubba Supersuite. Granitoids of the Dalgaringa Supersuite are metaluminous to weakly peraluminous, with whole-rock compositions similar to Andean-type subduction zone magmas (Sheppard et al., 2004), and is interpreted to have formed on the southern margin of the Glenburgh Terrane above a northwestern dipping subduction zone (Occhipinti et al., 2004; Sheppard et al. 2004; Johnson et al., 2010; 2013). Whole-rock Sm–Nd analyses of the Dalgaringa Supersuite record intial εNd values between -5.67 to -1.31, with model ages from 3720–2640 Ma (Sheppard et al., 2004). This was interpreted to indicate melting a source comprising a mixture of basaltic rock and some felsic rock(s) with an evolved isotopic composition, similar to the c. 2550 Ma protoliths of the Halfway Gneiss, as well as an additional felsic component (Sheppard et al., 2004). Similarly, zircon Lu–Hf isotopic data from the Glenburgh Terrane with age components of c. 2025–1955 Ma that show εHf_t values between -10.3 and +7.5, also indicating mixing between mantle-derived juvenile arc material and a rock(s) with similar isotopic compositions to those of the Halfway Gneiss (Johnson et al., 2011b; 2017). The Bertibubba Supersuite granitoids have initial εNd values between -11.09 and -3.51, with model Nd ages in the range of 2915–2675 Ma (Sheppard et al., 2004). These εNd values are more unradiogenic relative to the remainder of the Dalgaringa samples (-5.67 to -1.31), and Sheppard et al. (2004) interpreted the sources for the Bertibubba Supersuite consisted of Dalgaringa Supersuite with minor amounts of Archaean Narryer Terrane.

5.7.2 Timing of magmatism and significance of inherited ages

The analysed zircon from the Glenburgh Terrane samples cover a period of 1142 Myr, with individual $^{207}Pb/^{206}Pb$ ages ranging from c. 3025 Ma to c. 1883 Ma, with peaks at c. 2655–2545 Ma, c. 2100 Ma, c. 1995 Ma and c. 1965 Ma (Fig. 5.7). The Dalgaringa Supersuite samples are dominated by inherited material, with a total of 53% of concordant analyses indicating Palaeoproterozoic ages, ranging between c. 2539 and c. 2023 Ma. The magmatic ages established are in broad agreement with the c. 2005–1970 Ma age range established for the Dalgaringa Supersuite (Sheppard et al., 2004). Previous geochronology of the Dalgaringa Supersuite indicate individual (magmatic) $^{207}Pb/^{206}Pb$ ages zircon ages between c. 2024 Ma and c. 1923 Ma, and a limited number of inherited zircon (7%) with ages ranging between c. 2712–1928 Ma (Nelson, 2001e). Samples from the Bertibubba Supersuite have magmatic ages ranging between c. 1967 and 1944 Ma. Inherited ages are significantly older than those reported for the Dalgaringa Supersuite, with ages ranging between c. 3025 Ma and c. 2066 Ma.

The presence of Archaean inherited zircon components in the Bertibubba Supersuite can be attributed to their spatial location. The Bertibubba Supersuite intruded the northern margin of the Yilgarn Craton (Narryer Terrane), and the inherited material have mainly Archaean ages, which reflect the 3300–2640 Ma protolith ages established for the granitic gneisses of the Yarlarweelor Gneiss Complex (Nelson, 1998a; 1999i). Samples from both the Dalgaringa and Bertibubba Supersuites contain inherited zircon with ages similar to the c. 2550–2430 Ma protolith ages established for orthogneisses of the Halfway Gneiss (Johnson et al., 2011a). However, the majority of the inherited zircons yield $^{207}Pb/^{206}Pb$ ages that are between c. 2350 Ma and c. 2020 Ma, with a major peak at c. 2095 Ma. These ages are younger than the crystallisation ages of the Halfway Gneiss protoliths, however, rare magmatic grains with ages between c. 2342 Ma to c. 2082 Ma have been reported in other samples (e.g. Nelson, 2001e; Kinny et al., 2004; Wingate et al., 2010g). Johnson et al. (2010) reported similar aged inheritance from the Dalgaringa Supersuite (c. 2055–2020 Ma) and within the metasediments of the Camel Hill Metamorphics. These inherited and detrital zircon grains have moderately evolved Hf isotopic compositions, and Johnson et al. (2010) interpreted them as representing an older, unexposed proto-Dalgaringa arc. Detrital zircon in the metasedimentary units within the Gascoyne Province commonly preserve this age (c. 2095–2050 Ma), and support the interpretation that magmatism in the Dalgaringa Arc began prior to c. 2005 Ma, with erosional removal of arc crust occurring sometime before the deposition of the c. 2000–1955 Ma Camel Hill Metamorphics (Johnson et al., 2010).

All samples therefore provide evidence for Neoarchaean to Palaeoproterozoic events which occurred prior to the intrusion of the Dalgaringa Supersuite. The inherited zircon also indicate that significant proportions of crust of this age (Palaeoproterozoic) is present within, or was involved in the formation of the Dalgaringa Supersuite and Bertibubba Supersuite. In summary, the dominance of the inherited U–Pb ages, and the paucity of dated granitoids of this age, indicates that granitic magmatism in the Dalgaringa Arc likely started prior to ages indicated by currently exposed rocks. This supports the U–Pb and Hf isotopic evidence of Johnson et al. (2010) of a proto-Dalgaringa arc.

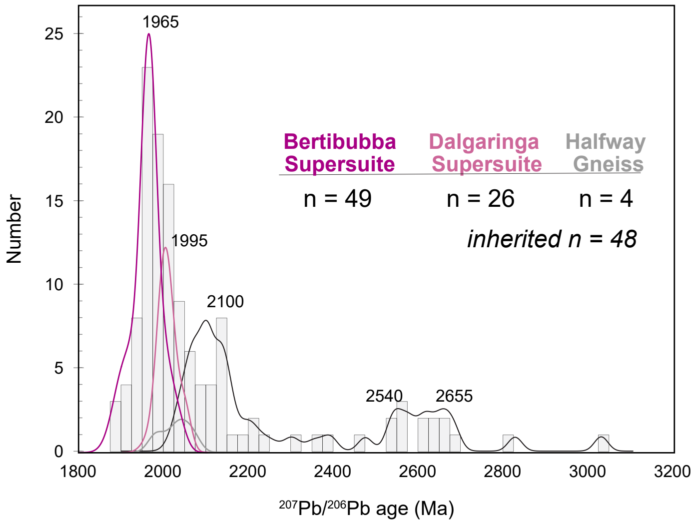

Figure 5.7 Probability plot of magmatic and inherited zircon U–Pb data

5.7.3 Development of crustal components – evidence from hafnium isotopes

The Dalgaringa Supersuite samples are characterised by negative εHf$_t$ values (-7.2 and 0). The predominance of evolved (unradiogenic) εHf$_t$ values in the samples suggests that suggests that extensive reworking appears to dominate, and implies that the magmas from which these zircon crystallised was derived, at least in part, from remelting of older crustal components with more evolved Lu/Hf compositions than CHUR. Hf model ages are 1100–677 Myr older than the crystallisation ages of the samples, which also indicates that there was significant contribution from older crustal material. Whole-rock geochemical and isotopic compositions indicate that the Dalgaringa Supersuite formed at a continental-margin arc above a northwestward dipping subduction zone (Sheppard et al. 2004). Subsequently, incorporation of older crustal material into the sources of the Palaeoproterozoic granites is assumed to occur through either crustal contamination, whereby juvenile mantle-like sources are mixed with older material during differentiation in the crust, or incorporation of material during emplacement, or contamination from subduction, where subducted sediments are mixed with depleted mantle.

Magmatic zircon with crystallisation ages between c. 2044–1959 Ma display dominantly unradiogenic initial $^{176}Hf/^{177}Hf$ ratios between 0.2813069 and 0.2815109 (εHf_t -7.2 to 0). Those with mantle like $\delta^{18}O$ values return T_{DM}^{C} ages between 3094 and 2668 Ma. Crustal evolution lines defined source $^{176}Lu/^{177}Hf$ values of 0.015 (Griffin et al., 2002) are plotted from analyses of the Halfway Gneiss (Archaean protolith) and the Yilgarn Craton (Fig. 5.5). The Dalgaringa Supersuite lie within the Halfway Gneiss isotopic envelope. This suggests that parental magmas of the c. 2044–1959 Ma granites interacted with, or were derived from reworking of a source possessing broadly similar $^{176}Lu/^{177}Hf$ ratios, such as the Halfway Gneiss. Inherited zircon grains have compositions which plot along this evolution line, and are consistent the interpretation that the Dalgaringa Supersuite was sourced from reworking of the Halfway Gneiss.

By contrast to the Dalgaringa Supersuite granites, the Hf isotope data for the c. 2002–1936 Ma granites from the Bertibubba Supersuite show a change to much more radiogenic initial $^{176}Hf/^{177}Hf$ ratios of 0.2813040–0.2816071 (εHf_t -8.8 to +2.8). Those with mantle like $\delta^{18}O$ values return T_{DM}^{C} ages between 3148 and 2440 Ma. The range in εHf_t values reflects a heterogeneous magma at the time of crystallisation, and suggests melt production from mixed sources: an older crustal component with T_{DM}^{C} ages of 3148 Ma and an additional juvenile component extracted from the mantle at c. 2440 Ma. The Hf-isotope array extends to highly negative εHf_t values, suggesting variable degrees of mixing with more evolved crustal components. As the Hf-isotope array lies within the Halfway Gneiss isotopic envelope, it would be possible to produce the isotopic array by mixing of high Lu/Hf mantle sources and enriched crustal sources with compositions similar to the Halfway Gneiss and/or the Dalgaringa Supersuite. However, inherited zircon with $^{207}Pb/^{206}Pb$ ages between c. 2823 and 2066 Ma have Hf compositions (εHf_t -6.8 to +6.5) that lie within both the Halfway Gneiss and Yilgarn Craton granites Hf–U–Pb field. This suggests that the Bertibubba Supersuite sourced a range of Yilgarn Craton and Halfway Gneiss material and mixed with an additional juvenile component at the time of emplacement. Therefore, the likely sources for the Bertibubba Supersuite are the Glenburgh Terrane granites, with minor amounts of Yilgarn Craton granites.

The shift from the dominantly unradiogenic εHf_t values of the Dalgaringa Supersuite granitoids to the more radiogenic values recorded in the Bertibubba Supersuite granitoids (Fig. 5.5) indicates a significant increase in juvenile mafic magma in the generation of these granitoids. It is possible that the change to more radiogenic sources was a response to slab break off, resulting in the partial melting of the mafic lower crust (Davies and von Blanckenburg, 1995). Magmatism generated due to slab detachment would also account for the narrow and linear distribution of the Bertibubba Supersuite along the Errabiddy Shear Zone (Fig. 5.1).

5.7.3.1 Enigmatic rocks – the case of sample GSWA 135497

GSWA 135497 is a metagranite recovered near an outcrop of the Bertibubba Supersuite within the Yarlarweelor Gneiss Complex and indicates two periods of metamorphism at 2015 ± 16 Ma (M) and 1905 ± 15 Ma (M2). The c. 2015 Ma rims indicate Dalgaringa Supersuite ages. However, geochemical and isotopic data indicates that the Dalgaringa Supersuite formed on the crust of the Glenburgh Terrane above a northwestward dipping subduction zone (Sheppard et al. 2004), i.e. no Dalgaringa Supersuite or Halfway Gneiss equivalents have been found on the Yilgarn Craton margin crust. Variably discordant (6–17%) analyses of cores indicate ^{207}Pb/^{206}Pb ages between 2851–1978 Ma, with the majority indicating Dalgaringa Supersuite ages (Fig. 5.3). It is possible that all zircon are inherited material from a gneiss which contains Dalgaringa Supersuite and Halfway Gneiss protoliths that were assimilated into c. 1965 Ma melts and emplaced in the YGC after the collision of Glenburgh Terrane and Yilgarn Craton, and any Bertibubba magmatism overprinted by the c. 1905 Ma event.

The c. 2015 Ma zircon indicates an initial ^{176}Hf/^{177}Hf ratio of 0.281290 (εHf$_t$ -7.5). The c. 1905 Ma indicate initial ^{176}Hf/^{177}Hf ratios between 0.2811227 and 0.2812584 (εHf$_t$ -16.7 and -11.1). If the metamorphic zircon formed by a pseudomorphic alteration process they will preserve its primary Hf isotopic composition (Zeh et al., 2010). However, if the metamorphic zircon precipitates from a fluid or melt, the Hf isotopic composition will reflect the isotopic composition of the external sources. The measured ^{176}Hf/^{177}Hf ratios (0.281139–0.281310) all indicate values more evolved than those of the Dalgaringa and Bertibubba Supersuite (0.281330–0.281650). However, they are comparable to the Halfway Gneiss analyses (0.281160–0.281260). This suggests that the Hf-isotopic composition of the metamorphic zircon reflects the initial isotopic composition of their magmatic cores. A possible scenario to explain these data is that the granite was initially of Halfway Gneiss protolith composition, which was intruded by Dalgaringa Supersuite during the early stages of the Glenburgh Orogeny and was subsequently deformed and metamorphosed.

5.7.4 Contamination of magmas

One of the major limitations in the interpretation of radiogenic isotopic data lies in identifying whether rocks with evolved isotopic signatures were derived from mixed juvenile and recycled metasedimentary sources, or from mantle derived sources that have aged in the deep crust. Isotopic partitioning in stable isotope systems (oxygen) occurs as a result of chemical, rather than nuclear, fractionation processes, and is therefore independent of time (Roberts and Spencer, 2015). Consequently, the measured δ^{18}O composition of magmatic zircon grains will reflect that of the source and associated contaminants, and can be used to trace different source contributions (Bindeman, 1999). Mantle magmas have an average δ^{18}O of 5.3 ± 0.6‰, and deviations from this value can only be achieved by mixing with material of a different $\delta^{18}O$ composition (Valley, 2003). High-$\delta^{18}O$ magmatic values (>6.5‰) are attributed to incorporation of an elevated $\delta^{18}O$ component, such as buried sediments or other supracrustal material, during magma generation (Valley et al. 2005, Cavosie et al., 2005). Magmatic zircon with low-$\delta^{18}O$ values are interpreted to result from incorporation of material that has undergone 'high temperature' alteration (Valley et al. 2005).

Zircon grains from the Glenburgh Terrane samples record average $\delta^{18}O$ values between 4.93 ± 1.05 and 6.9 ± 0.2‰ (2SD). With the exception of sample GSWA 142930 and GSWA 168947 all analyses have $\delta^{18}O$ values that are within error of the field of mantle zircon. This indicates that the magmas that the zircon crystallised from did not interact with any metasedimentary material, and contained significant low-$\delta^{18}O$ material representing an infracrustal source component with mantle-like $\delta^{18}O$. GSWA 142930 and GSWA 168947 record a range of $\delta^{18}O$ of 5.88–7.55‰, suggesting the involvement of an $\delta^{18}O$-enriched crustal material either through partial melting of a high-$\delta^{18}O$ material, or by assimilation into the host magma from surrounding crust during magma ascent and/or emplacement. The occurrence of minor amounts of low $\delta^{18}O$ values of magmatic and inherited zircon in sample GSWA 168951 (3.93–5.17‰) suggests possible interaction with waters derived from country rocks.

5.7.5 Potential magma sources: Hf–O modelling

εHf_t values of all Dalgaringa Supersuite samples are negative (-7.2 to 0) coupled with predominantly mantle-like $\delta^{18}O$ values (4.31–7.55‰, average 6.01 ± 1.24‰ 2SD, n = 19). The occurrence of magmatic and inherited zircon with high $\delta^{18}O$ values (6.88–7.55‰) indicates incorporation of a high $\delta^{18}O$ material into the melt source and may represent an additional metasedimentary source component. This Hf–O isotope array can be accounted for by either (1) the Dalgaringa Supersuite were sourced from melts that experienced magma mixing, or (2) they were sourced from depleted mantle and subsequently assimilated a significant proportion of an evolved crustal component during magma differentiation. There are essentially three end-member components involved: a juvenile (depleted-mantle) component, a low-$\delta^{18}O$ material representing an infracrustal source component with mantle-like $\delta^{18}O$ and an additional high-$\delta^{18}O$ metasedimentary component.

In order to estimate the proportion of old crust in the source necessary to drive a depleted mantle-derived melt to the Hf isotopic composition observed in the Glenburgh Terrane samples a simple two-component mixing model is used (Fig. 5.8). The Hf isotope composition of the crustal end-member was estimated from the average measured Hf data from the Halfway Gneiss samples calculated at c. 2000 Ma (εHf_t -11.8), and the mantle end-member uses a εHf_t value of

+8.6 (appropriate for the depleted-mantle at 2000 Ma; Fig. 5.5). A $\delta^{18}O$ value of 7.1‰ is used for the crustal component, and is based on the maximum $\delta^{18}O$ value measured from the Halfway Gneiss (Chapter 4). The proportion of mantle component is dependent on the concentration ratio of the mantle-derived magma and assimilated continental crust. The Hf concentration of the crustal end-member and mantle end-member was set at values 5.3, 1.9 and 0.2 ppm, estimates for the upper crust, lower crust and depleted mantle, respectively (Rudnick and Gao, 2003; Salters and Stracke, 2004). Following the methods of Roberts (2010), using depleted mantle combined with upper crustal values is compatible with a source contamination model; whereas using lower crust and average crust combined with upper crust values is compatible with a crustal contamination model. Bulk mixing curves for mixing between depleted mantle and the crustal end indicate that the majority of the data lies above the mixing curve. This suggests mixing between an alternative end-member. Using the maximum $\delta^{18}O$ value of mantle zircon of 5.9‰ for the depleted mantle component that approximates an enriched mantle (mixed mantle/crustal source) the mixing curve demonstrates that the Dalgaringa Supersuite granites can be modelled with bulk-mixing between a slightly enriched mantle component with a 15–55% contribution from an older crustal component (comparable with a Halfway Gneiss composition). The slightly elevated $\delta^{18}O$ compositions suggest introduction of a high-$\delta^{18}O$ component to the source region. The Bertibubba Supersuite indicate a 12–30 % contribution. The Halfway Gneiss protoliths have Hf–O compositions that are indistinguishable from the Archaean granitic components at

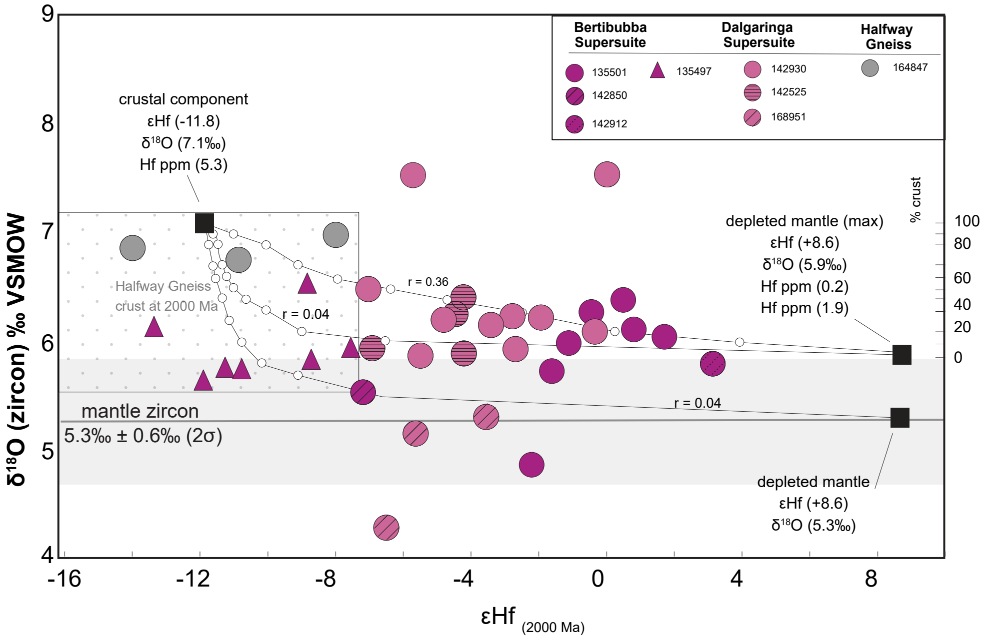

Figure 5.8 Plot of $\delta^{18}O$ versus εHf_t for zircon from the Glenburgh Terrane with bulk mixing model between depleted mantle and crustal source component. The parameters of end members are discussed in text. Bulk mixing curves are marked at 10% increments.

c. 2000 Ma (Fig. 5.8). Similarly, the metamorphic zircon from the Bertibubba Supersuite have compositions equivalent to the Halfway Gneiss, and could therefore have formed by melting of rocks with Halfway Gneiss composition. This supports the interpretation that the rock was initially of Halfway Gneiss composition which was intruded by Dalgaringa Supersuite, resulting in the growth of metamorphic rims at 2015 ± 16 Ma.

In subduction zones the interaction of fluids and/or melt derived from the subducting plate with the overlying mantle wedge, resulting in a heterogeneous mantle source (Pearce and Peate, 1995; Plank and Langmuir, 1998; Currie et al., 2007). The introduction of high-$\delta^{18}O$ material (i.e. sediments) to the mantle has been suggested to cause mantle oxygen isotope heterogeneity (e.g. Woodhead et al., 1993; Vroon et al., 2001; Lackey et al., 2005; Roberts et al., 2013), which can account for the derivation from pristine depleted-mantle values of 5.3 ± 0.6‰ (2σ; Valley et al., 2005) observed in the two component mixing model (Fig. 5.8).

5.8 SUMMARY

- The Dalgaringa and Bertibbua Superusite granites are characterised by variably evolved εHf_t coupled with mantle-derived to slightly elevated mean $\delta^{18}O$ compositions, indicating a period of crustal growth prior to and after continental collision. Two component mixing calculations indicate 45–85% mantle contribution.

- Hf–O isotope data show Glenburgh Orogeny magmatism involved recycling of previously formed continental crust, with bulk-mixing calculations indicating 20–55% involvement of a (low- $\delta^{18}O$ and variably evolved) mid- to lower-crustal component, with a composition equivalent to the Halfway Gneiss.

- Two component mixing modelling indicates the depleted mantle component had elevated $\delta^{18}O$, suggesting introduction of a high-$\delta^{18}O$ component to the source region, likely to have been incorporated by the interaction of fluids and/or melt derived from the subducting plate with the overlying mantle wedge.

CHAPTER 6

INTRACRUSTAL REWORKING — THE CAPRICORN OROGENY (c. 1820–1770 Ma)

6.1 INTRODUCTION

Granites are the direct product of the processes of partial melting and magmatic differentiation, and granitic suites commonly display significant variations in composition (Chappell, 2004). The differences in the isotopic compositions of granitic rocks are largely determined by the chemistry of their source rocks, as well as those of assimilated crustal components involved during their formation. Therefore, accurately identifying granitic sources, and the relative contributions of recycled crustal components, is essential to understanding the generation and evolution of the crust. Integrated U–Pb, Hf and O isotope analysis of zircon allows determination of magmatic and metamorphic ages, recognition of mantle-derived components and distinction between recycled metasedimentary (supracrustal) sources from pre-exisiting igneous (infracrustal) sources that have aged in the deep crust (e.g. Hawkesworth and Kemp, 2006).

The Capricorn Orogen records the Palaeoproterozoic collision of the Yilgarn and Pilbara Cratons to form the West Australian Craton, and over one billion years of subsequent intracontinental crustal reworking. U–Pb zircon geochronology records three discrete tectono-magmatic events that resulted in voluminous granitic magmatism: the 2005–1975 Ma Glenburgh Orogeny, the 1820–1770 Ma Capricorn Orogeny, and the 1680–1620 Ma Mangaroon Orogeny (Sheppard et al., 2010a; Johnson et al., 2013). The 1820–1770 Ma Capricorn Orogeny is associated with low- to medium-grade metamorphism and intense structural reworking, the intrusion of voluminous granitic magmas of the 1820–1775 Ma Moorarie Supersuite and, in the Gascoyne Province, deposition of the 1840–1810 Ma Leake Spring Metamorphics (Sheppard et al., 2010a; Johnson et al., 2011a, 2011b, 2013). Granitic rocks of the Moorarie Supersuite intruded across the Gascoyne Province and into adjacent Yarlarweelor Gneiss Complex and Ashburton Basin. Extensive whole-rock trace element and isotopic work has been directed towards identifying the sources of the Moorarie Supersuite granites in the Capricorn Orogen, and has revealed that all reflect reworking of older crust (Sheppard et al., 2003, 2004, 2010a; Johnson et al., 2017a). However, the nature of the recycling and any distinction between possible infracrustal and supracrustal components has not been established. This chapter presents U–Pb, trace element, hafnium and oxygen isotope data to identify the relative contributions of crust and mantle during granite petrogenesis, as well as determining the composition of the crustal source.

6.2 U–Pb GEOCHRONOLOGY

The 29 samples from the Moorarie Supersuite are grouped by geographic region, with reference to the recognised tectonometamorphic zones within the Gascoyne Province (Fig. 6.1; Sheppard et al., 2010a). Zircon grains obtained from heavy mineral separates provided by the GSWA are indicated in text. All other zircon grains are obtained through EMP as described in Chapter 3.

For many granitoid rocks of the Moorarie Supersuite, the crystallisation age has already been established as part of previous geochronological studies by the GSWA. In most cases, the age data obtained by LASS-ICPMS during this study are, within error or identical to those previously established ages. However, for 5 samples (169086, 168939, 178024, 88419 and 88415), ages were obtained that differ slightly (by 0.7 to 1.5%) from those constrained previously. A summary of zircon data is presented in Table 6.1, details of U–Pb sample analyses are given in Appendix D.

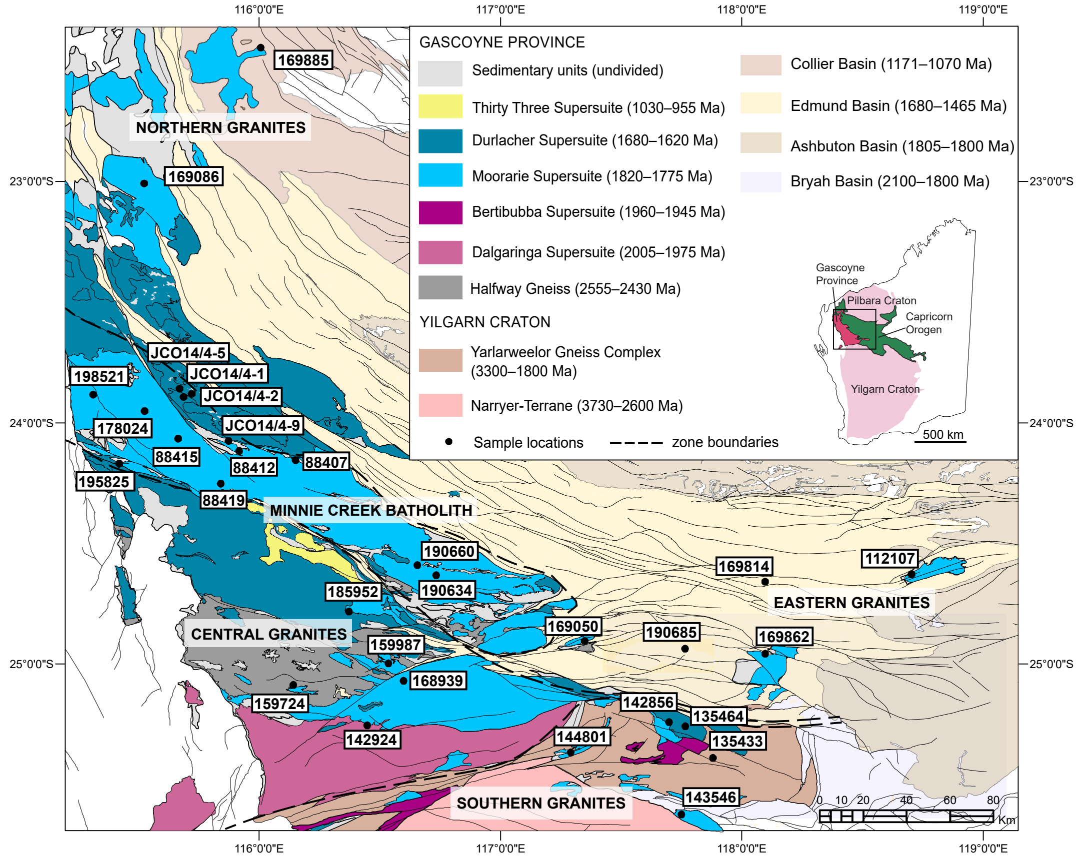

Figure 6.1 Simplified geological map of part of the Capricorn Orogen showing the Gascoyne Province and Yilgarn Craton margin, the principal tectonic units and sample locations mentioned in the text.

6.2.1 Southern granites (Yarlarweelor Gneiss Complex)

The Southern granites occur in the reworked northern margin of the Narryer Terrane, intruding the Yarlarweelor Gneiss Complex (YGC) (Fig. 6.1). The YGC consists of granitic gneisses with protolith ages between c. 3300 and c. 2600 Ma (Nelson, 1998a; 1999i) that were locally deformed and intruded by c. 1960 Ma plutons during the Glenburgh Orogeny (Sheppard et al., 2003).

6.2.1.1 GSWA 144801

Sample 148801 is a metamonzogranite. Zircon grains are brown to dark brown, 80–400 μm in length and subrounded to elongate in shape. CL images reveal faint oscillatory zoning; grains are commonly metamict. Forty-two analyses were conducted on 44 grains. Forty analyses were between 8 and 41% discordant, three analyses have <10% discordance. The analyses characterised by <10% discordance have $^{207}Pb/^{206}Pb$ ages ranging from 2730–2272 Ma. The remaining plotted data points do not define a meaningful discordance line and indicate a significant common-Pb component.

6.2.1.2 GSWA 143546

Sample 143546 is metagranite. Zircon grains are colourless to dark brown in colour, 80–220 μm in length and subrounded, elongate to stubby in shape. CL images reveal a range of textures including oscillatory zoning and homogenous domains. Some examples are metamict, and subrounded cores are present in some grains. Thin CL-bright overgrowths mantle some crystals, which are generally <5μm in length. A total of 47 analyses were obtained from 46 zircon grains. Twenty-seven analyses (Group D) are >5% discordant and are not considered further. Twenty analyses of oscillatory zoned and homogenous domains yield $^{207}Pb/^{206}Pb$ dates between c. 3506 and c. 2023 Ma, interpreted to reflect the ages of inherited material.

6.2.1.3 GSWA 135433

Sample 135433 is a metagranite. Zircon grains are yellow, pink and dark brown in colour, 50–200 μm in length and subrounded, elongate to stubby in shape. CL images reveal a range of textures including oscillatory zoning and homogenous domains, which are commonly overprinted by recrystallization zones. Forty-two analyses were obtained from 40 grains. Twenty-six analyses (Group D) are >5% discordant and are not considered further. Six analyses of oscillatory zoned grains (Group 1) yield a weighted mean $^{207}Pb/^{206}Pb$ date of 1838 ± 26 Ma (MSWD = 1.5), interpreted as the age of magmatic crystallization. Ten analyses of cores (Group X) yield $^{207}Pb/^{206}Pb$ dates between c. 3331 and c. 1903 Ma, interpreted as the ages of inherited material.

Table 6.1 Summary of sample descriptions and U–Pb LASS data

sample	Unit[1]	Lithology[2]	Pb–Pb age (Ma)[3]	Inheritance (Ma)	Pb–Pb age (Ma)[4]	T_{Ti} (°C)	Lat	Long
144801	SG	metamonzogranite	–	2730–2272	-	775–853	–25.36743	117.29085
143546	SG	metagranite	–	3506–2023	-	688–849	–25.6243	117.7502
135433	SG	metagranite	1838 ± 26	3331–1903	-	733	–25.38876	117.88123
135464	SG	monzogranite	1794 ± 13	2112–1853	-	759	–25.26451	117.75733
142856	SG	monzogranite	1785 ± 21	1857–1839	1801 ± 7	728	–25.24085	117.69802
169086	NG	monzogranite	1806 ± 13	2722–1846	1784 ± 5	729	–23.00884	115.52444
169885	NG	granodiorite	1802 ± 10	3329–1858	1796 ± 9	744	–22.4466	116.0077
190685	EG	metatonalite	(1796 ± 45)	2693–1898	1811 ± 5	-	–24.93638	117.76473
169050	EG	tonalite	n/a	-	1806 ± 5	828	–24.92847	117.37784
169814	EG	granitic rock	1805 ± 6	2294–1984	-	719	–24.65851	118.09598
169862	EG	granitic rock	1814 ± 17	2067–1973	-	718	–24.95796	118.09544
112107	EG	granodiorite	1774 ± 5	-	1797 ± 8	742	–24.6279	118.70389
159724	CG	monzogranite	1823 ± 8	2016–1882	1815 ± 4	760	-25.1264	116.1787
159987	CG	granodiorite	(1849 ± 23)	2495–1849	1810 ± 9	810	-24.9983	116.5352
168939	CG	monzogranite	1826 ± 10	2639–1988	1800 ± 7	689	-25.0699	116.5982
185952	CG	monzogranite	1808 ± 17	2153–1973	1799 ± 5	758	-24.78183	116.37321
142924	CG	granodiorite	-	2054–1930	1827 ± 14	–	-25.2717	116.4398
195821	MCB	metagranodiorite	1785 ± 9	-	1794 ± 5	690	-23.88417	115.31163
190634	MCB	metamonzogranite	1787±14	1837	1777 ± 5	695	-24.63234	116.73361
JCO14–4–02	MCB	metagranite	1799 ± 4	1893–1863	-	728	-23.857945	115.74535
88419	MCB	monzogranite	1801 ± 8	-	1781 ± 6	676	-24.2535	115.8416
178024	MCB	granodiorite	1798 ± 5	-	1783 ± 5	678	-23.9531	115.5255
88415	MCB	granodiorite	1802 ± 7	1893–1844	1777 ± 8	693	-24.0668	115.6653
88412	MCB	monzogranite	1803 ± 4	1982–1876	1801 ± 5	718	-24.1185	115.917
88407	MCB	monzogranite	1804 ± 5	1848	1794 ± 8	723	-24.1568	116.1523
JCO14–4–01	MCB	metagranite	1805 ± 3	1915–1857	-	720	-23.857773	115.74537
JCO14–4–09	MCB	metagranite	1817 ± 6	1865	-	708	-24.075952	115.87397
190660	MCB	felsic intrusive	(1814 ± 15)	2053–1808	1791 ± 4	-	-24.5902	116.655
JCO14–4–05	MCB	metagranite	1814 ± 28	1956–1858	-	564	-23.855011	115.70045

[1] SG = southern granites, NG = northern granites, EG = eastern granites, CG = central granites, MCB = Minnie Creek Batholith

[2] Petrographically characterisation established by GSWA

[3] Crystallisation age ($^{207}Pb/^{206}Pb$) established by LASS, ages in brackets indicate () minimum crystallisation age.

[4] Crystallisation age ($^{207}Pb/^{206}Pb$) established by SHRIMP (GSWA) (-) indicates no value obtained

6.2.1.4 GSWA 135464

Sample 135464 is a monzogranite.Zircon grains are colourless to dark brown in colour, 50–200 µm in length and subhedral and subrounded to elongate in shape. CL images reveals CL-intermediate cores with faint oscillatory zoning, sometimes convoluted, mantled by CL-darker rims of varying thicknesses and often overprinted by recrystallization zones. Forty-four analyses were obtained from 39 grains. Thirty-five analyses (Group X) are >5% discordant and are not considered further. Six analyses (Group 1) yield a weighted mean $^{207}Pb/^{206}Pb$ date of 1794 ± 13 Ma (MSWD = 0.54), interpreted as the crystallization age of the granite. Three analyses of cores (Group X) yield $^{207}Pb/^{206}Pb$ dates between c. 2113 and c. 1853 Ma, interpreted as the ages of inherited material.

6.2.1.5 GSWA 142856

Sample 142856 is a monzogranite. Zircon grains were hand-picked from heavy mineral concentrates provided by the GSWA. The grains are yellow-brown to pink-brown in colour, 120–250 µm in length and subrounded subhedral elongate to blocky in shape. CL images display oscillatory zoning which in places is contorted. Rounded cores are present within some grains. Forty-five analyses were obtained from 42 grains. Thirty-four analyses (Group D) are >5% discordant and are not considered further. Eight (Group 1) of oscillatory zoned grains yield a weighted mean $^{207}Pb/^{206}Pb$ date of 1785 ± 21 Ma (MSWD = 1.6), interpreted as the age of magmatic crystallization of the monzogranite. Three analyses of cores (Group X) yield $^{207}Pb/^{206}Pb$ dates between c. 1857 and c. 1839 Ma, interpreted to reflect the ages of inherited material. The crystallisation age of 1785 ± 21 Ma in broad agreement with the SHRIMP U–Pb crystallisation age previously established by the GSWA (1801 ± 7 Ma; Nelson, 1998b).

6.2.2 Northern granites (Boora Boora Zone)

The Northern granites occur in the northern-most part of the Gascoyne Province, the Boora Boora Zone. The granites intrude the Ashburton and Edmund Basin (Sheppard et al., 2010b).

6.2.2.6 GSWA 169086

Sample 169086 is a monzogranite dyke intruding a granodiorite (Nelson, 2004a). Zircon grains were hand-picked from heavy mineral concentrates provided by the GSWA. The grains are pale brown, red-brown to black in colour, 100–350 µm in length and subrounded to euhedral in shape. CL images display oscillatory zoning, which in places is contorted and sometimes overprinted by zones of recrystallization. Older cores are present within some grains, and thin homogeneous overgrowths mantle some crystals. Forty-six analyses were obtained from 44 grains. Twelve analyses (Group D) are >5% discordant, or indicate a high ^{204}Pb component, and are not considered further. Three analyses of rims returned ^{207}Pb/^{206}P dates between c. 1830 and c. 1779 Ma, indistinguishable from dates obtained from oscillatory-zoned grains. Fifteen analyses (Group 1), including both cores and rims identified in CL, yield a weighted mean ^{207}Pb/^{206}Pb date of 1806 ± 13 Ma (MSWD = 1.6), interpreted as the age of magmatic crystallization. Seventeen analyses of cores (Group X) yield ^{207}Pb/^{206}Pb dates ranging between c. 2722 and c. 1846 Ma, and are interpreted as ages of an inherited material. The crystallisation age of 1806 ± 13 Ma is (0.7%) older than the SHRIMP U–Pb crystallisation age previously established (1784 ± 5 Ma; Nelson, 2004a).

6.2.2.7 GSWA 169885

Sample 169885 is a granodiorite. Zircon grains are colourless to dark brown, subheadral elongate to stubby in shape and 100–200 µm in length. CL images reveal ubiquitous oscillatory zoning, with some grains having high-uranium, metamict zones. Older cores are present within some grains. Forty-nine analyses were obtained from 49 grains. Thirty-five analyses (Group D) are >5% discordant, and are not considered further. Seven analyses (Group 1) yield a weighted mean ^{207}Pb/^{206}Pb date of 1802 ± 10 Ma (MSWD = 0.49), interpreted as the crystallization age of the granite. Seven analyses of cores (Group X) yield ^{207}Pb/^{206}Pb dates of 3329–1858 Ma, interpreted as the ages of inherited material. The crystallisation age of 1802 ± 10 Ma is in agreement with SHRIMP U–Pb crystallisation age previously established (1796 ± 9 Ma; Wingate et al., 2014b).

6.2.3 Eastern granites

The Eastern granites occur east of the Gascoyne Province, intruding the Edmund Basin (Fig. 6.1).

6.2.3.1 GSWA 190685

Sample 190685 is a metagranodiorite. Zircon grains were hand-picked from heavy mineral concentrates provided by the GSWA. The grains are colourless to dark brown, ranging between 100–300µm in length, with subrounded, subhedral to elongate morphologies. CL images reveal variably contorted oscillatory zoned grains. Some crystals contain older cores. Many crystals contain metamict, high-uranium zones. Forty-eight analyses were obtained from 47 grains. Forty-five analyses (Group D) are >5% discordant and are not considered further. The remaining three analyses indicate ^{207}Pb/^{206}Pb dates between c. 2693nd c. 1898 Ma. All analyses indicate ages older than accepted age of the Moorarie Supersuite (1820–1770 Ma) and are therefore interpreted as the ages of inherited material incorporated into this granite. The age of 1898 ± 37 Ma indicated by the youngest analysis is interpreted to be the minimum age of crystallisation of the granodiorite.

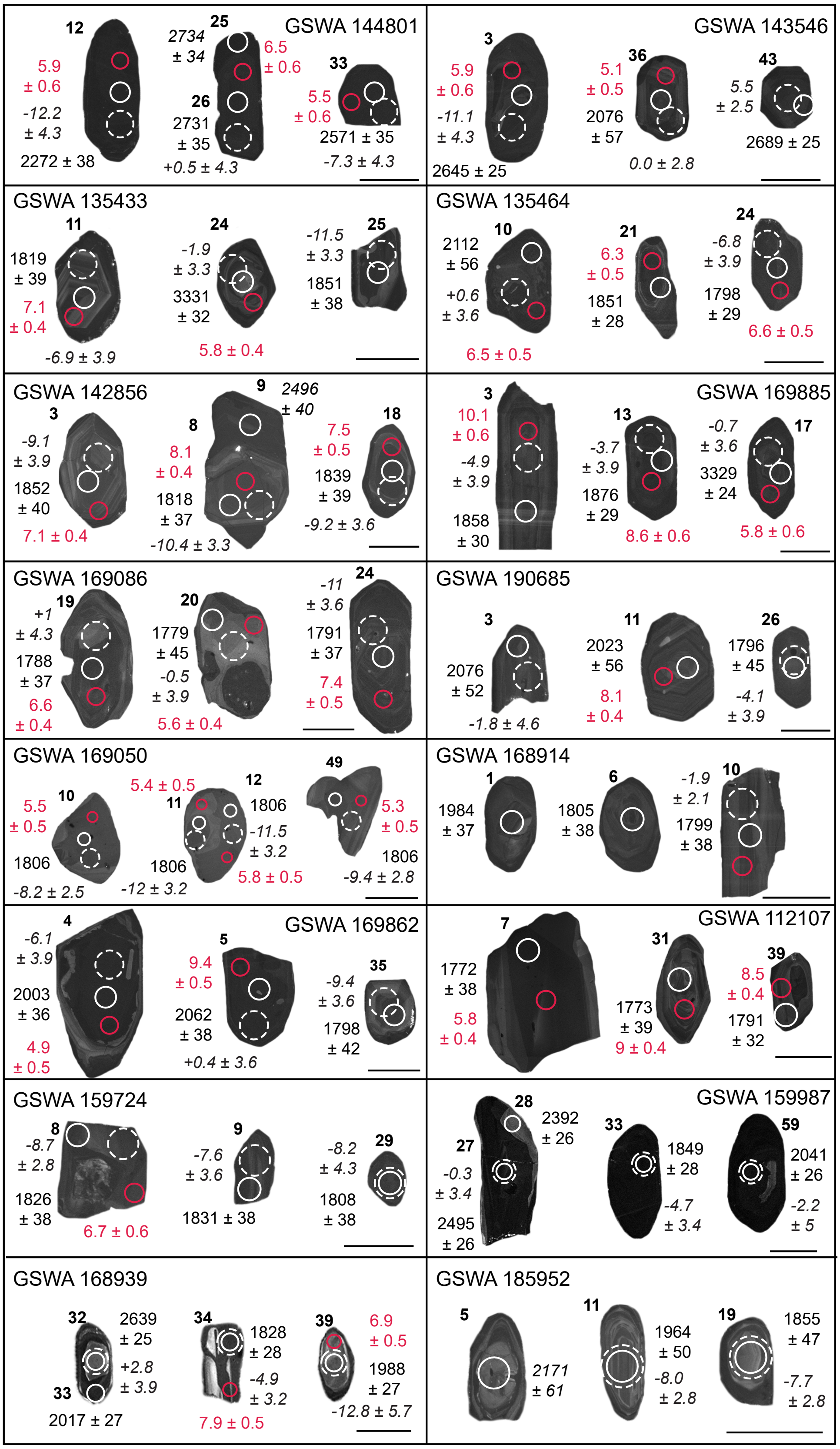

Figure 6.2 continues with caption overleaf

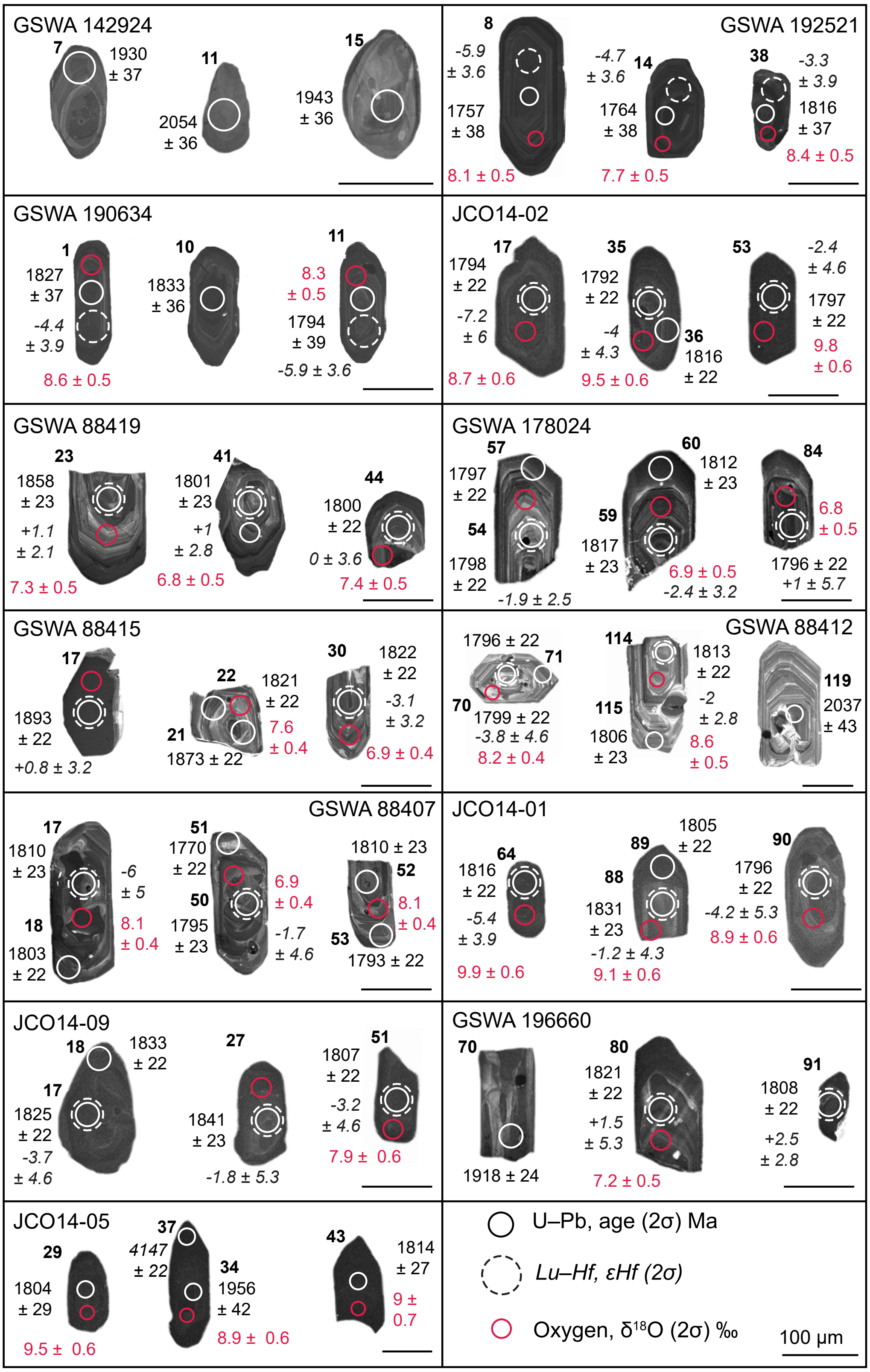

Figure 6.2 CL images of representative zircon grains from the Moorarie Supersuite. Grains are numbered by their analysis number. Ages in italics indicates discordance >10%.

6.2.3.2 GSWA 169050

Sample 169050 is a tonalite gneiss that occurs as a small dyke in a mafic gneiss that is interleaved with leucocratic gneiss (Nelson, 2002a). Zircon grains were hand-picked from heavy mineral concentrates provided by the GSWA. The grains are light pink-brown to dark red-brown, generally 150–250 μm in length, with subrounded, subhedral stubby to equant morphologies. CL images reveal weak broadly-zoned grains, many of which are structureless. Some grains contain older cores, and many are overprinted by recrystallization zones. Fifty analyses were obtained from 47 grains. Fifteen analyses (Group D) are >5% discordant and are not considered further. Thirty-three analyses (Group 1), including 5 recrystallised zones and 28 homogenous to weakly zoned grains, yield a weighted mean $^{207}Pb/^{206}Pb$ date of 1736 ± 7 Ma (MSWD = 0.76). One analyses (Group X) of a homogenous grain yields a $^{207}Pb/^{206}Pb$ date of c. 1841 Ma. The remaining analyses of an oscillatory zoned grain yields a $^{206}Pb/^{238}U$ date of c. 1558 Ma. The $^{207}Pb/^{206}Pb$ date of 1736 ± 6 Ma of Group 1 is significantly younger than any Moorarie Supersuite granites previously dated, and is younger than the SHRIMP U–Pb crystallisation age previously established by the GSWA (1806 ± 5 Ma; Nelson, 2002). All analyses in Group 1 are reversely discordant. Given that the majority of analyses were conducted on homogenous domains, the reverse discordance cannot be attributed to internal redistribution of radiogenic Pb from high-U zones to low U zones (e.g. Mattinson et al., 1984), but may be attributed to analytical artifacts, and the Pb–Pb ages are assumed to be unreliable. Therefore, any further calculations in section 6.4 use a U–Pb crystallisation age of 1806 ± 5 Ma (Nelson, 2002a).

6.2.3.3 GSWA 169814

Sample 168914 is a metagranitic rock. Zircon grains are colourless to light brown, 80–100μm in length, and subrounded elongate to stubby in shape. CL images display oscillatory zoning, which in places is contorted. Older cores are present within some grains, and homogenous overgrowths mantle some crystals. Forty-five analyses were obtained from 44 grains. Eight analyses are >5% discordant (Group D) and are not considered further, an additional six analyses are >5% discordant, but appear to have only been affected by recent radiogenic-Pb loss. Thirty-five analyses (Group 1) including 34 oscillatory zoned zircon and one rim identified in CL, yield a weighted mean $^{207}Pb/^{206}Pb$ date of 1805 ± 6 Ma (MSWD = 0.66), interpreted as the crystallization age of the granite. Two analyses of cores (Group X) yield $^{207}Pb/^{206}Pb$ dates of c. 2294 and c. 1984 Ma, interpreted to reflect the ages of inherited material.

6.2.3.4 GSWA 169862

Sample 169862 is granitic rock. Zircon grains are pink to brown in colour, 100–250 μm in length, and subhedral elongate to equant in shape. CL images display concentric growth zoning, and

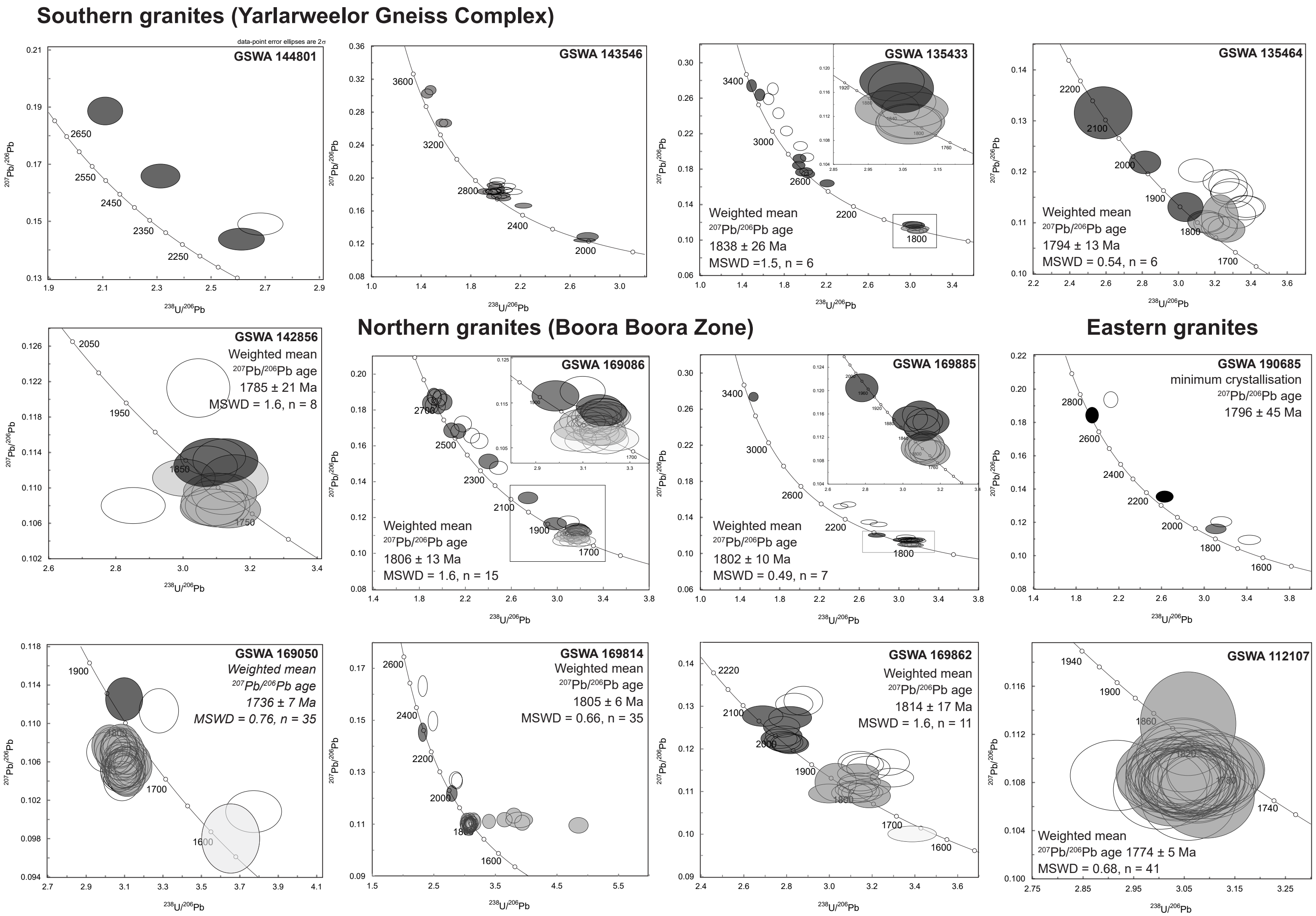

Figure 6.3 continues with caption overleaf

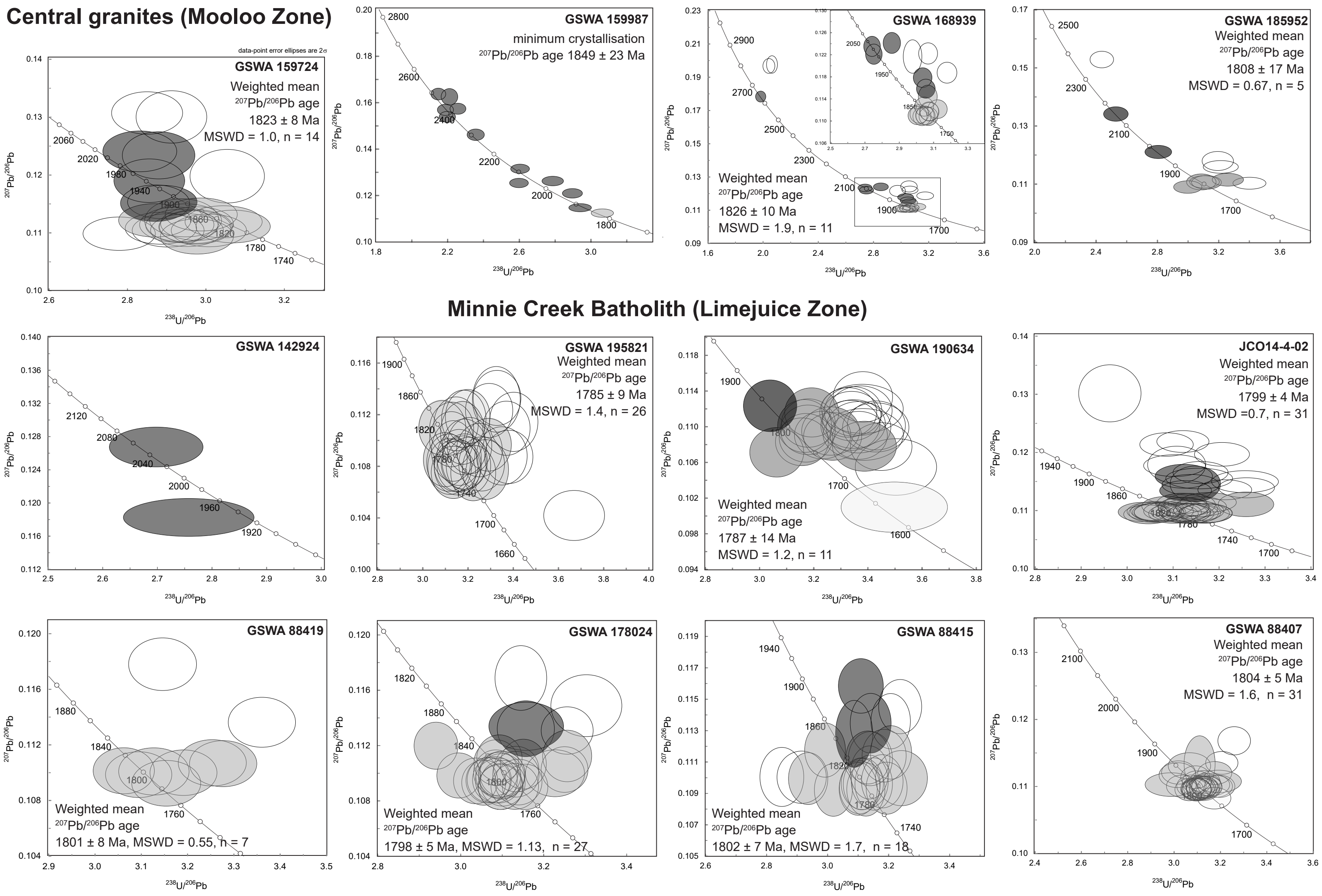

Figure 6.3 continues with caption overleaf

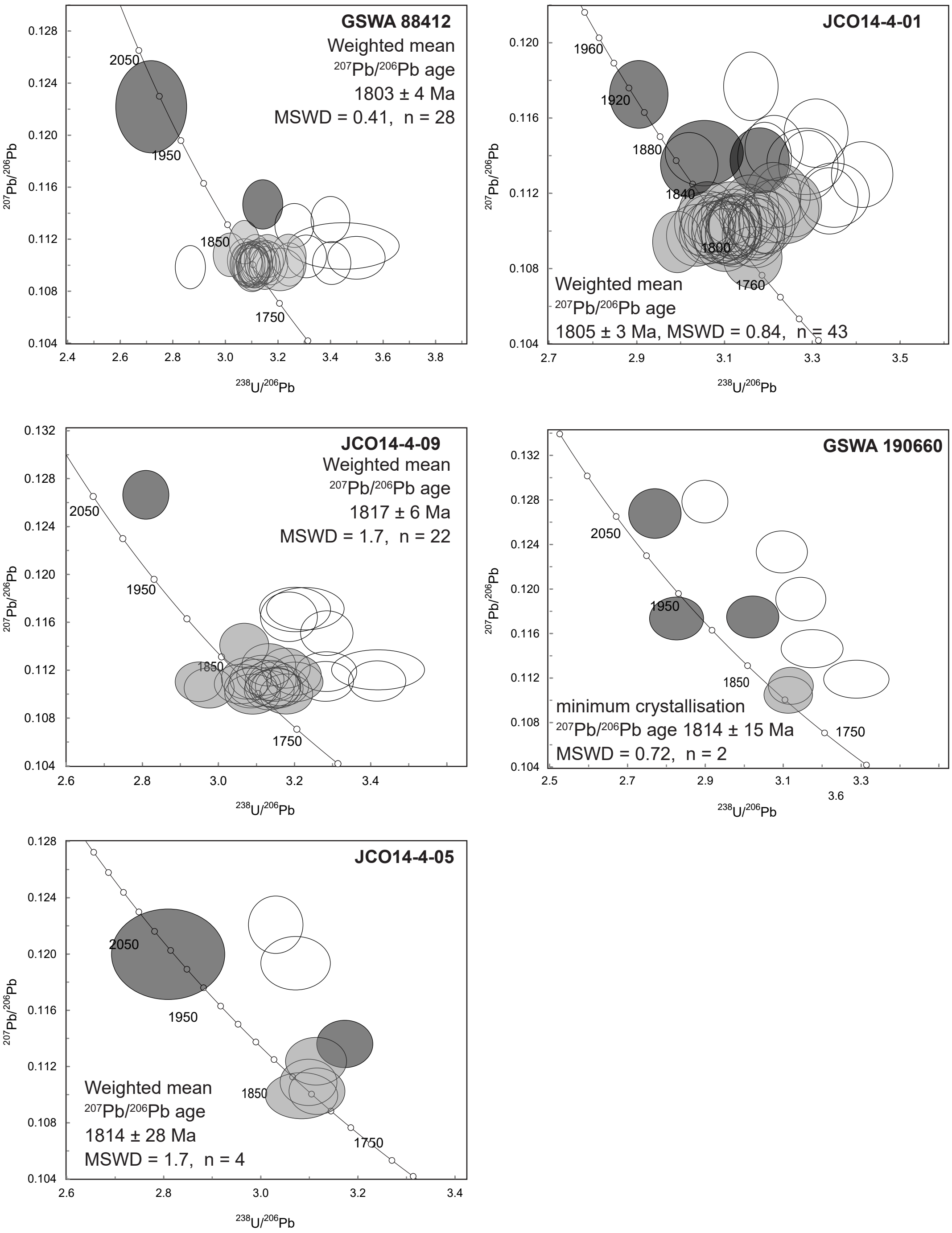

Figure 6.3 Concordia diagram showing the subset of results of zircon with <10% discordance. Concordia diagram shows <10% discordance, with grey ellipses analyses indicate analyses used to calculate Group 1 (crystallisation age), black ellipses indicate inherited zircon (Group X). Light grey ellipses indicate radiogenic Pb-loss (Group P). Hollow ellipses indicate outside discordance threshold (Group D).

some grains contain older cores, mantled by oscillatory zoned rims. Some sector zoned equant grains are present. Fort-nine analyses were obtained from 47 grains. Twenty-seven analyses are >5% discordant and are not considered further. Eleven analyses of sector zoned and oscillatory zoned grains (Group 1) yield a weighted mean $^{207}Pb/^{206}Pb$ date of 1814 ± 17 Ma (MSWD = 1.6), interpreted as the age of magmatic crystallization. Ten analyses zircon cores (Group X) yield $^{207}Pb/^{206}Pb$ dates between c. 2067 and c. 1973 Ma, interpreted to reflect the ages of inherited material. One analyses of a homogenous zircon (Group P) yielded a $^{207}Pb/^{206}Pb$ date of 1626 Ma, and is interpreted to have lost radiogenic Pb.

6.2.3.5 GSWA 112107

Sample 112107 is a granodiorite. Zircon grains were hand-picked from heavy mineral concentrates provided by the GSWA. The grains are colourless to light brown, ranging between 100–300μm in length, with subrounded, subhedral to anhedral morphologies. CL images reveal oscillatory zoning, which is commonly convoluted and overprinted by several phases of recrystallization. Forty-four analyses were obtained from 42 grains. Three analyses (Group D) are >5% discordant and are not considered further. The remaining 41 analyses define one coherent group (Group 1) that yield a weighted mean $^{207}Pb/^{206}Pb$ date of 1774 ± 5 Ma (MSWD = 0.68). Twenty-seven analyses of recrystallised, homogenous or convoluted zones returned $^{207}Pb/^{206}Pb$ dates between c. 1847 and c. 1744 Ma, indistinguishable from dates obtained from oscillatory zoned zircon. The age of 1774 ± 5 Ma of Group 1 is younger than the SHRIMP U–Pb crystallisation age previously established by the GSWA (1797 ± 8 Ma; Nelson, 1995). All analyses are reversely discordant, also observed in the GSWA SHRIMP analyses, which therefore cannot be attributed to analytical artefacts. All grains display at least two phases of recrystallization and low U concentration (69–624ppm). The reverse discordance may be attributed to fluid alteration resulting in U loss and/or Pb redistribution (e.g. Mattison et al., 1996).

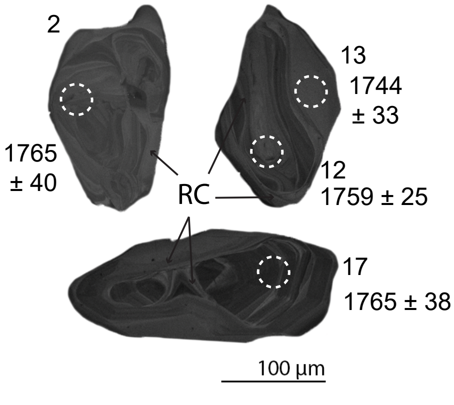

Fig. 6.4 CL images for zircon from sample GSWA 112107. LASS analytical sites are shown as dashed circles together with site number and the indicated U–Pb age in Ma. RC = recrystallised zone

6.2.4 Central granites (Mooloo Zone)

The Central granites occur in the Mooloo Zone, in the central part of the Gascoyne Province.

6.2.4.1 GSWA 159724

Sample 159724 is a metamonzogranite. Zircon grains were hand-picked from heavy mineral concentrates provided by the GSWA. The grains are dark yellow-brown to pink in colour, subrounded and subhedral, elongate to equant in shape and 80–200 µm in length. CL images reveal oscillatory zoning, which in many places is contorted. Older cores are present within some grains, and some grains are overprinted by recrystallization domains. Forty-seven analyses were obtained from 47 grains. Twenty-eight analyses (Group X) are >5% discordant, and are not considered further. Sixteen analyses (Group 1) of 14 oscillatory zoned zircon and two recrystallised domains yield a weighted mean ^{207}Pb/^{206}Pb date of 1823 ± 8 Ma (MSWD = 1.0), interpreted as the igneous crystallization age. Four analyses of cores (Group X) returned ^{207}Pb/^{206}Pb dates between c. 2016 Ma and c. 1882 Ma, interpreted as the ages of inherited material. The crystallisation age of 1823 ± 8 Ma is in agreement with the SHRIMP U–Pb crystallisation age previously established (1815 ± 4 Ma; Nelson, 2000b).

6.2.4.2 GSWA 159987

Sample 159987 is a metagranodiorite. Zircon grains were hand-picked from heavy mineral concentrates provided by the GSWA. The grains are brown, dark brown or colourless, ranging between 100–400 µm in length, with subrounded to rounded, subhedral, blocky to elongate morphologies. CL imaging reveal complex internal structures with cores displaying convoluted zoning; some grains have weak oscillatory zoning. Some zircons display CL-dark rims of varying thickness with transgressive recrystallization fronts overprinting oscillatory zoning. Fluid and mineral inclusions are common, many grains are highly fractured, and many are metamict. Thirty-four analyses were obtained from 30 grains. Twenty-two analyses (Group D) are >5% discordant or indicate high common Pb contents are not considered further. The remaining 12 analyses indicate ^{207}Pb/^{206}Pb dates between c. 2495 and c. 1849 Ma, interpreted as the ages of inherited material.

6.2.4.3 GSWA 168939

Sample 168939 is metamonzogranite. Zircon grains were hand-picked from heavy mineral concentrates provided by the GSWA. Grains from this sample range from in length from 60 to 250 µm, are typically yellow-brown to dark brown in colour, and sub-rounded elongate in shape. Cores typically show oscillatory zoning. Most cores are surrounded by homogenous CL-darker rims. Thirty analyses were obtained from 26 grains. Thirteen analyses (Group D) are >5% discordant and are not considered further. Group 1 comprises 11 analyses of nine cores and two recrystallized domains which yield a weighted mean ^{207}Pb/^{206}Pb date of 1826 ± 10 Ma (MSWD = 1.9), interpreted as the crystallization age of the granite. Six analyses (Group X) return ^{207}Pb/^{206}Pb dates between c. 2639 and c. 1988 Ma, and are interpreted to reflect the ages of inherited material. The crystallisation age of 1826 ± 11 Ma is older than the SHRIMP U–Pb crystallisation age previously established by the GSWA (1800 ± 7 Ma; Nelson, 2001b).

6.2.4.4 GSWA 185952

Sample 185952 is a metamonzogranite. Zircon grains are pale to dark brown in colour, 80–120 µm in length and subrounded subhedral elongate to equant in shape. CL images reveal variably contorted oscillatory zoning. Thirty-eight analyses were obtained from 38 grains. Thirty-one analyses (Group D) are >5% discordant and are not considered further. Five analyses of oscillatory zoned zircon (Group 1) yield a weighted mean ^{207}Pb/^{206}Pb date of 1810 ± 15 Ma (MSWD = 0.71), interpreted as the igneous crystallization age of the monzogranite. Two analyses of cores (Group X) return ^{207}Pb/^{206}Pb dates of c. 2153 and c. 1973 Ma, interpreted as the ages of inherited material incorporated into this granite. The crystallisation age of 1808 ± 13 Ma is in agreement with the SHRIMP U–Pb crystallisation age previously established by the GSWA (1799 ± 5 Ma; Wingate et al., 2010f).

6.2.4.5 GSWA 142924

Sample 142924 is a granodiorite. Zircon grains were hand-picked from heavy mineral concentrates provided by the GSWA. The grains are light pink, yellow to dark-brown and black, 100–250 µm in length and subrounded subhedral and blocky in shape. CL images reveal oscillatory zoning which in places is contorted. Rounded cores are present within some grains. Twenty-two analyses were obtained from 19 grains. Twenty-two analyses (Group D) are >5% discordant (high common-Pb component), and are not considered further. The remaining two analyses indicate ^{207}Pb/^{206}Pb dates of 2054 and 1930 Ma, interpreted as the ages of inherited material incorporated into this granite. The high number of discordant analyses is attributed to a common-Pb component.

6.2.5 Minnie Creek Batholith (Limejuice Zone)

The 270 km long by by 30–50km wide Minnie Creek Batholith occurs in the Limejuice Zone.

6.2.5.1 GSWA 195821

Sample 195821 is a metagranodiorite. Zircon grains were hand-picked from heavy mineral concentrates provided by the GSWA. Grains are brown, dark brown or colourless, ranging between

100–400µm in length, with subrounded to rounded, subhedral, blocky to elongate morphologies. CL images display ubiquitous oscillatory zoning. Some grains are locally overprinted by zones of recrystallization. Forty-six analyses were obtained from 44 grains. Twenty analyses (Group D) are >5% discordant and are not considered further. Twenty-six analyses (Group 1) including 24 oscillatory zoned zircon and two recrystallised zones identified in CL, yield a weighted mean ^{207}Pb/^{206}Pb date of 1785 ± 9 Ma (MSWD = 1.4), interpreted as the crystallization age of the granite. The crystallisation age of 1785 ± 9 Ma is in agreement with the SHRIMP U–Pb crystallisation age previously established by the GSWA (1794 ± 5 Ma; Wingate et al., 2013b).

6.2.5.2 GSWA 190634

Sample 190634 is a metamonzogranite. Zircon grains were hand-picked from heavy mineral concentrates provided by the GSWA. The grains are colourless to light-brown in colour, 100–300 µm in length and subrounded, euhedral and equant to elongate in shape. CL imaging reveals CL-intermediate cores with faint oscillatory zoning, sometimes convoluted, mantled by CL-darker rims of varying thicknesses and often overprinted by recrystallization zones. Fifty-four analyses were obtained from 48 grains. Thirty-nine analyses (Group D) are >5% discordant and are not considered further. Eleven analyses (Group 1) of nine oscillatory zoned grains and two recrystallised domain yield a weighted mean ^{207}Pb/^{206}Pb date of 1787 ± 14 Ma (MSWD = 1.2), interpreted as the age of magmatic crystallization. One analysis of a core (Group X) yields a ^{207}Pb/^{206}Pb date of c. 1837 Ma. One analysis (Group P) yielded a ^{207}Pb/^{206}Pb date of c. 1642 Ma and is interpreted to have lost radiogenic Pb. The crystallisation age of 1787 ± 14 Ma is in agreement with the SHRIMP U–Pb crystallisation age previously established by the GSWA (1777 ± 5 Ma; Wingate et al., 2012b).

6.2.5.3 JCO14–4–02

Sample JCO14–4–02 is a biotite metagranite. Zircon grains are pink to light-brown in colour, 60–200 µm in length and subrounded to euhedral, elongate to stubby in shape. CL images reveal oscillatory zoning, which in places is contorted. Older cores are present within some grains, and homogeneous overgrowths mantle some crystals. Fifty-four analyses were obtained from 37 grains. Twenty analyses (Group D) are >5% discordant, or are core-rim mixtures (14.1) and are not considered further. Three analyses of three rims returned ^{207}Pb/^{206}P dates between c. 1799 and c. 1791 Ma, indistinguishable from dates obtained from oscillatory zoned grains. Thirty-one analyses (Group 1), including both cores and rims identified in CL, yield a weighted mean ^{207}Pb/^{206}Pb date of 1799 ± 4 Ma (MSWD = 0.70), interpreted as the age of magmatic crystallization. Three analyses of cores (Group X) yield ^{207}Pb/^{206}Pb dates between c. 1893 and c. 1863 Ma, interpreted as the ages of inherited material.

6.2.5.4 GSWA 88419

Sample 88419 is a monzogranite. Zircon grains were hand-picked from heavy mineral concentrates provided by the GSWA. Grains range up to 500µm in length, typically brown to dark brown in colour, with sub-rounded, equant to stubby morphologies. Variable internal features can be observed and range from oscillatory zoning to convoluted zoning. Mineral inclusions are common. Thirty analyses were obtained from 25 grains. Twenty-three analyses (Group D) are >5% discordant and are not considered further. Group 1 comprises seven analyses of seven cores, yield a weighted mean $^{207}Pb/^{206}Pb$ date of 1801 ± 8 Ma (MSWD = 0.55), interpreted as the igneous crystallisation age. The crystallisation age of 1801 ± 8 Ma is older than the SHRIMP U–Pb crystallisation age previously established by the GSWA (1781 ± 6 Ma; Bodorkos et al., 2006e).

6.2.5.5 GSWA 178024

Sample 178024 is a granodiorite. Zircon grains were hand-picked from heavy mineral concentrates provided by the GSWA. Grains range between 100 and 350µm in length and are typically yellow-brown to dark brown in colour. They are subhedral-euhedral, equant to elongate grains. They are generally CL-intermediate and typically show oscillatory zoned cores mantled by homogenous rims. A few zircons show recrystallised zones that cross cut the original zoning. Some metamict cores and mineral inclusions are present. Thirty-nine analyses were obtained from 28 grains. Ten analyses (Group D) are >5% discordant, or indicate high common Pb and have been rejected. Nine rims were analysed, returning $^{207}Pb/^{206}P$ ages between c. 1855 and c. 1788 Ma, indistinguishable from ages obtained from cores. Twenty-seven analyses (Group 1), including both cores and rims identified in CL, yield a weighted mean $^{207}Pb/^{206}Pb$ date of 1798 ± 5 Ma (MSWD = 1.13), interpreted as the igneous crystallisation age of the monzogranite. Two analyses (Group X) of a core and rim yield $^{207}Pb/^{206}Pb$ dates of c. 1855 and c. 1851 Ma and are interpreted as ages of an inherited material incorporated into the granite. The crystallisation age of 1798 ± 5 Ma is older than the SHRIMP U–Pb crystallisation age previously established by the GSWA (1783 ± 5 Ma; Nelson et al., 2005b).

6.2.5.6 GSWA 88415

Sample 88415 is a granodiorite dyke, which contains inclusions of, and is comingled with a dolerite. Zircon grains were hand-picked from heavy mineral concentrates provided by the GSWA. Grains from this sample range between 80 and 350 µm in length, are typically colourless to dark brown in colour, and are subhedral to euhedral and elongate to equant in morphology. Grains generally display oscillatory zoning, and in some case, this zoning has become convoluted. Thin homogeneous CL-bright overgrowths mantle some crystals, typically <5 µm thick. Mineral inclusions are abundant. Thirty analyses were obtained from 18 grains. Nine analyses are

>5% discordant and are not considered further. Group 1 comprises 18 analyses of 17 cores and one CL-bright rim, and yields a weighted mean ^{207}Pb/^{206}Pb date of 1802 ± 7 Ma (MSWD = 1.7), interpreted as the igneous crystallisation age of the granodiorite. Group X comprises three analyses of three cores with ^{207}Pb/^{206}Pb dates ranging between c. 1893 and c. 1844 Ma, interpreted to date the ages of inherited zircon grains. The crystallisation age of 1802 ± 7 Ma is older than the SHRIMP U–Pb crystallisation age previously established by the GSWA (1777 ± 8 Ma; Bodorkos et al., 2006a).

6.2.5.7 GSWA 88407

Sample 88407 is a foliated monzogranite. Zircon grains were hand-picked from heavy mineral concentrates provided by the GSWA. Grains range in length from 100 to 400 µm, are typically pale-brown to colourless in colour, and subhedral to euhedral elongate in morphology. Grains show dominantly oscillatory zoning, although some grains display more chaotic zoning, mantled by homogenous or oscillatory zoned rims of variable thickness. Thirty-seven analyses were obtained from 23 grains. Five analyses are >5% discordant and are not considered further. Group 1 comprises 31 analyses of 30 cores and one oscillatory zoned rims, and yields a weighted mean ^{207}Pb/^{206}Pb date of 1804 ± 5 Ma (MSWD = 1.6), interpreted as the age of magmatic crystallisation. One analysis of an oscillatory zoned grain (Group P) yields a ^{207}Pb/^{206}Pb date of c. 1780 Ma, and is interpreted to have lost radiogenic Pb. The crystallisation age of 1804 ± 5 Ma is in agreement with the SHRIMP U–Pb crystallisation age previously established by the GSWA (1803 ± 6 Ma; Bodorkos et al., 2006c).

6.2.5.8 GSWA 88412

Sample 88412 is a foliated monzogranite. Zircon grains were hand-picked from heavy mineral concentrates provided by the GSWA. Grains are up to 350µm in length, are typically colourless to dark brown in colour, and euhedral elongate to stubby in morphology. CL images display oscillatory zoning, older cores are present within some grains, and oscillatory zoned overgrowths mantle some crystals. Twenty-eight analyses (Group D) are >5% discordant or indicate high common Pb contents, and are not considered further. Four analyses of oscillatory zoned rims returned ^{207}Pb/^{206}Pb dates between c. 1806 and c. 1794 Ma, indistinguishable from dates obtained from cores. Twenty-eight analyses (Group 1), including both cores and rims identified in CL, yield a weighted mean ^{207}Pb/^{206}Pb date of 1803 ± 4 Ma (MSWD = 0.41), interpreted as the crystallization age. Two analyses (Group X) located on an oscillatory zoned cores yield ^{207}Pb/^{206}Pb dates of c. 1876 and c. 1860 Ma, interpreted as the ages of inherited material. The crystallisation age of 1803 ± 4 Ma is in agreement with the SHRIMP U–Pb crystallisation age previously established by the GSWA (1801 ± 5 Ma; Bodorkos et al., 2006a).

6.2.5.9 JCO14–4–01

Sample JCO14–4–01 is a metagranite. Zircon grains are pink to brown in colour, 100–200 μm in length and subrounded to euhedral, elongate to stubby in shape. CL images reveal oscillatory zoning, which in places is contorted. Older cores are present within some grains, and homogeneous overgrowths mantle some crystals. Seventy analyses were obtained from 51 grains. Twenty-three analyses (Group D) are >5% discordant, and are not considered further. Three analyses of three rims returned ^{207}Pb/^{206}P dates between c. 1816 and c. 1808 Ma, indistinguishable from dates obtained from oscillatory zoned grains. Forty-three analyses (Group 1), including both cores and rims identified in CL, yield a weighted mean ^{207}Pb/^{206}Pb date of 1805 ± 3 Ma (MSWD = 0.84), interpreted as the age of magmatic crystallization. Four analyses of cores (Group X) yield ^{207}Pb/^{206}Pb dates between 1915–1857 Ma, interpreted as the ages of inherited material.

6.2.5.10 JCO14–4–09

Sample JCO14–4–09 is a metagranite. Zircon grains are colourless to dark brown, 60–200 μm in length and subrounded to euhedral, elongate to stubby in shape. CL images display oscillatory zoning, which in places is contorted and sometimes overprinted by recrystallization zones. Thirty-nine analyses were obtained from 35 grains. Sixteen analyses are >5% discordant (Group D) and are not considered further. Twenty two analyses of oscillatory zoned grains yield a weighted mean ^{207}Pb/^{206}Pb date of 1817 ± 6 Ma (MSWD = 1.7), interpreted as the age of magmatic crystallization.

6.2.5.11 GSWA 190660

Sample 190660 is a metamonzogranite. Zircon grains were hand-picked from heavy mineral concentrates provided by the GSWA. Grains are up to 500 μm in length, typically pale-brown to dark brown in colour and subhedral to euhedral elongate in morphology. CL textures range from irregular oscillatory zoning to convoluted zoning. Sixteen analyses were obtained from 16 grains. All analyses were between 2 and 48% discordant, with only five analyses <5% discordant. The analyses with <5% discordance have apparent ^{207}Pb/^{206}Pb ages ranging between c. 2053 and c. 1808 Ma. The two youngest concordant analyses yield an imprecise weighted mean ^{207}Pb/^{206}Pb date of 1814 ± 15 Ma (MSWD = 0.72), interpreted as the minimum age of magmatic crystallization. The remaining analyses c. 2053–1918 Ma are interpreted as representing the ages of inherited zircon grains. The minimum crystallisation age of 1814 ± 15 Ma is older than the SHRIMP U–Pb crystallisation age previously established by the GSWA (1791 ± 4 Ma; Wingate et al., 2012a).

6.2.5.12 JCO14–4–05

Sample JCO14–4–05 is a metagranite. Zircon grains are colourless to light-brown in colour, 60–200 µm in length and subrounded to euhedral, elongate to stubby in shape. CL images display oscillatory zoning, which in places is contorted and homogeneous CL-dark rims mantle some crystals. Thirty-two analyses were obtained from 24 grains. Twenty-four analyses (Group D) are >5% discordant, and are not considered further. One analysis of a homogenous rim returned a ^{207}Pb/^{206}P date of 1798 ± 28 Ma, indistinguishable from dates obtained from cores (c. 1838–1804 Ma). Four analyses (Group 1), including both cores and rim identified in CL, yield a weighted mean ^{207}Pb/^{206}Pb date of 1814 ± 28 Ma (MSWD = 1.7), interpreted as the crystallization age of magmatic crystallisation. Two analyses of oscillatory-zoned cores (Group X) yield ^{207}Pb/^{206}Pb dates of c. 1956 Ma and c. 1858 Ma, interpreted as the ages of inherited material.

6.3 ZIRCON TRACE-ELEMENT COMPOSITION

Zircon grains from the Moorarie Supersuite samples have trace-element compositions typical of continental zircon, with both magmatic and inherited populations plotting within continental arc-type zircon fields (Fig. 6.4; Grimes et al., 2007; 2015). Chondrite-normalised REE element patterns of magmatic zircons from the Moorarie Supersuite granites are characterised by strong positive Ce and negative Eu anomalies and a positive heavy REE (HREE) slope, consistent with growth of zircon in a magmatic environment (Rubatto 2007; Hoskin and Black, 2000; Hoskin and Ireland, 2000). There is no significant difference in the REE composition of zircon in overgrowths and/or recrystallised zones versus that in oscillatory-zoned cores (Fig. 5). Although there is some variation in Eu anomaly and HREE enrichment from group to group, the averages are similar for all groups (Table 3). All of the Moorarie Supersuite samples show similar REE patterns, which suggests that all the granites were derived from a source of similar composition and/or a similar degree of partial melting. Magmatic zircon trace element signatures indicate no evidence of co-crystallisation with garnet (Yb_N/Gd_N = 3–69, Eu/Eu* = 0.01–0.69), indicating formation pressures lower than around 1.2 GPa (<45 km depth; Rubatto and Hermann, 2007).

All Moorarie Supersuite samples record zircon Ti temperatures with averages between 682 and 828°C. These temperatures are comparable with the low-T inheritance-rich granitoids with T_{Zr} <800°C of Miller et al (2003) that are interpreted as forming in regions of crustal thickening. Estimates of crystallization temperatures were calculated using Ferry and Watson's (2007) calibration of the Ti-in-zircon thermometer.

6.4 Lu–Hf ISOTOPE DATA

Three hundred and twenty-five analyses were conducted on magmatic and inherited zircon grains from 27 samples from the Moorarie Supersuite granites (Table 2; Fig. 6.6). Thirty-six analyses have been rejected due to either poor U–Pb age data (high discordance) or the ablated area consisted of core-rim mixtures or cracks (see Appendix D).

Initial $^{176}Hf/^{177}Hf$ ratios of all analysed zircon grains range between 0.280405 and 0.281732, corresponding to εHf_t values of -13.8 and +3.3. Magmatic grains (n=213) yield a range of initial $^{176}Hf/^{177}Hf$ ratios between 0.281287 and 0.281732 (εHf_t -12.7 and +3.3), with median εHf_t values from each sample ranging between -11.1 ± 3.4 and +0.5 ± 1.2 (2SD). Inherited zircon grains (n=76) with $^{207}Pb/^{206}Pb$ ages ranging between c. 3506 to c. 1826 Ma yield a range of εHf_t values between -13.8 and +3.1.

6.4.1 Southern granites

Data from the southern granites consist of 49 analyses from five samples which have individual $^{207}Pb/^{206}Pb$ ages ranging between c. 3506 and c. 1758 Ma. Analyses of magmatic zircon from samples GSWA 135433, GSWA 135464 and GSWA 142856, with crystallisation ages of 1838 ± 26 Ma, 1794 ± 13 Ma and 1785 ± 21 Ma respectively, yield a range of initial $^{176}Hf/^{177}Hf$ ratios between 0.281293 to 0.281503, corresponding to εHf_t values between -12.7 and -5.2 (median εHf_t of -9.1 ± 4.3 2SD, n=19). The inherited zircon, with $^{207}Pb/^{206}Pb$ dates between c. 3506 and c. 1853 Ma, yield a wide range of initial $^{176}Hf/^{177}Hf$ ratios (0.280405–0.281462) with corresponding εHf_t values of -12.2 to +0.6.

6.4.2 Northern granites

A total of 22 zircon grains were analysed from two samples from the northern granites (GSWA 169086, GSWA 169885) and include analyses of groups that are interpreted to date crystallisation and inherited zircon. Analyses of magmatic zircon, with crystallisation ages of 1806 ± 13 Ma and 1802 ± 10 Ma, have a large range of initial $^{176}Hf/^{177}Hf$ ratios (0.281336–0.281732) with corresponding εHf_t values of -11 to +3.3 (median εHf_t of -5.3 ± 7.6, 2SD, n=15). Inherited zircon (n=7), with $^{207}Pb/^{206}Pb$ ages between c. 3329 and c. 1858 Ma, have a small range of initial $^{176}Hf/^{177}Hf$ compositions (0.280626–0.281577) and εHf_t values of -4.9 to 0.

6.4.3 Eastern granites

A total of 46 zircon grains were analysed from four samples from the eastern granites, and include analyses of groups that are interpreted to date crystallisation and inherited zircon. Analyses of magmatic zircon (n=36), with crystallisation ages between c. 1805 and c. 1814 Ma, have a large

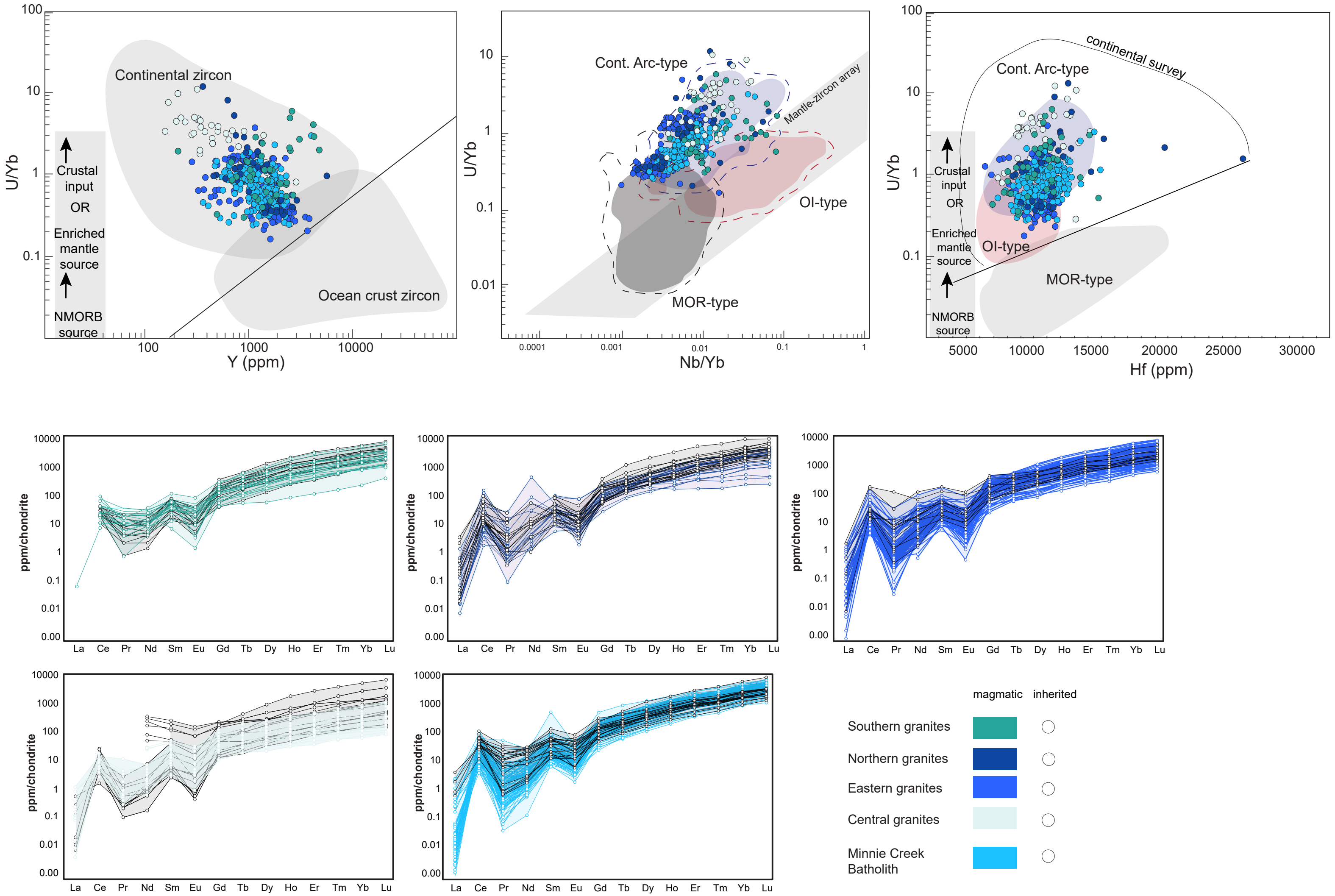

Figure 6.5 Discrimination diagrams and chondrite-normalised plots for trace elements

range of initial ^{176}Hf/^{177}Hf ratios (0.281287–0.281651) with corresponding εHf$_t$ values of -12.1 to -1.5 (median εHf$_t$ of -8.3 ± 6.8, n = 33). Analyses of inherited zircon with individual ^{207}Pb/^{206}Pb ages ranging between c. 2693 and c. 1898 Ma, have a range of initial ^{176}Hf/^{177}Hf compositions (0.280809–0.281660) and a large range of εHf$_t$ values between -13.8 to +4.9.

Table 6.2 Summary of zircon hafnium and oxygen isotope data

Sample	Unit[1]	Pb-Pb age (Ma)	εHf[2]	εHf range	TDMC[3]	δ^{18}O[4] (‰)	δ^{18}O range (‰)
144801	SG	–	-	-12.2 to +0.5	3621.0	-	4.93-6.51
143546	SG	1785 ± 21	-	-12.7 to -7.3	4093–3767	-	5.03-8.77
135433	SG	–	-9.1 ± 3.2 (5)	-11.4 to 0	3221	7.18 ± 0.42 (3)	7.03-7.42
135464	SG	1838 ± 26	-6.9 ± 2.4 (6)	-11.3 to-6.9	3053–2803	6.79 ± 0.79 (6)	6.34-7.47
142856	SG	1794 ± 13	-11.1 ± 3.4 (6)	-8.8 to -5.2	3192	6.92 ± 0.43 (5)	6.66-7.24
169086	NG	1802 ± 10	-0.8 ± 8.2 (8)	-9.2 to-2.8	2822–2360	6.29 ± 1.73 (9)	5.45-7.95
169885	NG	1806 ± 13	-5.9 ± 3.7 (7)	-11.0 to +3.3	n/a	9.01 ± 1.63 (7)	7.79-9.63
190685	EG	1826 ± 10	-3.5 (1)	-5.0 to -0.3	n/a	-	6.71-7.59
169050	EG	1806 ± 5	-9.5 ± 4.8 (15)	-12 to -2.8	3298–2977	5.47 ± 0.41 (13)	5.11-5.8
169814	EG	(1849 ± 28)	-3.3± 5.8 (9)	-8.8 to -4.8	n/a	9.42 ± 0.53 (7)	9.04-9.76
169862	EG	-	-9.7 ± 4.5 (8)	-8.8 to -4.4	3265	6.29 ± 0.96 (3)	5.22-7.07
112107	EG	1774 ±5	-	-	n/a	7.54± 0.96 (13)	5.75-9.0
142924	CG	(1796 ± 45)	-	-	-	-	-
159987	CG	1805 ± 6	-	-11.3 to -1.4	n/a	-	-
168939	CG	1814 ± 17	-5.7 ± 1.9 (8)	-12.1 to -4.9	n/a	8.09 ± 0.64 (7)	7.82-8.72
185952	CG	1776 ± 5	-6.8 ± 3.3 (5)	-	n/a	-	-
159724	CG	n/a	-7.3 ± 2 (12)	-11.8 to -2.8	3055–2873	6.51 ± 0.45 (7)	6.17-6.83
195821	MCB	1804 ± 5	-4.3 ± 2.6(15)	-7.4 to -2.5	n/a	7.94 ± 0.52 (11)	7.52-8.45
190634	MCB	1785 ± 9	-3.7 ± 2.9 (14)	-5.9 to -1.4	n/a	8.63 ± 0.73 (10)	8.19-9.23
JCO14–4–02	MCB	1817 ± 6	-3.9 ± 2.1 (15)	-7.2 to +0.8	n/a	9.42 ± 0.8 (13)	8.66-10.06
88419	MCB	1798 ± 5	+0.5 ± 1.2 (6)	-4.6 to +2.7	n/a	7.04 ± 0.62 (6)	6.66-7.37
178024	MCB	1803 ± 4	-0.5 ± 4.2 (15)	+1.5 to +2.5	n/a	7.22 ± 0.64 (11)	6.78-7.82
88415	MCB	1801 ± 8	-1.8 ± 0.6 (6)	-0.7 to +2.9	n/a	7.24 ± 0.54 (7)	6.86-8.17
88407	MCB	1787±14	-2.2 ± 1.5 (11)	-3.8 to +0.0	n/a	7.87 ± 0.82 (12)	6.94-8.35
88412	MCB	1799 ± 4	-2.0 ± 1.1 (12)	-4.4 to -1.4	n/a	8.33 ± 1.12 (14)	7.97-10.23
JCO14–4–01	MCB	1805 ± 3	-3.9 ± 1.9 (11)	-5.4 to +0.0	n/a	9.13 ± 0.76 (6)	8.72-9.92
JCO14–4–09	MCB	1814 ± 27	-2.1 ± 2 (11)	-5.5 to -1.55	n/a	8.03 ± 0.43 (8)	7.61-8.26
190660	MCB	1802 ± 7	2 ± 1.4 (2)	-6.4 to -1.7	n/a	-	7.22-8.42
JCO14–4–05	MCB	(1814 ± 15)	-	-	-	8.89 ± 1.11 (3)	8.15-9.48

[1] SG= Southern granites, NG = Northern granites, EG = Eastern granites, CG = Central granites, MCB = Minnie Creek Batholith.

[2] εHf values of magmatic zircon are expressed as median values in, ±2SD. Number of analyses donated in brackets.

[3] TDMC will only be quoted where δ^{18}O are within mantle (5.3 ± 0.6 ‰, 2σ) values

[4] δ^{18}O values of magmatic zircon are expressed as averages, ±2SD. Number of analyses donated in brackets. (-) indicates no value obtained. Where no value is obtained for magmatic zircon, the range reflects values from inherited zircon. n/a indicates not available

6.4.4 Central granites

A total of 42 zircon grains were analysed from four samples from the Central granites (GSWA 142924, GSWA 159724, GSWA 168939 and GSWA 185952), and include analyses of groups that are interpreted to date crystallisation and inherited zircon. Analyses of magmatic zircon, with crystallisation ages of 1823 ± 8 Ma, 1826 ± 10 Ma and 1808 ± 17 Ma, have a small range of initial ^{176}Hf/^{177}Hf ratios (0.281377–0.281586) with corresponding εHf$_t$ values of -8.8 to -1.4 (median εHf$_t$ of -6.5 ± 3.4, n=25). Analyses of inherited zircon with individual ^{207}Pb/^{206}Pb ages ranging between c. 2639 and c. 1849 Ma, have a range of initial ^{176}Hf/^{177}Hf compositions of 0.281120 to 0.281487, and a large range of εHf$_t$ values of -12.8 to +0.7.

6.4.5 Minnie Creek Batholith

Data from the Minnie Creek Batholith consist of 130 individual analyses from 12 samples and include analyses of groups that are interpreted to date crystallisation and inherited zircon. Analyses of magmatic zircon from groups with individual ages between c. 1843–1775 Ma have a range of initial ^{176}Hf/^{177}Hf ratios between 0.281440 and 0.281723, with corresponding εHf$_t$ values of -7.3 to +2.4 (median εHf$_t$ of -2.7 ± 4.4, n=119). Analyses of inherited zircon with individual ^{207}Pb/^{206}Pb ages ranging between c. 2069 and c. 1837 Ma, have a range of initial ^{176}Hf/^{177}Hf compositions of 0.281349 to 0.281705, and a large range of εHf$_t$ values of -4 to +3.1.

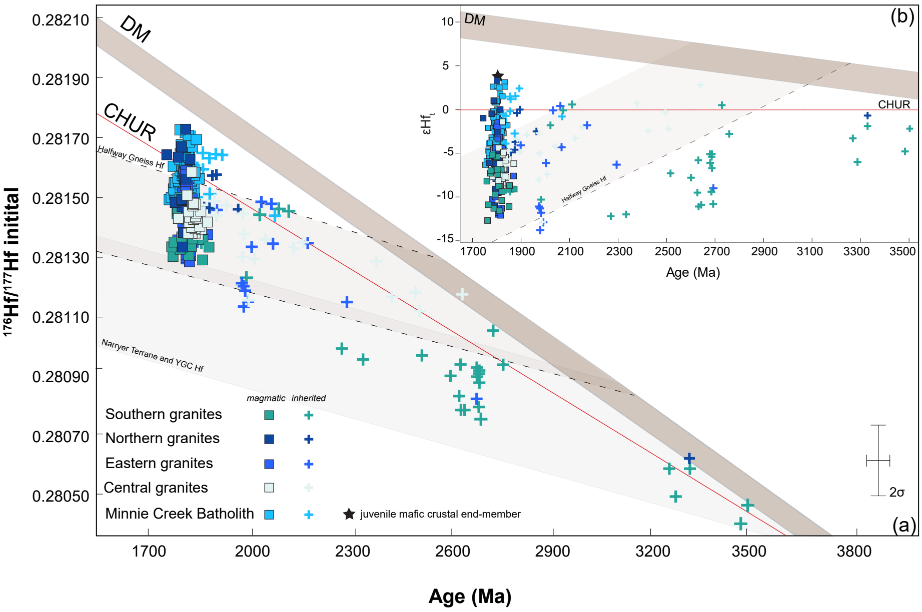

Figure 6.6 Lu–Hf isotope results from the Moorarie Supersuite. Grey shaded area: isotopic envelope for the Yilgarn Craton margin Hf (magmatic) (Narryer Terrane and Yarlarweelor Gneiss Complex) and striped area: isotopic envelope for the Halfway Gneiss Hf is from Chapter 4 analyses. The dashed line is a reference evolution line corresponding to a Lu/Hf ratio of 0.015. (a) Initial Hf evolution plot for the Mooarie Supersuite (n = 289), and (b) Hf evolution diagram for zircon grains from the Moorarie Supersuite, deviations of Hf (^{176}Hf/^{177}Hf) isotopic composition from the chondrite uniform reservoir (CHUR) standard are expressed in epsilon units, εHf$_t$.

6.5 OXYGEN ISOTOPE DATA

Two hundred and ninety-three analyses were conducted on magmatic and inherited zircon grains from 27 granitic rocks (Table 6.2; Fig. 6.7). Five analyses have been rejected due to ablated area consisting of core-rim mixtures, inclusions, cracks or edges (see Appendix D). $\delta^{18}O$ values of all analyses range between 3.91 and 10.23‰ . Magmatic grains (n=193) yield a range of $\delta^{18}O$ values between 5.11 to 10.23‰, with the average $\delta^{18}O$ magmatic zircon from each sample varying from 5.49 ± 0.43‰ to 9.42 ± 0.49‰, 2SD. Inherited zircon grains (n=90) with $^{207}Pb/^{206}Pb$ ages ranging between c. 3506 and c. 1818 Ma yield a range of $\delta^{18}O$ values between 3.91 and 10.06‰. Analyses with no reliable corresponding age data (n = 6) have $\delta^{18}O$ values between 5.96 and 9‰.

6.4.1 Southern granites

Data from the southern granites consist of 53 individual analyses from five samples. Analyses of magmatic zircon (n=15) from samples GSWA 135433, GSWA 135464 and GSWA 142856 record a range of $\delta^{18}O$ values from 6.34 to 7.47‰, and have means of 6.72 ± 1.62‰ (2SD, n=4), 6.79 ± 0.79‰ (n = 6) and 6.94 ± 0.43‰ (n=5), respectively. Inherited zircon grains (n=35) with $^{207}Pb/^{206}Pb$ ages between c. 3506 and c. 1818 Ma yield a range of $\delta^{18}O$ values ranging from 3.91to 8.77‰.

6.4.2 Northern granites

A total of 28 zircon grains were analysed from two samples. Analyses of magmatic zircon grains (n = 16) show large variation in $\delta^{18}O$ values, ranging from 5.45 to 9.84‰, and have means of 9.01± 1.63‰, (2SD; GSWA 169885; n=7) and 6.29 ± 1.73‰ (GSWA 169086; n=9), respectively. Analyses of inherited zircon grains (n=12) yield $\delta^{18}O$ values ranging from 5.8 to 10.06‰.

6.4.3 Eastern granites

A total of 46 zircon grains were analysed from five samples. Analyses of magmatic zircon grains (n=24) yield a range of $\delta^{18}O$ values between 5.22 and 9.76‰, and have average $\delta^{18}O$ of 7.54 ± 1.85‰ (2SD; GSWA 112107; n=13), 9.42 ± 0.49‰ (GSWA 169814; n=7), 6.29 ± 1.57‰ (GSWA 169862, n=3). Analyses of inherited zircon grains (n=8) with $^{207}Pb/^{206}Pb$ ages ranging between c. 2736 and c. 1997 Ma yield $\delta^{18}O$ values ranging from 4.7 to 8.81 ‰. Twelve analyses with no reliable age data record $\delta^{18}O$ values ranging between 5.11–8.06‰

6.4.4 Central granites

A total of 20 zircon grains were analysed from two samples (GSWA 168939 and GSWA 159724). Analyses of magmatic grains yield mean $\delta^{18}O$ values of 8.1 ± 0.6‰ (2SD, n=7) and 6.38 ±

0.77‰ (n=8), respectively. Analyses of inherited zircon grains (n=5) with ^{207}Pb/^{206}Pb ages ranging between c. 2008 and c. 1987 Ma yield δ^{18}O values ranging from 6.3 to 8.12‰.

6.4.5 Minnie Creek Batholith

Data from the Minnie Creek Batholith consist of 141 individual analyses from 12 samples. Analyses of magmatic grains (n=110) record δ^{18}O values ranging between 6.66 and 10.23‰, and have mean δ^{18}O values of: 7.87 ± 0.78‰ (GSWA 88407; 2SD, n=12); 8.33 ± 1.12‰ (GSWA 88412, n=14); 7.24 ± 0.54‰ (GSWA 88415, n=6); 7.04 ± 0.62‰ (GSWA 88419, n = 6); 7.22 ± 0.64‰ (GSWA 178024, n=11); 8.63 ± 0.73‰ (GSWA 190634, n=10); 7.94 ± 0.52‰ (GSWA 195821, n = 11); 9.13 ± 0.76‰ (JCO14–4–01, n = 6); 9.42 ± 0.8‰ (JCO14–4–02, n=15); 8.89 ± 1.11‰ (JCO14–4–05; n=3) and 8.03 ± 0.43‰ (JCO14–4–09 n=8). Analyses of inherited zircon grains (n=24) with ^{207}Pb/^{206}Pb ages ranging between c. 2113 to c. 1826 Ma yield a range of δ^{18}O values between 6.14 and 9.29‰. Analyses with no corresponding or reliable age data(n=12) have δ^{18}O values of 8.80 and 9.67‰.

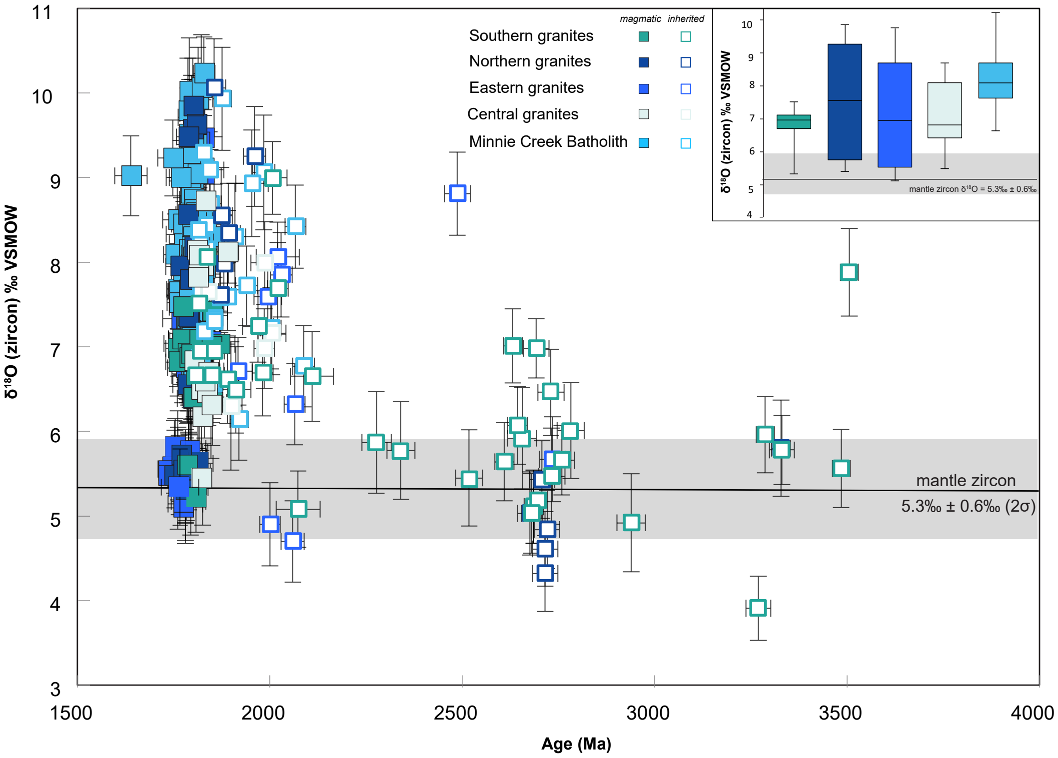

Figure 6.7 Oxygen isotope results from the Moorarie Supersuite. (n = 264). Inset shows box-and-whisker plots showing the range and median values of δ^{18}O VSMOW compositions.

6.6 DISCUSSION

6.6.1 Previous isotopic constraints

Granites of the Moorarie Supersuite are calc-alkaline and weakly peraluminous (Sheppard et al., 2010a), with whole-rock geochemical compositions similar to suprasubduction zone magmas of the Cordilleran Interior batholiths that were emplaced inboard (>600km) from active continental margins (Frost et al., 2001). Whole-rock Sm-Nd analyses of the Minnie Creek Batholith record εNd values between -5.5 and -1.7, corresponding T_{DM} model ages ranging between 2570 and 2250 Ma (Sheppard et al., 2010a). These εNd values are more radiogenic relative to the remainder of the Moorarie Supersuite samples (-14.3 to -4.0). Sheppard et al (2010a) interpreted that these values, along with the presence of mafic-ultramafic intrusions and mafic inclusions in the batholith, suggest a more juvenile (mantle derived) source due to lithospheric thinning in the centre of the province. Previous whole-rock and Sm-Nd isotope work of Sheppard et al. (2003; 2010a) on the southern granites constrain εNd to range between -14.3 and -11.6, suggesting the likely source for the granites were late Archaean and Palaeoproterozoic crustal components. Hf zircon analyses have been conducted on the Moorarie Supersuite granites (Johnson et al., 2017a). The resulting εHf_t array is compatible with mixing between radiogenic crust and highly evolved crust. By combining Hf and paired O isotopes, Johnson et al (2017a) have constrained the composition of a crustal component that they suggest was involved in the source of the Moorarie Supersuite granites. This crustal component is characterized by inherited zircon grains with ages ranging between c. 2280 and c. 2115 Ma with relatively low εHf_t and $\delta^{18}O$ values. These are considered to be evidence for a deep- or mid-crustal component that underlies much of the Gascoyne Province (Johnson et al., 2017a).

6.6.2 Timing of magmatism and significance of inherited ages

The analysed zircon from the Moorarie Supersuite samples span a period of 1880 Myr, with individual $^{207}Pb/^{206}Pb$ ages ranging from 3506 to 1626 Ma. Magmatic ages recorded in the individual Moorarie Supersuite samples range from c. 1838 to c. 1774 Ma. Magmatism in the southern and eastern part of the study area (i.e. samples from the southern granites, central granites and the eastern granites) generally have older crystallisation ages (c. 1838–1775 Ma) than magmatism recorded in the northern part of the study area (i.e. northern granites and Minnie Creek Batholith samples; c. 1817 to c. 1776 Ma). However, the trend is weak and its significance is unclear.

Further insight into the nature of the sources of the Moorarie Supersuite granites, and consequently into crustal evolutionary processes in this area, are provided by the inherited zircon population.

The individual $^{207}Pb/^{206}Pb$ ages of inherited grains range from c. 3506 to c. 1808 Ma, for which the age spectra show major peaks at c. 2690, c. 2535, c. 1983 and c. 1860 Ma, with minor peaks at c. 3490, c. 3290, c. 2520, c. 2150 and c. 2044 Ma (Fig. 6.8). The analysed zircon grains from the southern granites are dominated by inherited material, with a total of 68% of concordant analyses (<5% discordance) ranging between c. 3506 and c. 1818 Ma, the majority of which have Yilgarn-type ages (i.e. 2685–2630 Ma; Nutman et al., 1991; Champion and Cassidy, 2006). Similarly, the northern granite samples show a dominance of inherited material, with a total of 47% of concordant analyses indicating $^{207}Pb/^{206}Pb$ ages between c. 3329 and c. 1847 Ma, in which the majority have Palaeoproterozoic or Neoarchaean ages (i.e. 2695 and 1873 Ma; Fig. 6.8). The samples from the central granites also show a high number of inherited zircon grains, with a total of 51% indicating $^{207}Pb/^{206}Pb$ ages between c. 2639 and c. 1849 Ma. The samples from the eastern granites contain a more limited number of inherited zircon grains (14%), these show a dominance of Palaeoproterozoic ages, with the oldest analysis yielding a $^{207}Pb/^{206}Pb$ age of c. 2694 Ma. The Minnie Creek Batholith samples have a smaller number of inherited zircon grains (11%). These analyses show a dominance of Palaeoproterozoic ages (c. 1860 Ma), with oldest analysis yielding a $^{207}Pb/^{206}Pb$ age of 2397 Ma.

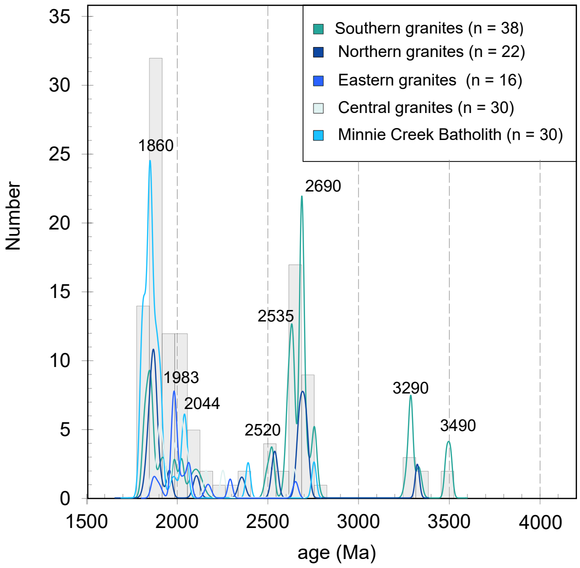

Figure 6.8 Probability plot of inherited ages, Moorarie Supserutie

The presence of Neoarchaean and Paleoarchaean inherited zircon components in the northern and southern granites can be attributed to their spatial location. The inherited material in the northern granites has ages similar to the Fortescue Group (c. 2775–c. 2629 Ma; Thorne and Trendal, 2001). The southern granites intruded the Yarlarweelor Gneiss Complex, and the inherited material have mainly Neoarchaean ages, which reflect the c. 3300–2640 Ma protolith ages. Within the Gascoyne Province, the Moorarie Supersuite intrudes metasedimentary rocks (Leake Spring Metamorphics) and igneous rocks (Glenburgh Terrane: Halfway Gneiss, Dalgaringa Supersuite). The Neoarchean-aged inherited material from the central granites reflect ages similar to the c. 2550–2430 Ma protolith ages established for orthogneisses of the Halfway Gneiss (Johnson et al., 2011a). The eastern granites intrude metasedimentary rocks, with the Yilgarn craton margin likely contributing the contaminating sedimentary components. The Minnie Creek Batholith samples show a paucity of Archaean-aged inherited zircons, with the majority of analyses yielding Palaeoproterozoic ages, with dominant peaks at c. 2050 and c. 1860 Ma. Although a lack of inherited zircon grains does not necessarily indicate the absence of older crust, the lack of Archaean inheritance in the Minnie Creek Batholith indicates that the granitoids were primarily generated from Palaeoproterozoic (c. < 2300 Ma) crustal components without the addition of significant Archaean-aged material.

The inherited zircon from all samples indicate that significant proportions of crust of Palaeoproterozoic age (c. 1860 Ma; Fig 6.8) is present within, or was involved in the formation of, the Moorarie Supersuite. Although existing data for igneous rocks within the Capricorn Orogen indicate that c. 1950–1840 Ma crustal components are currently unexposed, they can be matched with the Leake Spring Metamorphics which contain detrital zircon with ages that overlap with the c. 1950–1840 Ma component (Kirkland et al., 2009b; Wingate et al., 2011b, 2017c). This suggests that the abundant Palaeoproterozoic inherited material were incorporated from melting of the metasediments.

6.6.3 Development of crustal components – evidence from hafnium isotopes

The Moorarie Supersuite granitoids show a wide range in magmatic zircon Hf-isotope compositions, with εHf_t ranging between -12.1 to +2.5. Granites from individual regions show a more restricted range in values (Fig. 6.6), and there is a distinct spatial trend within the Moorarie Supersuite Hf data, with the northern samples (i.e. northern granites and Minnie Creek Batholith samples) having more radiogenic values. εHf_t values from magmatic zircon in the northern samples range between evolved (unradiogenic) values of -11 to more juvenile (radiogenic) values of +3.3. Median εHf_t values for individual samples range between -5.9 ± 3.7 (2SD; n=7) and -0.8 ± 3.7 (2SD; n=7). Those with mantle like $\delta^{18}O$ values return T_{DM}^{C} ages between c. 2822 and c. 2360 Ma. By contrast, εHf_t values of magmatic zircon from the southern part of the study area (i.e samples from the southern granites and the central granites) are all more evolved than CHUR, and all display a similar range of evolved εHf_t values of -11.4 to 0. Median εHf_t values for individual samples range between -11.1 ± 3.4 (2SD; n=6) and -6.9 ± 2.4 (2SD; n=6). Those with Mantle-like $\delta^{18}O$ values return T_{DM}^{C} ages between c. 3263 and c. 2770 Ma, older than those of the northern granites. Similarly, magmatic zircon grains from the eastern granites record a range of evolved εHf_t values of -12 to -1.4, and those with Mantle like $\delta^{18}O$ values return T_{DM}^{C} ages between 3298 and 2977 Ma. The dominance of unradiogenic εHf_t values in the southern and eastern samples suggests that these granites were formed mainly from the reworking of pre-existing isotopically evolved crustal components with little/no mantle input. By contrast, the Hf isotope data for the northern samples record more radiogenic εHf_t values that suggests mixing between a pre-existing crustal component and a juvenile component. These data suggest that the magmas that the zircon grains crystallised from were sourced from different, spatially discrete, crustal components.

Evolution lines defined by source $^{176}Lu/^{177}Hf$ values of 0.015 (Griffin et al., 2002) are plotted from analyses of Yilgarn Craton granites (Narryer Terrane and Yarlarweelor Gneiss Complex) and the Glenburgh Terrane granites (Halfway Gneiss, Dalgaringa Supersuite and Bertibubba Supersuite). These represent isotope arrays along which the Moorarie Supersuite may have evolved. Zircon Lu–Hf data for samples from the Halfway Gneiss yield a clearly-defined initial Hf array with crystallisation ages of c. 2689–2387 Ma, which correspond to T_{DM}^{C} ages of 3434–2771 Ma (Chapter 4; Johnson et al., 2017a). Crustal evolution lines show that the granites of the central granite samples lie within the Halfway Gneiss isotopic envelope. Therefore, these isotopic arrays indicate that the parental magmas were formed by reworking of a source possessing broadly similar $^{176}Lu/^{177}Hf$ ratios, such as the Halfway Gneiss. Inherited zircon grains have compositions which plot along this evolution line, and are consistent the interpretation that the central granites were sourced from reworking of the Halfway Gneiss. The southern granites have unradiogenic εHf_t values of -12.7 to -6.8 that, like the central granite samples, lie within the Halfway Gneiss isotopic envelope. In addition, inherited zircon grains with $^{207}Pb/^{206}Pb$ ages between c. 3506 and c. 2335 Ma have Hf compositions (εHf_t -12.2 to -1.9) that lie within the Yilgarn Craton granites Hf–U–Pb field (Fig. 6.6). However, a caveat is that the data do not distinguish whether the inherited zircon grains were incorporated into the host magma from surrounding crust during magma ascent, or derived from the magmatic source. It is possible that the southern granites sourced a range of Yilgarn Craton material and mixed with an additional juvenile component at the time of emplacement. However, there is a distinct absence of mafic-ultramafic material in the region associated with the southern granites and no field evidence to indicate magma mingling (Sheppard et al., 2003). In addition, the Hf signature only overlaps the most radiogenic Yilgarn Craton analyses. Therefore, it is more likely that the sources for the Southern granites are the Palaeoproterozoic granites of the southern Gascoyne Complex (with minor amounts of Archaean Yilgarn Craton granites). This indicates that crustal components of the Glenburgh Terrane were present under the margin of the Yilgarn Craton during the c. 1820–

1770 Ma Capricorn Orogeny. The presence of the Glenburgh Terrane below the Narryer Terrane is consistent with seismic reflection lines, which show south dipping crustal-scale thrusting, and indicate the existence of the Glenburgh Terrane below the Narryer Terrane at depths of 45–48 km (Johnson et al., 2013).

By contrast, the Hf isotope data for the Minnie Creek Batholith magmatic zircon define an array that includes values that are representative of more radiogenic (juvenile) crust (εHf_t -7.4 to +2.5). Inherited zircon grains with $^{207}Pb/^{206}Pb$ ages between c. 2069 and 1831 Ma have εHf_t values of -2.8 to +3.1. The range in isotopic composition in the Minnie Creek Batholith is more radiogenic than can be explained by reworking of the Glenburgh Terrane alone, and is compatible with melt sourced from two compositionally and isotopically distinct sources; an evolved component with an isotopic composition similar to that of the southern Gascoyne Province and a juvenile mantle-derived component. This interpretation is supported by the presence of mafic-ultramafic intrusions and mafic inclusions within the batholith, as well as field evidence of magma mingling (Sheppard et al., 2010a). This interpretation is essentially similar to that based on whole-rock geochemistry, which led Sheppard et al (2010a) to suggest that the Minnie Creek Batholith granites were generated by a mantle-derived mafic underplate beneath thinned lithosphere.

The eastern granite samples have εHf_t values of -12.1 to -1.4, those with mantle- like $\delta^{18}O$ values have corresponding to $T_{DM}{}^C$ ages that range from 3265 to 2977 Ma. These evolved Hf-isotope compositions imply that the magmas from which these zircon crystallised from were derived, at least in part, from remelting of more evolved crustal sources with lower Lu/Hf than CHUR. The Hf-isotopic range of this material overlaps the Glenburgh Terrane granites and suggests that the Glenburgh Terrane or its reworked equivalents were present as basement when magmatic rocks of the eastern granites were emplaced. This has implications for the interpretation of magnetotelluric studies of Dentith et al (2014) that suggest that the central part of the Collier Basin is underlain by rocks of the Glenburgh Terrane. Three inherited zircon grains with $^{207}Pb/^{206}Pb$ ages between c. 2693 and c. 1979 Ma have Hf compositions (εHf_t -13.8 to -9) that lie within the isotopic range exhibited by Yilgarn Craton granites. The eastern granites intrude metasedimentary rocks of the Padbury Group, and it is possible that the inherited zircon grains were sourced from a Yilgarn Craton detrital component within the upper crustal metasediments during emplacement. The northern granites have a range of εHf_t values (-11 to +3.3) that indicate mixing between an evolved component with crustal residence ages of more than c. 3100 Ma, and a juvenile component. One analysis of an inherited zircon grain with a $^{207}Pb/^{206}Pb$ age of 3329 Ma has a εHf_t value of -0.7 and $T_{DM}{}^C$ age of 3706 Ma, comparable with Pilbara Craton granites (Amelin et al., 2000). The northern granites intrude low-grade metasedimentary rocks of the Ashburton Formation, and like the samples from the eastern granites, it is possible that the inherited zircon grains were sourced from a Pilbara Craton detrital component within the upper crustal metasediments during emplacement. All the granitic rocks of the Moorarie Supersuite appear to share common source components, with variable mixing between upper and mid-to lower crustal components, with some depleted-mantle components.

6.6.4 Development of crustal components, evidence from oxygen isotopes

Oxygen isotope data for the magmatic zircon grains from the Moorarie Supersuite granites range from 5.47 ± 0.41‰ to 9.42 ± 0.53‰, 2SD. The magmatic zircon data show systematic variations in $\delta^{18}O$ with respect to spatial distribution, with the lowest $\delta^{18}O$ values observed in the southern granites within the Yarlarweelor Gneiss Complex (average $\delta^{18}O$ 6.79–7.18‰), increasing towards the northwest towards the central granites (average 6.51–8.09‰), Minnie Creek Batholith (average 7.04–9.42‰). The eastern and the northern granites show a larger range in $\delta^{18}O$, with averages between 5.47–9.42‰ and 6.29–9.01‰, respectively. The northern granites, eastern granites, southern granites and central granites have $\delta^{18}O$ values that are within error of the field of mantle zircon. This indicates that the magmas that these zircon crystallised from contained significant low-$\delta^{18}O$ material representing an infracrustal source component with mantle-like $\delta^{18}O$ (i.e. a meta-igneous crustal component that has not interacted significantly with shallow crustal material), and negligible amounts of supracrustal (metasedimentary) material. In contrast, the Minnie Creek Batholith is dominated by higher $\delta^{18}O$ (7–10‰; average 8.12 ± 1.6‰ 2SD). These high $\delta^{18}O$ zircon values are typical of magmas with a dominant metasedimentary component (~8-12‰; Appleby et al., 2010). The diversity of the data indicates that the magmas that the zircon grains crystallised from were sourced from multiple, isotopically distinct, crustal components. Individual samples from the southern granites display a narrow range of average $\delta^{18}O$ values (6.79 ± 0.42‰ to 7.18 ± 0.42‰) coupled with variably evolved εHf_t compositions (-11.4 to -5.2). Zircon with mantle $\delta^{18}O$ values indicate $T_{DM}{}^{C}$ ages of 3221–2803 Ma. The inherited Archaean zircon cores show $\delta^{18}O$ values ranging from 3.91 to 7.01‰, with the majority having mantle values. One grain has a higher $\delta^{18}O$ value of 7.88‰. Together, these data indicate derivation from an old or evolved crustal component that has not interacted significantly with shallow crustal material, with inherited material incorporated into the host magma from surrounding crust during magma ascent and/or emplacement within the mid- to low-crust. This is consistent with the U–Pb and Hf data which suggest reworking of Palaeoproterozoic granites of the southern Gascoyne Complex, and emplacement of magmas into the Yilgarn Craton margin.

Two samples from the central granites (GSWA 159724 and GSWA 168939) have contrasting average $\delta^{18}O$ of 6.51 ± 0.45‰ and 8.09± 0.64‰, coupled with moderately evolved εHf_t

compositions (median -7.3 to -5.7). The zircon with mantle $\delta^{18}O$ values indicate T_{DM}^{C} ages of 3003–2916 Ma. Johnson et al (2017) reported similar $\delta^{18}O$ ranges (6.8 ± 1.02‰ and 7.1 ± 0.9‰). Analyses from sample GSWA 157924 have low $\delta^{18}O$ that are within error of mantle zircon values. The origin of this low $\delta^{18}O$ magmas can be attributed to an infracrustal source component (igneous rock solidified at depth with limited interaction with shallow crustal material) and is consistent with the U–Pb and Hf data which suggest derivation from reworking of granites of the southern Gascoyne Complex. The higher $\delta^{18}O$ values observed in GSWA 168939 indicates incorporation of a high $\delta^{18}O$ material into the melt source and may represent an additional metasedimentary source component. Using a simple mixing (binary mixing) equation:

$$X_1 = (C_{mix} - C_2) / (C_1 - C_2) * 100$$

where:

X_1 is the proportion of end-member 1 in the crustal component
C_1 is concentration of end-member 1
C_2 is concentration of end-member 2
C_{mix} is concentration of the crustal component

and assuming an average Palaeoproterozoic sediment value of ~10–15‰, and an average magmatic value of ~8‰, this would imply an input of ~20–50% high $\delta^{18}O$ material in the GSWA 168939 magmas relative to average Glenburgh Terrane granite $\delta^{18}O$ values (~6.1‰). For sample GSWA 159724 an input of ~5-11% high $\delta^{18}O$ material is implied.

The eastern granites display similar Hf–O arrays, with samples indicating average $\delta^{18}O$ that range from mantle-like values 5.47 ± 0.41‰ to high-$\delta^{18}O$ values of 9.42 ± 0.53‰, coupled with variably evolved εHf_t compositions (median -9.5 to -3.3). This Hf–O isotope array can be accounted for by progressive contamination of magma batches due to crustal assimilation and wall-rock interaction, i.e. the granites were formed from melts generated from mixing of a low-$\delta^{18}O$ magmas (partial melts of a Halfway Gneiss-like component) with a minor metasedimentary component, while other broadly coeval granites formed from melts that incorporated larger amounts of metasedimentary component. The Minnie Creek Batholith analyses display variably evolved εHf_t compositions (-7.4 to +2.5) coupled with moderate to high-$\delta^{18}O$ values (6.7–10.2‰), indicating assimilation of buried sediments or other supracrustal material. Simple two-component mixing equation indicates an incorporation of ~25–55% high-$\delta^{18}O$ material in the generation of the Minnie Creek Batholith granites. It is possible that repeated intrusion of mantle-derived magmas induced crustal anatexis in lower and/or middle crustal levels, producing hybrid magmas within a deep crustal hot zone (Annen et al., 2006). The basaltic magmas can act as a lower- or mid-crustal heat source without contributing to the melts (e.g. Annen et al., 2006), as observed in the granites south of the Mutherbukin Zone. They can also mix with silicic magmas, as observed in the Minnie Creek Batholith granites. Extraction and subsequent migration of these melts could have occurred along deep-seated lithospheric structures into higher crustal reservoirs, where mixing may occur between different melt batches combined with partial melting with metasediments could precipitate zircon with high-δ^{18}O values and low εHf$_t$ values (e.g. Kemp et al., 2007). Metasedimentary enclaves (metre to kilometre-scale) in the Minnie Creek Batholith (Johnson et al., 2017a) are interpreted as evidence for bulk assimilation. These enclaves record low to very low metamorphic grade, and indicate that they have stayed at their current crustal levels since emplacement in the upper crust (Johnsone et al., 2011c). Absence of mantle δ^{18}O values in the Minnie Creek Batholith granites suggest remelting of mafic lower crust rather than mantle-derived magmas. This interpretation is supported by the Sm–Nd compositions of the mafic rocks which indicate more evolved compositions than that of the model depleted mantle (Johnson et al., 2017c).

Most of the samples have δ^{18}O values between 7 and 9‰, a characteristic consistent with derivation of the granite magmas from a source containing a significant component of weathered materials. Some samples have mantle like δ^{18}O values implying that not all magmas involved supracrustal contributions. This variation in δ^{18}O values may be explained if the zircon derived from magmas formed at different crustal levels. Magmas in the southern part of the Capricorn Orogen and adjacent Yilgarn Craton margin intruded at deeper mid- to lower- crust levels, which consisted largely of meta-igneous rocks, resulting in their lower δ^{18}O and evolved εHf$_t$ compositions. Towards the eastern and northern parts of the Capricorn Orogen these magmas intruded to shallow crustal levels, possibly along deep lithospheric-scale faults, and assimilated high-δ^{18}O crust resulting in higher δ^{18}O and variably evolved εHf$_t$ compositions. The U–Pb data indicate that most samples record a c. 1860 Ma component that can be matched detrital zircon populations within the Leake Spring Metamorphics, suggesting that they were derived in part from melting of upper crustal metasediments. This component is poorly constrained by Hf and O analyses, however the εHf$_t$ of these Palaeoproterozic inherited zircon (c. 1950–1850 Ma) range between -9.4 and +1.5, coupled with δ^{18}O values between 6.3 and 10.1‰, consistent with the interpretation that they represent upper crustal metasedimentary material. Heat provided by the emplacement and partial crystallisation of a significant number mantle-derived mafic magmas into the lower crust resulting in the development of deep crustal hot zones (e.g. Annen et al., 2006) may explain the thermal conditions that led to the generation of the Moorarie Supersuite granites. Downward increasing seismic velocities in the lower crust of the Glenburgh Terrane is consistent with magmatically underplated material, which is up to 16.5 km thick (Korsch et al., 2011).

The combination of high δ^{18}O and low εHf$_t$ values requires: (1) input of material into the source that was previously affected by low-temperature alteration at or near Earth's surface; (2) input of an evolved infracrustal material into the source, and (3) a juvenile input. Rocks that meet these criteria include upper crustal rocks, such as the Leake Springs Metamorphics and the Fortescue Group, and meta-igneous basement rocks of the Glenburgh Terrane. An εHf$_t$ versus δ^{18}O plot of Moorarie Supersuite zircon (Fig. 6.9) can show the relationship to potential supracrustal and infracrustal sources. The Hf–O compositions of the zircon indicate a wide array that require multiple crustal sources. The composition of the infracrustal source (crustal component 1) was estimated from the average δ^{18}O data and median Hf data from the Halfway Gneiss samples recalculated at 1790 Ma (Chapter 4). The composition of the second infracrustal source (crustal component 2) was estimated from the average δ^{18}O data and median Hf data from the Dalgaringa Suprsuite samples recalculated at 1790 Ma (Chapter 5). The juvenile mafic component uses a εHf$_t$ value of +3 (based on the whole-rock Nd isotopic composition of mafic rocks from Johnson et al., 2017c). There is a lack of data to constrain the supracrustal source (crustal component 3), however, using the median εHf$_t$ value of sedimentary units within the Gascoyne Province (GSWA, 2016) combined with δ^{18}O value of 10‰ (based on the average sediment value; Appleby et al., 2010), can approximate the composition of the supracrustal end-member. The Hf concentration of the crustal end-member and mantle end-member was set

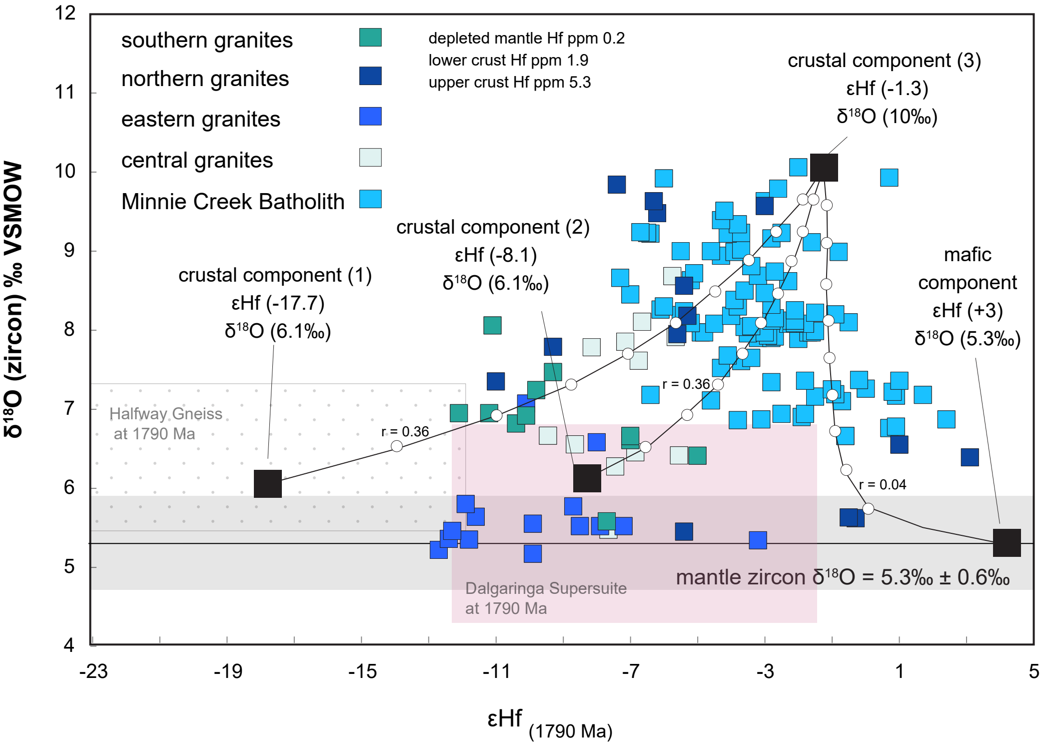

Figure 6.9 δ^{18}O vs εHf$_t$ for magmatic zircon from the Moorarie Supersuite. The stippled (crosses) box represents the Halfway Gneiss at 1790 Ma, the pink box represents the Dalgaringa Supersuite at 1790 Ma. The parameters of end members are discussed in text. Bulk mixing curves are marked at 10% increments.

at values 5.3, 1.9 and 0.2 ppm, estimates for the upper crust, lower crust and depleted mantle, respectively (Rudnick and Gao, 2003; Salters and Stracke, 2004). Based on the mixing lines between the depleted mantle component and the metasedimentary component (crustal component 2) the model indicates that the most radiogenic Minnie Creek Batholith samples require 70% input from a juvenile mafic crustal component. Simple mass balance equation of initial hafnium values will produce the same percentages. The eastern granites overlap composition fields of the Halfway Gneiss and Dalgaringa Supersuite (recalculated at 1790 Ma), and suggests that the infracrustal source represents a complicated mixture of Halfway Gneiss protoliths and Dalgaringa Supersuite granites. The central and southern granites lie on mixing lines between the metasedimentary end-member and the infracrustal sources (crustal component 1, 2) and do not require a depleted mantle component.

6.5 SUMMARY

- Moorarie Supersuite granites are interpreted to represent melts that were generated by the emplacement of basaltic magmas in the lower crust, resulting in a deep crustal hot zone that induced partial melting of mafic lower crustal rocks and surrounding metaigneous basement. Extraction of hybrid magmas and migration along crustal shear zones to shallow reservoirs in the upper crust facilitated crustal anatexis and metasedimentary rock assimilation.

- The Hf–O isotope data from granites south of the Mutherbukin Zone indicated mixing between a reworked meta-igneous component (40–100% contribution) with a composition similar to that of the Halfway Gneiss or the Dalgaringa Supersuite, and a metasedimentary component (20–60% contribution). The most radiogenic Minnie Creek Batholith analyses require 70% input from a juvenile mafic crustal component and 30–100% contribution from a metasedimentary component.

- The Hf–O compositions indicate melts were sourced from multiple, isotopically distinct sources: (1) a reworked meta-igneous component with a composition similar to that of the Halfway Gneiss/Dalgaringa Supersuite (2) a metasedimentary component and (3) a mafic, lower crustal component.

CHAPTER 7

INTRACRSTAL REWORKING — THE MANGAROON OROGENY (c. 1680–1620 Ma) AND EDMUNDIAN OROGENY (c. 1030–955 Ma)

7.1 INTRODUCTION

The Durlacher Supersuite is dominated by granites of granodioritic to monzogranitic composition, and intruded into the Gascoyne Province during the c. 1680–1620 Ma Mangaroon Orogeny (Sheppard et al., 2005). Granitic rocks of the Durlacher Supersuite intruded across the Gascoyne Province and into Yarlarweelor Gneiss Complex in the south. Previous geochemical and isotopic studies have suggested that the Durlacher Supersuite was generated by the melting and reworking of rocks similar in isotopic composition to the Moorarie Supersuite and also included a significant proportion of metasedimentary rock (Sheppard et al., 2005; Johnson et

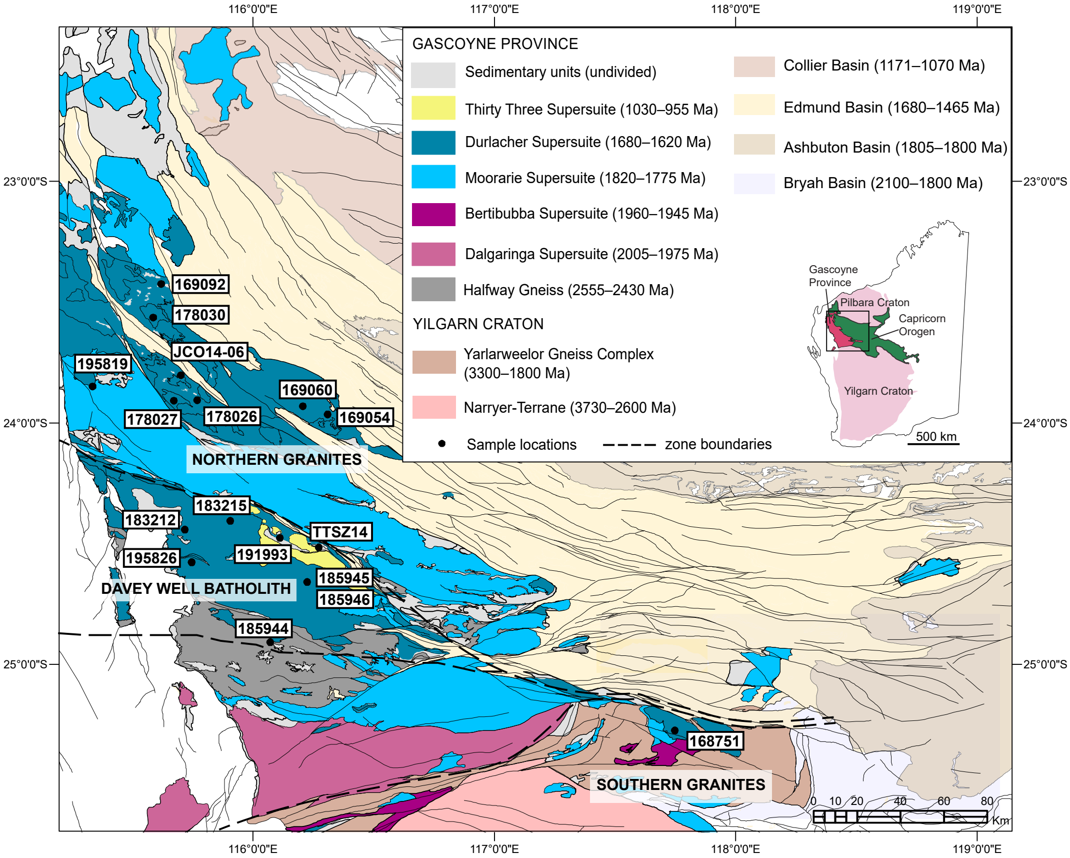

Figure 7.1 Simplified geological map of part of the Capricorn Orogen showing the Gascoyne Province and Yilgarn Craton margin, the principal tectonic units and sample locations mentioned in the text.

al., 2017a). However, the tectonic driver for melt generation is currently unknown. The c. 1030–955 Ma Edmundian Orogeny is interpreted as an intracratonic event that is associated with very low- to low-grade metamorphism and widespread deformation (Martin and Thorne, 2004; Sheppard et al., 2010a). Within the Gascoyne Province the Edmundian Orogeny is associated with high-temperature and low-pressure metamorphism (500–550°C, 3–4 kbar; Sheppard et al., 2007) within the Mutherbukin Zone, and the intrusion of the leucocratic granite plutons and rare element pegmatites of the c. 1030–955 Ma Thirty Three Supersuite (Sheppard et al., 2007, 2010b).

The identification of various granites in the Gascoyne Province have provided geochemical and geochronological constraints on the timing and nature of crustal growth within the Capricorn Orogen, and improved the understanding of its crustal evolution (Occhipinti et al., 1998, 1999; Sheppard et al., 2003, 2004, 2005, 2007; Johnson et al., 2010, 2011b, 2017a; Piechocka et al., 2017). This chapter presents U–Pb, trace element, hafnium and oxygen isotope data of the youngest two granitic supersuites, the Durlacher and Thirty Three Supersuite, which are used to constrain the relative contributions and compositions of crustal sources during their petrogenesis.

7.2 U–Pb GEOCHRONOLOGY

The 15 samples from the Durlacher Supersuite are grouped by geographic region, with reference to the tectonometamorphic zones of the Gascoyne Province (Fig. 7.1; Sheppard et al., 2010b). Samples are discussed in accordance to their geographical sub-divisions. Zircon grains obtained from heavy mineral separates provided for by the GSWA are indicated in text. All other zircon grains are obtained through EMP as described in Chapter 3. Representative CL images of zircon grains are shown in Fig. 7.2, all U–Pb Concordia diagrams showing the subset of results of zircon are shown in Fig. 7.3. Details of U–Pb sample analyses are given in Appendix E.

7.2.1 Southern Granites (Yarlarweelor Gneiss Complex)

The southern granite intrudes the Yarlarweelor Gneiss Complex, which is characterised by granitic gneisses with protolith ages of c. 3300–2630 Ma (Nelson, 1998a; 1999i) that were locally deformed and intruded by c. 1960 Ma plutons during the Glenburgh Orogeny (Sheppard et al., 2003) and intensely reworked during the 1820–1770 Ma Capricorn Orogeny.

7.2.1.1 GSWA 168751

Sample GSWA 168751 is a metamonzogranite. Zircon grains were hand-picked from heavy mineral concentrates provided by the GSWA. Zircon grains are colourless to light brown, typically 80–220 μm in size, with euhedral or subhedral, sub-rounded elongate to blocky

Table 7.1 Summary of sample descriptions and U–Pb LASS data

sample	Unit[1]	Lithology[2]	Pb–Pb age (Ma)[3]	Inheritance (Ma)	Pb–Pb age (Ma)[4]	T_{Ti} (°C)	Lat	Long
168751	SG	monzogranite	1651 ± 13	2061–1705	1644 ± 6	753	-25.25506	117.74676
183212	DWB	granitic gneiss	1684 ± 9	2409–1739	1666 ± 5	746	-24.42339	115.71645
183215	DWB	metamonzogranite	1666 ± 6	1742–1721	1667 ± 3	772	-24.38626	115.90343
185944	DWB	monzogranite	1667 ± 8	2246–1856	1653 ± 10	803	-24.8899	116.0697
191993	DWB	metamongranite	1658 ± 5	1724–1713	1666 ± 7	784	-24.4572	116.1106
195826	DWB	metamonzogranite	1674 ± 5	2565–1738	1664 ± 8	741	-24.5575	115.745
195819	NG	metamonzogranite	1682 ± 11	1765–1748	1670 ± 7	781	-23.83188	115.33255
169054	NG	metatonalite	1667 ± 15	2778–1746	1674 ± 4	708	-23.94653	116.30706
169060	NG	syenogranite	(1692 ± 23)	2265	1673 ± 15	-	-23.9129	116.2055
178027	NG	granodiorite	[1772 ± 10]	2222–1748	1677 ± 5	-	-23.88722	115.65568
178030	NG	granodiorite	1689 ± 5	2320–1747	1678 ± 6	716	-23.5456	115.5853
178026	NG	syenogranite	(1690 ± 16)	1920–1805	1691 ± 9	613	-23.8601	115.67
JCO14-4-06	NG	metagranite	(1683 ± 19)	1798	-	590	-23.792716	115.70107
169092	NG	monzogranite	-	-	1681 ± 10	-	-23.42301	115.64358
TTSZ14	33SS	metagranite	[1665 ± 5]	2233–1712	-	764	-24.5156	116.2357
185946	33SS	pegmatite	*1035 ± 7	1749–1634	*1030 ± 6	600	-24.6547	116.1677
185945	33SS	pegmatite	(*1028 ± 26)	1738–1558	*1000 ± 8	712	-24.65474	116.16774

[1] SG = southern granites, DWB = Davey Well Batholith, NG = northern granites, 33SS = Thirty Three Supersuite.

[2] Petrographically characterised (GSWA)

[4] Crystallisation age (^{207}Pb/^{206}Pb) established by LASS, ages in brackets indicate () minimum crystallisation age, asterix * indicates ^{206}Pb/^{238}U age

[3] Crystallisation age (^{207}Pb/^{206}Pb) established by SHRIMP (GSWA) (-) indicates no value obtained

morphology. CL images reveal oscillatory zoning which in places is contorted. Many grains are overgrown by thin (<10 µm thick) homogenous rims with low CL response. Forty-six analyses were obtained from 46 grains. Twenty-six analyses (Group D) are >5% discordant and are not considered further. Sixteen analyses (Group 1) from 15 cores and one rim yields a weighted mean ^{207}Pb/^{206}Pb date of 1651 ± 13 Ma (MSWD = 1.7), interpreted as the igneous crystallization age of the monzogranite. Four analyses of cores (Group X) yield ^{207}Pb/^{206}Pb dates of 2061 and 1705 Ma, interpreted as the ages of inherited material. The crystallisation age of 1651 ± 13 Ma is in agreement with the previously established SHRIMP U–Pb age (1644 ± 6 Ma; Nelson, 2001a).

7.2.2 Davey Well Batholith (Mutherbukin Zone)

The Davey Well Batholith samples occur in the Mutherbukin Zone in the central part of the Gascoyne Province (Fig. 7.1).

7.2.2.1 GSWA 183212

Sample GSWA 183212 is a granitic gneiss. Zircon grains were hand-picked from heavy mineral concentrates provided by the GSWA. Zircon grains are colourless to brown in colour, 60–180 µm in length and euhedral elongate to stubby in shape. CL images reveal grains with mainly low CL response, some grains display oscillatory zoning. Forty-six analyses were obtained from 45 grains. Twenty-two analyses (Group X) are >5% discordant and are not considered further. Twelve analyses (Group 1) yield a weighted mean $^{207}Pb/^{206}Pb$ date of 1684 ± 9 Ma (MSWD = 0.59), interpreted as the timing of magmatic crystallisation of the granite protolith. One analysis (Group P) yields a $^{207}Pb/^{206}Pb$ date of 1518 Ma interpreted to reflect ancient loss of radiogenic Pb. Eleven analyses (Group X) yield $^{207}Pb/^{206}Pb$ dates of c. 2409–1739 Ma, interpretedas the ages of inherited material. The crystallisation age of 1684 ± 9 Ma is older than the SHRIMP U–Pb age previously established by the GSWA (1666 ± 5 Ma; Kirkland et al., 2009).

7.2.2.2 GSWA 183215

Sample GSWA 183215 is a metamonzogranite. Zircon grains were hand-picked from heavy mineral concentrates provided by the GSWA. Zircons grains range from 100 to 500 μm in length and generally display sub-rounded, subhedral elongate morphologies. Grains typically show oscillatory zoning and in some cases this zoning has become convoluted. All grains display CL-dark peripheral rims, which are typically discontinuous and of varying thicknesses, typically <5 μm thick. Mineral inclusions are common. Twenty-nine analyses were obtained from 36 grains. Two analyses (Group D) are >5% discordant and have been rejected. Twenty-four analyses of 22 grains (Group 1) yield a weighted mean $^{207}Pb/^{206}Pb$ date of 1666 ± 6 Ma (MSWD = 1.6), interpreted as the age of magmatic crystallisation. Two analyses of rims yield $^{207}Pb/^{206}Pb$ dates of c. 1663 and c. 1658 Ma, indistinguishable from dates obtained from cores. Two analyses (Group X) yield $^{207}Pb/^{206}Pb$ dates of c. 1742 and c. 1721 Ma, interpreted to represent inherited material. The crystallisation age of 1666 ± 6 Ma is in agreement with the SHRIMP U–Pb age previously established by the GSWA (1667 ± 3 Ma; Wingate et al., 2009b).

7.2.2.3 GSWA 185944

Sample GSWA 185944 is a monzogranitic. Zircon grains are colourless or pale yellowish-brown, typically 120–280 μm in length, with euhedral or subhedral, sub-rounded elongate to blocky morphology. CL images generally display oscillatory zoned centres, and in some case, this zoning has become convoluted. Many zircons display rounded high uranium cores and oscillatory zoned overgrowths mantle many crystals. Thirty analyses were obtained from 29 grains. Eleven analyses (Group D) are >5% discordant and are not considered further. Seventeen analyses (Group 1) of cores yield a weighted mean $^{207}Pb/^{206}Pb$ date of 1667 ± 8 Ma (MSWD = 1.8), interpreted as the age of magmatic crystallization. Two analyses (Group X) return $^{207}Pb/^{206}Pb$ dates of c. 2246 and c. 1856 Ma, interpreted as the ages of inherited material. The crystallisation age of 1667 ± 8 Ma is in agreement with the SHRIMP U–Pb age previously established by the GSWA (1653 ± 10 Ma; Wingate et al., 2010a).

7.2.2.4 GSWA 191993

Sample GSWA 191993 is a metamonzogranite. Zircon grains from this sample are up to 400 µm in length and typically colourless to light-pinkish brown in colour. The general morphology is subhedral-euhedral, sub-rounded, equant to elongate. Grains generally display oscillatory zoned cores, and in some case, this zoning has become convoluted. Uranium rich rims of varying thicknesses are present on the majority of grains. Thirty-nine analyses were obtained from 31 grains. Twelve analyses (Group X) are >5% discordant and are not considered further. Twenty-four analyses (Group 1) from 17 cores and rims, yield a weighted mean ^{207}Pb/^{206}Pb date of 1658 ± 5 Ma (MSWD = 0.63), interpreted as the igneous crystallization age of the monzogranite. Three analyses of cores return ^{207}Pb/^{206}Pb dates between c. 1721 and c. 1713 Ma, interpreted as the ages of inherited material. The crystallisation age of 1658 ± 5 Ma is in agreement with the SHRIMP U–Pb age previously established by the GSWA (1663 ± 7 Ma; Wingate et al., 2009a).

7.2.2.5 GSWA 195826

Sample GSWA 195826 is a metamonzogranite. Zircon grains were hand-picked from heavy mineral concentrates provided by the GSWA. Zircon grains are typically subrounded elongate to equant in shape, colourless to light honey-brown in colour and generally 150–350 µm in size. CL images reveal poorly luminescent, convolute or oscillatory zoned grains mantled by thin CL-bright rims. Some grains contain subhedral cores. Forty-five analyses were obtained from 45 grains. Eleven analyses (Group D) are >5% discordant and are not considered further. Twenty-three analyses of 19 cores and four recrystallized domains (Group 1) yield a weighted mean ^{207}Pb/^{206}Pb date of 1675 ± 5 Ma (MSWD = 1.06), interpreted as the crystallisation age. Six analyses (Group X) of cores yield ^{207}Pb/^{206}Pb ages ranging between c. 2565 to 1738 Ma, interpreted as inherited material. Four analyses (Group P) yield ^{207}Pb/^{206}Pb dates between c. 1630 and c. 1546 Ma, and one analysis with a ^{206}Pb/^{238}U date of c. 1401 Ma. The analyses in Group P are interpreted to reflect grains that have suffered ancient loss of radiogenic Pb. The crystallisation age of 1675 ± 5 Ma is in agreement with the SHRIMP U–Pb age previously established by the GSWA (1664 ± 8 Ma; Wingate et al., 2013c).

The sample was analysed again in 2015, zircon were hand-picked from heavy mineral separates provided by the GSWA. Forty-five analyses were obtained from 38 grains. Twelve analyses (Group D) are >5% discordant and are not considered further. Twenty-nine analyses including 3 homogenous rims (Group 1) yield a weighted mean ^{207}Pb/^{206}Pb date of 1675 ± 8 Ma (MSWD = 1.3), interpreted as the crystallisation age. Three analyses (Group X) of cores yield ^{207}Pb/^{206}Pb ages ranging between c. 2288 to c. 1852 Ma, interpreted as inherited material. One analyses of a homogenous rim (Group M) returned a ^{206}Pb/^{238}U date of c. 1217 Ma, interpreted as the age of a metamorphic event. The crystallisation age of 1675 ± 8 Ma is in agreement with the SHRIMP U–Pb age previously established by the GSWA (1664 ± 8 Ma; Wingate et al., 2013c).

7.2.3 Northern granites (Limejuice and Mangaroon Zone)

The northern granites occur north of the Davey Well Batholith within the Limejuice and Mangaroon Zone. Within the Mangaroon Zone the granite plutons intrude the Pooranoo Metamorphics.

7.2.3.1 GSWA 195819

Sample GSWA 195819 is a metamonzogranite. Zircon grains are colourless to dark brown, 100–300 µm in length and euhedral elongate to stubby in shape. CL images display oscillatory zoning which in places is contorted and CL-dark homogenous overgrowths mantle many crystals. Forty-four analyses were obtained from 39 grains. Twenty analyses (Group D) are >5% discordant and are not considered further. Five analyses of homogenous overgrowths returned $^{207}Pb/^{206}Pb$ dates between c. 1725 and 1641 Ma, indistinguishable from dates obtained from oscillatory zoned grains. Twenty-two analyses (Group 1) including 17 oscillatory zoned zircon and 5 homogenous overgrowths identified in CL, yield a weighted mean $^{207}Pb/^{206}Pb$ date of 1682 ± 11 Ma (MSWD = 1.6), interpreted as the age of magmatic crystallization. Two analyses of an oscillatory zoned rim and one core return $^{207}Pb/^{206}Pb$ dates between c. 1765 and 1748 Ma, interpreted as the ages of inherited material. The crystallisation age of 1682 ± 11 Ma is in agreement with the SHRIMP U–Pb age previously established by the GSWA (1670 ± 7 Ma; Wingate et al., 2013a).

7.2.3.2 GSWA 169054

Sample GSWA 169054 is a metatonalite. Zircon grains were hand-picked from heavy mineral concentrates provided by the GSWA. Zircon grains are pale to dark brown in colour, 60–120 µm in length, and are subhedral, subrounded stubby to elongate in shape. CL imaging reveal complex internal structures with cores displaying convoluted zoning, some grains with oscillatory zoning are present. Some zircons display CL-dark rims of varying thicknesses, most are <15 µm thick. Twenty-seven analyses were obtained from 27 grains. Six analyses (Group D) are >5% discordant and are not considered further. Six analyses (Group 1) of cores yield a weighted mean weighted mean $^{207}Pb/^{206}Pb$ date of 1667 ± 15 Ma (MSWD = 0.72), interpreted as the age of magmatic crystallization. Fifteen analyses of cores (Group X) return $^{207}Pb/^{206}Pb$ dates between 2778 and 1746 Ma, interpreted as the ages of inherited material incorporated into this granite. The crystallisation age of 1662 ± 12 Ma is in agreement with the SHRIMP U–Pb age previously established by the GSWA (1674 ± 6 Ma; Nelson, 2002b).

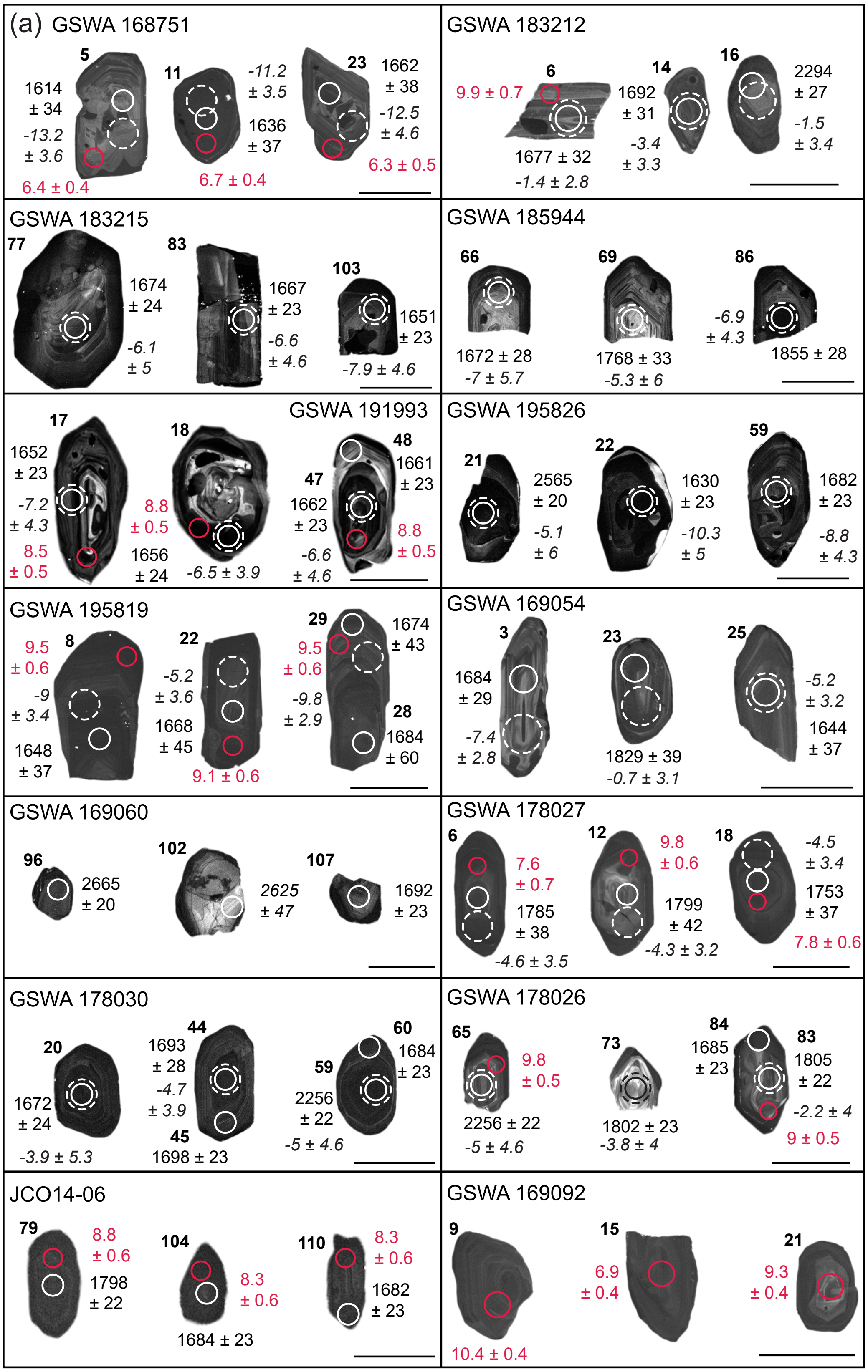

Figure 7.2 continues with caption overleaf

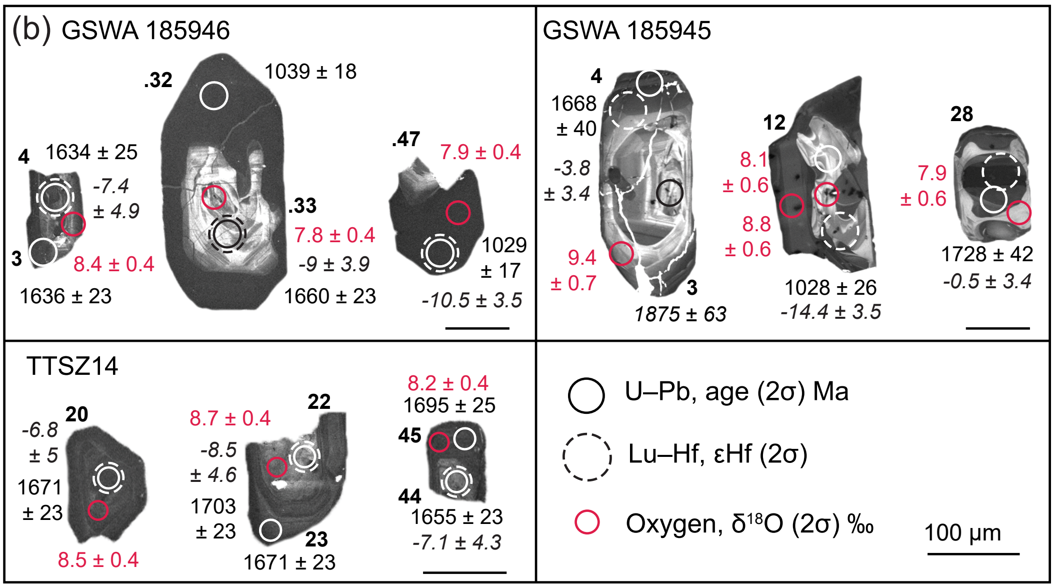

Figure 7.2 CL images of representative zircon grains from (a) Durlacher Supersuite and (b) Thirty Three Supersuite. Grains are numbered by their analysis number. Ages in italics indicates discordance >10%.

7.2.3.3 GSWA 169060

Sample GSWA 169060 is a syenogranite. Zircon grains were hand-picked from heavy mineral concentrates provided by the GSWA. Zircon grains range from 50 to 120 μm in length, are sub-rounded to elongate in shape, and are typically pinkish-brown to dark brown or black in colour and subhedral, subrounded and stubby or irregular fragments. CL imaging reveals cores that typically show oscillatory zoning, and in some cases this has become convoluted. Many are metamict. Ten analyses were obtained from 10 grains. Eight analyses are >5% discorant and are not considered further. The remaining analyses have $^{207}Pb/^{206}Pb$ ages of c. 2665 and c. 1692 Ma. The date of the youngest concordant analysis (1692 ± 23 Ma) is interpreted as the best estimate of the maximum The remaining plotted data points do not define a meaningful discordance line and indicate a significant common-Pb component. The maximum crystallisation age of 1692 ± 23 Ma is in broad agreement with the SHRIMP U–Pb age previously established by the GSWA (1673 ± 15 Ma; Nelson, 2005a).

7.2.3.4 GSWA 178027

Sample GSWA 178027 is a granodiorite. Zircon grains were hand-picked from heavy mineral concentrates provided by the GSWA. Zircon grains are light yellowish-brown to dark brown in colour, between 60–200 μm in length, subrounded elongate to stubby in shape. CL images reveal a range of textures including oscillatory zoning and homogenous domains, often overprinted by recrystallization zones. Forty-seven analyses were obtained from 47 grains. Twenty-six analyses (Group D) are >5% discordant and are not considered further. Seventeen analyses (Group X1) of oscillatory zoned and homogenous domains yield a weighted mean ^{207}Pb/^{206}Pb date of 1774 ± 9 Ma (MSWD = 1.14). Four analyses of cores (Group X) yield ^{207}Pb/^{206}Pb dates between 2222 and 1858 Ma. The age of 1774 ± 9 Ma is significantly older than any Durlacher Supersuite granite.

A geochronological dataset for this sample has previously been described by Nelson (2005d). Twelve analyses yielded a weighted mean ^{207}Pb*/^{206}Pb* date of 1677 ± 5 Ma (MSWD = 1.4), interpreted as the age of crystallisation. Fourteen analyses indicate ^{207}Pb*/^{206}Pb* dates between c. 2822 and c. 1705 Ma, of which five analyses yielding a ^{207}Pb*/^{206}Pb* date of 1793 ± 9 Ma (MSWD = 0.55), interpreted as the ages of inherited zircon grains. The LASS ^{207}Pb/^{206}Pb date of 1774 ± 9 Ma is within error of the ^{207}Pb*/^{206}Pb* date of 1793 ± 9 Ma. Subsequently, the age of 1774 ± 9 Ma indicated by Group X1 and remaining analyses indicating ^{207}Pb/^{206}Pb dates between 2222 and 1858 Ma (this study) are interpreted to be of inherited zircon grains.

7.2.3.5 GSWA 178030

Sample GSWA 178030 is a granodiorite. Zircon grains were hand-picked from heavy mineral concentrates provided by the GSWA. Zircon grains range between 150 and 350 µm in size, and are typically colourless to light-honey brown in colour, and euhedral to subhedral elongate in shape. CL images display weakly concentric narrowly spaced oscillatory zoning, occasionally convoluted zoning is present. Some grains contain rounded CL-darker older cores mantled by homogenous or oscillatory zoned rims of variable thickness. Sixty-one analyses were obtained from 36 grains. Fifteen analyses (Group D) are >5% discordant, and are not considered further. Thirty-seven analyses (Group 1) of 30 cores and seven rims a weighted mean ^{207}Pb/^{206}Pb date of 1689 ± 5 Ma (MSWD = 1.5), interpreted as the igneous crystallisation age of the monzogranite. Nine analyses (Group X) of cores and one rim return ^{207}Pb/^{206}Pb dates ranging between 2320 and 1747 Ma, interpreted as the ages of inherited material. The crystallisation age of 1689 ± 5 Ma is in agreement with the SHRIMP U–Pb age previously established by the GSWA (1678 ± 6 Ma; Nelson, 2005e).

7.2.3.6 GSWA 178026

Sample GSWA 178026 is a syenogranite. Zircon grains were hand-picked from heavy mineral concentrates provided by the GSWA. Zircon grains range from 100 to 280 µm in length, sub-rounded to elongate in shape, and are typically yellow-brown to pinkish in colour. CL imaging reveals cores that typically show oscillatory zoning, and in some cases this has become convoluted. Grains are mantled by CL-darker rims of varying thicknesses and often overprinted by recrystallization zones. Twenty-five analyses were obtained from 23 grains. Fourteen analyses

(Group D) are >5% discordant and are not considered further. Two analyses (Group 1) of one oscillatory zoned core and one homogenous recrystallised domain with Th/U ratios of 0.02 and 0.05 yield a weighted mean ^{207}Pb/^{206}Pb date of 1690 ± 16 Ma (MSWD = 0.21), interpreted as the best estimate of the maximum age of crystallisation. Eight analyses (Group X) of cores and one recrystallised domain return ^{207}Pb/^{206}Pb dates of c. 1920–1805 Ma, interpreted as the ages of inherited material. The maximum crystallisation age of 1690 ± 16 Ma is in agreement with the SHRIMP U–Pb age previously established by the GSWA (1691 ± 9 Ma; Nelson, 2005c).

7.2.3.7 JCO14–4–06

Sample JCO14**–4–06** is a metagranite. Zircon grains are light-brown to brown in colour, 80-220 µm in size and subrounded to euhedral, elongate to stubby in shape. CL images display oscillatory zoning, which in places is contorted. Thirty-six analyses (Group D) are >5% discordant or indicated low Pb counts, and are not considered further. Two analyses of oscillatory zoned cores yield a weighted mean ^{207}Pb/^{206}Pb date of 1683 ± 19 Ma (MSWD = 0.13), interpreted as the best estimate of the maximum age of magmatic crystallisation. Three analyses (Group X) return ^{207}Pb/^{206}Pb dates between c. 1804 and 1798 Ma, interpreted as the ages of inherited material.

7.2.3.8 GSWA 169092

Sample GSWA 169092 is a monzogranite. Zircon grains were hand-picked from heavy mineral concentrates provided by the GSWA. Zircon grains range from 100 to 250 µm in length, subrounded subhedral elongate to irregular in shape, and are typically light-brown to brown in colour. CL images reveal structureless to oscillatory zoned grains, frequently mantled by thin structureless of finely zoned rims. U–Pb data is not available for this sample due to problems during collection.

A geochronological dataset for this sample has previously been described by Nelson (2004b). Twelve analyses of 12 zircon yielded a weighted mean ^{207}Pb*/^{206}Pb* date of 1681 ± 10 Ma (MSWD = 1.48), interpreted as the age of crystallisation.

7.2.4 Thirty Three Supersuite (Mutherbukin Zone)

The Thirty Three Supersuite comprises a belt of plutons and widespread pegmatite dykes and sheets within the Mutherbukin zone. The supersuite crops out over an area 70 km long by 10 km wide and is structurally bound to the north by the Ti Tree Shear Zone.

7.2.4.1 TTSZ14

Sample TTSZ14 is a leucocratic metagranite. Zircon grains are typically subhedral, subrounded stubby to elongate in shape, pale to dark brown in colour, and 100–250 µm in length. CL imaging reveals cores that typically show oscillatory zoning, and in some cases this has become convoluted. Rounded homogenous cores are present in some zircon grains. Some grains are mantled by faintly oscillatory zoned rims. Forty-one analyses were obtained from 34 grains. Nineteen analyses (Group D) are >5% discordant and are not considered further. Seventeen analyses of 14 cores and 3 oscillatory zoned rims (Group X1) yield a weighted mean $^{207}Pb/^{206}Pb$ date of 1665 ± 5 Ma (MSWD = 1.02). Four analyses of cores (Group X) yield $^{207}Pb/^{206}Pb$ ages ranging between c. 2233 to 1991 Ma, interpreted as inherited material.

A biotite–tourmaline monzogranite sampled 700 m to the east (GSWA 183288) yielded a U–Pb age of 1650 ± 6 Ma (Wingate et al., 2017b). Based on field relationships (the granite cross-cuts Neoproterozoic metamorphic fabrics) and previous geochronology the date of 1650 ± 6 Ma was interpreted as the age of an inherited component (Wingate et al., 2017b). Hence, the $^{207}Pb/^{206}Pb$ date of 1665 ± 5 Ma indicated by Group X1 is interpreted to reflect the age of an inherited component.

7.2.4.2 GSWA 185946

Sample GSWA 185946 is a 1m wide pegmatite dyke. Zircon grains were hand-picked from heavy mineral concentrates provided by the GSWA. Zircon grains are colourless to dark brown, and up to 600 µm in size, with euhedral to subhedral, sub-rounded elongate morphology. CL images reveal oscillatory zoning. Some grains display cores of CL-bright responses, surrounded by thick CL-dark rims. Fractures are observed in cores of CL-bright cores. Fifty-three analyses were obtained from 34 zircons. Twenty-nine analyses (Group D) are >5% discordant and are not considered further. The remaining 24 analyses can be divided into three groups, based on their Th/U ratios and ages. Group 1 comprises 11 analyses with Th/U ratios of 0.00–0.02 which yield a weighted mean $^{206}Pb/^{238}U$ date of 1035 ± 5 Ma (MSWD = 1.12). Eleven analyses of cores with Th/U ratios of 0.48–1.82 return $^{207}Pb/^{206}Pb$ dates between c. 1749–1634 Ma. Group X includes nine analyses (Group X2) that yield a weighted mean $^{207}Pb/^{206}Pb$ age of 1656 ± 8 Ma (MSWD 1.03). Two analyses (Group P) return a $^{206}Pb/^{238}U$ dates of c. 1425 and 1004 Ma, and are interpreted to have undergone ancient radiogenic-Pb loss. The age of 1035 ± 5 Ma indicated by Group 1 is interpreted as the age of magmatic crystallisation, with the remaining analyses from Groups X2 and X interpreted as the ages of inherited material. The crystallisation age of 1035 ± 5 Ma is in agreement with the SHRIMP U–Pb age previously established by the GSWA (1030 ± 6 Ma; Wingate et al., 2010e).

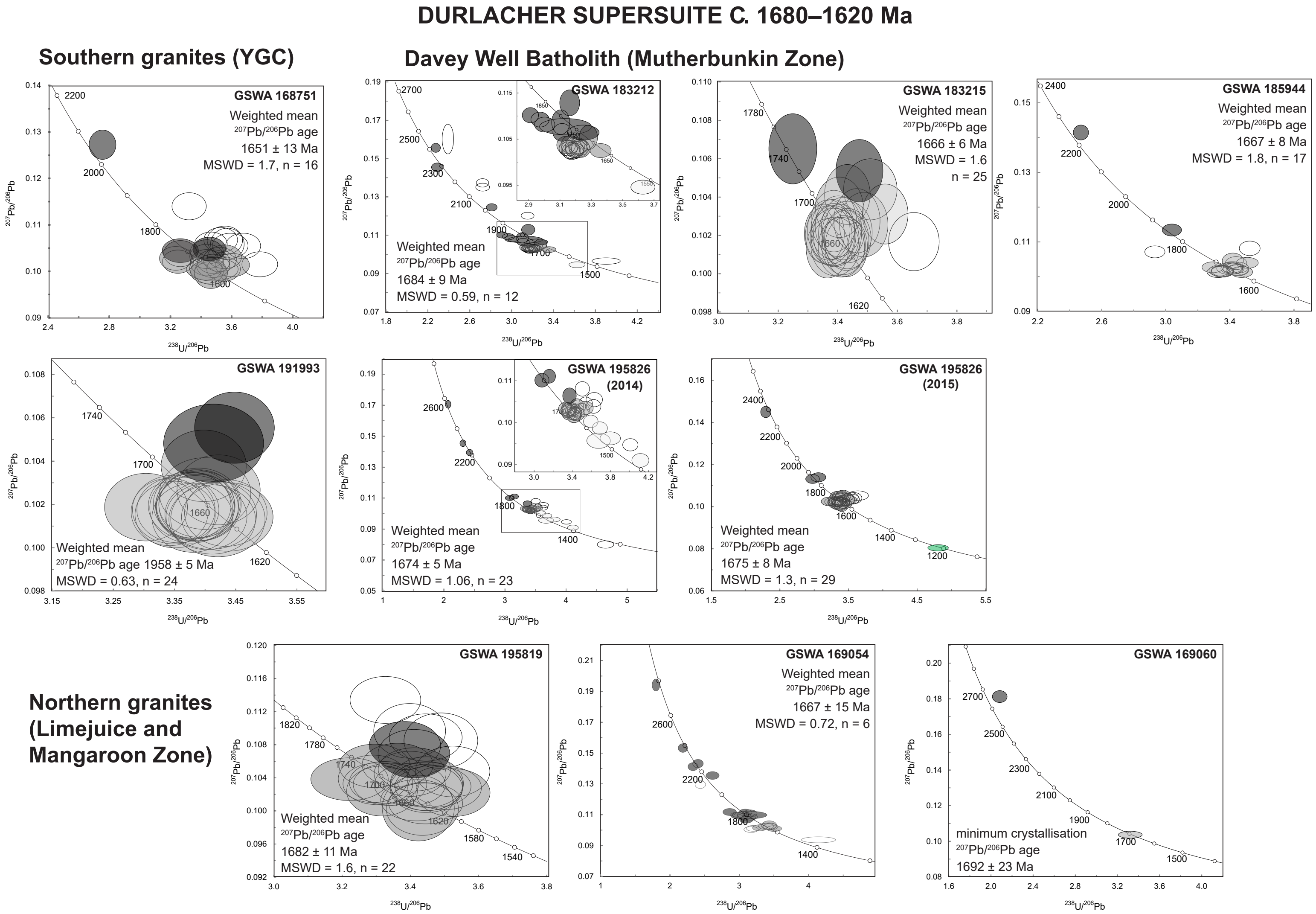

Figure 7.3 continues with caption overleaf

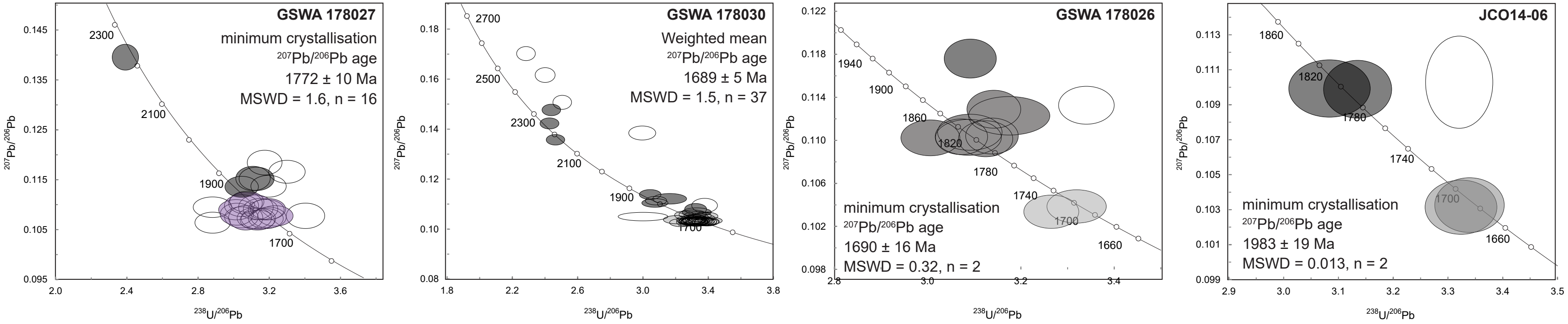

THIRTY THREE SUPERSUITE c. 1035–955 Ma

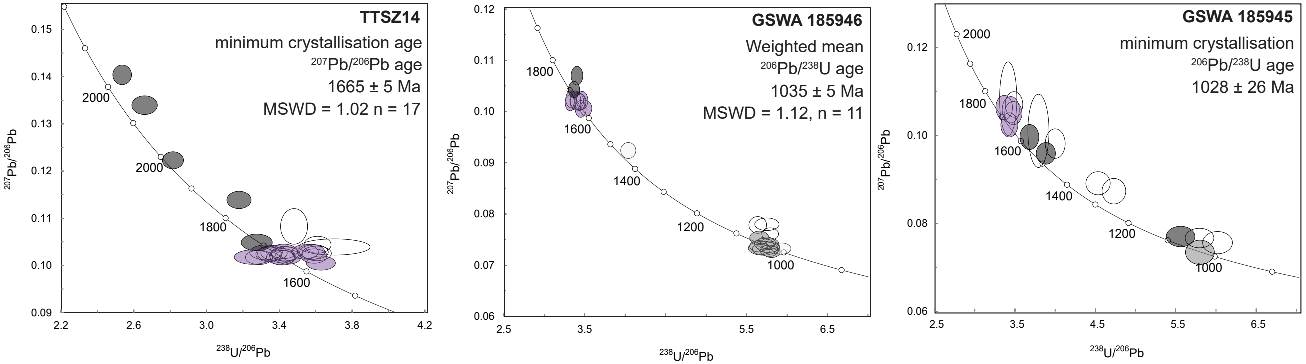

Figure 7.3 Concordia diagram showing the subset of results of zircon with <10% discordance. Grey ellipses indicate analyses used to calculate Group 1 (crystallisation age). Black ellipses indicate inherited zircon (Group X). Purple ellipses indicate analyses used to calculate Group 2 (inherited zircon group). Light grey ellipses indicate radiogenic Pb-loss (Group P). Hollow ellipses indicate outside discordance threshold (Group D). Green ellipses indicate metamorphic zircon (Group M). YGC = Yarlarweelor Gneiss Complex

7.2.4.3 GSWA 185945

Sample GSWA 185945 is a pegmatite lens in metamonzogranite. Zircon grains were hand-picked from heavy mineral concentrates provided by the GSWA. Zircon grains are colourless to dark brown, between 120–300 µm in length, with euhedral to subhedral, sub-rounded elongate to stubby morphology. CL images reveal oscillatory zoning which is commonly convoluted and overprinted by zones of recrystallization. Many grains are surrounded by thin rims of CL-bright response. Twenty-one analyses were obtained from 18 grains. Thirteen analyses are >5% discordant (Group D) and are not considered further. Four analyses yield a weighted mean ^{207}Pb/^{206}Pb age of 1713 ± 49 Ma (MSWD 2.4). Five analyses return ^{206}Pb/^{238}U dates ranging between c. 1558and c. 1028 Ma.

A geochronological dataset for this sample has previously been described by Wingate et al (2010d). Fifteen analyses yielded a concordia age of 1000 ± 8 Ma (MSWD = 1.5), interpreted as the age of crystallisation. Twenty-three analyses yield a ^{207}Pb*/^{206}Pb*date of 1648 ± 6 Ma (MSWD = 0.55), interpreted as the ages of inherited zircon grains from the host monzogranite.

Table 7.2 Summary of hafnium and oxygen isotope data

Sample	Unit[1]	Pb-Pb age[2] (Ma)	εHf[3]	εHf range	TDMC[4]	$\delta^{18}O$[5] (‰)	$\delta^{18}O$ range (‰)
168751	SG	1651 ± 13	-10.7 ± 3 (14)	-13.2 to -8.1	3169–3046	6.38 ± 1.39 (12)	5.46–7.39
183212	DWB	1684 ± 9	-3.2 ± 1.8 (3)	-3.4 to -1.4	n/a	8.96 ± 0.82 (7)	8.49–9.85
183215	DWB	1666 ± 6	-6.6 ± 3.2 (12)	-9.1 to -3.6	n/a	-	-
185944	DWB	1667 ± 8	-8.9 ± 2.3 (6)	-10.2 to -8.2	n/a	-	-
191993	DWB	1658 ± 5	-6.4 ± 2.7 (14)	-8.4 to -3.1	n/a	8.65 ± 0.38 (13)	8.29–8.98
195826	DWB	1674 ± 5	-8.1 ± 3.3 (21)	-10.9 to -5.1	n/a	7.85 ± 1.01 (10)	6.95–9.02
195819	NG	1682 ± 11	-6.9 ± 3.9 (13)	-9.8 to -3.9	n/a	9.02 ± 0.77 (14)	8.33–9.64
169054	NG	1667 ± 15	-6.3 ± 3.5 (4)	-7.8 to -3.5	n/a	-	-
169060	NG	(1692 ± 23)	-	-	n/a	-	-
178027	NG	[1772 ± 10]	-4 ±2.7 (11)	-5.7 to -1.4	2702		-
178030	NG	1689 ± 5	-3.9 ± 2.3 (13)	-6.2 to -1.3	n/a	-	-
178026	NG	(1690 ± 16)	*-2.5 ± 3 (1)*	-	n/a	9.59 ± 0.49 (1)	6.74–9.82
JCO14–4–06	NG	(1683 ± 19)	-	-	n/a	8.58 ± 0.05 (3)	8.28–8.33
169092	NG	-	-	-	n/a	-	6.87–10.41
TTSZ14	33SS	[1665 ± 5]	-	-10.9 to -0	n/a	-	5.59–8.92
185946	33SS	*1035 ± 7	-10 ± 1.2 (4)	-10.5 to -8.9	n/a	8.32 ± 0.96 (3)	7.93–8.99
185945	33SS	(*1028 ± 26)	-15.4 ± 2.1(2)	-16.5 to -14.4	n/a	8.84 ± 0.96 (1)	-

[1] SG= Southern granites, DWB = Davey Well Batholith, NG = Northern granites.

[2] [*] indicates ^{206}Pb/^{238}U age,

[3] εHf values of magmatic zircon are expressed as median values in, ±2SD. Number of analyses donated in brackets.

[4] TDMC will only be quoted where $\delta^{18}O$ are within mantle (5.3 ± 0.6 ‰, 2σ) values

[5] $\delta^{18}O$ values of magmatic zircon are expressed as averages, ±2SD. Number of analyses donated in brackets. (-) indicates no value obtained. Where no value is obtained for magmatic zircon, the range reflects values from inherited zircon. n/a indicates not available

The youngest concordant analyses with a $^{206}Pb/^{238}U$ age of 1028 ± 26 Ma is interpreted as the maximum age of crystallisation, and the age of 1713 ± 49 Ma indicated by Group X are interpreted to be of inherited zircon grains.

7.3 ZIRCON TRACE-ELEMENT COMPOSITION

Zircon grains from the Durlacher and Thirty Three Supersuite samples have trace-element compositions typical of continental zircon, with both magmatic and inherited populations plot within continental arc-type zircon fields (Fig. 7.3a; Grimes et al., 2007; 2015). All Durlacher and Thirty Three Supersuite samples record zircon Ti temperatures with averages between 600 and 803°C. These temperatures are comparable with the low-T inheritance-rich granitoids with T_{Zr} <800°C of Miller et al (2003) that are interpreted as forming in regions of crustal thickening.

7.3.1 Durlacher Supersuite

Chondrite-normalised REE element patterns of the magmatic zircon from the Durlacher Supersuite granites are characterised by strong positive Ce and negative Eu anomalies and a positive heavy REE (HREE) slope, consistent with magmatic zircon (Rubatto 2007; Hoskin and Black, 2000; Hoskin and Ireland, 2000). There is no significant difference in REE composition between zircon overgrowth/recrystallised composition and oscillatory zoned cores (Fig. 7.3b). Magmatic zircon trace element signatures indicate no evidence of co-crystallisation with garnet (i.e. flat HREE pattern with Lu/Gd <3 and no negative Eu anomaly, Eu/Eu* >0.75). The zircon record a range of Yb_N/Gd_N of 2-43 and Eu/Eu* of 0.04–0.74, indicating formation in lower pressures than eclogitic minerals (<1.2 GPa, <45 km depth; Rubatto and Hermann, 2007).

7.3.2 Thirty Three Supersuite

Magmatic zircon have a steep positive M-HREE slope (Yb_N/Gd_N = 31–36) and small Eu anomlay (Eu/Eu* = 0.46–1.13). Inherited zircon have a steep M–HREE slope (Yb_N/Gd_N = 5–51) and slightly more pronounced Eu anomalies (Eu/Eu* = 0.02–0.82).

7.4 Lu–Hf ISOTOPE DATA

A total of 209 analyses were obtained from 12 samples and include analyses of groups that are interpreted to date crystallisation, inherited and metamorphic zircon (Fig, 7.4). Twenty-eight analyses have been rejected due to either poor U–Pb age data (high discordance), no available U–Pb data or the ablated area consisted of core-rim mixtures, epoxy or cracks (see Appendix E).

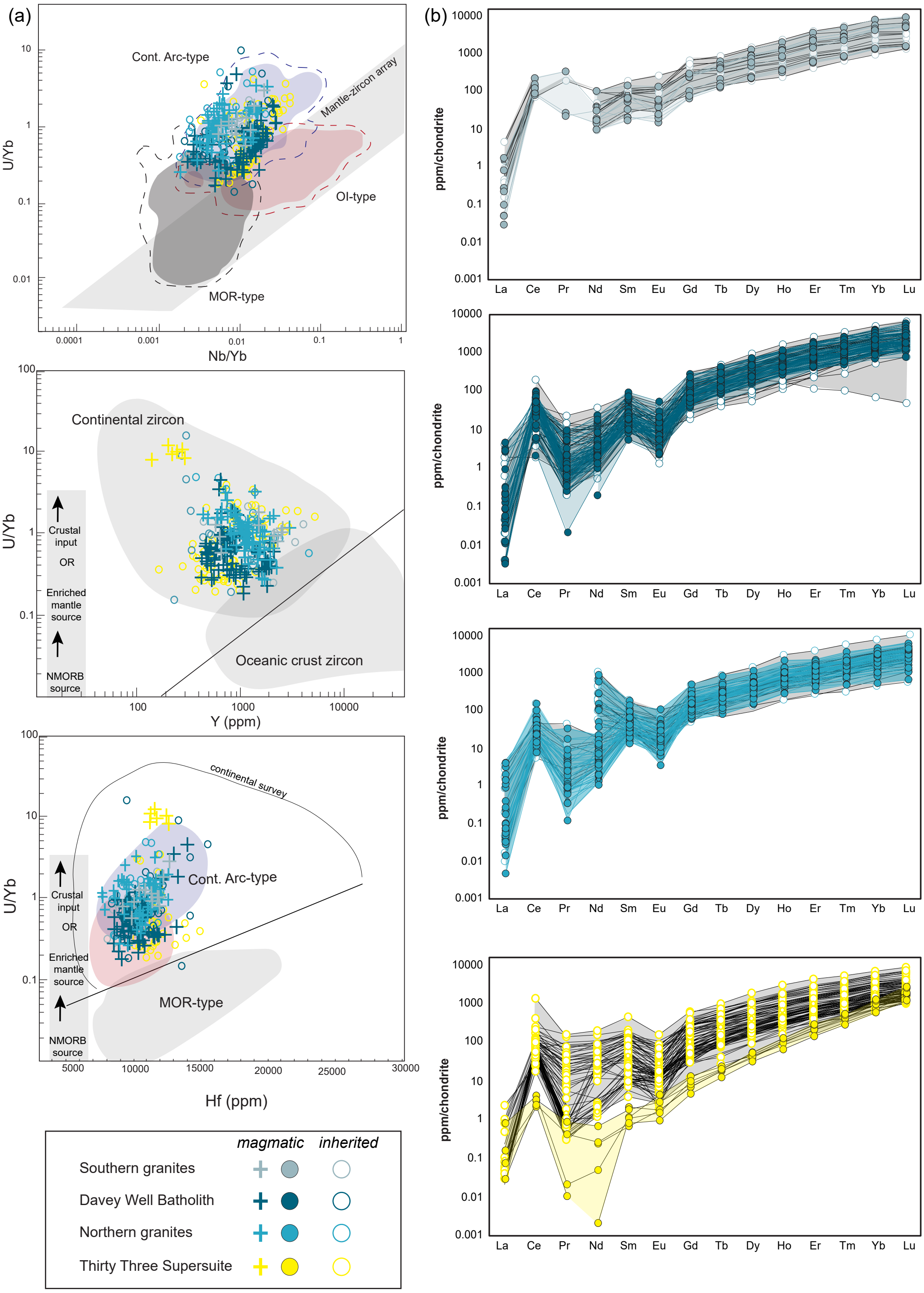

Figure 7.4 Discrimination diagrams and chondrite-normalised plots for trace elements

7.4.1 Durlacher Supersuite

Initial $^{176}Hf/^{177}Hf$ ratios of all analysed zircon grains range between 0.281002 and 0.281873, corresponding to εHf_t values of -19.8 and +5.6. Magmatic grains (n=101) yield a range of initial $^{176}Hf/^{177}Hf$ ratios between 0.281347 and 0.281677 (εHf_t -13 and -1.3), with median εHf_t values from each sample ranging between -10.7 ± 2.7 and -3.2 ± 1.8, 2SD. Inherited zircon grains (n=48) with $^{207}Pb/^{206}Pb$ ages ranging between c. 2565 and c. 1671 Ma yield a range of εHf_t values between -10.8 and -0.7. One analysis of a rim dated at c. 1217 Ma returned an initial $^{176}Hf/^{177}Hf$ ratio of 0.281456 (εHf_t -19.8).

7.4.1.1 Southern granites

A total of 18 zircon grains were analysed from one sample (GSWA 168751). Analyses of magmatic zircon grains with a crystallisation age of 1658 ± 11 Ma have a narrow range of initial $^{176}Hf/^{177}Hf$ ratios (0.281347– 0.281509) with corresponding εHf_t values of -13 to -8.6 (median εHf_t of -10.5 ± 3, n=14). The inherited zircon, with $^{207}Pb/^{206}Pb$ ages between c. 2061 and c. 1700 Ma, yield a range of initial $^{176}Hf/^{177}Hf$ ratios (0.281245–0.281479) with corresponding εHf_t values of -9.3 to -7.7.

7.4.1.2 Davey Well Batholith

Data from the Davey Well Batholith consists of 73 analyses from five samples, and include analyses of groups that are interpreted to date magmatic crystallisation, inherited and metamorphic zircon grains. Magmatic grains (n=56) yield a range of initial $^{176}Hf/^{177}Hf$ ratios between 0.281416 and 0.281677 (εHf_t -10.9 and -1.4). Median values (magmatic) range between -8.9 ± 2.3 and -3.2 ± 1.8. Inherited zircon grains (n=16) with $^{207}Pb/^{206}Pb$ ages ranging between c. 2294 and c. 1671 Ma yield a range of εHf_t values between -10.8 and -1.1. One analysis of a rim dated at c. 1217 Ma returned an initial $^{176}Hf/^{177}Hf$ ratio of 0.281456 (εHf_t -19.8).

7.4.1.3 Northern granites

A total of 59 zircon grains were analysed from five samples. Magmatic grains (n=31) yield a range of initial $^{176}Hf/^{177}Hf$ ratios between 0.281442 and 0.281674 (εHf_t -9.8 and -1.5). Median values range between -6.3 ± 3.9 and -3.9 ± 2.6 (2SD). Inherited zircon grains (n=14) with $^{207}Pb/^{206}Pb$ ages ranging between c. 2384 and c. 2702 1678 Ma range of εHf_t values between -8.2 and -0.7.

7.4.2 Thirty Three Supersuite

A total of 31 zircon grains were analysed from three samples. Magmatic grains (n=5) yield a range of initial $^{176}Hf/^{177}Hf$ ratios between 0.281723 and 0.281873 (εHf_t -14.4 and -8.9). One sample

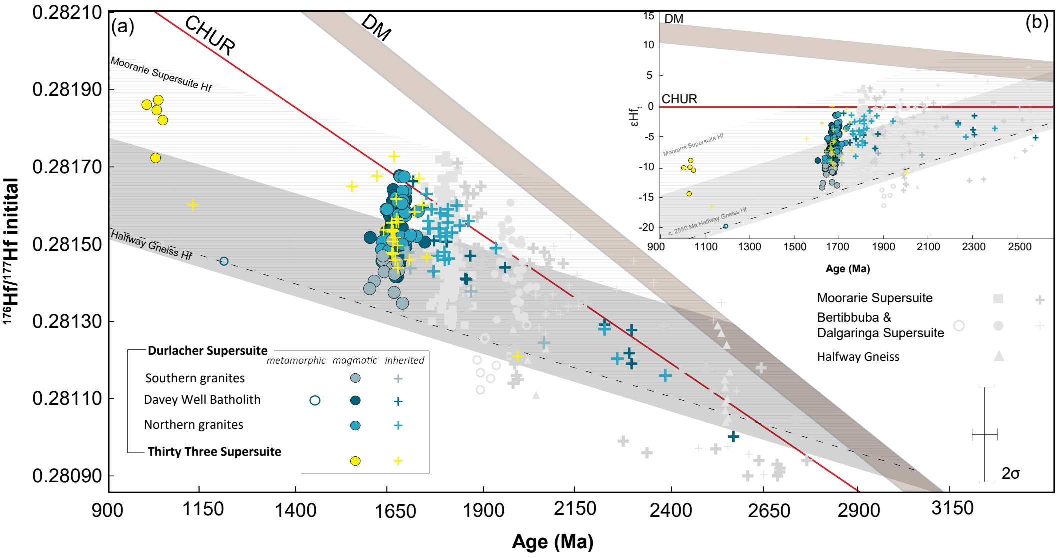

Figure 7.5 Lu–Hf isotope results from the Durlacher Supersuite Thirty Three Supersuite. Grey shaded area: isotopic envelope for the Halfway Gneiss Hf (Chapter 4) and striped area: isotopic envelope for the Moorarie Supersuite Hf (Chapter 6). The dashed line is a reference evolution line corresponding to a Lu/Hf ratio of 0.015 (a) Initial Hf evolution plot for the Durlacher and Thirty Three Supersuite (n=181), (b) εHf$_t$ evolution diagram for zircon from the Duralcher Supersuite.

returned a median εHf$_t$ value of -10 ± 1.2, 2SD. Inherited zircon grains (n=26) with ^{207}Pb/^{206}Pb ages ranging between 1991 and 1127 Ma yield a range of εHf$_t$ values between -16.5 and 0.

7.5 OXYGEN ISOTOPE DATA

A total of 151 zircon grains were analysed from 12 samples (Fig. 7.5) and include analyses of groups that are interpreted to date crystallisation and inherited material. Three analyses were rejected due to ablated area consisting of metamict patches or edges (see Appendix E).

7.5.1 Durlacher Supersuite

A total of 104 zircon grains were analysed from 9 samples. δ^{18}O values of all analysed zircon grains range between 5.46 and 10.95‰. Magmatic grains (n=59) yield a range of δ^{18}O values between 5.46 and 9.85‰, with average δ^{18}O from each sample ranging between 6.38 ± 1.39 and 8.97 ± 0.72‰ 2SD. Inherited zircon grains (n=32) with ^{207}Pb/^{206}Pb ages ranging between 2288 and 1713 Ma yield a range of δ^{18}O values between 5.46 and 10.95‰. Analyses with no corresponding or reliable age data (n=13) have δ^{18}Ovalues between 6.87 and 10.41‰.

7.5.1.1 Southern granite

Data from GSWA 168751 consists of 13 individual analyses. Analyses of magmatic zircon grains record a range of $\delta^{18}O$ values from 5.46 to 7.39‰, with an average $\delta^{18}O$ of 6.38 ± 1.39‰ (2SD, n=12). One analyses of an inherited zircon returns a $\delta^{18}O$ value of 7.21‰.

7.5.1.2 Davey Well Batholith

Data from the Davey Well Batholith granites consist of 40 individual analyses from three samples. Analyses of magmatic zircon from samples GSWA 195826, GSWA 191993 and GSWA 183212 record a range of $\delta^{18}O$ values between 6.95 and 9.85‰, and have averages of 7.85 ± 1.01‰ (n=10), 8.65 ± 0.38‰ (n=13) and 8.96 ± 0.82‰ (2SD, n=7), respectively. Analyses of inherited zircon grains (n=6) record $\delta^{18}O$ values that range between 5.46 and 9.34‰. Analyses with no reliable age data (n=4) have $\delta^{18}O$values between 7.58 and 9.04‰.

7.5.1.3 Northern granites

Data from the northern granites consist of 51 individual analyses from five samples. Analyses of magmatic zircon (n=18) record a range of $\delta^{18}O$ values from 8.28 to 9.64‰, and have averages of 8.31 ± 0.05‰ (JCO14-06; n =2) and 9.02 ± 0.77‰ (GSWA 195819; n = 14). Analyses of inherited zircon grains (n=26) record $\delta^{18}O$ values that range between 6.46 and 10.95‰. One sample with no age data (GSWA 169092, n=8) records $\delta^{18}O$ values ranging between 6.87–10.41‰. One analysis with reliable age data has a $\delta^{18}O$ value of 8.87‰.

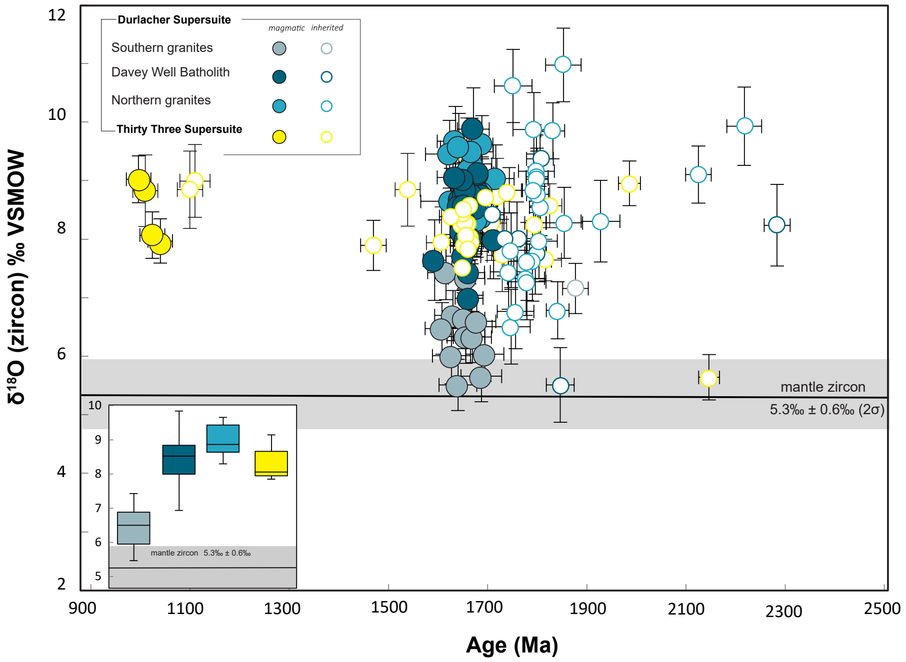

Figure 7.6 Oxygen isotope results from the Durlacher and Thirty Three Supersuite (n = 124). Inset shows box-and-whisker plots showing the range and median values of $\delta^{18}O$ VSMOW compositions.

7.5.2 Thirty Three Supersuite

A total of 44 analyses were obtained from three samples. $\delta^{18}O$ values of all analysed zircon grains range between 5.46 and 9.69‰. Magmatic grains (n= 4) yield a range of $\delta^{18}O$ values between 7.93 and 8.99‰ (average 8.32 ± 0.96‰, 2SD). Analyses of inherited zircon grains (n= 29) yield a range of $\delta^{18}O$ values between 5.59 and 9.43‰. Eleven analyses with no corresponding or reliable age data record $\delta^{18}O$ values between 7.73 and 9.69‰.

7.6 DISCUSSION

7.6.1 Previous isotopic constraints

Previous geochronology has dated Durlacher Supersuite magmatism at 1682–1619 Ma (Wingate et al., 2013, Nelson, 1998a) and leucocratic granitic magmatism of the Thirty Three Supersuite at 1030–889 Ma (Sheppard et al., 2007; Piechocka et al., 2017). The geodynamic driver for melt generation is currently unknown (Johnson et al., 2017a). Granites of the Durlacher Supersuite are calc-alkaline and weakly- to strongly-peraluminous (Johnson et al., 2017a, GSWA, 2016). Whole-rock Sm-Nd analyses of the Durlacher Supersuite record εNd values between -7.9 and -4.1 (Johnson et al., 2017), the unradiogenic values were interpreted to indicate that the granites formed without significant contribution from depleted mantle melts. Hf and oxygen zircon analyses have been conducted on the Durlacher Supersuite granites (Johnson et al., 2017a), with magmatic zircon recording εHf_t values between -13.8 and +0.4 and $\delta^{18}O$ compositions, from 6.3 to 10.5‰. The Hf–O arrays have been interpreted to indicate formation from melts sourced from reworking of older crustal material, with compositions similar to the Moorarie Supersuite, and subsequent contamination by upper crustal rocks during magma emplacement and crystallization (Johnson et al., 2017).

7.6.2 Timing of magmatism and significance of inherited ages

The analysed zircon from the Durlacher Supersuite samples cover a period of 1570 Myr, with individual $^{207}Pb/^{206}Pb$ ages ranging between between c. 2778 and c. 1209 Ma. Granites were generated during one main magmatic episode at c. 1685–1645 Ma. The northern granites have older crystallisation ages (c. 1690–1667 Ma) than magmatism recorded in the Davey Well Batholith granites in central part of the study area (c. 1674–1658 Ma). The youngest magmatism is recorded in the southern granite sample (c. 1651 Ma). Individual ages for the samples from the Thirty Three Supersuite range between c. 2233 and 1004 Ma, with magmatic crystallisation constrained at c. 1030 Ma. The magmatic ages established are in broad agreement with the c. 1682–1619 Ma age range established for the Durlacher Supersuite (Sheppard et al., 2005) and the c. 1030–889 Ma age range of the Thirty Three Supersuite (Piechocka et al., 2017, Sheppard et al., 2007).

Inherited zircon grains from the Durlacher Supersuite indicate $^{207}Pb/^{206}Pb$ ages of c. 2778–1700 Ma, with two main magmatic events identified at 1805 and 1762 Ma, and a minor peak at c. 2290–2225 Ma. In the Gascoyne Province the Durlacher Supersuite intrude the Poorarnoo Metamophics, and the major group of inherited material at c. 1762 Ma reflects the c. 1760–1680 Ma depositional ages established for the metasediments (Nelson, 2004d; Sheppard et al., 2007). The major group of inherited material at c. 1805 Ma reflect ages similar to the c. 1820–1775 Ma Moorarie Supersuite. The granitic rocks contain abundant enclaves of partially assimilated granitic gneisses of the Moorarie Supersuite and metasedimentary rocks of the Pooranoo Metamorphics (Johnson et al., 2017a). The main group of inherited zircon grains at c. 1805 and c. 1762 Ma have ages that reflect the ages of the Moorarie Supersuite and Pooranoo Metamorphics, and indicate that the Durlacher Supersuite granitoids assimilated these rocks during emplacement and crystallisation. The c. 2290–2250 Ma inherited material may have been assimilated from upper crustal components; currently no exposed crustal components of this age have been identified. Johnson et al (2017a) reported similar aged inheritance from the Moorarie and Durlacher Supersuites (c. 2280–2115 Ma), and interpreted them as representing a deep- or mid-crustal component that underlies much of the Gascoyne Province. However, with inherited zircon (with the exception of one) with comparable ages from the Durlacher Supersuite indicate elevated $\delta^{18}O$ values (7.83–9.9‰), suggesting a sedimentary origin. The pegmatites and granitoids of the Thirty Three Supersuite intrude the Durlacher Supersuite in the central part of the Gascoyne Province (Mutherbukin Zone) and inherited material of the Thirty Three Supersuite have $^{207}Pb/^{206}Pb$ ages of c. 2233–1700 Ma ages, with one major peak at c. 1663 Ma, which reflects the c. 1680–1620 Ma ages established for the Durlacher Supersuite.

7.6.3 Isotopic constraints on crustal components

U–Pb data reveals three main periods of magmatic activity at c. 1850–1770, c. 1663, and c. 1030 Ma, and a minor c. 2295–2225 event. Zircon from these samples yield initial $^{176}Hf/^{177}Hf$ ratios between 0.281160 and 0.281873 (εHf_t -14.4 to 0). The majority of the analyses indicate evolved εHf_t values (median -6.3), indicating that these granites were formed mainly from the reworking of crustal components with little to no significant mantle input.

The c. 2295–2225 Ma zircon form a small group indicate moderately evolved εHf_t compositions (-5 to -1.5) and $\delta^{18}O$ values between 5.59 and 9.9‰. The Durlacher Supersuite extensively intrude rocks of the 1740–1680 Ma Pooranoo Metamorphics, and the age range of these inherited zircon are comparable to the detrital components identified in metasedimentary rocks of the Pooranoo Metamorphics (Bodorkos et al., 2006; Wingate et al., 2017a, Wingate et al., 2010a, 2010b, 2010c). This suggests that the zircons are likely to have been sourced from their current host metasedimentary country rocks during magma ascent and emplacement. The zircon with elevated $\delta^{18}O$ (8.2–9.9‰) are characteristic of metasedimentary component (~8-12‰; Appleby et al., 2010), and are consistent with the interpretation that the inherited zircon were incorporated from assimilated Pooranoo Metamorphics. The $\delta^{18}O$ value of 5.59‰ in one inherited grain indicates that the magma that this zircon crystallised from contained significant low-$\delta^{18}O$ material representing an infracrustal source component with mantle-like $\delta^{18}O$. It may either infer that the granite sourced an older deep crustal component, such as the one identified by Johnson et al (2017a), but does not rule out an inherited (detrital) component assimilated from host country rock. The c. 1850–1770 Ma zircon indicate a large range in εHf_t values (-8.2 to -0.7) and δ18O values ranging between 5.56 and 10.95‰. These U–Pb ages and Hf–O isotope data are identical to the c. 1820–1775 Ma Moorarie Supersuite (Fig. 7.5), and imply that the Moorarie Supersuite was incorporated into host magma, either during magma ascent during crustal anatexis.

Analyses of c. 1665 Ma magmatic zircon indicate εHf_t values between -13 and -1.1, with $\delta^{18}O$ values between 5.46 and 9.85‰. Like the Moorarie Supersuite (Chapter 6), there is a distinct spatial trend within the data. The samples located within the Yarlarweelor Gneiss Complex (southern granite) have more unradiogenic εHf_t and lower $\delta^{18}O$ values than those located within the Gascoyne Province (northern granites and Davey Well Batholith). This indicates that the magmas that the zircon grains crystallised from were sourced from different, spatially discrete, crustal components. The southern granite sample has initial $^{176}Hf/^{177}Hf$ ratios between 0.281347 and 0.281509 (εHf_t -13 to -7.8, median -10.7 ± 2.7, 2SD), and those with mantle like $\delta^{18}O$ values return T_{DM}^{C} ages between c. 3216 and 3046 Ma. The zircon grains have mantle-like $\delta^{18}O$ values between 5.46 and 7.39‰ (average: 6.38 ± 1.39, 2SD). The Hf–O array indicates derivation from an old or evolved crustal component that has not interacted significantly with shallow crustal material.

On an εHf_t versus $\delta^{18}O$ plot (Fig 7.7a) where the εHf_t of the Moorarie Supersuite recalculated at c. 1665 Ma (based on data presented in Chapter 6) the Durlacher Supersuite is indistinguishable from the older supersuite. The southern granite sample falls within the central and southern granite samples Hf–O array. These Moorarie Supersuite samples were interpreted to have been sourced from melts resulting from the reworking of pre-existing crust which had isotopic compositions similar to that of the Halfway Gneiss protoliths. Therefore it is probable that the southern granite sourced a range of southern Gascoyne Province Palaeoproterozoic granites that were present below the Narryer Terrane at the time of emplacement. Crustal evolution lines show that the southern sample lies within the Halfway Gneiss and Moorarie Supersuite isotopic

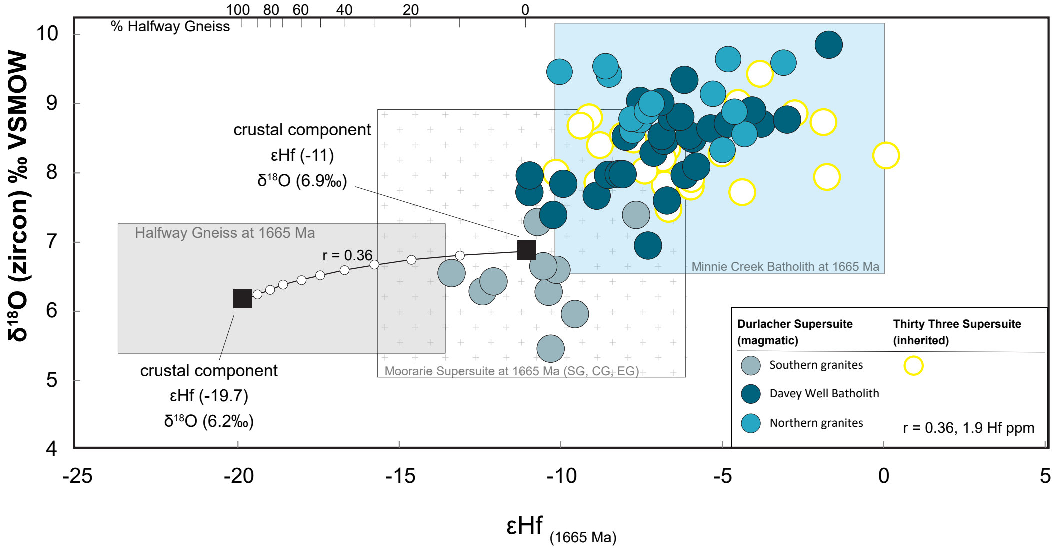

Figure 7.7 Plot of $\delta^{18}O$ versus εHf_t for magmatic zircon from the Durlacher Supersuite and inherited zircon from the Thirty Three Supersuite. The blue box represents the Minnie Creek Batholith at 1665 Ma, the stippled (crosses) box represents the Southern, Central and Eastern Granites of the Moorarie Supersuite at 1665 Ma, grey box represents the Halfway Gneiss granitoids at 1665 Ma (based on Hf–O data presented in Chapter 4 and 6). The parameters of end members are discussed in text. Bulk mixing curves are marked at 10% increments.

envelope (Fig. 7.5), supporting the interpretation that the southern granite was sourced from the reworking of the Halfway Gneiss and Moorarie Supersuite (southern granites) granitoids. The shape of the Hf–O arrays shown in Fig. 7.7 can reveal the nature and relative contributions of crustal components (end-members) to the source of the magma (Kemp et al., 2007), with the shape of the arrays (and mixing curves) dependent on the relative Hf concentrations of the end-members. Using lower crustal values (1.9 ppm, Rudnick and Gao, 2003) combined with upper crustal values (5.3 ppm, Rudnick and Gao, 2003) is compatible with a crustal contamination model (Roberts, 2010). Using the average measured εHf_t and $\delta^{18}O$ values for the Halfway Gneiss and Moorarie Supersuite (Chapter 4 and 6), the two-component mixing modelling indicates that the c. 1665 Ma southern granite may represent mixing between 88–100% Moorarie Supersuite and 0–12% Halfway Gneiss rocks.

The northern granites and Davey Well Batholith samples display dominantly unradiogenic initial $^{176}Hf/^{177}Hf$ ratios between 0.281509 and 0.281416 (εHf_t -10.9 to -1.1) with median εHf_t for individual samples between -8.5 ± 4.3 and -3.2 ± 1.8, 2SD. The magmatic zircon form homogenous oxygen isotope populations with average $\delta^{18}O$ values between 7.85 ± 1.01 and 8.97 ± 0.72‰, 2SD. The Hf–O array can be generated from a source containing a large component of weathered materials, i.e metasediments. Granites of the Minnie Creek Batholith have identical Hf and O isotope composition to the ones of the Durlacher Supersuite (Fig. 7.7), and therefore constitute the likely candidate for the granite source. This is supported by the occurrence of

c. 1850–1770 Ma zircon inherited that have compositions which plot in the U–Pb–Hf field of the Moorarie Supersuite (Fig. 7.5).

The c. 1030 Ma magmatic zircon from the Thirty Three Supersuite have unradiogenic initial ^{176}Hf/^{177}Hf ratios that range between 0.281723 and 0.281873 (εHf$_t$ -14.4 to -8.9). The δ^{18}O values range between 7.93–8.99‰. Crustal evolution lines defined by a source a ^{176}Lu/^{177}Hf value of 0.015 (Griffin, 2002), show that the younger granites lie within the Durlacher Supersuite and Moorarie Supersuite granites isotopic envelope. Therefore, these isotopic arrays indicate that the melts were formed by reworking of an infracrustal source possessing similar ^{176}Lu/^{177}Hf ratios, such as the c. 1800–1600 Ma granites. Inherited zircon have U–Pb ages and Hf–O isotope compositions comparable to the Durlacher Supersuite, indicating that the c. 1030 Ma granites and pegmatites were sourced from reworking of the c. 1665 Ma granites. Fig. 7.8 shows the Hf-O range the Durlacher and Moorarie Supersuite would have at c. 1030 Ma. The Thirty Three Supersuite zircon have εHf$_t$ values that are more radiogenic than can be explained by remelting of the Durlacher Supersuite alone, and instead suggests mixing with an alternative end-member. The Hf–O array of the Thirty Three Supersuite zircon requires an end member with more radiogenic εHf$_t$ composition than that of the Durlacher Supersuite, and high-δ^{18}O values. Mixing between the Durlacher Supersuite and an alternative metasedimentary end-member (εHf$_t$ value of -0.5 coupled with δ^{18}O value of 9‰) indicates a 38–62% contribution from the metasedimentary component. Using mid-crustal values (4.4 ppm, Rudnick and Gao, 2003) combined with upper

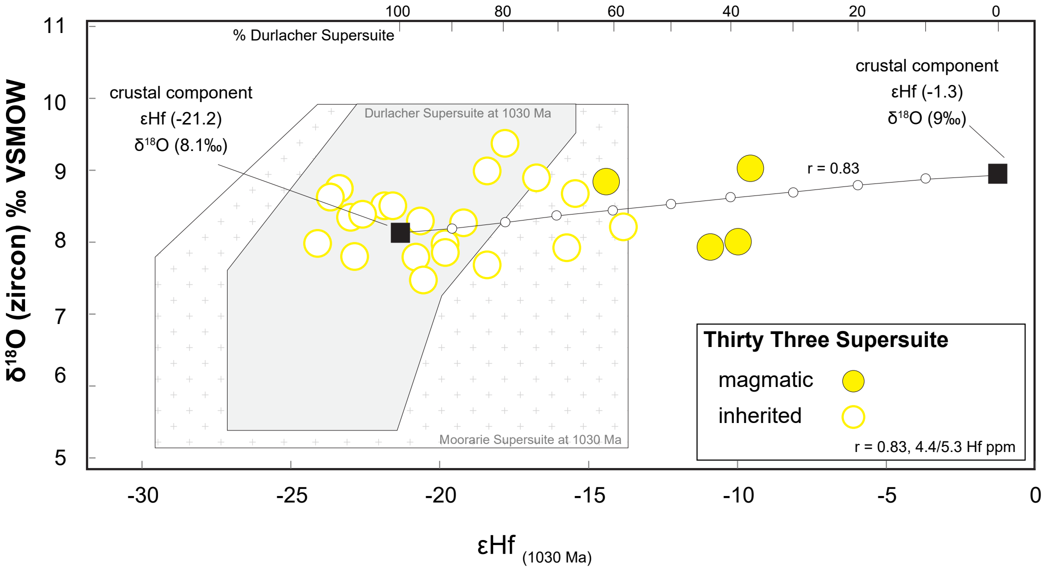

Figure 7.8 Plot of δ^{18}O versus εHf$_t$ for magmatic and inherited zircon from the Thirty Three Supersuite. The grey area represents the Durlacher Supersuite at 1030 Ma, the stippled (crosses) area represents Moorarie Supersuite at 1030 Ma (based on Hf–O data presented in chapter 6). The parameters of end members are discussed in text. Bulk mixing curves are marked at 10% increments.

crustal values (5.3 ppm, Rudnick and Gao, 2003) is compatible with a crustal contamination model. It is worth noting that there is limited published Hf isotope data for the metasedimentary units within the study area. Therefore the end-member of the metasedimentary component uses the average εHf_t value of the sedimentary units within the Gascoyne Province (GSWA, 2016), which may not represent the metasedimentary components within the Mutherbukin Zone that the pegmatites intrude, therefore this model requires further data to be tested.

7.7 SUMMARY

- U–Pb and Hf–O data provide evidence that the primary source for the Durlacher Supersuite magmatism was predominantly from recycling of previously formed continental crust, with compositions equivalent to the Moorarie Supersuite granitoids. Hf zircon isotopic compositions indicate no contribution from juvenile components, and do not require an additional metasedimentary source to account for the Hf–O array observed in the Durlacher Supersuite granites.

- The U–Pb, hafnium and oxygen isotopes from the c. 1680–1620 Ma Durlacher Supersuite within the Gascoyne Province indicate derivation from reworking of the Moorarie Supersuite, while those that intruded the northern margin of the Yilgarn Craton indicate mixing between 88–100% Moorarie Supersuite and 0–12% Halfway Gneiss rocks.

- U–Pb and Hf–O data provide evidence that the primary source for the Thirty Three Supersuite magmatism was also predominantly from recycling of previously formed continental crust, equivalent to the Durlacher Supersuite granitoids, with an additional metasedimentary source.

CHAPTER 8

DISCUSSION

8.1 CRUSTAL EVOLUTION ALONG THE YILGARN CRATON MARGIN

Archaean cratons are the stable remnants of Earth's early continental crust, assembled from crustal fragments through accretionary and collisional tectonics (Cawood et al., 2009). Accretionary processes such as terrane accretion, rifting and reattachment occur along the craton margins, and can modify the craton's spatial-extent over time. These processes contribute to crustal growth, and involve the variable reworking of pre-existing continental crust and generation of new juvenile material. Therefore, distinguishing the nature of craton margin processes, and identifying the relative crust and mantle contributions to specific magmatic episodes can help to constrain the temporal evolution of a crustal block.

The Capricorn Orogen is considered to have developed as a response to the convergence and amalgamation of the Pilbara Craton, Glenburgh Terrane and Yilgarn Craton (Cawood and Tyler 2004). The reworked northwestern margin of the Yilgarn Craton, the Narryer Terrane, records the collision between the Archean craton and the Glenburgh Terrane during the formation of the West Australian Craton. The Archaean granites and granitic gneisses of the Yarlarweelor Gneiss Complex were reworked and formed part of the melt source for the younger granitic magmatism. In the east, the Palaeoproterozoic Yerrida, Bryah, Padbury and Eraheedy Basins from a belt about 700 km along the northern margin of the Yilgarn Craton, and contain the Archaean Marymia and Goodin inliers. The inliers consist of several tectonically juxtaposed lithotectonic fragments which crop out in sedimentary basins, and are the northernmost extent of the Yilgarn Craton.

The data presented in Chapter 4 were used to infer possible sources as well as clarifying possible genetic relations between the various Archaean crustal components associated with the Yilgarn Craton. Here we will discuss their tectonic implications for the crustal evolution of the Yilgarn Craton margin. The following history represents a summary of the research presented in Chapter 4 integrated with existing geochronological and geochemical data.

8.1.1 Crustal evolution in the early Archaean (3700–3100 Ma)

The oldest period of granite magmatism is observed in samples from the Narryer Terrane and

Marymia Inlier. These samples record zircon U–Pb crystallisation ages between c. 3365 and c. 3330 Ma. Based on their U–Pb ages, Lu–Hf and oxygen-isotope composition, the c. 3350 Ma granitoids exposed in the Marymia Inlier are interpreted to represent a Narryer Terrane crustal component (Chapter 4). It has been proposed that Narryer Terrane zircon grains formed from heterogeneous magma sources, including older crustal rocks and mantle-derived mafic component with an Eoarchaean extraction age (Kemp et al., 2010, Nebel-Jacobsen et al., 2010). The Hf–O data presented in Chapter 4 confirms that an Eoarchaean component contributed to the Paleo- to Mesoarchaean magmatism in the Narryer Terrane-Marymia Inlier.

The geodynamic setting of the Paleoarchaean Narryer Terrane and its relationship with the Murchison Domain prior to amalgamation and cratonisation of the Yilgarn Craton is unclear, mainly due to the general uncertainty regarding the nature of plate tectonics in the Archaean (Condie and Pease, 2008). Previously, models involved accretion of the allochthonous Narryer Terrane with the Murchison Domain during (or prior) to widespread granitoid emplacement at c. 2750–2620 Ma (Nutman et al., 1993; Myers, 1995). Recently, detailed geochemical and isotopic studies have recognised evidence of c. 2700 Ma mantle-plume activity in the northern Murchison Domain (Czarnota et al., 2010; Ivanic et al., 2012; Van Kranendonk et al., 2011; 2013). These datasets have been used to propose a combination of both plume and arc related volcanism involving autochthonous development for the Narryer and Youanmi Terranes, followed by rifting and re-accretion of the Narryer Terrane (Wyman and Kerrich, 2012). Based on the presence of arc-related rocks (boninite- and sanukitoid-like rocks) in the northern Murchison, this period of rifting was followed by development of a subduction zone between the Narryer and Youanmi Terrane at c. 2800–2740 Ma, with the subduction zone dipping to the southeast (Champion and Cassidy, 2002; Wyman and Kerrich, 2012). If the Narryer Terrane is not exotic to the Murchison Domain and represents an exposed portion of the Youanmi Terrane basement, it would account for the c. 4350–3130 Ma ages of detrital zircon recorded in the Southern Cross Domain (Wyche et al., 2004), the c. 4000 Ma inherited zircon in Murchison Domain granites (Nelson et al., 2000e) and Hf model ages of >4000 Ma in the Youanmi Terrane (Ivanic et al., 2012; Wyche et al., 2012).

The Lu–Hf and O isotopic compositions of the Paleoarchaean crustal components indicate extensive reworking of an evolved crustal component older than 3800 Ma (Chapter 4). These data also indicate that the c. 3350 Ma zircon require an input of a component with a more radiogenic Hf signature (i.e. juvenile input) not observed in the Narryer Gneiss Complex meta-igneous zircon. The oxygen isotope compositions of these zircon are within error of mantle zircon ($\delta^{18}O = 5.3 \pm 0.6$, 2σ, Valley et al., 2005), and suggests that the juvenile input was from the partial (re) melting of a mantle-derived source component. Models for crustal growth in the

Narryer Terrane (Kemp et al., 2010) involved the partial melting of a thickened mafic (basaltic) crust, i.e. a volcanic plateau, producing intermediate-felsic components. Similar models have been proposed for Paleoarchaean crustal growth in the East Pilbara Terrane (Smithies et al., 2009; Van Kranendonk et al., 2015; Gardiner et al., 2017) and Kaapvaal cratons (Van Kranendonk et al., 2015) and Acasta Gneiss Complex (Reimink et al., 2016), whereby episodic thermal anomalies (mantle plume heat source) resulted in renewed partial melting of the mafic to intermediate crustal sources at various crustal levels to produce the younger evolved granites. The proposed model can account for the reworking trend towards more unradiogenic compositions over time observed in the Hf-isotope data (median εHf_t -2.2 to -4.7 at c. 3350 Ma, to -6.8 at c. 3100 Ma), the mantle-like oxygen-isotope values.

While these models do not require a plate tectonic regime for the generation of Paleoarchaean crust, the addition of a mantle-derived source component (i.e. magmatic underplating) is also observed in a number of modern tectonic settings, including extensional continental areas, rift zones and continental margins (Thybo and Artemieva, 2013). However, these settings are not unique to either plate tectonic or mantle-plume dominated environments. Whether the driving force for the protracted crustal reworking in the Narryer Terrane was either through subduction or plume activity cannot be determined from the Hf–O isotope data alone, as either process could result in voluminous magmatic underplating and subsequent crustal anatexis could produce the Hf–O array observed in the zircon. There is no clear geochemical or isotopic evidence of crustal growth through tectonic accretion until c. 2750 Ma (Wyman and Kerrich, 2012).

8.1.2 Crustal evolution in the Neoarchaean

Following the somewhat cryptic evolution of the Paleoarchaean crust, the northern margin of the Yilgarn Craton was affected by contemporaneous magmatic events at c. 2750–2600 Ma. Generation of granitic magmatism and development of the Neoarchaean crust is observed in: (1) the Narryer Terrane/YGC between c. 2730–2615 Ma, (2) the Marymia Inlier at c. 2700–2690 Ma, (3) the Kalgoorlie Terrane at c. 2670 Ma, (4) the Goodin Inlier at c. 2660–2620 Ma, and (5) the Halfway Gneiss at c. 2550–2440 Ma. The Lu–Hf data of these granitoids also indicate four significantly distinct isotopic sources:

1. Narryer Terrane/YGC: median εHf_t value of -7.9, median T_{DM}^{C} of c. 3650 Ma
2. Goodin Inlier: median εHf_t value of -6.3, median T_{DM}^{C} of c. 3500 Ma
3. Halfway Gneiss: median εHf_t of -2, median T_{DM}^{C} of c. 3200 Ma
4. Marymia Inlier and Kalgoorlie Terrane: median εHf_t +2, median T_{DM}^{C} of c. 3100 Ma

As discussed in Chapter 4, the Marymia and Goodin Inliers, the Narryer Terrane/YGC and Halfway Gneiss are isotopically distinct, with the Marymia and the Goodin Inliers correlated to the EGST and Youanmi Terrane, respectively. The Halfway Gneiss has isotopic similarities with both the Youanmi Terrane and the Kalgoorlie Terrane, and is interpreted to represent a reworked portion of the Yilgarn Craton, re-accreted during the Glenburgh Orogeny.

The overall architecture of the Yilgarn Craton is dominated by a central nucleus, the Youanmi Terrane which acted like a protocraton onto which the Narryer Terrane was accreted in the northwest, the Southwestern Terrane in the southwest, and the EGST developed on to the east. Currently there are two essentially opposing models for the crustal evolution and formation of the Yilgarn Craton: (1) convergent plate tectonic model, involving subduction zone magmatism and the accretion of allochthonous terranes in a Cordilleran-style accretionary orogen at c. 2660–2620 Ma (e.g. Barley et al., 1989; Myers, 1995; Krapež and Barley, 2008; Korsch et al., 2011) and (2) an autochthonous model, involving plume-driven rifting along the lithospheric margin, followed by (re)accretion of the Narryer Terrane, Southwestern Terrane and EGST to the Proto-Yilgarn craton at 2750–2630 Ma (Campell and Hill, 1988; Barnes et al., 2014; Ivanic et al., 2012, Wyman and Kerrich, 2012; Van Kranendonk et al., 2013; Mole et al., 2013).

8.1.3 Exotic terranes or rifted fragments?

The new Lu–Hf isotopic data from the c. 2700 Ma Marymia Inlier granitoids are equivalent to the isotopic signature recorded in the Kalgoorlie and Kurnalpi Terranes (Wyche et al., 2012), consistent with the interpretation that the Marymia Inlier is a northwestern extension of the EGST (Vielreicher et al., 2002; Griffin et al., 2004; Gazley, 2011; Gazley et al., 2011). The boundary between the EGST and the Youanmi Terrane is the Ida Fault. However, boundary between the two terranes at the Marymia Inlier is not clearly defined. The northern extent of the Ida Fault has been truncated by a series of thrust faults, the Waroonga Fault System, which is interpreted to extend under the Yerrida Basin towards the Plutonic Greenstone Belt (Blewett and Hitchman, 2006). The isotopic data from this study is consistent with this interpretation, and indicates that the region of the Marymia Inlier that is correlative with the EGST includes the eastern part of the inlier area and extends to the area north of the Plutonic Greenstone Belt. The data also indicates that the c. 2700–2690 Ma magmatism in the Marymia Inlier is isotopically distinct from the c. 2730–2620 Ma Narryer Terrane/YGC granites, and as such, is interpreted to have formed from separate sources. The area southwest of the greenstone belt which contains c. 3350 Ma crust is proposed to be part of the Narryer Terrane. This interpretation is supported by presence of c. 3800–2980 Ma inherited zircon recorded in various samples southwest of the greenstone belt (Vielreicher and McNaughton, 2002; Lu et al., 2017).

While the isotopic data from this study does not provide constraints on the evolution of the EGST, it does offer a better understanding of the relationship between various terranes, specifically the Narryer, Youanmi, Kalgoorlie and Glenburgh Terranes. Development of the Neoarchaean crust in the Murchison Domain has been interpreted as a plume event at c. 2810 Ma producing voluminous mafic-ultramafic and komatiitic volcanism (Ivanic et al., 2010). This event was accompanied by east-west extension and incipient rifting in the northern Murchison Domain marked by radiogenic Hf-isotopes and younger model ages (Champion and Cassidy, 2007; Van Krandendonk et al., 2011; Ivanic et al., 2012; Mole et al., 2014), as well as numerous layered intrusions in the Youanmi Terrane (Ivanic et al., 2010; Ivanic et al., 2012). Intra-cratonic rifting is followed by rifting along the eastern margin of the Youanmi Terrane, which produced multiple Yilgarn fragments, i.e the Kalgoorlie and Burtville Terrane (Pawley et al., 2012 Ivanic et al., 2012; Wyche et al., 2012; Wyman and Kerrich, 2012; Van Krandendonk et al., 2013).

Although the Hf–O compositions of the Paleoarchaean crustal components in the Narryer Terrane and western Marymia Inlier indicates a comagmatic origin, it remains unclear whether the Marymia Inlier and Narryer Terrane stayed contiguous following the proposed rifting from the proto-Youanmi Terrane at c. 2835 Ma. It is possible that rifting of the Narryer Terrane from the Younami Terrane did not include the Marymia Inlier crustal portion. Juxtaposition of the Narryer Terrane with the Youanmi Terrane occurred prior to the intrusion of voluminous c. 2750–2620 Ma granitoids, which may have formed as response to the final amalgamation of the Narryer and Youanmi Terrane (Myers, 1995; Nutman et al., 1993; Spaggiari et al., 2008). Magmatism at c. 2730–2615 Ma recorded in the Narryer Terrane has a median T_{DM}^{C} age of c. 3650 Ma, and is interpreted to represent further reworking of the Paleoarchean crust, and the addition of a juvenile component. Two component mixing Hf evolution model indicates a minimum mantle contribution of approximately 55% is necessary to explain the most radiogenic portions of the c. 2730–2615 Ma array. A scenario which can account for the elevated Hf ratios relative to the Paleoarchaean crust in the c. 2730–2615 Ma Narryer Terrane granitoids involves the asthenospheric upwelling following post-collisional slab break-off or lithospheric delamination (Davies and von Blanckenburg, 1995; van Hunen and Allen, 2011), with the advection of mantle-generated mafic magma into the lower crust leading to crustal anatexis.

A second phase of plume magmatism at c. 2720–2675 Ma produced further mafic intrusions and volcanism in the Youanmi Terrane (Ivanic et al., 2012; Van Kranendonk et al., 2013), followed by crustal anatexis and younger felsic magmatism. This period of juvenile input is also recorded in the Kalgoorlie and Kurnalpi Terranes (Campbell and Hill, 1988; Wyche et al., 2012; Barnes et al., 2012; Mole et al., 2013). Thermo-tectonic modelling of Rey et al (2003) demonstrated that conductive heat from a mantle plume combined with thermal blanketing can induce crustal anatexis 20–40 Myr after the emplacement of the plume. This is compatible with the generation of the c. 2700 Ma granites. Mole et al (2014) used the variable isotopic signatures of the crust as proxies for lithospheric thickness, where radiogenic εHf_t values reflect relatively thin lithosphere, while unradiogenic values reflect thicker lithosphere. The period of felsic magmatism is observed in the Marymia Inlier and Kalgoorlie Terrane granitoids which are characterised by radiogenic εHf_t values (median εHf_t +1.9) and younger median $T_{DM}{}^{C}$ age of 3100 Ma, and the Goodin Inlier samples which have unradiogenic εHf_t values (median εHf_t -6.3) and older median $T_{DM}{}^{C}$ age of 3500 Ma. Models that involve terrane accretion are difficult to reconcile with the widespread c. 2720 Ma komatiitic volcanism across the Youanmi, Kalgoorlie and Kurnalpi Terranes, unless amalgamation of the Youanmi and Kalgoorlie Terranes was complete prior to 2720 Ma (e.g. Smithies and Champion, 1999).

The differences in the observed εHf_t values reflects the how the thickness of the crust influences the isotopic signal during an interaction with a mantle-plume. The older Youanmi Terrane which consists of a thicker lithosphere, the addition of mantle-derived material into the crust results in extensive reworking of the pre-existing crust, leading to the unradiogenic isotopic signal observed in the Goodin Inlier. By contrast, the Kalgoorlie Terrane which consists of thinner lithosphere at craton margin/extensional areas, mantle-derived magmas can reach the crust more easily, resulting in the predominance of a juvenile signature. The melts also incorporate a minor component of Paleoarchaean crust (Youanmi Terrane), as indicated by $T_{DM}{}^{C}$ ages up to 3361 Ma.

Whether the Narryer and Kalgoorlie terranes are either exotic terranes or crustal blocks rifted off the Youanmi Terrane have implications for the interpreted crustal evolution of the Archaean components of the Capricorn Orogen. Previous studies that have interpreted significant magmatic and isotopic histories for the Glenburgh Terrane and the Yilgarn Craton have led to the suggestion that the Halfway Gneiss was an exotic terrane accreted to the Yilgarn Craton margin during the Glenburgh Orogeny at c. 2005–1945 Ma (Johnson et al., 2011). However, the similarity in Lu–Hf data between the Glenburgh Terrane and the Youanmi and Kalgoorlie Terranes at c. 2973–2620 Ma suggests that a component with a Yilgarn Craton Hf-isotopic composition made a contribution to the c. 2550 Ma magmatism. The similarities in Lu–Hf data between the Youanmi Terrane, Kalgoorlie Terrane and Narryer Terranes have been used to interpret an autochthonous crustal evolution in the early Archaean, with a c. 2810 Ma plume event leading to rifting and fragmentation along the eastern Youanmi terrane. Based on the present day configuration of the terranes, it is possible that the Glenburgh Terrane developed along the northeastern margin of the Younami Terrane. The Hf–O data presented in Chapter 4 provide evidence for the formation of c. 2550 Ma crust from variable reworking of c. 3300 Ma crustal components with an additional c. 2770 Ma juvenile component. This is similar to the terrane transfer described by Kirkland et al. (2011) in the Albany-Fraser Orogen, where the addition of juvenile input dilutes the isotopic signal from the basement through times and reflects the influence of Palaeoproterozoic juvenile input into non-radiogenic Archaean sources. These data are compatible with the Halfway Gneiss representing a remnant fragment of the Yilgarn, produced during c. 2810 Ma plume induced rifting along the eastern margin of the Youanmi Terrane.

8.1.4 Lu–Hf contour maps

In Chapter 4 the U–Pb, Hf and O isotope data were used to identify regions with a shared history of granite emplacement corresponding to a common geological and crustal evolution. The Lu-Hf system in zircon provides a greater understanding of the source regions of the crustal magmas, by distinguishing between juvenile mantle derived crust from reworked older crust. When integrated with U-Pb zircon geochronology, the data can constrain the age and type of source from which the crust formed at a particular time. As each data point has its time of crystallisation constrained prior to analysis, and has its spatial location known, these data can be used to map crustal evolution in both space and time. The U–Pb and Hf–isotope data were used to generate an interpolation map of the Yilgarn Craton margin to better define the crustal history of the Archaean inliers within the Capricorn Orogen, and identify areas of crustal growth or reworking present within the region. In order to generate the Lu–Hf contour maps, single εHf_t values (rather than an array) are required. Median values account for the data distribution within an array, and are therefore more representative of the spread of data. Mole (2012) demonstrated that this method reduces potential bias and is representative of the entire dataset, including the oldest, reworked and youngest, most juvenile material found throughout the craton.

ESRI ArcMap 10.1 was used to generate the contour maps, and extensions including Spatial Analyst and Geostatistical Analyst were used to process the data to create the final map. Following the methods of Mole (2012), an inverse distance weighted (IDW) interpolation method was used to contour the Hf dataset. Data were grouped using equal interval method, which divides the range of attribute values into equal-sized subranges. This method best emphasizes the amount of an attribute value relative to other values.

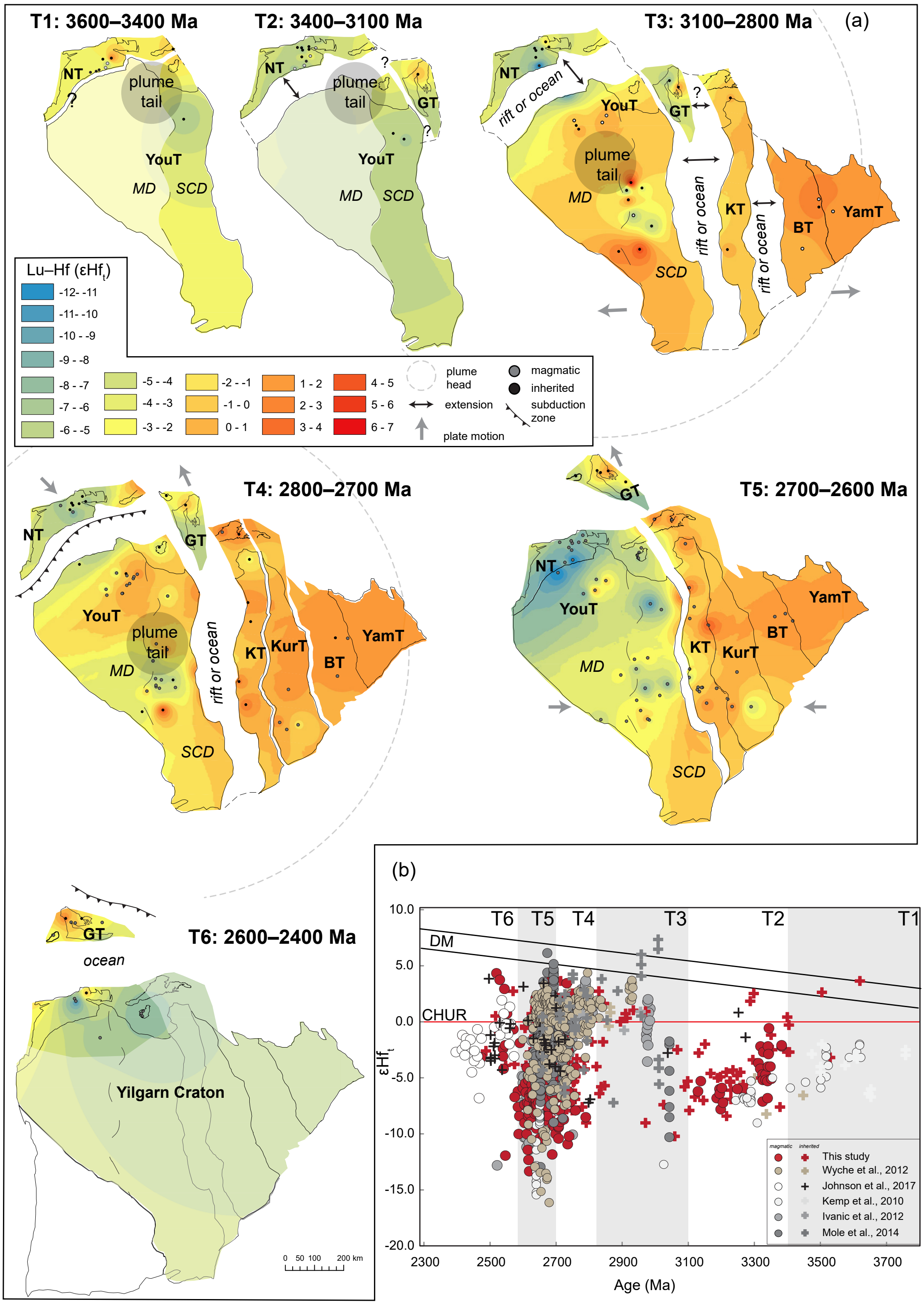

Figure 8.1 caption overleaf

Figure 8.2 A schematic model for Archaean crustal evolution along the Yilgarn Craton (a) Lu–Hf isotopic maps of the Yilgarn Craton shown as six timeslices (T1–T6) illustrating the spatial–temporal evolution of the Yilgarn Craton. (T1–T2) Development of granites in the NT by crustal anatexis driven by repeated thermal anomalies (mantle-plumes), development is assumed to be autochthonous with development in northern YT, rifting of NT occurs sometime within this period, (T3) Impingement of plume results in thinning of crust and juvenile input in northern MD, and crustal extension and rifting along the eastern margin of the YT, producing multiple fragments including GT, KT, BT and YamT, (T4) Development of a subduction zone between NT and YT, accretion/re-attachment of NT to YT occurring at c. 2750 Ma, resulting in extensive c. 2730 Magmatism in NT. Second plume event affects YT and KT at c. 2720–2675 Ma (T5) Plume induced magmatism is observed as reworking in the YT, and juvenile input in KT. Migration of GT northwards in response to closure of rift/ocean between YT and KT. Convergence between the multiple eastern fragments and YT occurs between c. 2715 and c. 2660 Ma (T6) Development of a subduction zone north of the GT results in magmatism involving reworking of basement and juvenile input at c. 2550 Ma (Halfway Gneiss). Modified from Cassidy, 2004 and Wyman and Kerrich, 2012. [BT, Burtville Terrane; GT, Glenburgh Terrane; KT, Kalgoorlie Terrane; KurT, Kurnalpi Terrane; NT, Narryer Terrane; MD, Murchison Domain; SCD, Southern Cross Domain; YamT, Yamarna Terrane; YouT, Youanmi Terrane] Approximate location and scale of plume head and tail were taken from Mole, 2012 and adapted from Campbell et al., 1989 and Barnes et al., 2012. (b) εHf_t versus age for all collated data. A total of 27 samples from this study (Chapter 4) were combined with 86 granitoid samples collated from previously published sources (Kemp et al., 2010; Wyche et al., 2012; Ivanic et al., 2012; Mole et al., 2014; Johnson et al., 2017a).

8.1.5 An Archaean tectonic synthesis

Figure 8.2 depicts the crustal evolution of the Yilgarn Craton during the Archaean through an isotopic perspective

T1–2 (3600–3100 Ma): Development of granites in the Narryer Terrane by crustal anatexis driven by repeated thermal anomalies (mantle-plumes), development is assumed to be autochthonous with development in northern Youanmi Terrane. Inherited grains are observed in the Glenburgh Terrane and Southern Cross Domain. Rifting of Narryer Terrane occurs sometime within this period, the Marymia Inlier component is not detached.

T3 (3100–2800 Ma): Impingement of plume at c. 2830–2810 Ma in northern Murchison Domain results voluminous mafic-ultramafic and komatiitic volcanism in the northern Murchison Domain, leading to significant east-west extension/crustal thinning in northern Murchison Domain. Crustal extension and rifting also occurred along the eastern margin of the Youanmi Terrane. Rifting produces multiple fragments including Glenburgh, Kalgoorlie, Burtville and Yamarna Terranes.

T4 (2800–2700 Ma): Development of a subduction zone between Narryer and Youanmi Terranes, bonanites in the northern Murchison Domain suggest southeastward subduction, with accretion/re-attachment of Narryer Terrane to the Youanmi Terrane occurring at c. 2750 Ma. Second plume event at c. 2720–2690 Ma impinges on the thicker and older Youanmi Terrane, resulting attenuation of the lithosphere and extensive komatitiic-basaltic volcanic magmatism across the Youanmi Terrane and EGST.

T5 (2700–2600 Ma): Narryer and Youanmi Terrane are amalgamated and cratonised, widespread c. 2730–2615 Ma magmatism in Narryer Terrane is a response to post-collisional slab break-off or lithospheric delamination. Second plume event at c. 2720–2675 Ma, komatitiic-basaltic volcanic magmatism observed in Youanmi, Kalgoorlie and Kurnalpi Terranes. Crustal anatexis leading to granite magmatism observed in the Kalgoorlie Terrane (Marymia Inlier) and Youanmi Terrane (Goodin Inlier) at c. 2700 Ma. The significant contrast in isotopic signature between the Kalgoorlie (median εHf_t +1.9) and Youanmi Terranes (median εHf_t -6.3) are reflections of their crustal thicknesses. Glenburgh Terrane represents a detached crustal fragment by c. 2600 Ma.

T6 (2600–2400 Ma): By 2600 Ma all of the Yilgarn Craton is stabilised, predominance of unradiogenic εHf_t values in Yilgarn Craton indicates that granite magmatism involves intracrustal melting of variably older felsic crust. Magmatism in the northern Murchison Domain has been interpreted to reflect lithospheric delamination at c. 2640 Ma (Van Krandendonk et al., 2013). The Glenburgh Terrane has a predominance of radiogenic εHf_t values and involves the addition of juvenile material, possibly in a continental-margin arc environment. Magmatism developed as a response to southward subduction under the Glenburgh Terrane.

8.2 PROTEROZOIC CRUSTAL EVOLUTION

The Capricorn Orogen formed during the early Palaeoproterozoic as a response to the accretion of three discrete crustal components, the Pilbara Craton, the Yilgarn Craton and the Glenburgh Terrane. The orogen records over a billion years of repeated basin formation and magmatism. The following history represents a summary of the research presented in chapters 5–7 integrated with existing geochronology and geochemical data and previous models in order to rationalise the crustal evolution of the Capricorn Orogen.

8.2.1 Palaeoproterozoic rifting

Lithospheric extension along the northern Yilgarn Craton at c. 2200–2100 Ma resulted in the formation of the Yerrida Basin (Pirajno et al., 2004, Occhipinti et al., 2017). The c. 2660–2620 Ma Goodin Inlier, a northward extension of the Youanmi Terrane forms basement to the Yerrida Basin. Pirajno and Occhipinti (2000) interpreted that the Goodin Inlier resulted from basement uplift due to compressional phase in the Yerrida Basin development. Continued rifting along the Yilgarn Craton margin resulted in backarc sea-floor spreading and rifting, and led to the development of the Bryah sub-basin at c. 2030 Ma and generation of voluminous mafic to ultramafic magmatism (Pirajno et al., 2004, Occhipinti et al., 2017). During this event, the backarc rifting has been interpreted as separating the southeast portion of the Marymia Inlier from the Yilgarn Craton (Pirajno and Occhipinti, 2000). Recent studies have interpreted the Marymia Inlier as a rifted fragment of the Yilgarn Craton formed during continental rifting and deposition in the Yerrida Basin at c. 2174 Ma (Dentith et al., 2014; Olierook et al., 2017). Extensional processes ended following the start of nothwestard subduction of the Yilgarn Craton beneath the Glenburgh Terrane during the c. 2005–1950 Ma Glenburgh Orogeny (Sheppard et al., 2004; Occhipinti et al., 2017). Ocean closure and collision along the Yilgarn Craton margin resulted in the sedimentation in the Padbury Basin, which is interpreted as developing in a retro-arc forland basin (Martin, 1994; Occhipinti et al., 2017).

8.2.2 Palaeoproterozoic accretion (Part 1)

The Capricorn Orogen developed between the Pilbara and Yilgarn Cratons during the two-stage formation of the Western Australian Craton (WAC; Occhipinti et al., 2004). The first stage involved the accretion of the Glenburgh Terrane with the southern margin of the Pilbara Craton during the c. 2215–2145 Ma Ophthalmian Orogeny (Occhipinti, 2004; Occhipinti et al., 2004; Johnson et al., 2013). The second stage involved the collision of the combined Glenburgh Terrane-Pilbara Craton with the passive margin of the Yilgarn Craton during the 2005–1950 Ma Glenburgh Orogeny (Occhipinti et al., 2004; Sheppard et al., 2004).

The southern Pilbara Craton is interpreted to have evolved from a passive to an active continental margin at c. 2500 Ma (Blake and Barley, 1992; Krapež, 1997; Powell et al., 1999), followed by ocean closure and accretion with a continent to the south during the c. 2215–2145 Ma Ophthalmian Orogeny (Blake and Barley, 1992; Martin et al., 2000; Rasmussen et al., 2005; Martin and Morris, 2010). Based on detailed studies on the tectonic evolution of the southern margin of the Glenburgh Terrane, Sheppard et al. (2004) and Occiphinti et al. (2004) suggested that the continent that the Pilbara Craton collided with was likely to be the Glenburgh Terrane. However, there is no clearly defined arc magmatism associated with this event, and the polarity of the subduction has not been constrained. Deep seismic survey results of Korsch et al. (2011) indicate the Lyons River Fault is suture zone between the Glenburgh Terrane and the Bandee Seismic Province, interpreted to be a component that was accreted to Pilbara Craton at some stage prior to c. 2775 Ma (Johnson et al., 2013).

Mafic magmatism at c. 2200 Ma in the southern Pilbara has been interpreted to suggest a northward subduction zone beneath the Pilbara Craton (Blake and Barley, 1992; Martin and Morris, 2010). However, previous studies have also interpreted the mafic magmatism to be the product of rifting (Krapež, 1999; Müller et al., 2005) or foreland basin evolution (Martin et al., 1998; Powell et al., 1999; Martin et al., 2000). Recent isotopic data from Johnson et al., (2017a) identified a c. 2280–2115 Ma inherited zircon population that contributed to the granites of the Moorarie and Durlacher Supersuites. They interpreted these zircon as representing a crustal component that was a product of arc magmatism within the Glenburgh Terrane that developed above a southward dipping subduction zone during the Ophthalmian Orogeny. Granites from the Dalgaringa and Bertibubba Supersuites from this study contain inherited material that have similar ages as those reported by Johnson et al. (2017a). The Hf–O composition of these c. 2280–2100 Ma components are consistent with the moderately evolved Hf-isotope (εHf_t -12.2 to +3.5) and light to moderate O-isotope ($\delta^{18}O$ 3.39‰ to 6.48‰) array described by Johnson et al. (2017a). The development of the c. 2280–2100 Ma crustal component within the Glenburgh Terrane suggests that the subduction of the ocean crust was south directed. This crustal component was reworked and later contributed to the Glenburgh Orogeny magmatism.

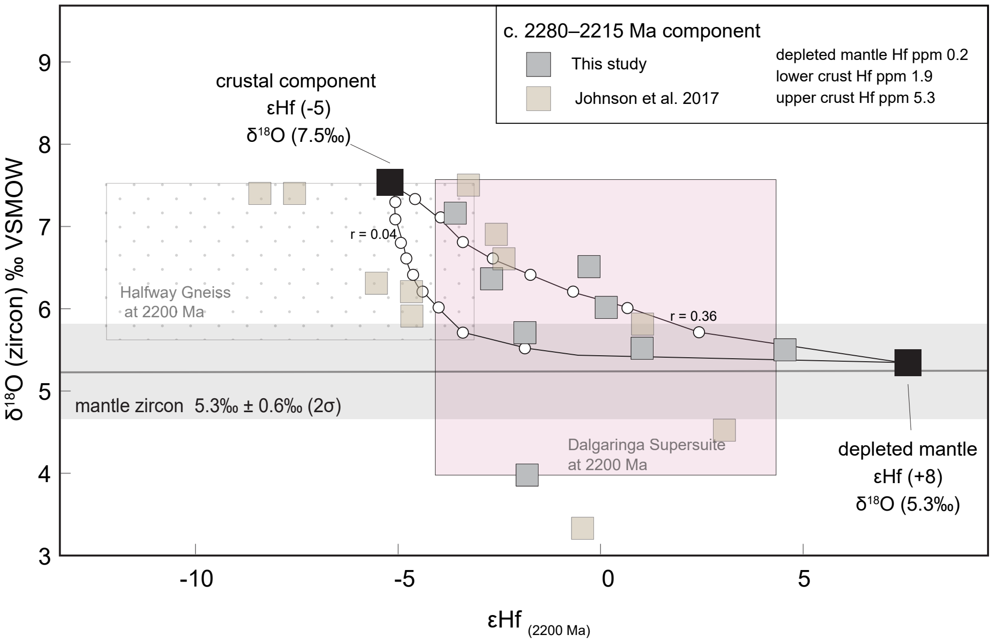

Figure 8.2 Plot of δ^{18}O versus εHf_t showing the c. 2280–2100 Ma crustal component at 2200 Ma. The stippled (crosses) box represents Halfway Gneiss at 2200 Ma (based on Hf–O data presented in Chapter 4), and the pink box represents the Dalgaringa Supersuite at 2200 Ma. Composition of crustal endmembers are based on low Hf coupled with maximum measured δ^{18}O value from Halfway Gneiss samples (Chapter 4). Bulk mixing curves are marked at 10% increments.

On an εHf_t versus δ^{18}O plot (Fig. 8.2) where the εHf_t of the c. 2280–2100 Ma components recalculated at c. 2200 Ma, most of the data fall between mixing lines that represent mixing between a juvenile (depleted-mantle) component and a crustal component (Halfway Gneiss composition). The majority of the c. 2280–2100 Ma components in this study can be modelled with bulk-mixing between a juvenile (depleted mantle) component with a 10–80% contribution from an older crustal component (comparable with a Halfway Gneiss composition). Analyses of inherited zircon with δ^{18}O values above 7.5‰ were assumed to represent crustal contamination, i.e. metasedimentary components that were incorporated into the melt source, either by assimilation or wall-rock interaction. The crystallisation ages of individual samples range between c. 2280 and 2100 Ma, and are broadly similar to the age of the 2215–2125 Ma Ophthalmian Orogeny, supporting the interpretation that magmatism was generated in an arc environment on the northern margin of the Glenburgh Terrane (e.g. Johnson et al., 2011, 2017a).

8.2.3 Palaeoproterozoic accretion (Part 2)

In the mid-Palaeoproterozoic, magmatism was generated in an Andean-type continental arc setting on the southern margin of the Glenburgh Terrane during the accretion of the combined

Glenburgh Terrane-Pilbara Craton with the passive margin of the Yilgarn Craton (Occhipinti et al., 1999; Sheppard et al., 2004). Arc magmatism is suggest to have initiated at c. 2090–2050 Ma, with the outboard arc components now lost by subduction erosion (Johnson et al., 2011b; Chapter 5). The Hf–O data from the c. 2005–1970 Ma Dalgaringa Supersuite is consistent with previous isotopic studies that determined that they formed by mixing of juvenile mantle-derived material with Archaean crust (Sheppard et al., 2004; Johnson et al., 2011a), with bulk-mixing calculations indicating 12–55% involvement of a (low-δ^{18}O with variably evolved εHf_t) mid- to lower-crustal component, which has a isotopic composition equivalent to the Halfway Gneiss (Chapter 5). Inherited zircon with ages between c. 2280–2215 Ma have Hf–O compositions that are indistinguishable from Archaean granitic components at c. 2000 Ma (Fig. 8.2). This supports the interpretation that the c. 2280–2115 Ma zircon grains represent an Ophthalmian arc related crustal component, and was subsequently incorporated into the magmas generated during the Glenburgh Orogeny at c. 2000 Ma. Deformation during the early stages of the Glenburgh Orogeny is constrained between c. 2005–1990 Ma (Nelson, 1999; Occhipinti et al., 2001) and resulted in the deformation of the Archaean basement of the Glenburgh Terrane and older (c. 2000 Ma) Dalgaringa Supersuite granitic rocks to form the Halfway Gneiss (Occhipinti et al., 2001, 2004). Previous studies have shown that the combined use of Lu–Hf and O isotope data in order to evaluate the relative contributions from mantle, crust, and recycled reservoirs within magmas have their limitations (Roberts et al., 2012; Roberts and Spencer, 2015; Payne et al., 2016). Processes such as the incorporation of continental crustal-derived materials in the mantle at subduction zones may alter the Hf–O signatures of mantle-derived melts (e.g. Nebel et al., 2011; Roberts et al., 2013; Couzinié et al. 2016; Wang et al., 2016). These hybrid mantle sources may not have DM-like Hf isotope compositions or pristine mantle O isotope compositions, as observed in the Dalgaringa and Bertibubba Supersuite granites (Chapter 5). This crustal contamination primarily affects newly formed crust at convergent plate settings (Nebel et al., 2011). As such, interpretations of crustal growth at subduction zones need careful evaluation.

Collision and accretion of the Glenburgh Terrane and Yilgarn Craton formed the north-northeasterly trending Errabiddy Shear Zone (Occhipinti and Reddy, 2004). The Errabiddy Shear Zone includes metasedimentary rocks of the Camel Hill Metamorphics, and fault slices of the Yilgarn Craton and southern Glenburgh Terrane, which were intruded by the Bertibubba Supersuite at c. 1965–1945 Ma, marking the end of the Glenburgh Orogeny (Occhipinti et al., 2004). The Hf–O data presented in Chapter 5 indicates that magmatism was generated as a response to slab breakoff. This process can account for the shift from dominantly unradiogenic εHf_t values of the Dalgaringa Supersuite towards the radiogenic compositions observed in the Hf-isotope data. Following slab breakoff, continued compression resulted in steepening and eventual overturning of the suture (Davies and von Blanckenburg, 1995). Reworking of the Errabiddy Shear Zone by the Cardilya Fault resulted in the southern margin of the Glenburgh Terrane being thrust back to the south under the Narryer Terrane (Sheppard et al., 2003; Johnson et al., 2011c).

8.2.4 From crustal growth to crustal reworking

The Palaeoproterozoic collisional phase was followed by a 115 Myr hiatus in magmatic activity, after which the Capricorn Orogen was affected by widespread granitic magmatism and deformation at c. 1820–1770 Ma. Although magmatism is observed mainly in the western portion of the orogen (Gascoyne Province) and in the Yilgarn Craton (Yarlarweelor Gneiss Complex), it is also recognised in the eastern extent within the Edmund Basin. The geodynamic setting during the Capricorn Orogeny is unclear. Previous models for crustal growth during the Capricorn Orogeny (Tyler and Thorne, 1990; Myers, 1990; Evans, 1993) involved oblique collision of the Yilgarn and Pilbara Cratons, with the suture near or at the Minnie Creek Batholith. More recently, Sheppard et al (2010a) re-evaluated the spatial and temporal patterns of sedimentation, and presented whole-rock geochemistry of granites and volcanics associated with the Capricorn Orogeny which indicated that there was no requirement for subduction related processes. They proposed an intracratonic setting for the Capricorn Orogen, with reworking and magmatism interpreted to be a response to far-field plate tectonic processes.

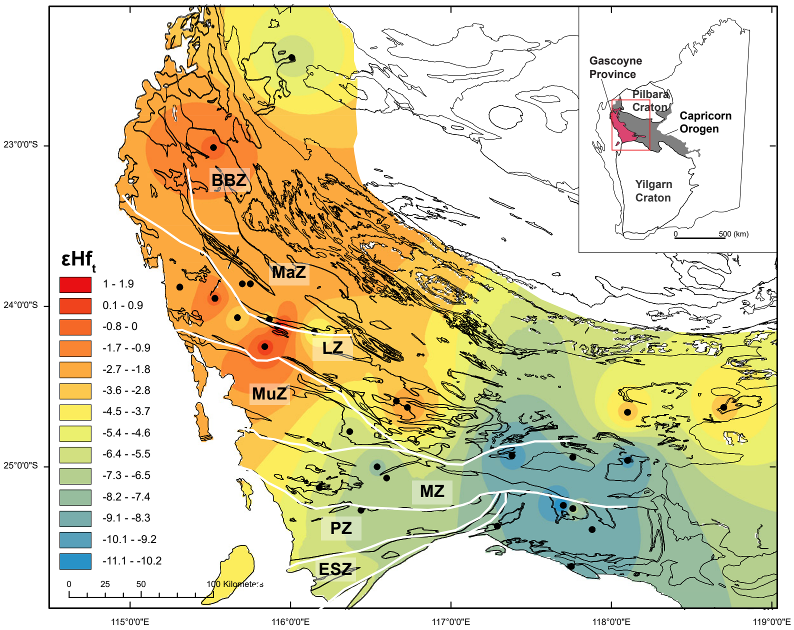

Figure 8.3 Distribution of median εHf$_t$ values for the Moorarie Supersuite samples, showing subdivision of the region after the structural-metamorphic zones of Sheppard et al. (2010a). BBZ: Boora Boora Zone, MaZ: Mangaroon Zone, LZ: Limejuice Zone, MuZ: Mutherbukin Zone, Mz: Mooloo Zone, PZ: Paradise zone, ESZ: Errabiddy Shear Zone.

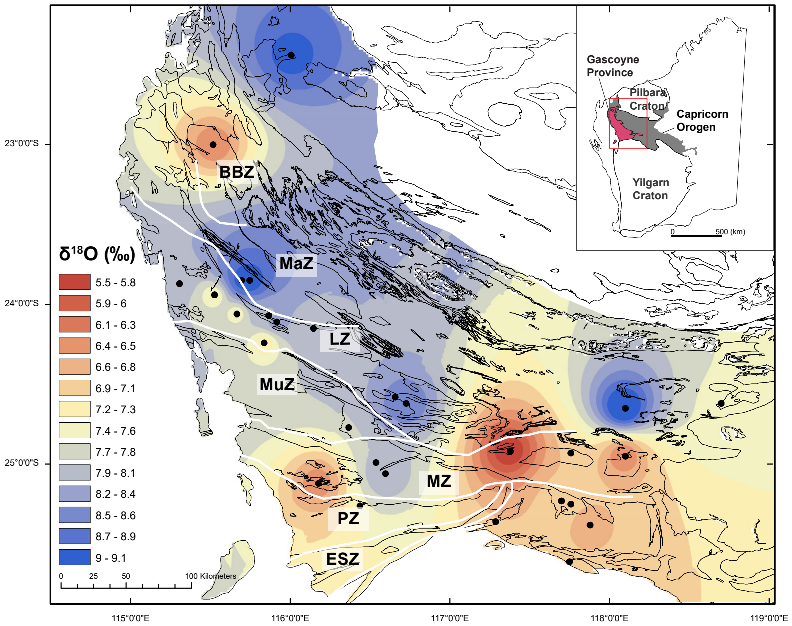

Figure 8.4 Distribution of average δ^{18}O values for the Moorarie Supersuite samples, showing subdivision of the region after the structural-metamorphic zones of Sheppard et al. (2010a). BBZ: Boora Boora Zone, MaZ: Mangaroon Zone, LZ: Limejuice Zone, MuZ: Mutherbukin Zone, Mz: Mooloo Zone, PZ: Paradise zone, ESZ: Errabiddy Shear Zone.

The isotopic characteristics of the c. 1820–1775 Ma Moorarie Supersuite granites record a significant change from the mantle-derived magmatism and crustal growth recorded during the Glenburgh Orogeny to magmatism dominated by reworking and an increased incorporation of metasedimentary material. The Hf–O data presented in Chapter 6 identified three isotopically distinct sources for the Moorarie Supersuite granites which include: (1) juvenile component/mafic lower crustal rocks, (2) evolved crustal components with a compositions equivalent to the Halfway Gneiss and Dalgaringa Supersuite and (3) a metasedimentary/upper crustal component. This interpretation is consistent with previous isotopic studies (Sheppard et al., 2010a; Johnson et al., 2017a). The Hf data shows a distinct spatial trend, with increasing heterogeneity in $\varepsilon\mathrm{Hf}_t$ composition and involvement of a more juvenile source observed from south to north (Fig. 8.3). In addition, the oxygen isotope data shows the same spatial trend, with the southern samples indicating mantle-derived values, increasing to high-δ^{18}O values towards the north (Fig. 8.4).

A geodynamic model for the Moorarie Supersuite must account for the systematic geographical variations in isotopic composition, the generation of large volumes of granitic melts, and the lack of geochemical characteristics of subduction-related magmatic activity (Sheppard et al., 2010a). As discussed in Chapter 6, the northward trend of the Hf–O isotope compositions was interpreted to reflect differences in the depth of melting, with the southern and central granites (Errabiddy

Shear Zone to Mooloo Zone) forming at mid-crustal levels, which consisted of largely of the evolved meta-igneous Glenburgh Terrane rocks, resulting in the unradiogenic εHf_t coupled with mantle-like $\delta^{18}O$ values (Fig. 8.4, 8.5). The radiogenic (juvenile) input observed in the Minnie Creek Batholith (Limejuice Zone) was interpreted to represent the mafic-ultramafic and mafic inclusions observed in the batholith (Sheppard et al., 2010a). Johnson et al. (2017c) reported the Nd isotopic compositions of the mafic rocks, which overlap with the most radiogenic rocks of the Minnie Creek Batholith, consistent with field observations of magma mingling (Sheppard et al., 2010b) and supports the Hf isotope data which indicate incorporation of juvenile material during the genesis of the Minnie Creek Batholith granites (Chpater 6). The high $\delta^{18}O$ values recorded in the granites north of the Mooloo Zone was interpreted to reflect melting at higher levels (i.e. upper-crustal levels), resulting in the higher incorporation of metasedimentary materials and the greater heterogeneity observed in the Hf–O array (εHf_t values range from -7.9 to +2.5, total of 10.4 εHf_t units; Chapter 6). Crustal deformation during extension and shortening is often accommodated by large-scale mid-crustal shear zones (Jolievet et al., 1998; Rey et al., 2009). These crustal shear zones can act as migration pathways for melts from their lower-crustal source to emplacement in the upper crust (D'lemos et al., 1992; Ferré et al., 2012; Diener et al., 2014; Carvalho et al., 2016). Migration of melts along shear zones (i.e. Ti Tree Shear Zone, Lyons River Fault) into upper crustal reservoirs where they incorporated the Leake Spring Metamorphics accounts for the enclaves of low-grade metasedimentary material observed in the Minnie Creek Batholith (Sheppard et al., 2010a).

Based on the presence enclaves with metamorphic assemblages consistent with upper crustal origin, the source of the high-$\delta^{18}O$ material in the Minnie Creek Batholith granites (average $\delta^{18}O$ values 8–9‰) was interpreted to be the Leake Spring Metamorphics into which they intruded (Johnson et al., 2017a; Chapter 6). Data presented in Chapter 7 indicates that the Moorarie Supersuite, specifically the Minnie Creek Batholith, was the primary source component for the younger c. 1680–1620 Ma Durlacher Supersuite granites. Within the Mutherbukin Zone, Durlacher Supersuite granites (Davey Well Batholith) are interpreted to have been emplaced at mid-crustal levels (>650°C, 4.7–7 kbar; Korhonen et al., 2017; Johnson et al., 2011b). This suggests that the high-$\delta^{18}O$ signature of the Durlacher Supersuite and Moorarie Supersuite represents partial melting and incorporation of high-$\delta^{18}O$ components at mid-crustal levels, which is difficult to reconcile with the melting and recycling of the upper crustal Minnie Creek Batholith. This suggests the Leake Spring Metamorphics is not the source for the high $\delta^{18}O$ signature recorded in the Minnie Creek Batholith, and an alternative metasedimentary source component at mid-crustal levels is required. The introduction of high-$\delta^{18}O$ material to mid-crustal levels may have occurred by tectonic burial (i.e. retroarc underthrusting) during subduction that preceded the Capricorn

Orogeny, namely during the Glenburgh Orogeny. This process has been used to account for the formation of S-type granites within the Coast Mountains batholith, British Columbia (Pearson et al., 2017). During the c. 2005–1950 Ma Glenburgh Orogeny the rocks of the Glenburgh Terrane experienced shortening, which was accommodated by the development of faults, and may have resulted in the southward underthrusting of sediments (c. 2240–2125 Ma Moogie Metamorphics) to mid-crustal levels. Although no direct evidence of mid-crustal metasediments from the Gascoyne Province has not been identified, the isotopic compositions of the granites north of the Mooloo Zone strongly suggest a mid-crustal metasedimentary source, and the localised variation in radiogenic isotope composition observed in the Moorarie Supersuite granites is compatible with the tectonic burial of a crustal component. Two-component mixing modelling based on the data from the Thirty Three Supersuite indicated a 38–62% contribution from an unknown metasedimentary component that used an average Moogie Metamorphic εHf_t value (Chapter 7). Similarly, the mixing model for the Moorarie Supersuite (Chapter 6) also used an average Moogie Metamorphic εHf_t value, which suggests that the metasedimentary component is compatible with the interpretation of a mid-crustal Moogie Metamorphics component. Generation of Minnie Creek Batholith granitic melts involved mixing between hybrid magmas from deep crustal hot zones and a metasedimentary component at mid-crustal levels. These melts migrated along shear zones to higher crustal levels, where they assimilated local wall-rocks (Leake Spring Metamorphics), which did not significantly change isotopic composition of the magmas.

Intracontinental orogenic events have been recognised to occur as a response to the transferral of stresses from active plate boundaries to intra-plate regions, and are controlled by the presence of heterogeneities in the lithosphere (Vauchez et al., 1998; Gorczyk et al., 2013). Examples of intra-plate orogenic events within Australia are observed in the Neoproterozoic to Phanerozoic Petermann and Alice Springs Orogens of central Australia (Hand and Sandiford, 1999; Scott et al., 2000; Wade et al., 2006, 2008; Smithies et al., 2011; Kennet and Iaffaldano, 2013; Raimondo et al., 2014). Processes such as terrane accretion can significantly weaken the lithosphere, and deformation associated with subsequent orogenic events is likely to be concentrated in zones of pre-existing lithospheric weaknesses (Vauchez et al., 1998; Audet and Bürgermann, 2011; Gorczyk et al., 2013; Calignano et al., 2015). The Capricorn Orogen records the collision between the Pilbara Craton, the Glenburgh Terrane and the Yilgarn Craton (Sheppard et al., 2010a). The suture zones between the three crustal blocks have been indentified as the Lyons River Fault in the north and Errabiddy Shear Zone in the south (Johnson et al., 2011c). These zones have remained a site of lithospheric weakness and have been subject to reactivation, in extensional, compressional and oblique-slip settings during subsequent Palaeoproterozoic events (Johnson et al., 2013). The c. 1820–1770 Ma Capricorn Orogeny overlaps with the c. 1800–

1765 Ma Yapungku Orogeny in the Rundal Complex of the Paterson Orogen (Bagas and Smithies, 1997; Bagas, 2004) and the c. 1860–1820 Ma Stafford tectonic event and the c. 1780–1770 Ma Yambah Event of the Arunta Inlier in central Australia (Collins and Shaw, 1995; Hand and Buick, 2001). The Yapungku Orogeny has been interpreted to represent collision between the West Australian and North Australian Cratons (c. 1800–1765 Ma; Smithies and Bagas, 1997; Li, 2000; Bagas, 2004; Payne et al., 2009). The timing of this event is constrained by the age of granitoid intrusions of 1802 ± 14 Ma and 1765 ± 15 Ma (Nelson, 1995a, 1995b) which are interpreted to pre- and post-date high-pressure metamorphism resulting from the collisional event (Smithies and Bagas, 1997; Bagas, 2004). The polarity of subduction is currently unconstrained, previous models have suggested a north-eastwards direction (Smithies and Bagas, 1997; Betts and Giles, 2006), although this does not preclude a south-westward direction (Payne et al., 2009). Maidment (2017) has suggested that the amalgamation took place at a later stage, and the c. 1800–1765 Ma magmatism may have developed as a consequence of extensional conditions, but does not rule out a convergent setting. Initiation of subduction may have started prior to c. 1800 Ma, and the transferral of stresses from the plate boundaries to the Capricorn Orogen could have been the driver of the intraplate deformation.

Granite magmatism during the Capricorn Orogeny primarily reflects crustal partial melting during the emplacement of mantle-derived melts (Chapter 6). However, identification of the driver of mantle melting in an intracratonic setting remains problematic. Recent numerical experiments have suggested the removal of the lower lithosphere by gravitational instabilities (Rayleigh-Taylor instability) and subsequent asthenospheric upwelling can produce magmatism in intracratonic regions (Elkins-Tanton, 2007; Gorczyck et al., 2012; Gorczyk and Vogt, 2015; Wang and Currie, 2015). This process is used to account for magmatism associated with the Giles Event in the Musgrave region in central Australia (Smithies et al., 2015). Numerical modelling by Gorczyk and Vogt (2015) have demonstrated that mechanical removal of part of the lithosphere can be initiated as a result of heterogeneities within the lithosphere, where horizontal compression facilitates the localisation of strain and deformation within the zones of lithospheric weakness, resulting in plastic delamination and can generate mantle melts within 8.1 Myr. Rayleigh-Taylor instability and subsequent delamination initiated as a response to far field stress is a viable mechanism that can account for the production and emplacement of basaltic magmas in the lower crust, leading to the development of a deep crustal hot zone, and inducing crustal anatexis.

Although the geodynamic driver for the Capricorn Orogeny has not been unequivocally identified, the timing of magmatism and deformation is synchronous with events in central Australia, and as such, it is suggested that these orogenic events resulted in the propagation of stresses that lead to the localisation of strain and deformation within zones of lithospheric weakness and reactivation of the pre-existing suture zones within the Capricorn Orogen which resulted in the intracratonic Capricorn Orogeny.

8.2.5 The last of the granites

The c. 1680–1620 Ma the Mangaroon Orogeny involved heterogeneous deformation and metamorphism, reactivation of faults and shear zones, and was accompanied by coeval voluminous granitic magmatism of the Durlacher Supersuite (Sheppard et al., 2005). Deformation and amphibolite to greenschist facies metamorphism is concentrated within the Mangaroon Zone in the Gascoyne Province, and is interpreted to have occurred in an extensional tectonic setting (Sheppard et al., 2005).

Magmatism is predominantly observed in the Gascoyne Province, with minor amounts observed in the Yarlarweelor Gneiss Complex to the south. The Lu–Hf and O isotopic compositions of the Durlacher Supersuite indicate the primary source for the melts consisted of reworking of the Moorarie Supersuite granites with minor amounts of metasedimentary material, and no evidence of input from mantle-derived material (Chapter 7). The Hf–O composition of the granites that intrude the Yarlarweelor Gneiss Complex can be modelled with mixing between 88–100% Moorarie Supersuite and 0–12% Halfway Gneiss rocks, while the remainder of the Durlacher Supersuite are indistinguishable from the Minnie Creek Batholith granites (Chapter 7). The Hf–O composition of the southern granite indicates that they were generated at mid-crustal levels, with a similar distribution observed as the southern granites of the Moorarie Supersuite. Inherited ages of zircon are consistent with an origin from the Pooranoo Metamorphics into which they intruded, and are interpreted as representing late stage magmatic contamination in the upper crust. The similarities in the distribution of granites (intrusion into the Yarlarweelor Gneiss Complex and in the Gascoyne Province) suggests melt migration was controlled along the crustal scale shear zones within the Gascoyne Province.

Development of the Mangaroon Orogeny and associated magmatism of the Durlacher Supersuite has been interpreted as intracontinental reworking as a response to the amalgamation of the West Australian, North Australian and South Australian cratons during the Kimban-Nimrod-Strangways Orogeny at c. 1740–1690 Ma (Sheppard et al., 2005; Betts et al., 2008; Huston et al., 2012). However, the heat source required to generate Durlacher Supersuite magmatism has not been established. Sheppard et al. (2005) reported field evidence of magma mingling between gabbros and granites within the Mangaroon Zone. This suggests that some addition of mantle-derived material was involved, possibly as a response of the extensional processes associated with the Mangaroon Orogeny, and provided heat necessary for partial melting of mid-to upper-crustal rocks. However, this is not observed in the Hf–O compositions of the Durlacher Supersuite, as mixing would be expected to produce a more radiogenic Hf-isotope composition in the granites than is recorded. This suggests that precipitation of zircon from crustal-derived melts may have occurred prior to the mingling with gabbros.

In the absence of isotopic evidence for a large contribution of mantle-derived magmas associated with the generation of the Durlacher Supersuite, alternative processes to generate the heat necessary to induce partial melting of the source rocks are required. An additional source for heat causing widespread crustal anatexis is the contribution from radiogenic heat production (e.g. Gerdes et al., 2000; Sandiford and McLaren, 2002; Korhohen and Johnson, 2015). Another form of internal heat production is through crustal scale shear heating, and several studies have quantitatively demonstrated that shear heating is a plausible mechanism to induce anatexis within the shear zone and adjacent rocks in mid- to upper crustal levels (Leloup et al., 1999; Nablek and Liu, 2004; Nablek et al., 2010; Devès et al., 2014; Carvalho et al., 2016). Although evidence for shear heating within the Gascoyne Province has not been substantiated, deformation and metamorphism was strongly partitioned into the Mangaroon Zone (Sheppard et al., 2005). Several crustal scale shear zones intersect this zone, including the crustal scale Lyons River Fault and the Tagla-Godfrey Faults, these shear zones acted as pathways for fluids and melts and may have been the sites of partial melting. Korhonen and Johnson (2015) demonstrated that heat-producing elements have been progressively concentrated within the shallow crust of the Capricorn Orogen. A combination of these mechanisms would increase the heat within the crust, and produce the conditions necessary for crustal anatexis to occur. For example, the concentration of heat-producing elements in the crust could result in a higher thermal gradient, and effectively preheat the crust within the Gascoyne Province. During the Mangaroon Orogeny crustal extension was accompanied by high-temperature-low-pressure metamorphism, shear heating and emplacement of small volumes of mafic melts within the crust, further increasing the thermal gradient within the crust, facilitating crustal anatexis.

Within the Gascoyne Province the c. 1030–955 Ma Edmundian Orogeny is associated with amphibolite facies metamorphism (500–550°C and 3–4 kbar; Sheppard et al., 2007), deformation and intrusion of leucocratic granite plutons and rare element pegmatites of the c. 1030–890 Ma Thirty Three Supersuite concentrated within the Mutherbukin Zone (Sheppard et al., 2007, 2010a; Johnson et al., 2013; Piechocka et al., 2017). No magmatic zircon from the Thirty Three Supersuite granite plutons were identified in this study, however, inherited zircon indicate ages and Hf–O compositions equivalent to the Durlacher Supersuite granites, suggesting they were generated by the remelting of these c. 1680–1620 Ma granites. The data in presented in Chapter 7 indicated that the Hf–O composition of c. 1030 Ma magmatic zircon from the rare element pegmatites cannot be modelled with a single Durlacher Supersuite source, and require an additional source with a more radiogenic Hf signature. Two-component mixing modelling indicated a 38–68% contribution from a metasedimentary component. The crustal component was modelled used an average εHf_t value of the Moogie Metamorphics, and supports the interpretation of a mid-crustal metasedimentary component that was underthrust during the Glenburgh Orogney.

The generation of granites during previous events resulted in the concentration of radiogenic elements in the shallow to mid-crust of the Capricorn Orogen, creating a weak zone, raising the thermal gradient and localising deformation during later tectonic events (Pysklywec and Beaumont, 2004; Korhonen and Johnson, 2015; Korhonen et al., 2017). Previous studies have attributed the Edmundian Orogeny to far-field stresses related to tectonic activity on the western margin of the WAC during the formation of Rodinia (Occhipinti and Reddy, 2009), and magmatism may have been related to reactivation along the Ti Tree Shear Zone driven by plate margin processes. The Hf–O data presented in this study show that crustal evolution of the Capricorn Orogen is defined by four periods of granite emplacement which evolved from crustal growth during continental collision to intracratonic reworking, and ultimately resulting in the stabilisation of the crust 1100 Myr after terrane amalgamation.

8.2.6 A Palaeoproterozoic tectonic synthesis

Figure 8.5 depicts the crustal evolution of the Capricorn Orogen through an isotopic perspective.

T1 (3600–3000 Ma): Development of granites in the Narryer Terrane by crustal antaexis driven by repeated thermal anomalies (Chapter 4). Inherited grains are observed in Glenburgh Terrane and northern Gascoyne Province (present day location).

T2 (3000–2500 Ma): Widespread magmatism in Narryer Terrane at c. 2730–2600 Ma is dominated by crustal reworking. Magmatism is gnerated in response to accretion/re-attachment to the northern Murchison Domain. Rifting of Glenburgh Terrane from the Yilgarn Craton occurs sometime in this period. Initiation of a subduction zone results in the development of arc magmatism on the southern part of the Gleburgh Terrane at c. 2550 Ma, forming the protolith the the Halfway Gneiss. Magmatism is dominated by juvenile input.

T3 (2500–2100 Ma): Development of a subduction zone between the Glenburgh Terrane and the Pilbara Craton at c. 2300. Inherited grains in the Gascoyne Province indicate radiogenic εHf_t suggest southeastward subduction, with accretion completed by the end of the Opthalmian Orogeny at c. 2145 Ma (Rasmussen et al., 2005).

T4 (2100–1900 Ma): The combined Glenburgh Terrane-Pilbara Craton is accreted to the passive margin of the Yilgarn Craton during the 2005–1950 Ma Glenburgh Orogeny. Magmatism was generated in an arc environment on the southern margin of the Glenburgh Terrane at c. 2005–1970 Ma. Zircon indicate high amounts of crustal reworking during generation of arc magmas. Ocean closure and accretion is completed by the end of the Glenburgh Orogeny, indicated by suturing magmatism recorded in the Narryer Terrane and southern Gascoyne Province at c. 1960–1945 Ma.

T5 (1900–1730 Ma): Generation of granites at c. 1800 Ma during the Capricorn Orogeny indicates some juvenile input in the northern Gascoyne Province, while predominance of unradiogenic Hf values in southern Gascoyne Province indicates that granite magmatism involved mainly intracrustal melting of variably older felsic crust.

T6 (1730–950 Ma): Granites developed during the c. 1680–1620 Ma Mangaroon Orogeny and c. 1030–955 Ma Edmundian Orogeny have unradiogenic εHf_t values, indicating widespread reworking. These granites are the final stages in the cratonisation of the Capricorn Orogen.

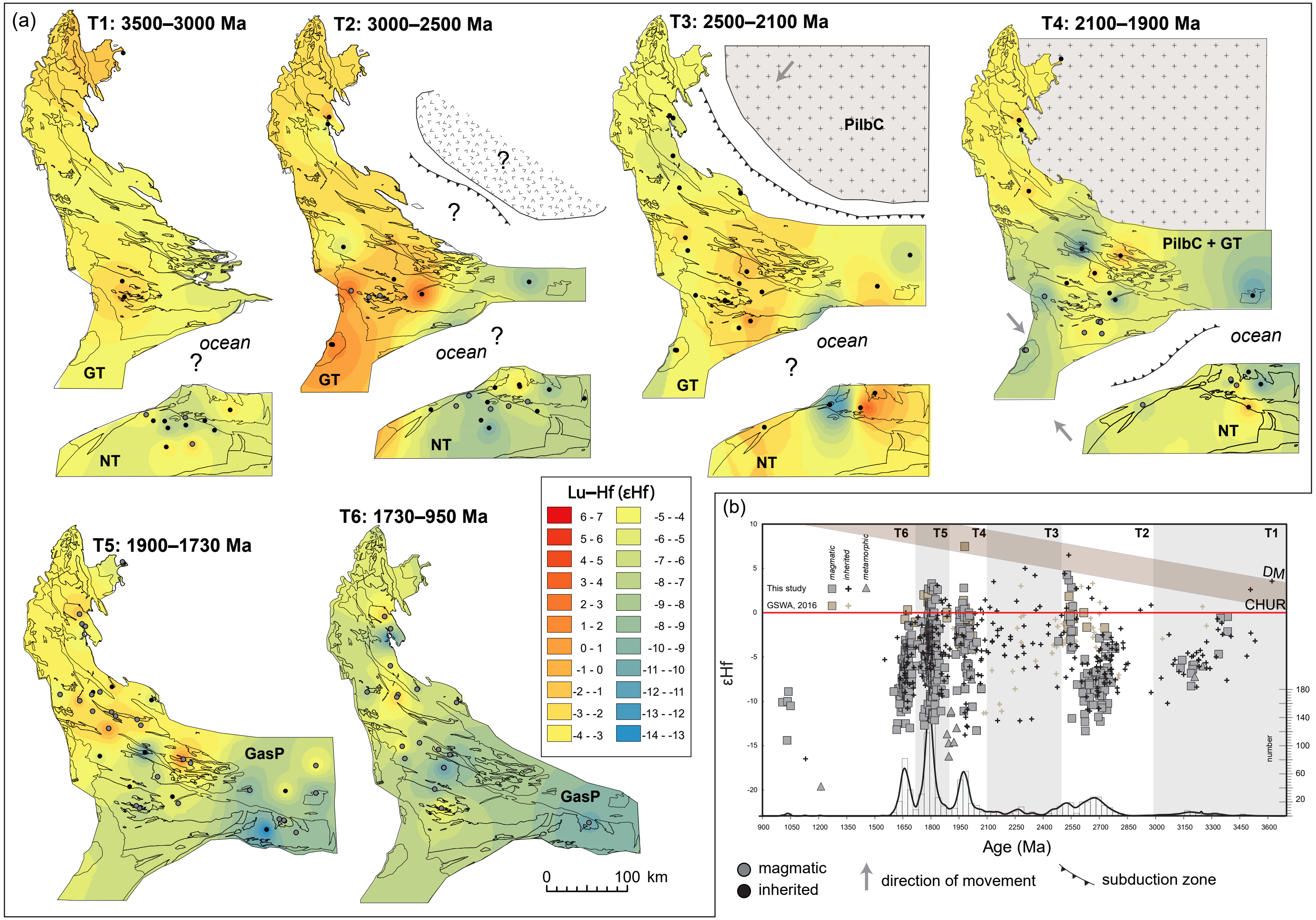

Figure 8.5 caption overleaf

Figure 8.5 A schematic model for Palaeoproterozoic crustal evolution in the Gascoyne Province (a) Lu–Hf isotopic maps of the Gascoyne Province shown as six timeslices (T1–T6) illustrating the spatial–temporal evolution of the Gascoyne Province. (T1) Granite magmatism in the NT is observed as reworking. Inherited grains are observed in GT and northern GasP. (T2) Crustal reworking observed in the northern NT. Development of a subduction zone north of the GT results in magmatism involving reworking of basement and juvenile input at c. 2550 Ma (Halfway Gneiss). (T3) Development of a subduction zone between northern GT and PilbT during the Ophthalmian Orogeny. Juvenile input is recorded in magmatism in the GT, suggesting southeastward subduction. (T4) Arc magmatism generated on southern margin of GT, involving large contribution from intracrustal sources. Magmatism is observed in the northern NT, with ocean closure and accretion completed by c. 1950 Ma. (T5) Granite magmatism records juvenile input in northern GasP, and reworking of intracrustal components in the southern areas. (T6) Granite magmatism is observed as reworking within the GasP, with no contribution from juvenile sources. [GasP, Gascoyne Province; GT, Glenburgh Terrane; PilbC, Pilbara Craton; NT, Narryer Terrane]. (b) εHf_t versus age for all collated data. A total of 74 samples (Chapter 4–7) were combined with data from 14 granitoid samples from GSWA data (Appendix F).

8.2.7 The isotopic barcode, relating Hf isotopic arrays to crustal evolution

Hf isotope ratios measured in zircon can be used to distinguish between mantle and crustal input into magmas. Variations in Hf isotope ratios and corresponding arrays are largely controlled by the magmatic source, which can be related to specific tectonic environments (e.g. Kemp et al., 2009; Collins et al., 2011; Næraa et al., 2012; Boekhout et al., 2015). Changes in Hf isotopic arrays indicate fundamental changes in tectonic conditions which reflect regional-scale geodynamics, and can be used to distinguish between different styles of orogenesis (e.g. Collins et al., 2011; Spencer et al., 2018). Orogens can be divided into three types; accretionary, collisional and intracontinental (Cawood et al. 2009). Accretionary orogens form on the exterior of continental masses and form by the continuous subduction of oceanic lithosphere. Collisional orogens form through collisional of crustal components and form within the interior of continental masses. Intracratonic orogens form within continents, away from an active plate boundaries and are driven by transmission of far-field stresses (Cawood et al., 2009; 2016). Using εHf arrays of Phanerozoic orogenic systems Collins et al. (2011) described two distinct isotopic trends that correlated with two types of orogenic systems; external and internal orogens. External orogens (i.e. circum-Pacific accretionary orogens) form on the exterior of a continental mass and are characterised by a trend towards increasingly positive εHf values, which reflect the removal of lower crust and lithospheric mantle during the subduction of oceanic lithosphere (Fig. 8.6; Cawood et al., 2009; Collins et al., 2011). By contrast, internal orogens (i.e. Alpine-Himalayan-Indonesian collisional orogens) form during the collision between continental fragments, and are characterised by a shift to both positive and negative εHf values resulting in a 'fanning' isotopic array (Fig. 8.6; Collins et al., 2011). This fanning out array is attributed to lower crust and lithospheric mantle being replaced by continental lithosphere from accreting continental fragments. Accretionary orogens involve on-going subduction-related activity that is associated with periods of ocean closure, and is generally followed by termination of subduction and final continental collision (Cawood et al., 2009). Collision-related magmatism records the transition from a convergent plate boundary to intraplate evolution, after which the tectonic activities cease following final cratonisation.

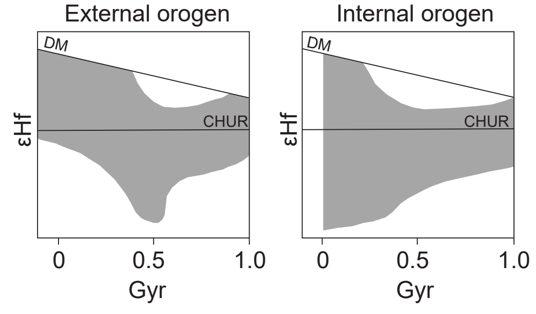

Figure 8.6 The pattern of zircon Hf data for internal and external orogens (based on Collins et al., 2011).

The Hf isotope array for the Capricorn Orogen granites show a distinctive pattern, with an initial episode of an increase of positive εHf values followed by punctuated vertical arrays trending towards increasingly negative εHf values over time, resulting in a similar 'fanning' pattern as for the start of an internal orogen (Collins et al., 2011). The internal-type orogen interpretation supports the geochemical and isotopic evidence of continent-continent collision, which indicates juvenile input during arc magmatism prior to collision (Dalgaringa Arc, Chapter 5) and a significant input of an unradiogenic component due to reworking of an evolved crustal component (Halfway Gneiss and Yilgarn Craton, Chapter 5). Other Proterozoic examples of collisional orogens include the Mesoproterozoic Grenville orogen (Petersson et al., 2015; Spencer et al., 2018), Palaeoproterozoic Rudall Province (Kirkland et al., 2013; Gardiner et al., 2018), Palaeoproterozoic Limpopo Belt (Zeh et al., 2007). Following assembly of the West Australian Craton three punctuated periods of granitic magmatism (Moorarie, Durlacher and Thirty-Three Supersuites) were generated in an intracratonic setting (Chapter 6 and 7). The Hf isotopic compositions of the granitic suites form large vertical arrays, and the strongly negative εHf values reflecting extensive reworking of Paleoproterozoic and older crustal sources, with limited input from mantle components. This pattern is similar to the zircon Hf isotope trends of magmatic rocks from the Rudall Province (Gardiner et al., 2018), which records a collisional event between the West Australian Craton and the North Australian Craton, followed by reworking of Archaean basement rocks. Current studies that relate Hf isotope variations to tectonic evolution have primarily focused on accretionary and collisional orogens, and establishing links between the isotopic signature of these types of orogens and their relation to crustal growth in the supercontinent cycles (i.e. Collins et al., 2011; Roberts, 2012; Smits et al., 2014; Gardiner et al., 2016; Li et al., 2016). By contrast, relatively few studies have been conducted that offer an isotopic perspective on intracratonic orogens. Granitic rocks from the Capricorn Orogen offer a comprehensive isotopic insight into the crustal evolution of an orogen, and record Hf isotopic trends that document the evolution from an active continental margin to intracratonic reworking and to subsequent cratonisation.

CHAPTER 9

THESIS SUMMARY

This aim of this thesis was to characterise the granites within the Capricorn Orogen in order to establish new constraints on the crustal evolution of the Capricorn Orogen. The following summarises the findings and key outcomes of this study in consideration of these aims.

Archaean magmatism The geochronological, geochemical and isotopic data presented in this chapter 4 was used to identify regions with a shared history of granite emplacement corresponding to a common geological and crustal evolution, and were used to constrain the relationships between the basement inliers and the Yilgarn and Pilbara Cratons.

Sylvania Inlier U–Pb zircon geochronology from the Sylvania Inlier date magmatism between 3196 ± 9 Ma and 2879 ± 16 Ma. Hf–O data indicates that magmatism in the Sylvania Inlier was derived from mixing between a juvenile component and an older crustal component with compositions similar to the Eastern Pilbara Terrane. The new U–Pb ages and Hf–isotopic data indicate correlations to the Eastern Pilbara Terrane, however, with a separate evolution after c. 3200 Ma. This supports previous interpretations that the Sylvania Inlier is part of the Kurrana Terrane, and represents a rifted portion of the Eastern Pilbara Terrane (Hickman, 2004; Hickman et al., 2010).

Goodin Inlier Magmatic zircon U–Pb data from the Goodin Inlier reveal one main period of granite emplacement at c. 2660–2620 Ma, contemporaneous with the c. 2760–2620 Ma voluminous granite emplacement observed in the Narryer Terrane, Youanmi Terrane and Marymia Inlier. Zircon analyses indicate predominantly evolved Hf-isotope compositions (median εHf_t -6.3, $T_{DM}{}^{C}$ 3500 Ma) coupled with mantle-like $\delta^{18}O$ (average $\delta^{18}O$ 5.88‰), interpreted as indicating the zircons crystallised from a magma generated by melting of pre-existing igneous rocks mixed with evolved sources at lower- to mid- crustal levels. These isotopic compositions are comparable with, and interpreted to be part of, the Youanmi Terrane in the Yilgarn Craton.

Marymia Inlier Analysed magmatic zircons from the Marymia Inlier indicate two periods of magmatism at c. 3300 and c. 2700. The c. 3300 Ma samples are the first to date magmatism of this age in the Marymia Inlier. The dominance of evolved εHf_t values in the c. 3330 Ma zircon (median εHf_t -4.2 , $T_{DM}{}^{C}$ 3931 Ma) coupled with slightly enriched $\delta^{18}O$ (average $\delta^{18}O$ 6.38‰), and are comparable to that of the Narryer Terrane and Yarlarweelor Gneiss granites of equivalent age, and suggests that part of the Marymia is an extension of the Narryer Terrane. By contrast, the c. 2700 Ma granites show a change to much more radiogenic values and younger crustal model ages (median εHf_t +1.7, $T_{DM}{}^{C}$ 3076 Ma) coupled with slightly enriched $\delta^{18}O$(average $\delta^{18}O$ 6.1‰), indicating that melts were generated from variable degrees of mixing of juvenile components with more evolved crustal components. These isotopic compositions are comparable to those recorded in the Kalgoorlie and Kurnalpi Terranes (Wyche et al., 2012), consistent with the interpretation that the Marymia Inlier is a northwestern extension of the Eastern Goldfields Superterrane (Vielreicher et al., 2002; Griffin et al., 2004; Gazley, 2011; Gazley et al., 2011).

Halfway Gneiss, Glenburgh Terrane The c. 2600–2430 Ma Halfway Gneiss is considered to be exotic to the adjacent Pilbara and Yilgarn Cratons based on the absence of late Paleoprotoerozoic magmatism within the Yilgarn Craton, lack of similarities in tectonomagmatic history with the Yilgarn Craton, and contrasting Hf-isotope signatures (Johnson et al., 2011b; Occhipinti et al., 2004; Sheppard et al., 2004). The Archean protoliths of the Halfway Gneiss samples have εHf_t values ranging from -4.2 to +4.3, and those with mantle like $\delta^{18}O$ values return $T_{DM}{}^{C}$ ages between 3312 and 2771 Ma. The range in εHf_t values suggests melt production from mixed sources: an older crustal component with $T_{DM}{}^{C}$ ages of >c. 3320 Ma and an additional juvenile component extracted from the mantle at c. 2770 Ma. Crustal evolution lines show that there is a degree of overlap in the most unradiogenic components of the Halfway Gneiss and the most juvenile values of the Narryer Terrane/YGC. Additionally, inherited zircon show Lu–Hf compositions that overlap Yilgarn Craton compositions from the Murchison and Kalgoorlie Terrane, and suggests that a component with a Yilgarn Hf-isotope composition made a contribution to the c. 2550 Ma magmatism. The Hf–isotope data from the Halfway Gneiss indicate that it is not exotic to the Yilgarn Craton and may represent a rifted fragment of the Yilgarn Craton that separated from the craton during plume related magmatism initiated at c. 2800 Ma and then reaccreted during the Glenburgh Orogeny.

Palaeoproterozoic magmatism The U–Pb zircon geochronology, hafnium and oxygen isotope data from granitoids associated with the Glenburgh Orogeny were used to constrain the temporal evolution of the Palaeoproterozoic crust, and identify relative contributions of crust and mantle during their petrogenesis. Inherited zircon indicate that significant proportions of crust was generated during the Palaeoproterozoic (c. 2353–2030 Ma), and show that granitic magmatism during the Glenburgh extends to ages older than those indicated by current exposed rocks, consistent with previous interpretations that arc magmatism was initiated prior to 2005 Ma (Johnson et al., 2017a). Hf–O isotope data show Glenburgh Orogeny magmatism involved significant recycling of previously formed continental crust, with bulk-mixing calculations indicating 20–55% involvement of a mid- to lower-crustal component, with a composition equivalent to the Halfway Gneiss. The Hf–O data show a shift from dominantly unradiogenic εHf_t values (median -4.1) during Dalgaringa Supersuite magmatism, to more radiogenic εHf_t values (median -1.8), indicating a significant increase in juvenile mafic magma in the generation of these granitoids, interpreted as reflecting slab break off. Modelling indicated a depleted mantle component with slightly elevated $\delta^{18}O$, interpreted as the addition of a high $\delta^{18}O$ material into the source region, through the interaction of fluids and/or melt derived from the subducting plate with the overlying mantle wedge.

From crustal growth to crustal reworking The U–Pb zircon geochronology, hafnium and oxygen isotope data from granitoids associated with the Capricorn Orogeny were used to identify relative contributions of crust and mantle during their petrogenesis. The Hf–O compositions indicate melts were sourced from multiple, isotopically distinct sources: (1) a reworked meta-igneous component with a composition similar to that of the Halfway Gneiss/Dalgaringa Supersuite (2) a metasedimentary component and (3) a mafic, lower crustal component. The Hf–O granites south of the Mutherbukin Zone indicated mixing between a reworked meta-igneous component (40–100% contribution) with a composition similar to that of the Halfway Gneiss or the Dalgaringa Supersuite, and a metasedimentary component (20–60% contribution). Data from chapter 7 indicated that the metasedimentary component was likely to have been incorporated into melts at mid-crustal levels. The introduction of high-$\delta^{18}O$ material to mid-crustal levels may have occurred by tectonic burial (i.e. retroarc underthrusting) during the later stages of the Glenburgh Orogeny. The most radiogenic Minnie Creek Batholith analyses require 70% input from a juvenile mafic crustal component and 30–100% contribution from a metasedimentary component. Moorarie Supersuite granites are interpreted to represent melts that were generated by the intraplating of basaltic magmas in the lower crust, resulting in a deep crustal hot zone that induced partial melting of mafic lower crustal rocks and surrounding metaigneous basement. The basaltic magmas can act as a lower- or mid-crustal heat source without contributing to the melts, as observed in the granites south of the Mutherbukin Zone. Repeated intrusion of basalt may lead to partial melting of previous underplates which mix with silicic magmas, as observed in the Minnie Creek Batholith granites. Extraction of hybrid magmas and migration along crustal shear zones to shallow reservoirs in the middle and upper crust facilitated crustal anatexis and metasedimentary rock assimilation. Granite magmatism during the Capricorn Orogeny primarily reflects crustal partial melting during the emplacement of mantle-derived melts in an intracontinental setting. Mantle melts may have been generated by the Rayleigh-Taylor instabilities which developed in response to transferral of stresses from plate boundaries during subduction between the North and West Australian Cratons.

The last of the granites The U–Pb zircon geochronology, hafnium and oxygen isotope data from granitoids associated with the Mangaroon and Edmundian Orogenies were used to identify relative contributions of crust and mantle during their petrogenesis. U–Pb and Hf–O data show that the primary source for the Durlacher Supersuite magmatism was predominantly recycling of previously formed crust, with compositions equivalent to the Moorarie Supersuite granitoids. Isotopic modelling indicates no contribution from juvenile components and do not require an additional metasedimentary source to account for the Hf–O array observed in the Durlacher Supersuite granites. Development of the Mangaroon Orogeny has been interpreted as intracontinental reworking as a response to the amalgamation of the West Australian, North Australian and South Australian cratons during the Kimban-Nimrod-Strangways Orogeny at 1740–1690 Ma (Sheppard et al., 2005; Betts et al., 2008; Huston et al., 2012). Radiogenic heat production combined with crustal scale shear heating are mechanisms that could account for increasing the thermal gradient within the crust, facilitating crustal anatexis. The Thirty Three Supersuite zircon have εHf_t values that are more radiogenic than can be explained by remelting of the Durlacher Supersuite alone, and instead suggests mixing with an alternative end-member. Two-component mixing modelling indicated a 38–68% contribution from a metasedimentary component. The crustal component was modelled used an average εHf_t value of the Moogie Metamorphics, and supports the interpretation of a mid-crustal metasedimentary component that was underthrust during the Glenburgh Orogney.

BIBLIOGRAPHY

AITKEN, A. R. A., OCCHIPINTI, S. A., LINDASY, M. D., JOLY, A., HOWARD, H. M., JOHNSON, S. P., HOLLIS, J. A., SPAGGIARI, C. V., TYLER, I. M., MCCUAIG, T. C. & DENTITH, M. C. 2017. The tectonics and mineral systems of Proterozoic Western Australia: Relationships with supercontinents and global secular change. *Geoscience Frontiers*.

AMELIN, Y., LEE, D. C., HALLIDAY, A. N. & PIDGEON, R. T. 1999. Nature of the Earth's earliest crust from hafnium isotopes in single detrital zircons. *Nature,* 399, 252–255.

AMELIN, Y., LEE, D-C. & HALLIDAY, A. N. 2000. Early-middle Archaean crustal evolution deduced from Lu-Hf and U-Pb isotopic studies of single zircon grains. *Geochimica et Cosmochimica Acta,* 64, 4205–4225.

AMELIN, Y. & ZAITSEV, A. N. 2002. Precise geochronology of phoscorites and carbonatites: The critical role of U-series disequilibrium in age interpretations. *Geochimica et Cosmochimica Acta,* 66, 2399–2419.

ANDERS, E. & GREVESSE, N. 1989. Abundances of the elements: Meteoritic and solar. *Geochimica et Cosmochimica Acta,* 53, 197–214.

ANNEN, C., BLUNDY, J. D. & SPARKS, R. S. J. 2006. The Genesis of Intermediate and Silicic Magmas in Deep Crustal Hot Zones. *Journal of Petrology,* 47, 505–539.

APPLEBY, S. K., GILLESPIE, M. R., GRAHAM, C. M., HINTON, R. W., OLIVER, G. J. H. & KELLY, N. M. 2010. Do S-type granites commonly sample infracrustal sources? New results from an integrated O, U–Pb and Hf isotope study of zircon. *Contributions to Mineralogy and Petrology,* 160, 115–132.

ARCHIBALD, N. J., BETTENAY, L. F., BINNS, R. A., GROVES, D. I. & GUNTHORPE, R. J. 1978. The evolution of Archaean greenstone terrains, Eastern Goldfields Province, Western Australia. *Precambrian Research,* 6, 103–131.

ARCHIBALD, N. J., BETTENAY, L. F., BICKLE, M. J. & GROVES, D. I. 1981. volution of Archaean crust in the eastern Goldfields province of the Yilgarn Block, Western Australia. *Geological Society of Australia Special Publications,* 7, 491–504.

ARNDT, N. T. 2013. The formation and evolution of the continental crust. *Geochemical Perspectives,* 2, 405–405.

AUDET, P. & BÜRGERMANN, R. 2011. Dominant role of tectonic inheritance in supercontinent cycles. *Nature Geoscience,* 4, 184–187.

BAGAS, L. 1999. Early tectonic history of the Marymia Inlier and correlation with the Archaean Yilgarn Craton, Western Australia. *Australian Journal of Earth Sciences,* 46, 115–125.

BAGAS, L. 2004. Proterozoic evolution and tectonic setting of the northwest Paterson Orogen, Western Australia. *Precambrian Research,* 128, 475–496.

BAGAS, L. & SMITHIES, R. H. 1997. Palaeoproterozoic tectonic evolution of the Rudall Complex, and comparison with the Arunta Inlier and Capricorn Orogen. *Western Australia Geological Survey, Annual Review*, 100–115.

BARLEY, M.E., EISENLOHR, B.N., GROVES, D.I., PERRING, C.S. & VEARNCOMBE, J.R., 1989. Late Archean convergent margin tectonics and gold mineralization: A new look at the Norseman-Wiluna Belt, Western Australia. Geology, 17(9), pp.826-829.
BARLEY, M. E., BROWN, S. J. A., CASSIDY, K. F., CHAMPION, D. C., GARDOLL, S. J. & KRAPEŽ, B. 2003. An integrated geological and metallogenic framework for the eastern Yilgarn Craton: developing geodynamic models of highly mineralised Archaean granite–greenstone terranes. *Amira International Limited,* AMIRA Project P763.

BARLEY, M. E., BROWN, S. J. A., CASSIDY, K. F., CHAMPION, D. C., GARDOLL, S. J. & KRAPEŽ, B. 2003. An integrated geological and metallogenic framework for the eastern Yilgarn Craton: developing geodynamic models of highly mineralised Archaean granite–greenstone terranes. *Amira International Limited,* AMIRA Project P763.

BARNES, S. J., VAN KRANENDONK, M. J. & SONNTAG, I. 2012. Geochemistry and tectonic setting of basalts from the Eastern Goldfields Superterrane. *Australian Journal of Earth Sciences*, 59, 707–735.

BARNES, S.J. & VAN KRANENDONK, M.J., 2014. Archean andesites in the east Yilgarn craton, Australia: Products of plume-crust interaction? *Lithosphere*, 6, 80–92.

BELOUSOVA, E.A., KOSTITSYN, Y.A., GRIFFIN, W.L., BEGG, G.C., O'REILLY, S.Y. & PEARSON, N.J. 2010. The growth of the continental crust: constraints from zircon Hf-isotope data. *Lithos*, 119, 457–466.

BETTS, P. G. & GILES, D. 2006. The 1800–1100 Ma tectonic evolution of Australia. . *Precambrian Research,* 144, 92–125.

BETTS, P. G., GILES, D. & SCHAEFER, B. F., 2008. Comparing 1800–1600 Ma accretionary and basin processes in Australia and Laurentia: Possible geographic connections in Columbia. *Precambrian Research*, 166, 81–92.

BINDEMAN, I. 2008. Oxygen Isotopes in Mantle and Crustal Magmas as Revealed by Single Crystal Analysis. *Reviews in Mineralogy and Geochemistry,* 69, 445–478.

BLACK, L. P., KORSCH, R. J., FOUDOULIS, C., ALLEN, C. M., CAMPBELL, I. H., WILLIAMS, I. S., KAMO, S. L., DAVIS, D. W., ALEINIKOFF, J. N., VALLEY, J. W. & MUNDIL, R. 2004. Improved ^{206}Pb/^{238}U microprobe geochronology by the monitoring of a trace-element-related matrix effect; SHRIMP, ID-TIMS, ELA-ICP-MS and oxygen isotope documentation for a series of zircon standards. *Chemical Geology,* 205, 115–140.

BLAKE, T. S. & BARLEY, M. E. 1992. Tectonic evolution of the Late Archaean to Early Proterozoic Mount Bruce Megasequence Set, Western Australia. *Tectonics,* 11, 1415–1425.

BLEWETT, R. S. 2000. *Atlas of North Pilbara: Geology and Geophysics: 1: 1.5 Million Scale*, Australian Geological Survey Organisation.

BLICHERT-TOFT, J. 2008. The Hf isotopic composition of zircon reference material 91500. *Chemical Geology,* 253, 252–257.

BLICHERT-TOFT, J. & ALBARÈDE, F. 1997. The Lu-Hf isotope geochemistry of chondrites and the evolution of the mantle-crust system. *Earth and Planetary Science Letters,* 148, 243–258.

BODORKOS, S., LOVE, G. J., NELSON, D. R. & WINGATE, M. T. D. 2006a. 88415: porphyritic granodiorite dyke, Nurunah Hill; Geochronology dataset 613, in Compilation of geochronology data, June 2006 update. *Western Australia Geological Survey*.

BODORKOS, S., LOVE, G. J., NELSON, D. R. & WINGATE, M. T. D. 2006b. 178747: metamorphosed feldspathic sandstone, North East Bore; Geochronology dataset 643, in Compilation of geochronology data, June 2006 update. *Western Australia Geological Survey*.

BODORKOS, S., LOVE, G. J. & WINGATE, M. T. D. 2006c. 88407: porphyritic monzogranite, Dunnise Well; Geochronology dataset 607, in Compilation of geochronology data, June 2006 update. *Geological Survey of Western Australia*.

BODORKOS, S., LOVE, G. J. & WINGATE, M. T. D. 2006d. 88412: foliated porphyritic monzogranite, Bently Well; Geochronology dataset 611, in Compilation of geochronology data, June 2006 update. *Western Australia Geological Survey*.

BODORKOS, S., LOVE, G. J. & WINGATE, M. T. D. 2006e. 88419: porphyritic monzogranite, Hatches Soak; Geochronology dataset 614, in Compilation of geochronology data, June 2006 update. *Western Australia Geological Survey*.

BOEKHOUT, F., ROBERTS, N. M., GERDES, A. & SCHALTEGGER, U., 2015. A Hf-isotope perspective on continent formation in the south Peruvian Andes. *Geological Society, London, Special Publications*, 389, 305–321.

BROWN, M. 1994. The generation, segregation, ascent and emplacement of granite magma: the migmatite-to-crustally-derived granite connection in thickened orogens. *Earth Science Reviews,* 36, 83–130.

BROWN, M. 2013. Granite; from genesis to emplacement. *Geological Society of America Bulletin,* 125, 1079–1113.

CALIGNANO, E., SOKOUTIS, D., WILLINGSHOFER, E., GUEYDAN, F. & CLOETINGH, S. 2015. Asymmetric vs. symmetric deep lithospheric architecture of intra-plate continental orogens. *Earth and Planentary Science Letters,* 424, 38–50.

CAMPBELL, I. H. & HILL, R. I. 1988. A two-stage model for the formation of the granite-greenstone terrains of the Kalgoorlie-Norseman area, Western Australia. *Earth and Planetary Science Letters,* 90, 11–25.

CARVALHO, B.B., SAWYER, E.W., & JANASI, V.A., 2016. Crustal reworking in a shear zone: transformation of metagranite to migmatite. *Journal of Metamorphic Geology,* 34, 237–264.

CASSIDY, K. F., CHAMPION, D. C., MCNAUGHTON, N. J., FLETCHER, I. R., WHITAKER, A. J., BASTRAKOVA, I. V. & BUDD, A. R. 2002. Characterisation and metallongenic significance of Archaean granitoids of the Yilgarn Craton, Western Australia. *Minerals and Energy Research Institute of Western Australia (MERIWA),* Report 222, 514.

CASSIDY, K. F. & CHAMPION, D. C. 2004. Crustal evolution of the Yilgarn Craton from Nd isotopes and granite geochronology: implications for metallogeny. *SEG*, 317–320.

CASSIDY, K. F., CHAMPION, D. C. & HUSTON, D. L. 2005. Crustal evolution constraints on the metallogeny of the Yilgarn Craton. *In*: Mao J., Bierlein F. B. (eds.) Mineral Deposit Research: Meeting the Global Challenge: Proceedings of the Eighth Biennial SGA Meeting Beijing, China, 18–21 August 2005. Berlin, Heidelberg: Springer Berlin Heidelberg.

CASSIDY, K. F., CHAMPION, D. C., KRAPEŽ, B., BARLEY, M. E., BROWN, S. J. A., BLEWETT, R. S., GROENEWALD, P. B. & TYLER, I. M. 2006. A revised geological framework for the Yilgarn Craton, Western Australia. *Western Australia Geological Survey.*

CAVOSIE, A. J., VALLEY, J. W., WILDE, S. A. & E.I.M.F, S. A. 2005. Magmatic $\delta^{18}O$ in 4400–3900 Ma detrital zircons: A record of the alteration and recycling of crust in the Early Archean. *Earth and Planetary Science Letters,* 235, 663–681.

CAWOOD, P. A., KRÖNER, A., COLLINS, W. J., KUSKY, T. M., MOONEY, W. D. & WINDLEY, B. F. 2009. Accretionary orogens through Earth history. *Geological Society, London, Special Publications,* 318, 1–36.

CAWOOD, P. A. & TYLER, I. M. 2004. Assembling and reactivating the Proterozoic Capricorn Orogen; lithotectonic elements, orogenies, and significance. *Precambrian Research,* 128, 201–218.

CAWOOD, P. A., KRÖNER, A., COLLINS, W. J., KUSKY, T. M., MOONEY, W. D. & WINDLEY, B. F., 2009. Accretionary orogens through Earth history. *Geological Society, London, Special Publications*, 318, 1–36.

CAWOOD, P. A., STRACHAN, R. A., PISAREVSKY, S. A., GLADKOCHUB, D. P. AND MURPHY, J. B., 2016. Linking collisional and accretionary orogens during Rodinia assembly and breakup: Implications for models of supercontinent cycles. *Earth and Planetary Science Letters*, 449, 118–126.

CHAMPION, D. C. & CASSIDY, K. F. 2002. Granites of the Leonora-Laverton transect area, northeastern Yilgarn Craton. *Geoscience Australia, Record,* 2002/18.

CHAMPION, D. C. & CASSIDY, K. F. 2007. An overview of the Yilgarn Craton and its crustal evolution. *In:* In: Bierlein F. P. & Knox-Robinson C. M. (eds.) *Proceedings, Geoscience Australia*, Geoconferences (WA) Inc. Kalgoorlie '07, Kalgoorlie, Western Australia, 25 September 2007, Record 2007/14, 8–13.

CHAMPION, D. C. & SHERATON, J. W. 1997. Geochemistry and Nd isotope systematics of Archaean granites of the Eastern Goldfields, Yilgarn Craton, Australia: implications for crustal growth processes. *Precambrian Research,* 83, 109–132.

CHAPPELL, B. W. 1996. Magma Mixing and the Production of Compositional Variation within Granite Suites: Evidence from the Granites of Southeastern Australia. *Journal of Petrology,* 37, 449–470.

CHAPPELL, B. W. 2004. Towards a unified model for granite genesis. *Earth and Environmental Science Transactions of the Royal Society of Edinburgh,* 95, 1–10.

CHAPPELL, B. W. & WHITE, A. J. R. 1974. Two contrasting granite types. *Pacific geology,* 8, 173–174.

CHAUVEL, C., LEWIN, E., CARPENTIER, M., ARNDT, N. T. & MARINI, J.-C. 2008. Role of recycled oceanic basalt and sediment in generating the Hf–Nd mantle array. *Nature Geoscience,* 1, 64–67.

CHEN, S. F., RIGANTI, A., WYCHE, S., GREENFIELD, J. E. & NELSON, D. R. 2003. Lithostratigraphy and tectonic evolution of contrasting greenstone successions in the central Yilgarn Craton, Western Australia. *Precambrian Research,* 127, 249–266.

CHEN, R.-X., ZHENG, Y.-F. & XIE, L. W. 2010. Metamorphic growth and recrystallization of zircon: distinction by simultaneous in-situ analyses of trace elements, U–Th–Pb and Lu–Hf isotopes in zircons from eclogite-facies rocks in the Sulu orogen. *Lithos,* 114, 132–154.

CHEW, D. M., SYLVESTER, P. J. & TUBRETT, M. N. 2011. U– Pb and Th– Pb dating of apatite by LA-ICPMS. *Chemical Geology,* 280, 200–216.

COCHERIE, A. & ROBERT, M. 2008. Laser ablation coupled with ICP-MS applied to U–Pb zircon geochronology: A review of recent advances. *Gondwana Research,* 14, 597–608.

COLLINS, W. J. & SHAW, R. D. 1995. Geochronological constraints on orogenic events in the Arunta Inlier: a review. *Precambrian Research,* 71, 315–346.

COLLINS, W. J., BELOUSOVA, E. A., KEMP, A. I. & MURPHY, J. B., 2011. Two contrasting Phanerozoic orogenic systems revealed by hafnium isotope data. *Nature Geoscience*, 4, 333.

COMPSTON, W., WILLIAMS, I. S., CAMPBELL, I. H. & GRESHAM, J. J. 1986. Zircon xenocrysts from the Kambalda volcanics: age constraints and direct evidence for older continental crust below the Kambalda-Norseman greenstones. *Earth and Planetary Science Letters*, 76, 299–311.

CONDIE, K.C., BICKFORD, M.E., ASTER, R.C., BELOUSOVA, E. & SCHOLL, D.W. 2011. Episodic zircon ages, Hf isotopic composition, and the preservation rate of continental crust. *GSA Bulletin*, 123, 951–957.

COTTLE, J. M., KYLANDER-CLARK, A. R. & VRIJMOED, J. C. 2012. U–Th/Pb geochronology of detrital zircon and monazite by single shot laser ablation inductively coupled plasma mass spectrometry (SS-LA-ICPMS). *Chemical Geology,* 332-333, 136–147.

COUZINIÉ, S., LAURENT, O., MOYEN, J-F., ZEH, A., BOUILHOL, P & VILLAROS, A. 2016. Post collisional magmatism: crustal growth not identified by zircon Hf–O isotopes. *Earth and Planetary Science Letters,* 456, 182-195.

CURRIE, C. A., BEAUMONT, C. & HUISMANS, R. S. 2007. The fate of subducted sediments: a case for backarc intrusion and underplating. *Geology*, 35, 1111-1114.

CUTTEN, H. N., JOHNSON, S. P., THORNE, A. M., WINGATE, M. T. D., KIRKLAND, C. L., BELOUSOVA, E. A., BLAY, O. A. & ZWINGMANN, H. 2016. Deposition, provenance, inversion history and mineralization of the Proterozoic Edmund and Collier Basins, Capricorn Orogen. *Geological Survey of Western Australia,* Report 127, 74.

CZARNOTA, K., CHAMPION, D. C., GOSCOMBE, B., BLEWETT, R. S., CASSIDY, K. F., HENSON, P. A. & GROENEWALD, P. B. 2010. Geodynamics of the eastern Yilgarn Craton. *Precambrian Research,* 183, 175–202.

DAVIES, J. H. & VON BLANCKENBURG, F. 1995. Slab breakoff: a model of lithosphere detachment and its test in the magmatism and deformation of collisional orogens. *Earth and Planetary Science Letters,* 129, 85–102.

DENTITH, M., JOHNSON, S. P., EVANS, S., AITKEN, A., JOLY, A., THIEL, S. & TYLER, I. M. 2014. A magnetotelluric traverse across the eastern part of the Capricorn Orogen. *Geological Survey of Western Australia,* Report 135, 49.

DEVÈS, M.H., TAIT, S.R., KING, G.C. & GRANDIN, R. 2014. Strain heating in process zones; implications for metamorphism and partial melting in the lithosphere. *Earth and Planetary Science Letters*, 394, 216–228.

DIENER, J.F., WHITE, R.W. & HUDSON T.J. 2014. Melt production, redistribution and accumulation in mid-crustal source rocks, with implications for crustal-scale melt transfer. *Lithos*, 200, 212–225.

DHUIME, B., HAWKESWORTH, C. AND CAWOOD, P., 2011. When continents formed. *Science*, 331, 54–155.

DHUIME, B., HAWKESWORTH, C.J., CAWOOD, P.A. & STOREY, C.D., 2012. A change in the geodynamics of continental growth 3 billion years ago. *Science*, 335, 1334–1336.

D'LEMOS, R. S., BROWN, M. & STRACHAN, R. A. 1992. Granite magma generation, ascent and emplacement within a transpressional orogen. *Journal of the Geological Society,* 149, 487–490.

DRUMMOND, B. J., GOLEBY, B. R. & SWAGER, C. P. 2000. Crustal signature of Late Archaean tectonic episodes in the Yilgarn craton, Western Australia: evidence from deep seismic sounding. *Tectonophysics,* 329, 193–221.

EGGINS, S. M., KINSLEY, L. P. J. & SHELLEY, J. M. G. 1998. Deposition and element fractionation processes during atmospheric pressure laser sampling for analysis by ICP-MS. *Applied Surface Science,* 129, 278–286.

ELKINS-TANTON, L.T., 2007. Continental magmatism, volatile recycling, and a heterogeneous mantle caused by lithospheric gravitational instabilities. *Journal of Geophysical Research: Solid Earth,* 112(B3).

EVANS, D. A. D., SIRCOMBE, K. N., WINGATE, M. T. D., DOYLE, M., MCCARTHY, M., PIDGEON, R. T. & VAN NIEKERK, H. S. 2003. Revised geochronology of magmatism in the western Capricorn Orogen at 1805–1785 Ma: diachroneity of the Pilbara–Yilgarn collision. *Australian Journal of Earth Sciences*, 50, 853–864.

FERRÉ, E. C., GALLAND, O., MONTANARI, D. & KALAKAY, T. J., 2012. Granite magma migration and emplacement along thrusts. *International Journal of Earth Sciences,* 101, 1673-1688.

FISHER, C. M., VERVOORT, J. D. & HANCHAR, J. M. 2014. Guidelines for reporting zircon Hf isotopic data by LA-MC-ICPMS and potential pitfalls in the interpretation of these data. *Chemical Geology,* 363, 125–133.

FISHWICK, S. & READING, A. M. 2008. Anomalous lithosphere beneath the Proterozoic of western and central Australia: A record of continental collision and intraplate deformation? *Precambrian Research,* 166, 111–121

FLETCHER, I. R., WILLIAMS, S. J., GEE, R. D. & ROSMAN, K. J. R. 1983. Sm-Nd model ages across the margins of the Archaean Yilgarn Block, Western Australia; northwest transect into the proterozoic gascoyne province. *Journal of the Geological Society of Australia,* 30, 167–174.

FROST, B. R., BARNES, C. G., COLLINS, W. J., ARCULUS, R. J., ELLIS, D. J. & FROST, C. D. 2001. A Geochemical Classification for Granitic Rocks. *Journal of Petrology,* 42, 2033–2048.

FU, B., PAGE, F., CAVOSIE, A., FOURNELLE, J., KITA, N. T., LACKEY, J., WILDE, S. A. & VALLEY, J. 2008. Ti-in-zircon thermometry: applications and limitations. *Contributions to Mineralogy and Petrology,* 156, 197–215.

GARDINER, N. J., HICKMAN, A. H., KIRKLAND, C. L., LU, Y., JOHNSON, T. & ZHAO, J.-X. 2017. Processes of crust formation in the early Earth imaged through Hf isotopes from the East Pilbara Terrane. Precambrian Research, 297, 56–76.

GARDINER, N. J., MAIDMENT, D. W., KIRKLAND, C. L., BODORKOS, S., SMITHIES, R. H. AND JEON, H., 2018. Isotopic insight into the Proterozoic crustal evolution of the Rudall Province, Western Australia. *Precambrian Research*, 313, 31–50.

GAZLEY, M. F. 2011. *Metamorphism, geochronology and stratigraphy of an amphibolite-facies greenstone-hosted gold deposit: Plutonic Gold Mine, Marymia Inlier, Western Australia.* Doctoral dissertation. University of Wellington, New Zealand.

GAZLEY, M. F., VRY, J. K. & BOORMAN, J. C. 2011. P-T evolution in greenstone-belt mafic amphibolites: An example from plutonic gold mine, marymia inlier, western australia. *Journal of Metamorphic Geology,* 29, 685–697.

GEE, R. D. 1979. Structure and tectonic style of the Western Australian Shield. *Tectonophysics,* 58, 327–369.

GEE, R. D. 1987. Peak Hill, W.A. (2nd edition). *Geological Survey of Western Australia 1:250 000 Geological Series Explanatory Notes.*

GEHRELS, G. E., VALENCIA, V. A. & RUIZ, J. 2008. Enhanced precision, accuracy, efficiency, and spatial resolution of U-Pb ages by laser ablation–multicollector–inductively coupled plasma–mass spectrometry. *Geochemistry, Geophysics, Geosystems,* 9.

GERDES, A., WÖRNER, G. & HENK, A., 2000. Post-collisional granite generation and HT–LP metamorphism by radiogenic heating: the Variscan South Bohemian Batholith. *Journal of the Geological Society*, 157, 577–587.

GORCZYK, W., HOBBS, B., & GERYA, T. 2012. Initiation of Rayleigh-Taylor instabilities in intra-cratonic settings. *Tectonophysics,* 514–517, 146–155.

GORCZYK, W., HOBBS, B., GESSNER, K. & GERYA, T. 2013. Intracratonic geodynamics. *Gondwana Research,* 24, 838–848.

GORCZYK, W., & VOGT, K. 2015. Tectonics and melting in intra-continental settings. *Gondwana Research,* 27, 196–208.

GRIFFIN, W. L., PEARSON, N. J., BELOUSOVA, E. A., JACKSON, S. E., VAN ACHTERBERGH, E., O'REILLY, S. Y. & SHEE, S. R. 2000. The Hf isotope composition of cratonic mantle: LAM-MC-ICPMS analysis of zircon megacrysts in kimberlites. *Geochimica et Cosmochimica Acta,* 64, 133–147.

GRIFFIN, W. L., WANG, X., JACKSON, S. E., PEARSON, N. J., O'REILLY, S. Y., XU, X. & ZHOU, X. 2002. Zircon chemistry and magma mixing, SE China: in-situ analysis of Hf isotopes, Tonglu and Pingtan igneous complexes. *Lithos,* 61, 237–269.

GRIFFIN, W. L., BELOUSOVA, E. A., SHEE, S. R., PEARSON, N. J. & O'REILLY, S. Y. 2004. Archean crustal evolution in the northern Yilgarn Craton: U–Pb and Hf-isotope evidence from detrital zircons. *Precambrian Research,* 131, 231–282.

GRIMES, C. B., JOHN, B. E., KELEMEN, P. B., MAZDAB, F. K., WOODEN, J. L., CHEADLE, M. J., HANGHOJ, K. & SCHWARTZ, J. J. 2007. Trace element chemistry of zircons from oceanic crust; a method for distinguishing detrital zircon provenance. *Geology,* 35, 643–646.

GRIMES, C., WOODEN, J., CHEADLE, M. & JOHN, B. 2015. "Fingerprinting" tectono-magmatic provenance using trace elements in igneous zircon. *Contributions to Mineralogy and Petrology,* 170, 1–26.

GROVES, D. I. & BIERLEIN, F. P. 2007. Geodynamic settings of mineral deposit systems. *Journal of the Geological Society,* 164, 19–30.

GSWA. 2016. *Interactive geological map (GeoVIEW.WA),* Geological Survey of Western Australia, accessed 20 June 2017, <https://geoview.dmp.wa.gov.au/GeoViews/?Viewer=GeoVIEW>.

HANCHAR, J. M. & MILLER, C. F. 1993. Zircon zonation patterns as revealed by cathodoluminescence and backscattered electron images: Implications for interpretation of complex crustal histories. *Chemical Geology,* 3, 37–42.

HANCHAR, J. M. & VAN WESTRENEN, W. 2007. Rare earth element behavior in zircon-melt systems. *Elements,* 110, 1–13.

HAND, M. & SANDIFORD, M. 1999. Intraplate deformation in central Australia, the link between subsidence and fault reactivation. *Tectonophysics,* 305, 121–140.

HAND, M. & BUICK, I. S. 2001. Polymetamorphism and reworking of the Reynolds and Anmatjira Ranges, central Australia. *In:* Miller, J. A., Holdsworth, R. E., Buick, I. S & Hand, M (ed.) *Continental Reactivation and Reworking.* Geological Society, London, Special Publications.

HARLEY, S. L. & KELLY, N. M. 2007. Zircon: Tiny but timely. *Elements,* 3, 13–18.

HARRISON, T. M., AIKMAN, A. B. & WATSON, E. B. 2007. Temperature spectra of zircon crystallization in plutonic rocks. *Geology,* 35, 635–638.

HAWKESWORTH, C. J. & KEMP, A. I. S. 2006. Evolution of the continental crust. *Nature,* 443, 811.

HAWKESWORTH, C. J. & KEMP, A. I. S. 2006a. Using hafnium and oxygen isotopes in zircons to unravel the record of crustal evolution. *Chemical Geology*, 226, 144–162.

HICKMAN, A. H. 2004. Two contrasting granite–greenstone terranes in the Pilbara Craton, Australia: evidence for vertical and horizontal tectonic regimes prior to 2900 Ma. *Precambrian Research,* 131, 153–172.

HICKMAN, A. H. 2012. Review of the Pilbara Craton and Fortescue Basin, Western Australia: Crustal evolution providing environments for early life. *Island Arc,* 21, 1–31.

HICKMAN, A. H., SMITHIES, R. H. & TYLER, I. M. 2010. Evolution of active plate margins: West Pilbara Superterrane, De Grey Superbasin, and the Fortescue and Hamersley Basins — a field guide. *Geological Survey of Western Australia,* Record 2010/3, 74.

HORSTWOOD, M. S. A., KOŠLER, J., GEHRELS, G., JACKSON, S. E., MCLEAN, N. M., PEARSON, N. J., SIRCOMBE, K., SYLVESTER, P., VERMEESCH, P., BOWRING, J. F., CONDON, D. J. & SCHOENE, B. 2016. Community-derived standards for LA-ICP-MS U-Th-Pb geochronology - uncertainty propagation, age interpretation and data reporting. *Geostandards and Geoanalytical Research*, 40, 311-332.

HOSKIN, P. W. O. & BLACK, L. P. 2000. Metamorphic zircon formation by solid-state recrystallization of protolith igneous zircon. *Journal of Metamorphic Geology,* 18, 423–439.

HOSKIN, P. W. O. & IRELAND, T. R. 2000. Rare earth element chemistry of zircon and its use as a provenance indicator. *Geology,* 28, 627–630.

HOSKIN, P. W. O. & SCHALTEGGER, U. 2003. The composition of Zircon and Igneous and Metamorphic Petrogenesis. *In:* Hanchar, J.M. & Hoskin, P.W.O (eds.) Zircon. Washington, DC: Reviews in Mineralogy and Geochemistry.

HUPPERT, H. E. & SPARKS, S. J. 1988. The generation of granitic magmas by intrusion of basalt into continental crust. *Journal of Petrology,* 29, 599–624.

HUSTON, D. L., BLEWETT, R. S. & CHAMPION, D. C., 2012. Australia through time: a summary of its tectonic and metallogenic evolution. *Episodes*, 35, 23–43.

IRELAND, T. R. & WILLIAMS, I. S. 2003. Considerations in zircon geochronology by SIMS. *In:* Hanchar, J.M., Hoskin, P.W.O (ed.) *Zircon.* Washington, DC: Reviews in Mineralogy and Geochemistry.

IVANIC, T. J., VAN KRANENDONK, M. J., KIRKLAND, C. L., WYCHE, S., WINGATE, M. T. D. & BELOUSOVA, E. A. 2012. Zircon Lu–Hf isotopes and granite geochemistry of the Murchison Domain of the Yilgarn Craton: Evidence for reworking of Eoarchean crust during Meso-Neoarchean plume-driven magmatism. *Lithos,* 148, 112–127.

JACKSON, S. E., PEARSON, N. J., GRIFFIN, W. L. & BELOUSOVA, E. A. 2004. The application of laser ablation-inductively coupled plasma-mass spectrometry to in situ U–Pb zircon geochronology. *Chemical Geology,* 211, 47–69.

JAFFEY, A. H., FLYNN, K. F., GLENDENIN, L. E., BENTLEY, W. C. & ESSLING, A. M. 1971. Precision measurement of half-lives and specific activities of U 235 and U 238. *Physical Review C,* 4, 1889.

JOHNSON, S. P., SHEPPARD, S., RASMUSSEN, B., WINGATE, M. T. D., KIRKLAND, C. L., MUHLING, J. R., FLETCHER, I. R. & BELOUSOVA, E. A. 2010. The Glenburgh Orogeny as a record of Paleoproterozoic continent–continent collision. *Geological Survey of Western Australia,* Record 2010/5, 54.

JOHNSON, S. P., SHEPPARD, S., RASMUSSEN, B., WINGATE, M. T. D., KIRKLAND, C. L., MUHLING, J. R., FLETCHER, I. R. & BELOUSOVA, E. A. 2011a. Two collisions, two sutures: Punctuated pre-1950 Ma assembly of the West Australian Craton during the Ophthalmian and Glenburgh Orogenies. *Precambrian Research,* 189, 239–262.

JOHNSON, S. P., SHEPPARD, S., WINGATE, M. T. D., KIRKLAND, C. L. & BELOUSOVA, E. A. 2011b. Temporal and hafnium isotopic evolution of the Glenburgh Terrane basement: an exotic crustal fragment in the Capricorn Orogen. *Geological Survey of Western Australia,* Report 110, 27.

JOHNSON, S. P., THORNE, A. M. & TYLER, I. M. 2011c. Capricorn Orogen seismic and magnetotelluric (MT) workshop 2011: extended abstracts. *Geological Survey of Western Australia,* Record 2011/25, 120.

JOHNSON, S. P., THORNE, A. M., TYLER, I. M., KORSCH, R. J., KENNETT, B. N., CUTTEN, H. N., GOODWIN, J., BLAY, O., BLEWETT, R. S., JOLY, A., DENTITH, M. C., AITKEN, A. A., HOLZSCHUH, J., SALMON, M., READING, A., HEINSON, G., BOREN, G., ROSS, J., COSTELLOE, R. D. & FOMIN, T. 2013. Crustal architecture of the Capricorn Orogen, Western Australia and associated metallogeny. *Australian Journal of Earth Sciences,* 60.

JOHNSON, S. P., KORHONEN, R. J., KIRKLAND, C. L., CLIFF, J. B., BELOUSOVA, E. A. & SHEPPARD, S. 2017a. An isotopic perspective on growth and differentiation of Proterozoic orogenic crust: From subduction magmatism to cratonization. *Lithos,* 268-271, 76–86.

JOHNSON, T. E., BROWN, M., GARDINER, N. J., KIRKLAND, C. L. & SMITHIES, R. H. 2017b. Earth's first stable continents did not form by subduction. *Nature,* 543.

JOHNSON, S. P., KORHONEN, F. J., KIRKLAND, C. L., CLIFF, J. A., BELOUSOVA, E. A. & SHEPPARD, S. 2017c. Crustal differentiation in the Proterozoic Capricorn Orogen. *Geological Survey of Western Australia,* Report 168, 22.

JOHNSTON, S., GEHRELS, G., VALENCIA, V. & RUIZ, J. 2009. Small-volume U–Pb zircon geochronology by laser ablation-multicollector-ICP-MS. *Chemical Geology,* 259, 218–229.

KEMP, A. I. S. & HAWKESWORTH, C. J. 2004. Granites and differentiation of the continental crust. *Geochimica et Cosmochimica Acta,* 68, A667–A667.

KEMP, A. I. S., HAWKESWORTH, C. J., PATERSON, B. A. & KINNY, P. D. 2006. Episodic growth of the Gondwana supercontinent from hafnium and oxygen isotopes in zircon. *Nature,* 439, 580.

KEMP, A. I. S., HAWKESWORTH, C. J., FOSTER, G. L., PATERSON, B. A., WOODHEAD, J. D., HERGT, J. M., GRAY, C. M. & WHITEHOUSE, M. J. 2007. Magmatic and crustal differentiation history of granitic rocks from Hf-O isotopes in zircon. *Science* 315, 980.

KEMP, A. I. S., HAWKESWORTH, C. J., COLLINS, W. J., GRAY, C. M. & BLEVIN, P.L., 2009. Isotopic evidence for rapid continental growth in an extensional accretionary orogen: The Tasmanides, eastern Australia. *Earth and Planetary Science Letters*, 284, 455–466.

KEMP, A. I. S., WILDE, S. A., HAWKESWORTH, C. J., COATH, C. D., NEMCHIN, A., PIDGEON, R. T., VERVOORT, J. D. & DUFRANE, S.A., 2010. Hadean crustal evolution revisited: new constraints from Pb–Hf isotope systematics of the Jack Hills zircons. *Earth and Planetary Science Letters*, 296, 45–56.

KEMP, A. I. S., HICKMAN, A. H., KIRKLAND, C. L. & VERVOORT, J. D. 2015. Hf isotopes in detrital and inherited zircons of the Pilbara Craton provide no evidence for Hadean continents. *Precambrian Research,* 261, 112–126.

KENNETT, B. L. N. & IAFFALDANO, G. 2013. Role of lithosphere in intra-continental deformation: Central Australia. *Gondwana Research,* 24, 958–968.

KINNY, P. D. & NUTMAN, A. P. 1996. Zirconology of the Meeberrie gneiss, Yilgarn Craton, Western Australia: an early Archaean migmatite. *Precambrian Research,* 78, 165–178.

KINNY, P. D., WILLIAMS, I. S., FROUDE, D. O., IRELAND, T. R. & COMPSTON, W. 1988. Early archaean zircon ages from orthogneisses and anorthosites at Mount Narryer, Western Australia. *Precambrian Research,* 38, 325–341.

KINNY, P. D. & MAAS, R., 2003. Lu–Hf and Sm–Nd isotope systems in zircon. *In:* Hanchar, J.M. & Hoskin, P.W.O (eds.) Zircon. Washington, DC: Reviews in Mineralogy and Geochemistry.

KINNY, P. D., NUTMAN, A. P. & OCCHIPINTI, S. A. 2004. Reconnaissance dating of events recorded in the southern part of the Capricorn Orogen. *Precambrian Researc*h, 128, 279–294.

KIRKLAND, C. L., WINGATE, M. T. D., BODORKOS, S., SHEPPARD, S. & FARRELL, T. R. 2009. 183212: granitic gneiss, O'Malley Well; Geochronology Record 755. *Geological Survey of Western Australia*, 4.

KIRKLAND, C. L., WINGATE, M. T. D., BODORKOS, S. & FARRELL, T. R. 2009b. 180935: psammitic schist, Leake Spring; Geochronology Record 749. *Geological Survey of Western Australia*, 5.

KIRKLAND, C.L., JOHNSON, S.P., SMITHIES, R.H., HOLLIS, J.A., WINGATE, M.T.D., TYLER, I.M., HICKMAN, A.H., CLIFF, J.B., TESSALINA, S., BELOUSOVA, E.A. AND MURPHY, R.C., 2013. Not-so-suspect terrane: constraints on the crustal evolution of the rudall province. *Precambrian Research*, 235, 131–149.

KITA, N.T., USHIKUBO, T., FU, B. & VALLEY, J.W., 2009. High precision SIMS oxygen isotope analysis and the effect of sample topography. *Chemical Geology*, 264, 43-57.

KORHONEN, F. J., JOHNSON, S. P., FLETCHER, I. R., RASMUSSEN, B., SHEPPARD, S., MUHLING, J. R., DUNKLEY, D. J., WINGATE, M. T. D., ROBERTS, M. P. & KIRKLAND, C. L. 2015. Pressure–temperature–time evolution of the Mutherbukin Tectonic Event, Capricorn Orogen. *Geological Survey of Western Australia,* Report 146, 6.

KORHONEN, F. J., JOHNSON, S. P., WINGATE, M. T. D., KIRKLAND, C. L., FLETCHER, I. R., DUNKLEY, D. J., ROBERTS, M. P., SHEPPARD, S., MUHLING, J. R. & RASMUSSEN, B. 2017. Radiogenic heating and craton-margin plate stresses as drivers for intraplate orogeny. *Journal of Metamorphic Geology,* 35, 631–661.

KORSCH, R. J., JOH., TYLER, I. M., THORNE, A. M., BLEWETT, R. S., CUTTEN, H. N., JOLY, A., DENTITH, M. C., AITKEN, A. R. A., GOODIN, J. A. & KENNETT, B. L. N. 2011. Geodynamic implications of the Capricorn deep seismic survey: from the Pilbara Craton to the Yilgarn Craton. *In:* Johnson, S. P., Thorne, A.M. & Tyler, I.M (ed.) *Capricorn Orogen seismic and magnetotelluric (MT) workshop 2011: extended abstracts.* Geological Survey of Western Australia, Record 2011/25.

KOSITCIN, N., BROWN, S. J. A., BARLEY, M. E., KRAPEŽ, B., CASSIDY, K. F. & CHAMPION, D. C. 2008. SHRIMP U-Pb zircon age constraints on the Late Archaean tectonostratigraphic architecture of the Eastern Goldfields Superterrane, Yilgarn Craton, Western Australia. *Precambrian Research,* 161, 5–33.

KRAPEŽ, B. 1997. Sequence-stratigraphic concepts applied to the identification of depositional basins and global tectonic cycles. *Australian Journal of Earth Sciences*, 44, 1–36.

KRAPEŽ, B. 1999. Stratigraphic record of an Atlantic-type global tectonic cycle in the Palaeoproterozoic Ashburton Province of Western Australia. *Australian Journal of Earth Sciences*, 46, 71–87.

KRAPEŽ, B. & MARTIN, D. M. 1999. Sequence stratigraphy of the Palaeoproterozoic Nabberu Province of Western Australia. *Australian Journal of Earth Sciences,* 46, 89–103.

KRAPEŽ, B. & MCNAUGHTON, N. J. 1999. SHRIMP zircon U–Pb age and tectonic significance of the Palaeoproterozoic Boolaloo Granodiorite in the Ashburton Province, Western Australia. *Australian Journal of Earth Sciences,* 46, 283–287.

KYLANDER-CLARK, A. R. C., HACKER, B. R. & COTTLE, J. M. 2013. Laser ablation split stream ICP petrochronology. *Chemical Geology,* 345, 99–112.

LACKEY, J. S., VALLEY, J. W. & SALEEBY, J. B. 2005. Supracrustal input to magmas in the deep crust of Sierra Nevada batholith: evidence from high-$\delta^{18}O$ zircon. *Earth and Planetary Science Letters*, 235, 315-330.

LELOUP, P. H., RICARD, Y., BATTAGLIA, J. & LACASSIN, R. 1999. Shear heating in continental strike-slip shear zones: model and field examples. *Geophysical Journal International*, 136, 19–40.

LI, Z. X. 2000. Palaeomagnetic evidence for unification of the North and West Australian cratons by ca. 1.7 Ga: new results from the Kimberley Basin of northwestern Australia. *Geophysical Journal International,* 142, 173-180.

LI, X-H., LONG, W-G., LI, Q. L., LIU, Y., ZHENG, Y-F., YANG, Y-H., CHAMBERLAIN, K. R., WAN, D-F., GUO, C-H., WANG, C-C. & TAO, H. 2010. Penglai Zircon Megacrysts: A Potential New Working Reference Material for Microbeam Determination of Hf–O Isotopes and U–Pb Age. *Geostandards and Geoanalytical Research,* 34, 117–134.

LI, S., CHUNG, S. L., WILDE, S. A., WANG, T., XIAO, W. J. & GUO, Q.Q., 2016. Linking magmatism with collision in an accretionary orogen. *Scientific reports*, 6, 25751.

LIBBY, W. G., DE LAETER, J. R. & MYERS, J. S. 1986. Geochronology of the Gascoyne Complex. *Geological Survey of Western Australia.*

LU, Y. J., LOURCKS, R. R., FIORENTINI, M. L., MCCUAIG, T. C., EVANS, N. J., YANG, Z. M., HOU, Z. Q., KIRKLAND, C. L., PARRA-AVILA, L. A. & KOBUSSEN, A. 2016. Zircon compositions as a pathfinder for porphyry Cu ± Mo ± Au deposits. *Society of Economic Geologists Special Publication,* 19, 329–347.

LU, Y., WINGATE, M. T. D., BLAY, O. & THORNE, A. M. 2017. 216142: granite gneiss, Lawson Well; Geochronology Record 1430. *Geological Survey of Western Australia*, 4.

LUDWIG, K. R. 2012. User's Manual for Isoplot/Ex, v.3.75, A Geochronological Toolkit for Microsoft Excel. *Berkeley Geochronological Center Special Publications, 5.*

MAIDMENT, D. W. 2017, Geochronology of the Rudall Province, Western Australia: implications for the amalgamation of the West and North Australian Cratons: *Geological Survey of Western Australia,* Report 161, 95.

MARTIN, D. M. 1994. *Sedimentology, sequence stratigraphy, and tectonic setting of a Palaeoproterozoic turbidite complex, Lower Padbury Group, Western Australia.* Doctoral dissertation, University of Western Australia, Perth.

MARTIN, D. M. 1998. Lithostratigraphy and structure of the Palaeoproterozoic lower Padbury Group, Milgun 1:100 000 sheet, Western Australia. *Western Australia Geological Survey,* Report 62, 58.

MARTIN, D. M., POWELL, C. M. & GEORGE, A. D. 2000. Stratigraphic architecture and evolution of the early Paleoproterozoic McGrath Trough, Western Australia. *Precambrian Research,* 99, 33–64.

MARTIN, D. M. & THORNE, A. M. 2004. Tectonic setting and basin evolution of the Bangemall Supergroup in the northwestern Capricorn Orogen. *Precambrian Research,* 128, 385–409.

MARTIN, D. M. & MORRIS, P. A. 2010. Tectonic setting and regional implications of ca 2.2 Ga mafic magmatism in the southern Hamersley Province, Western Australia. *Australian Journal of Earth Sciences,* 57, 911–931.

MARTIN, H. 1999. Adakitic magmas: modern analogues of Archaean granitoids. *Lithos,* 46, 411–429.

MATTINSON, J. M., GRAUBARD, C. M., PARKINSON, D. L. & MCCLELLAND, W. C. 1996. U-Pb Reverse Discordance in Zircons: The Role of Fine-Scale Oscillatory Zoning and Sub-Micron Transport of Pb. *In:* HART, A. B. A. S. (ed.) *Earth Processes: Reading the Isotopic Code.* Washington D.C.: American Geophysical Union.

MCCUAIG, T. C. & HRONSKY, J. 2014. The mineral systems concept: the key to exploration targeting. *Applied Earth Science,* 126, 77–78.

MCCULLOCH, M. T. & COMPSTON, W. 1981. Sm–Nd age of Kambalda and Kanowna greenstones and heterogeneity in the Archaean mantle. *Nature,* 294, 322-327.

MCCULLOCH, M. T., COMPSTON, W. & FROUDE, D. 1983. Sm-Nd and Rb-Sr dating of Archaean gneisses, eastern Yilgarn Block, Western Australia. *Journal of the Geological Society of Australia,* 30, 149–153.

MCLENNAN, S. M. 1988. Recycling of the continental crust. *pure and applied geophysics,* 128, 683–724.

MEINHOLD, G. 2010. Rutile and its applications in earth sciences. *Earth-Science Reviews,* 102, 1–28.

MILLER, C. F., MCDOWELL, S. M. & MAPES, R. W. 2003. Hot and cold granites? Implications of zircon saturation temperatures and preservation of inheritance. *Geology* 31, 529–532.

MOLE, D. R. 2012. *Evaluating the Lithospheric Architecture of the Yilgarn Craton in Space and Time: Implications for Komatiite Volcanism and Earth Evolution* Doctoral dissertation, University of Western Australia.

MOLE, D. R., FIORENTINI, M. L., CASSIDY, K. F., KIRKLAND, C. L., THEBAUD, N., MCCUAIG, T. C., DOUBLIER, M. P., DUURING, P., ROMANO, S. S. & MAAS, R. 2013. Crustal evolution, intra-cratonic architecture and the metallogeny of an Archaean craton. *Geological Society, London, Special Publications,* 393.

MOLE, D. R., FIORENTINI, M. L., THEBAUD, N., CASSIDY, K. F., MCCUAIG, T. C., KIRKLAND, C. L., ROMANO, S. S., DOUBLIER, M. P., BELOUSOVA, E. A., BARNES, S. J. & MILLER, J. S. 2014. Archean komatiite volcanism controlled by the evolution of early continents. *Proceedings of the National Academy of Sciences of the United States of America,* 111, 10083.

MOLE, D. R., FIORENTINI, M. L., THEBAUD, N., MCCUAIG, T. C., CASSIDY, K. F., BARNES, S. J., BELOUSOVA, E. A., MUDROVSKA, I. & DOUBLIER, M. P. 2010. Lithospheric controls on the localization of komatiite-hosted nickel-sulfide deposits. *Fifth International Archean Symposium Abstracts: Geological Survey of Western Australia, Record,* 18, 101–103.

MOLE, D. R., FIORENTINI, M. L., THEBAUD, N., MCCUAIG, T. C., CASSIDY, K. F., KIRKLAND, C. L., WINGATE, M. T. D., ROMANO, S. S., DOUBLIER, M. P. & BELOUSOVA, E. A. 2012. Spatio-temporal constraints on lithospheric development in the southwest–central Yilgarn Craton, Western Australia. *An International Geoscience Journal of the Geological Society of Australia,* 59, 625–656.

MOREL, M. L. A., NEBEL, O., NEBEL-JACOBSEN, Y. J., MILLER, J. S. & VROON, P. Z. 2008. Hafnium isotope characterization of the GJ-1 zircon reference material by solution and laser-ablation MC-ICPMS. *Chemical Geology,* 255, 231–235.

MUHLING, J. R. 1988. The nature of Proterozoic reworking of early Archaean gneisses, Mukalo Creek Area, Southern Gascoyne Province, Western Australia. *Precambrian Research,* 40, 341–362.

MÜLLER, S., KRAPEZ, B., BARLEY, M. E. & FLETCHER, I. R. 2005. Giant iron-ore deposits of the Hamersley province related to the breakup of Paleoproterozoic Australia: New insights from in situ SHRIMP dating of baddeleyite from mafic intrusions. *Geology,* 33, 577–580.

MYERS, J. S. 1990. Precambrian tectonic evolution of part of Gondwana, southwestern Australia. *Geology,* 18, 537-540.

MYERS, J. S. 1993. Precambrian history of the West Australian Craton and adjacent orogens. *Annual Review of Earth and Planetary Sciences,* 21, 453–485.

MYERS, J. S. 1995. The generation and assembly of an Archaean supercontinent: evidence from the Yilgarn craton, Western Australia. *Geological Society, London, Special Publications,* 95, 143–154.

MYERS, J. S. 1997. Geology of granite. *Journal of the Royal Society of Western Australia,* 80, 87–100.

NABELEK, P. I. & LIU, M., 2004. Petrologic and thermal constraints on the origin of leucogranites in collisional orogens. *Earth and Environmental Science Transactions of the Royal Society of Edinburgh*, 95, 73–85.

NABELEK, P. I., WHITTINGTON, A. G. & HOFMEISTER, A. M., 2010. Strain heating as a mechanism for partial melting and ultrahigh temperature metamorphism in convergent orogens: Implications of temperature-dependent thermal diffusivity and rheology. J*ournal of Geophysical Research: Solid Earth*, 115(B12).

NÆRAA, T., SCHERSTÉN, A., ROSING, M. T., KEMP, A. I. S., HOFFMANN, J. E., KOKFELT, T. F. & WHITEHOUSE, M. J., 2012. Hafnium isotope evidence for a transition in the dynamics of continental growth 3.2 Gyr ago. *Nature*, 485, 627.

NASDALA, L., ZHANG, M., KEMPE, U., PANCZER, G., GAFT, M., ANDRUT, M. & PLÖTZE, M. 2003. Spectroscopic methods applied to zircon. *In:* Hanchar, J.M., Hoskin, P.W.O (ed.) *Zircon.* Washington, DC: Reviews in Mineralogy and Geochemistry.

NEBEL-JACOBSEN, Y., MÜNKER, C., NEBEL, O., GERDES, A., MEZGER, K. & NELSON, D. R. 2010. Reworking of Earth's first crust: Constraints from Hf isotopes in Archean zircons from Mt. Narryer, Australia. *Precambrian Research,* 182, 175–186.

NEBEL, O., CAPITANIO, F. A., MOYEN, J-F,. WEINBERG , R. F., CLOS, F,. NEBEL-JACOBSEN, Y. J., CAWOOD , P. A. 2018. When crust comes of age: on the chemical evolution of Archaean, felsic continental crust by crustal drip tectonics. *Philosophical Transactions of the Royal Society A: Mathematical, Physical and Engineering Sciences.* 376. 20180103

NELSON, D. R. 1995. 112107: granodiorite, Jillawarra Sub-basin; in Compilation of SHRIMP U–Pb zircon geochronology data, 1994. *Western Australia Geological Survey,* Record 1995/3, 9–11.

NELSON, D. R. 1995a. 112379: biotite monzogranite (augen) gneiss, Split Rock; in Compilation of SHRIMP U–Pb zircon geochronology data, 1994. *Western Australia Geological Survey,* Record 1995/3, 195–198.

NELSON, D. R. 1995b. 112310: granodiorite gneiss, Dunn Creek west; in Compilation of SHRIMP U–Pb zircon geochronology data, 1994. *Western Australia Geological Survey,* Record 1995/3, 2.

NELSON, D. R. 1997a. 118957: coarse-grained augen gneiss, Peak Hill ruins; in Compilation of SHRIMP U–Pb zircon geochronology data, 1996. *Western Australia Geological Survey,* Record 1997/2, 94–97.

NELSON, D. R. 1997b. 118963: porphyritic syenogranite, Goodin Dome; in Complication of SHRIMP U–Pb zircon geochonology data, 1996. *Western Australia Geological Survey,* Record 1997/2, 90–93.

NELSON, D. R. 1998a. 142847: granite gneiss, Stevies Well; in Compilation of SHRIMP U–Pb zircon geochronology data, 1997. *Western Australia Geological Survey,* Record 1998/2, 172–175.

NELSON, D. R. 1998b. 142856: monzogranite, west of Round Yard Bore; in Compilation of SHRIMP U–Pb zircon geochronology data, 1997. *Western Australia Geological Survey,* Record 1998/2, 198–200.

NELSON, D. R. 1998c. 142896: leucocratic gneiss, Dingo Bore; in Compilation of SHRIMP U–Pb zircon geochronology data, 1997. *Western Australia Geological Survey,* Record 1998/2, 201–203.

NELSON, D. R. 1999a. 142848: foliated biotite monzogranite, Stevies Well; in Compilation of geochronology data, 1998. *Western Australia Geological Survey,* Record 1999/2, 17–20.

NELSON, D. R. 1999b. 142850: foliated monzogranite, Nanular Bore; in Compilation of geochronology data, 1998. *Western Australia Geological Survey,* Record 1992/2, 21–23.

NELSON, D. R. 1999c. 142912: foliated biotite monzogranite, Gidgee Bore; in Compilation of geochronology data, 1998. *Western Australia Geological Survey,* Record 1999/2, 40–43.

NELSON, D. R. 1999d. 142914: porphyritic biotite-hornblende monzogranite, Bullbadger Bore; in Compilation of geochronology data, 1998. *Western Australia Geological Survey,* Record 1999/2, 48–50.

NELSON, D. R. 1999e. 142924: biotite-muscovite granodiorite, Two Wells Well; in Compilation of geochronology data, 1998. *Western Australia Geological Survey,* Record 1999/2, 55–58.

NELSON, D. R. 1999f. 142925: biotite monzogranite, Challenger Well; in Compilation of geochronology data, 1998. *Western Australia Geological Survey,* Record 1999/2, 59–62.

NELSON, D. R. 1999g. 142927: foliated biotite-oligoclase granodiorite, Mulunka Well; in Compilation of geochronology data, 1998. *Western Australia Geological Survey,* Record 1999/2, 67–70.

NELSON, D. R. 1999h. 142930: coarse leucocratic pegmatite, Fred Well; in Compilation of geochronology data, 1998. *Western Australia Geological Survey,* Record 1999/2, 79–81.

NELSON, D. R. 1999i. 142903: foliated porphyritic biotite monzogranite, Bullaroo Hill; in Compilation of geochronology data, 1998. *Western Australia Geological Survey,* Record 1999/2, 24–27.

NELSON, D. R. 2000a. 139459: foliated porphyritic biotite monzogranite, Black Hills Bore; in Compilation of geochronology data, 1999. *Western Australia Geological Survey,* Record 2000/2, 18–21.

NELSON, D. R. 2000b. 159724: foliated biotite monzogranite, Geringee Bore; in Compilation of geochronology data, 1999. *Western Australia Geological Survey,* Record 2000/2, 42–45.

NELSON, D. R. 2000c. 159987: foliated porphyritic biotite granodiorite, Madonga Creek; in Compilation of geochronology data, 1999. *Western Australia Geological Survey,* Record 2000/2, 46–49.

NELSON, D. R. 2000d. 164309: foliated porphyritic biotite granodiorite, Middle Well; in Compilation of geochronology data, 1999. *Western Australia Geological Survey, Record,* 2000/2, 58–61.

NELSON, D. R. 2000e. Compilation of geochronology data, 1999. *Geological Survey of Western Australia,* Record 2001/2.

NELSON, D. R. 2001a. 168751: biotite monzogranite, Round Yard Bore; in Compilation of geochronology data, 2000. *Western Australia Geological Survey,* Record 2001/2, 21–23.

NELSON, D. R. 2001b. 168939: biotite monzogranite, Trickery Bore; in Compilation of geochronology data, 2000. *Western Australia Geological Survey,* Record 2001/2, 28–30.

NELSON, D. R. 2001c. 168947: biotite-muscovite monzogranite gneiss, Weedarrah Homestead; in Compilation of geochronology data, 2000. *Western Australia Geological Survey,* Record 2001/2, 49–51.

NELSON, D. R. 2001d. 168951: foliated biotite-muscovite monzogranite, Salt Well; in Compilation of geochronology data, 2000. *Western Australia Geological Survey,* Record 2001/2, 69–71.

NELSON, D. R. 2001e. Compliation of geochronology data, 2000. *Western Australia Geological Survey,* Record 2001/2, 205.

NELSON, D. R. 2002a. 169050: leucocratic gneiss, Mount Remarkable Bore; in Compilation of geochronology data, 2001. *Western Australia Geological Survey,* Record 2002/2, 28–30.

NELSON, D. R. 2002b. 169054: metatonalite, Fraser Prospect; in Compilation of geochronology data, 2001. *Geological Survey of Western Australia,* Record 2002/2, 39–42.

NELSON, D. R. 2004a. 169086: biotite monzogranite, Boora Boora Bore; Geochronology dataset 117; in Compilation of geochronology data, June 2006 update. *Western Australia Geological Survey*.

NELSON, D. R. 2004b. 169092: biotite-muscovite monzogranite, Red Rock Bore; Geochronology dataset 103; in Compilation of geochronology data, June 2006 update. *Western Australia Geological Survey*.

NELSON, D. R. 2004c. 178012: biotite tonalite gneiss, Quartz Hill; Geochronology dataset 96; in Compilation of geochronology data, June 2006 update. *Western Australia Geological Survey*.

NELSON, D. R. 2004d, 169091: metasandstone, Hogan Well; Geochronology dataset 120; in Compilation of geochronology data, June 2006 update: *Western Australia Geological Survey*.

NELSON, D. R. 2005a. 169060: porphyritic syenogranite, Yangibana Bore; in Compilation of geochronology data, 2001. *Western Australia Geological Survey,* Record 2002/2, 56-58.

NELSON, D. R. 2005b. 178024: biotite granodiorite, Minga Well; Geochronology dataset 533; in Compilation of geochronology data, June 2006 update. *Western Australia Geological Survey*.

NELSON, D. R. 2005c. 178026: muscovite-biotite syenogranite, Russell Well; Geochronology dataset 535; in Compilation of geochronology data, June 2006 update. *Western Australia Geological Survey*.

NELSON, D. R. 2005d. 178027: biotite-muscovite granodiorite, Mangaroon Homestead; Geochronology dataset 536; in Compilation of geochronology data, June 2006 update. *Western Australia Geological Survey*.

NELSON, D. R. 2005e. 178030: biotite granodiorite, Robinson Well; Geochronology dataset 539; in Compilation of geochronology data, June 2006 update. *Western Australia Geological Survey*.

NELSON, DR 2005f, 178014: biotite monzogranite, Quartz Hill; Geochronology Record 551: *Geological Survey of Western Australia*, 4p.

NELSON, DR 2005g, 178013: quartz diorite gneiss, Quartz Hill; Geochronology Record 550: *Geological Survey of Western Australia*, 4p.

NOWELL, G. M., KEMPTON, P. D., NOBLE, S. R., FITTON, J. G., SAUNDERS, A. D., MAHONEY, J. J. & TAYLOR, R. N. 1998. High precision Hf isotope measurements of MORB and OIB by thermal ionisation mass spectrometry: insights into the depleted mantle. *Chemical Geology,* 149, 211–233.

NUTMAN, A.P., 2006. Comment on "Zircon thermometer reveals minimum melting conditions on earliest Earth" II. *Science*, 311, 779b-779b.

NUTMAN, A. P., KINNY, P. D., COMPSTON, W. & WILLIAMS, I. S. 1991. SHRIMP U-Pb zircon geochronology of the Narryer Gneiss Complex, Western Australia. *Precambrian Research,* 52, 275–300.

NUTMAN, A. P., BENNETT, V., KINNY, P. D. & PRICE, R. 1993. Large-scale crustal structure of the Northwestern Yilgarn Craton, western Australia: Evidence from Nd isotopic data and zircon geochronology. *Tectonics,* 12, 971–981.

OCCHIPINTI, S. A., SHEPPARD, S., NELSON, D. R., MYERS, J. S. & TYLER, I. M. 1998. Syntectonic granite in the southern margin of the Palaeoproterozoic Capricorn Orogen, Western Australia. *Australian Journal of Earth Sciences,* 45, 509–512.

OCCHIPINTI, S. A. & SHEPPARD, S. 2000. Geology of the Glenburgh 1:100 000 sheet. *1:100 000 Geological Series Explanatory Notes.* Geological Survery of Western Australia.

OCCHIPINTI, S. A., SHEPPARD, S., MYERS, J. S., TYLER, I. M. & NELSON, D. R. 2001. Archaean and Palaeoproterozoic geology of the Narryer Terrane (Yilgarn Craton) and the southern Gascoyne Complex (Capricorn Orogen), Western Australia— a field guide. *Western Australia Geological Survey,* Record 2001/8, 70.

OCCHIPINTI, S. A., SHEPPARD, S., PASSCHIER, C., TYLER, I. M. & NELSON, D. R. 2004. Palaeoproterozoic crustal accretion and collision in the southern Capricorn Orogen: the Glenburgh Orogeny. *Precambrian Research,* 128, 237–255.

OCCHIPINTI, S. A. & REDDY, S. M. 2004. Deformation in a complex crustal-scale shear zone: Errabiddy Shear Zone, Western Australia. . *In:* Alsop G. I., Holdsworth, R. E., McCaffery, K. J. W. & Hand, M. (ed.) *Flow Processes in Faults and Shear Zones.* Geological Society, London, Special Publication.

OCCHIPINTI, S. A., HOCKING, R., LINDSAY, M. D., AITKEN, A., COPP, I., JONES, J., SHEPPARD, S., PIRAJNO, F. & METELKA, V. 2017. Paleoproterozoic basin development on the northern Yilgarn Craton, Western Australia. *Precambrian Research,* 300, 121–140.

OLIEROOK, H. K., MERLE, R. E. & JOURDAN, F., 2017. Toward a Greater Kerguelen large igneous province: Evolving mantle source contributions in and around the Indian Ocean. *Lithos*, 282, 163–172.

PATON, C., WOODHEAD, J. D., HELLSTROM, J. C., HERGT, J. M., GREIG, A. & MAAS, R. 2010. Improved laser ablation U-Pb zircon geochronology through robust downhole fractionation correction. *Geochemistry, Geophysics, Geosystems - G (super 3),* 11.

PATON, C., HELLSTROM, J. C., PAUL, B., WOODHEAD, J. D. & HERGT, J. M. 2011. Iolite: Freeware for the visualisation and processing of mass spectrometric data. *Journal of Analytical Atomic Spectrometry,* 26, 2508–2518.

PAWLEY, M. J., ROMANO, S. S., HALL, C. R., WYCHE, S. & WINGATE, M. T. D. 2009. The Yamarna Shear Zone: a new terrane boundary in the northeastern Yilgarn Craton. *Geological Survey of Western Australia,* Annual Review 2007/08, 26–32.

PAWLEY, M. J., WINGATE, M. T. D., KIRKLAND, C. L., WYCHE, S., HALL, C. E., ROMANO, S. S. & DOUBLIER, M. P. 2012. Adding pieces to the puzzle: episodic crustal growth and a new terrane in the northeast Yilgarn Craton, Western Australia. *Australian Journal of Earth Sciences,* 59, 603–623.

PAYNE, J. L., HAND, M., BAROVICH, K. M., REID, A. & EVANS, D. A. 2009. Correlations and reconstruction models for the 2500-1500 Ma evolution of the Mawson Continent. *Geological Society, London, Special Publications,* 323, 319–355.

PAYNE, J.L., MCINERNEY, D.J., BAROVICH, K.M., KIRKLAND, C.L., PEARSON, N.J. & HAND, M., 2016. Strengths and limitations of zircon Lu-Hf and O isotopes in modelling crustal growth. *Lithos*, 248, 175–192.

PEARCE, J. A. 1996. Sources and settings of granitic rocks. *Episodes,* 19, 120–125.

PEARCE, J. A., HARRIS, N. B. W. & TINDLE, A. G. 1984. Trace element discrimination diagrams for the tectonic interpretation of granitic rocks. *Journal of Petrology,* 25, 956–983.

PEARCE, J.A. & PEATE, D.W. 1995. Tectonic implications of the composition of volcanic arc magmas. *Annual Review of Earth and Planetary Sciences*, 23, 251-285.

PEARSON, D. M., MACLEOD, D. R., DUCEA, M. N., GEHRELS, G. E. & PATCHETT, J. P., 2017. Sediment underthrusting within a continental magmatic arc: Coast Mountains batholith, British Columbia. *Tectonics*, 36, 2022–2043.

PETFORD, N., CRUDEN, A. R., MCCAFFREY, K. J. W. & VIGNERESSE, J. L. 2000. Granite magma formation, transport and emplacement in the Earth's crust. *Nature,* 408, 669.

PIDGEON, R. T. & WILDE, S. A. 1990. The distribution of 3.0 Ga and 2.7 Ga volcanic episodes in the Yilgarn Craton of Western Australia. *Precambrian Research,* 48, 309–325.

PIECHOCKA, A. M., GREGORY, C. J., ZI, J.-W., SHEPPARD, S., WINGATE, M. T. D. & RASMUSSEN, B. 2017. Monazite trumps zircon: applying SHRIMP U–Pb geochronology to systematically evaluate emplacement ages of leucocratic, low-temperature granites in a complex Precambrian orogen. *Contributions to Mineralogy and Petrology,* 172, 63.

PIRAJNO, F. & OCCHIPINTI, S. A. 2000. Three Palaeoproterozoic basins—Yerrida, Bryah and Padbury—Capricorn Orogen, Western Australia. *Australian Journal of Earth Sciences,* 47, 675–688.

PIRAJNO, F., JONES, J. A., HOCKING, R. M. & HALILOVIC, J. 2004. Geology and tectonic evolution of Palaeoproterozoic basins of the eastern Capricorn Orogen, Western Australia. *Precambrian Research,* 128, 315–342.

PLANK, T. & LANGMUIR, C. H. 1998. The chemical composition of subducting sediment and its consequences for the crust and mantle. *Chemical Geology*, 145, 325-394.

POWELL, C. M., OLIVER, N. H. S., LI, Z.-X., MARTIN, D. M. & RONASZEKI, J. 1999. Synorogenic hydrothermal origin for giant Hamersley iron oxide ore bodies. *Geology,* 27, 175–178.

PYSKLYWEC, R.N. & BEAUMONT, C., 2004. Intraplate tectonics: feedback between radioactive thermal weakening and crustal deformation driven by mantle lithosphere instabilities. *Earth and Planetary Science Letters,* 221, 275–292.

RAIMONDO, T., HAND, M. & COLLINS, W. J. 2014. Compressional intracontinental orogens: Ancient and modern perspectives. *Earth-Science Reviews,* 130, 128–153.

RASMUSSEN, B., FLETCHER, I. R. & SHEPPARD, S. 2005. Isotopic dating of the migration of a low-grade metamorphic front during orogenesis. *Geology,* 33, 773–776.

REDDY, S. M. & OCCHIPINTI, S. A. 2004. High-strain zone deformation in the southern Capricorn Orogen, Western Australia: kinematics and age constraints. *Precambrian Research,* 128, 295–314.

REIMINK, J. R., CHACKO, T., STERN, R. A. & HEAMAN, L. M., 2016. The birth of a cratonic nucleus: lithogeochemical evolution of the 4.02–2.94 Ga Acasta Gneiss Complex. *Precambrian Research*, 281, 453–472.

REY, R. P., TEYSSIER, C. & WHITNEY, D. L. 2009. Extension rates, crustal melting, and core complex dynamics. *Geology,* 37, 391–394.

ROBERTS, N. M. W. 2010. *From crystal to crust: the Proterozoic crustal evolution of southwest Norway.* Doctoral Dissertation, University of Leicester.

ROBERTS, N. M., 2012. Increased loss of continental crust during supercontinent amalgamation. *Gondwana Research*, 21, 994–1000.

ROBERTS, N. M., SLAGSTAD, T., PARRISH, R. R., NORRY, M. J., MARKER, M. & HORSTWOOD, M. S. 2013. Sedimentary recycling in arc magmas: geochemical and U–Pb–Hf–O constraints on the Mesoproterozoic Suldal Arc, SW Norway. *Contributions to Mineralogy and Petrology*, 165, 507–523.

ROBERTS, N. M. W. & SPENCER, C. J. 2015. The zircon archive of continent formation through time. *Geological Society, London, Special Publications,* 389, 197–225.

RUBATTO, D. & HERMANN, J. 2007. Zircon Behaviour in Deeply Subducted Rocks. *Elements,* 3, 31-35.

RUDNICK, R. 1995. Making continental crust. *Nature,* 378, 571.

RUDNICK, R. L. & GAO, S. 2003. Composition of the continental crust. *Treatise on geochemistry,* 3, 659.

SALTERS, V. J. M. & STRACKE, A. 2004. Composition of the depleted mantle. *Geochemistry, Geophysics, Geosystems, 5.*

SANDIFORD, M. & MCLAREN, S., 2002. Tectonic feedback and the ordering of heat producing elements within the continental lithosphere. *Earth and Planetary Science Letters*, 204, 133–150.

SAWYER, E. W. 1996. Melt segregation and magma flow in migmatites: implications for the generation of granite magmas. *Geological Society of America Special Papers,* 315, 85–94.

SAWYER, E. W. 1998. Formation and Evolution of Granite Magmas During Crustal Reworking: the Significance of Diatexites. *Journal of Petrology,* 39, 1147–1167.

SCHALTEGGER, U., SCHMITT, A. K. & HORSTWOOD, M. S. A. 2015. U– Th– Pb zircon geochronology by ID- TIMS, SIMS, and laser ablation ICP-MS: Recipes, interpretations, and opportunities. *Chemical Geology,* 402, 89–110.

SCHERER, E., MÜNKER, C. &MEZGER, K., 2001. Calibration of the lutetium-hafnium clock. *Science*, 293, 683-687.

SCHOENE, B., LATKOCZY, C., SCHALTEGGER, U. & GÜNTHER, D. 2010. A new method integrating high-precision U–Pb geochronology with zircon trace element analysis (U–Pb TIMS-TEA). *Geochimica et Cosmochimica Acta,* 74, 7144–7159.

SELWAY, K., SHEPPARD, S., THORNE, A. M., JOHNSON, S. P. & GROENEWALD, P. B. 2009. Identifying the lithospheric structure of a Precambrian orogen using magnetotellurics: The Capricorn Orogen, Western Australia. *Precambrian Research,* 168, 185–196.

SHEPPARD, S., OCCHIPINTI, S. A., NELSON, D. R. & TYLER, I. M. 1999. The Significance of ca. 2.0 Ga crust along the southern margin of the Gascoyne Complex. *Geological Survey of Western Australia,* Annual Review 1998-1999, 56–61.

SHEPPARD, S., OCCHIPINTI, S. A. & TYLER, I. M. 2003. The relationship between tectonism and composition of granitoid magmas, Yarlarweelor Gneiss Complex, Western Australia. *Lithos,* 66, 133–154.

SHEPPARD, S., OCCHIPINTI, S. A. & TYLER, I. M. 2004. A 2005–1970 Ma Andean-type batholith in the southern Gascoyne Complex, Western Australia. *Precambrian Research,* 128, 257–277.

SHEPPARD, S., OCCHIPINTI, S. A. & NELSON, D. R. 2005. Intracontinental reworking in the Capricorn Orogen, Western Australia: the 1680−1620 Ma Mangaroon Orogeny*. *Australian Journal of Earth Sciences,* 52, 443–460.

SHEPPARD, S., RASMUSSEN, B., MUHLING, J. R., FARRELL, T. R. & FLETCHER, I. R. 2007. Grenvillian- aged orogenesis in the Palaeoproterozoic Gascoyne Complex, Western Australia: 1030– 950 Ma reworking of the Proterozoic Capricorn Orogen. *Journal of Metamorphic Geology,* 25, 477–494.

SHEPPARD, S., BODORKOS, S., JOHNSON, S. P., WINGATE, M. T. D. & KIRKLAND, C. L. 2010a. The Paleoproterozoic Capricorn Orogeny: intracontinental reworking not continent–continent collision. *Geological Survey of Western Australia,* Report 108, 33.

SHEPPARD, S., JOHNSON, S. P., WINGATE, M. T. D., KIRKLAND, C. L. & PIRAJNO, F. 2010b. Explanatory notes for the Gascoyne Province. *Geological Survey of Western Australia.* 336.

SCHALTEGGER, U., FANNING, C. M., GÜNTHER, D., MAURIN, J. C., SCHULMANN, K. & GEBAUER, D., 1999. Growth, annealing and recrystallization of zircon and preservation of monazite in high-grade metamorphism: conventional and in-situ U-Pb isotope, cathodoluminescence and microchemical evidence. Contributions to Mineralogy and Petrology, 134, 186-201.

SLÁMA, J., KOŠLER, J., CONDON, D. J., CROWLEY, J. L., GERDES, A., HANCHAR, J. M., HORSTWOOD, M. S. A., MORRIS, G. A., NASDALA, L., NORBERG, N., vSCHALTEGGER, U., SCHOENE, B., TUBRETT, M. N. & WHITEHOUSE, M. J. 2008. Plešovice zircon — A new natural reference material for U–Pb and Hf isotopic microanalysis. *Chemical Geology,* 249, 1–35.

SMITHIES, R. H. & BAGAS, L. 1997. High pressure amphibolite-granulite facies metamorphism in the Paleoproterozoic Rudall Complex, central Western Australia. *Precambrian Research,* 83, 243–265.

SMITHIES, R. H. & CHAMPION, D. C. 1999. Late Archaean felsic alkaline igneous rocks in the Eastern Goldfields, Yilgarn Craton, Western Australia: a result of lower crustal delamination? *Journal of the Geological Society,* 156, 561–576.

SMITHIES, R. H., CHAMPION, D. C. & VAN KRANENDONK, M. J. 2009. Formation of Paleoarchean continental crust through infracrustal melting of enriched basalt. *Earth and Planetary Science Letters,* 281, 298–306.

SMITHIES, R. H., KIRKLAND, C. L., KORHONEN, F. J., AITKEN, A. R. A., HOWARD, H. M., MAINER, W. D., WINGATE, M. T. D., QUENTIN DE GROMARD, R. & GESSNER, K. 2015. The Mesoproterozoic thermal evolution of the Musgrave Province in central Australia — Plume vs. the geological record. *Gondwana Research,* 27, 64–94.

SMITS, R. G., COLLINS, W. J., HAND, M., DUTCH, R. & PAYNE, J., 2014. A Proterozoic Wilson cycle identified by Hf isotopes in central Australia: implications for the assembly of Proterozoic Australia and Rodinia. *Geology*, 42, 231–234.

SPENCER, C. J., KIRKLAND, C. L. & TAYLOR, R. J. M. 2016. Strategies towards statistically robust interpretations of in situ U–Pb zircon geochronology. *Geoscience Frontiers,* 7, 581–589.

SPENCER, K. J., HACKER, B. R., KYLANDER-CLARK, A. R. C., ANDERSEN, T. B., COTTLE, J. M., STEARNS, M. A., POLETTI, J. E. & SEWARD, G. G. E. 2013. Campaign-style titanite U–Pb dating by laser-ablation ICP: Implications for crustal flow, phase transformations and titanite closure. *Chemical Geology,* 341, 84–101.

SPENCER, C. J., KIRKLAND, C. L., PRAVE, A. R., STRACHAN, R. A. & PEASE, V., 2018. Crustal reworking and orogenic styles inferred from zircon Hf isotopes: Proterozoic examples from the North Atlantic region. *Geoscience Frontiers*.

SPAGGIARI, C. V., WARTHO, J. A. & WILDE, S. A., 2008. Proterozoic deformation in the northwest of the Archean Yilgarn Craton, Western Australia. *Precambrian Research*, 162, 354–384.

STERN, R. A. 2001. *A new isotopic and trace-element standard for the ion microprobe: preliminary thermal ionization mass spectrometry (TIMS) U-Pb and electron-microprobe data*, Ressources naturelles Canada.

STERN, R. A., BODORKOS, S., KAMO, S. L., HICKMAN, A. H. & CORFU, F. 2009. Measurement of SIMS instrumental mass fractionation of Pb isotopes during zircon dating. *Geostandards and Geoanalytical Research,* 33, 145–168.

SWAGER, C. P., GOLEBY, B. R., DRUMMOND, B. J., RATTENBURY, M. S. & WILLIAMS, P. R. 1997. Crustal structure of granite-greenstone terranes in the Eastern Goldfields, Yilgarn Craton, as revealed by seismic reflection profiling. *Precambrian Research,* 83, 43–56.

THOMPSON, A. B. & CONNOLLY, J. A. D. 1995. Melting of the continental crust: Some thermal and petrological constraints on anatexis in continental collision zones and other tectonic settings. *Journal of Geophysical Research: Solid Earth,* 100, 15565–15579.

THORNE, A. M. & SEYMOUR, D. B. 1991. Geology of the Ashburton Basin, Western Australia. *Geological Survey of Western Australia Bulletin.* Geological Survey of Western Australia.

THORNE, A. M. & TRENDALL, A. F. 2001. Geology of the Fortescue Group, Pilbara Craton, Western Australia. *Western Australia Geological Survey, Bulletin,* 144, 249.

THYBO, H. & ARTEMIEVA, I. M. 2013. Moho and magmatic underplating in continental lithosphere. *Tectonophysics*, 609, 605–619.

TYLER, I. M. 1991. The geology of the Sylvania Inlier and the southeas Hamersley Basin,. *Geological Survey of Western Australia, Bulletin,* 138.

TYLER, I. M. & THORNE, A. M. 1990. The northern margin of the Capricorn Orogen, Western Australia—an example of an Early Proterozoic collision zone. *Journal of Structural Geology,* 12, 685–701.

TYLER, I. M., FLETCHER, I. R., DE LAETER, J. R., WILLIAMS, I. R. & LIBBY, W. G. 1992. Isotope and rare earth element evidence for a late archaean terrane boundary in the southeastern pilbara craton, western australia. *Precambrian Research,* 54, 211–229.

TYLER, I. M., PIRAJNO, F., BAGAS, L., MYERS, J. S. & PRESTON, W. 1998. The geology and mineral deposits of the Proterozoic in Western Australia. *AGSO Journal of Australian Geology and Geophysics,* 17, 223–244.

VALLEY, J. W. 2003. Oxygen isotopes in zircon. *Reviews in mineralogy and geochemistry,* 53, 343–385.

VALLEY, J., LACKEY, J., CAVOSIE, A., CLECHENKO, C., SPICUZZA, M., BASEI, M., BINDEMAN, I., FERREIRA, V., SIAL, A., KING, E., PECK, W., SINHA, A. & WEI, C. 2005. 4.4 billion years of crustal maturation: oxygen isotope ratios of magmatic zircon. *Contributions to Mineralogy and Petrology,* 150, 561–580.

VAN HUNEN, J. & ALLEN, M. B., 2011. Continental collision and slab break-off: A comparison of 3-D numerical models with observations. *Earth and Planetary Science Letters*, 302, 27–37.

VAN KRANENDONK, M. J., SMITHIES, R. H., HICKMAN, A. H. & CHAMPION, D. C. 2007. Paleoarchean Development of a Continental Nucleus: the East Pilbara Terrane of the Pilbara Craton, Western Australia. *Developments in Precambrian Geology,* 15, 307–337.

VAN KRANENDONK, M. J., SMITHIES, R. H., HICKMAN, A. H., WINGATE, M. T. D. & BODORKOS, S. 2010. Evidence for Mesoarchean (~3.2 Ga) rifting of the Pilbara Craton: The missing link in an early Precambrian Wilson cycle. *Precambrian Research,* 177, 145–161.

VAN KRANENDONK, M. J., IVANIC, T. J., WINGATE, M. T., KIRKLAND, C.L. & WYCHE, S. 2013. Long-lived, autochthonous development of the Archean Murchison Domain, and implications for Yilgarn Craton tectonics. *Precambrian Research*, 229, 49–92.

VAN KRANENDONK, M. J., SMITHIES, R. H., GRIFFIN, W. L., HUSTON, D. L., HICKMAN, A. H., CHAMPION, D. C., ANHAEUSSER, C. R. & PIRAJNO, F. 2015. Making it thick: a volcanic plateau origin of Palaeoarchean continental lithosphere of the Pilbara and Kaapvaal cratons. *Geological Society, London, Special Publications,* 389, 83–111.

VAUCHEZ, A., TOMMASI, A. & BARRUOL, G. 1998. Rheological heterogeneity, mechanical anisotropy and deformation of the continental lithosphere. *Tectonophysics,* 296, 61–68.

VERVOORT, J.D., PATCHETT, P.J., SÖDERLUND, U. & BAKER, M., 2004. Isotopic composition of Yb and the determination of Lu concentrations and Lu/Hf ratios by isotope dilution using MC-ICPMS. *Geochemistry, Geophysics, Geosystems,* 5.

VERVOORT, J.D. & KEMP, A.I., 2016. Clarifying the zircon Hf isotope record of crust–mantle evolution. *Chemical Geology*, 425, 65–75.

VIELREICHER, N. M. & MCNAUGHTON, N. J. 2002. SHRIMP U–Pb geochronology of magmatism and thermal events in the Archaean Marymia Inlier, central Western Australia. *International Journal of Earth Sciences,* 91, 406–432.

VIELREICHER, N. M., RIDLEY, J. R. & GROVES, D. I. 2002. Marymia: an Archean, amphibolite facies-hosted, orogenic lode-gold deposit overprinted by Palaeoproterozoic orogenesis and base metal mineralisation, Western Australia. *International Journal of Geology, Mineralogy and Geochemistry of Mineral Deposits,* 37, 737–764.

VROON, P. Z., LOWRY, D., VAN BERGEN, M. J., BOYCE, A. J. & MATTEY, D. P. 2001. Oxygen isotope systematics of the Banda Arc: Low $\delta^{18}O$ despite involvement of subducted continental material in magma genesis. *Geochimica et Cosmochimica Acta*, 65, 589-609.

WADE, B. P., BAROVICH, K. M., HAND, M., SCRIMGEOUR, I. R. & CLOSE, D. F. 2006. Evidence for early Mesoproterozoic arc magmatism in the Musgrave Block, central Australia: implications for Proterozoic crustal growth and tectonic reconstructions of Australia. *The Journal of Geology,* 114, 43–63.

WADE, B. P., KELSEY, D. E., HAND, M. & BAROVICH, K. M. 2008. The Musgrave Province: stitching north, west and south Australia. *Precambrian Research,* 166, 370–386.

WANG, Q. , SCHIOTTE, L. & CAMPBELL, I.H. 1996. Geochronological constraints on the age of komatiites and nickel mineralisation in the Lake Johnston greenstone belt, Yilgarn Craton, Western Australia. *Australian Journal of Earth Sciences,* 43, 381–385.

WANG, Q., SCHIØTTE, L. & CAMPBELL, I. H. 1998. Geochronology of supracrustal rocks from the Golden Grove area, Murchison Province, Yilgarn Craton, Western Australia. *Australian Journal of Earth Sciences,* 45, 571–577.

WANG, H. & CURRIE, C. A. 2015. Magmatic expressions of continental lithosphere removal. *Journal of Geophysical Research: Solid Earth,* 120, 7239–7260.

WATSON, E. B. 1996. Dissolution, growth and survival of zircons during crustal fusion: kinetic principles, geological models and implications for isotopic inheritance. *Geological Society of America Special Papers,* 315, 43–56.

WATSON, E. B. & HARRISON, T. M. 1983. Zircon saturation revisited: temperature and composition effects in a variety of crustal magma types. *Earth and Planetary Science Letters,* 64, 295–304.

WENDT, I. & CARL, C. 1991. The statistical distribution of the mean squared weighted deviation. Chemical Geology: Isotope Geoscience Section, 86, 275–285.

WIEDENBECK, M., ALLÉ, P., CORFU, F., GRIFFIN, W. L., MEIER, M., OBERLI, F., VON QUADT, A., RODDICK, J. C. & SPIEGEL, W. 1995. Three natural zircon standards for U–Th–Pb, Lu–Hf, trace element and REE analyses. *Geostandards Newsletter,* 19, 1–23.

WILLIAMS, S. J. 1986. Geology of the Gascoyne Province, Western Australia. Govt. Print. Office.

WINGATE, M. T. D., KIRKLAND, C. L., BODORKOS, S., FARRELL, T. R. & SHEPPARD, S. 2009a. 191993: foliated metamonzogranite, Nardoo Well; Geochronology Record 774. *Geological Survey of Western Australia*, 4.

WINGATE, M. T. D., KIRKLAND, C. L., BODORKOS, S., SHEPPARD, S. & FARRELL, T. R. 2009b. 183215: porphyritic metamonzogranite, Davey Well; Geochronology Record 771. *Geological Survey of Western Australia*, 4.

WINGATE, M. T. D., KIRKLAND, C. L., JOHNSON, S. P. & SHEPPARD, S. 2010a. 185944: porphyritic metamonzogranite, Mombo Creek; Geochronology Record 900. *Geological Survey of Western Australia*, 4.

WINGATE, M. T. D., KIRKLAND, C. L., JOHNSON, S. P. & SHEPPARD, S. 2010b. 185953: quartzite, Mount James; Geochronology Record 906. *Geological Survey of Western Australia*, 4.

WINGATE, M. T. D., KIRKLAND, C. L., JOHNSON, S. P. & SHEPPARD, S. 2010c. 185954: quartzite, Mount James; Geochronology Record 907. *Geological Survey of Western Australia*, 5.

WINGATE, M. T. D., KIRKLAND, C. L., SHEPPARD, S. & JOHNSON, S. P. 2010d. 185945: pegmatite lenses in metamonzogranite, Yinnetharra Homestead; Geochronology Record 901. *Geological Survey of Western Australia*, 5.

WINGATE, M. T. D., KIRKLAND, C. L., SHEPPARD, S. & JOHNSON, S. P. 2010e. 185946: pegmatite dyke, Yinnetharra Homestead; Geochronology Record 902. *Geological Survey of Western Australia*, 4.

WINGATE, M. T. D., KIRKLAND, C. L., SHEPPARD, S. & JOHNSON, S. P. 2010f. 185952: gneissic monzogranite, Salt Well; Geochronology Record 905. *Geological Survey of Western Australia*, 4.

WINGATE, M. T. D., KIRKLAND, C. L., SHEPPARD, S. & JOHNSON, S. P. 2010g. 185955: leucocratic granitic gneiss, Wabli Creek; Geochronology Record 908. *Geological Survey of Western Australia*, 4.

WINGATE, M. T. D., KIRKLAND, C. L. & JOHNSON, S. P. 2011. 190685: biotite metagranodiorite, Hibernian gold deposit; Geochronology Record 1004. *Geological Survey of Western Australia*, 5.

WINGATE, M. T. D., KIRKLAND, C. L., SHEPPARD, S. & JOHNSON, S. P. 2011b. 190666: quartzite, Minierra Well; Geochronology Record 1002. *Geological Survey of Western Australia*, 7.

WINGATE, M. T. D., KIRKLAND, C. L. & JOHNSON, S. P. 2012a. 190660: metamonzogranite, Midway Bore; Geochronology Record 1036. *Geological Survey of Western Australia*, 4.

WINGATE, M. T. D., KIRKLAND, C. L., JOHNSON, S. P. & SHEPPARD, S. 2012b. 190634: metamonzogranite, Minierra Well; Geochronology Record 1034. *Geological Survey of Western Australia*, 4.

WINGATE, M. T. D., KIRKLAND, C. L. & JOHNSON, S. P. 2013a. 195819: metamonzogranite, Bee Well Creek; Geochronology Record 1098. *Geological Survey of Western Australia*, 4.

WINGATE, M. T. D., KIRKLAND, C. L. & JOHNSON, S. P. 2013b. 195821: metagranodiorite, Wirradong Well; Geochronology Record 1100. *Geological Survey of Western Australia*, 4.

WINGATE, M. T. D., KIRKLAND, C. L. & JOHNSON, S. P. 2013c. 195826: monzogranitic gneiss, McCarthy Well; Geochronology Record 1104. *Geological Survey of Western Australia*, 5.

WINGATE, M. T. D., KIRKLAND, C. L. & JOHNSON, S. P. 2014a. 195870: metamonzogranite, Stalley Well; Geochronology Record 1154. *Geological Survey of Western Australia*, 4.

WINGATE, M. T. D., KIRKLAND, C. L., THORNE, A. M. & JOHNSON, S. P. 2014b. 169885: biotite granodiorite, Stuarts Well; Geochronology Record. *Geological Survey of Western Australia,* Record 1208, 4.

WINGATE, M. T. D., KIRKLAND, C. L., KORHONEN, F. J. & JOHNSON, S. P. 2017a. 208371: quartzite, Emu Creek Bore; Geochronology Record 1359. *Geological Survey of Western Australia*, 6.

WINGATE, M. T. D., LU, Y. & JOHNSON, S. P. 2017b. 183288: biotite–tourmaline monzogranite, Perseverance Well; Geochronology Record 1352. *Geological Survey of Western Australia*, 4.

WINGATE, M. T. D., LU, Y., KIRKLAND, C. L. & JOHNSON, S. P. 2017c. 190668: metasandstone, Nardoo Creek; Geochronology Record 1354. *Geological Survey of Western Australia*, 6.

WOODHEAD, J. D., GREENWOOD, P., HARMON, R. S. & STOFFERS, P. 1993. Oxygen isotope evidence for recycled crust in the source of EM-type ocean island basalts. *Nature*, 362, 809–813.

WOODHEAD, J., HERGT, J., SHELLEY, M., EGGINS, S. AND KEMP, R., 2004. Zircon Hf-isotope analysis with an excimer laser, depth profiling, ablation of complex geometries, and concomitant age estimation. *Chemical Geology,* 209, 121–135.

WOODHEAD, J. D. & HERGT, J. M. 2005. A Preliminary Appraisal of Seven Natural Zircon Reference Materials for In Situ Hf Isotope Determination. *Geostandards and Geoanalytical Research,* 29, 183–195.

WYCHE, S. 2008. Kalgoorlie, Youanmi, and Narryer Terranes of the Yilgarn Craton — a field guide. *Geological Survey of Western Australia,* Record 2008/12, 67.

WYCHE, S., KIRKLAND, C. L., RIGANTI, A., PAWLEY, M. J., BELOUSOVA, E. & WINGATE, M. T. D. 2012. Isotopic constraints on stratigraphy in the central and eastern Yilgarn Craton, Western Australia. *An International Geoscience Journal of the Geological Society of Australia,* 59, 657–670.

WYCHE, S., NELSON, D. R. & RIGANTI, A. 2004. 4350–3130 Ma detrital zircons in the Southern Cross Granite–Greenstone Terrane, Western Australia: implications for the early evolution of the Yilgarn Craton. *Australian journal of Earth sciences,* 51, 31–45.

WYMAN, D. A. & KERRICH, R. 2012. Geochemical and isotopic characteristics of Youanmi terrane volcanism: the role of mantle plumes and subduction tectonics in the western Yilgarn Craton. *Australian Journal of Earth Sciences,* 59, 671–694.

XIE, L., ZHANG, Y., ZHANG, H., SUN, J. & WU, F., 2008. In situ simultaneous determination of trace elements, U-Pb and Lu-Hf isotopes in zircon and baddeleyite. Chinese Science Bulletin, 53, 1565–1573.

YEATS, C. J., MCNAUGHTON, N. J. & GROVES, D. I. 1996. SHRIMP U-Pb geochronological constraints on Archean volcanic-hosted massive sulfide and lode gold mineralization at Mount Gibson, Yilgarn Craton, Western Australia. *Economic Geology and the Bulletin of the Society of Economic Geologists,* 91, 1354–1371.

YUAN, H.L., GAO, S., DAI, M.N., ZONG, C.L., GÜNTHER, D., FONTAINE, G.H., LIU, X.M. & DIWU, C., 2008. Simultaneous determinations of U–Pb age, Hf isotopes and trace element compositions of zircon by excimer laser-ablation quadrupole and multiple-collector ICP-MS. *Chemical Geology,* 247, 100–118.

ZEH, A., GERDES, A., BARTON JR, J. & KLEMD, R., 2010. U–Th–Pb and Lu–Hf systematics of zircon from TTG's, leucosomes, meta-anorthosites and quartzites of the Limpopo Belt (South Africa): constraints for the formation, recycling and metamorphism of Palaeoarchaean crust. *Precambrian Research*, 179, 50–68.

ZEH, A., GERDES, A., WILL, T. M. & FRIMMEL, H. E. 2010. Hafnium isotope homogenization during metamorphic zircon growth in amphibolite-facies rocks: Examples from the Shackleton Range (Antarctica). *Geochimica et Cosmochimica Acta,* 74, 4740–4758.

APPENDICES

APPENDIX A

ZIRCON STANDARD DATA (CHAPTER 3)

SUPPLEMENTARY DATA FILE[1]

The attached Excel spreadsheet contains the following tables:

Table AA.1 LASS data (U–Pb and trace elements)
Table AA.2 Summary of Lu–Hf isotope data
Table AA.3 Summary of oxygen isotope data
Table AA.4 List of samples

---

[1] Data tables have been embedded due to thesis submission restrictions

APPENDIX B

ZIRCON SAMPLE DATA (CHAPTER 4)

SUPPLEMENTARY DATA FILE[1]

The attached Excel spreadsheet contains the following tables:

Table AB.1 LASS U–Pb data, Chapter 4
Table AB.2 Trace element data, Chapter 4
Table AB.3 Lu–Hf data, Chapter 4
Table AB.4 Oxygen isotope data, Chapter 4

---

[1] Data tables have been embedded due to thesis submission restrictions

APPENDIX C

ZIRCON SAMPLE DATA (CHAPTER 5)

SUPPLEMENTARY DATA FILE[1]

The attached Excel spreadsheet contains the following tables:

Table AC.1 LASS U–Pb data, Chapter 5
Table AC.2 Trace element data, Chapter 5
Table AC.3 Lu–Hf data, Chapter 5
Table AC.4 Oxygen isotope data, Chapter 5

---

[1] Data tables have been embedded due to thesis submission restrictions

APPENDIX D

ZIRCON SAMPLE DATA (CHAPTER 6)

SUPPLEMENTARY DATA FILE[1]

The attached Excel spreadsheet contains the following tables:

Table AD.1 LASS U–Pb data, Chapter 6
Table AD.2 Trace element data, Chapter 6
Table AD.3 Lu–Hf data, Chapter 6
Table AD.4 Oxygen isotope data, Chapter 6

---

[1] Data tables have been embedded due to thesis submission restrictions

APPENDIX E

ZIRCON SAMPLE DATA (CHAPTER 7)

SUPPLEMENTARY DATA FILE[1]

The attached Excel spreadsheet contains the following tables:

Table AE.1 LASS U–Pb data, Chapter 7
Table AE.2 Trace element data, Chapter 7
Table AE.3 Lu–Hf data, Chapter 7
Table AE.4 Oxygen isotope data, Chapter 7

---

[1] Data tables have been embedded due to thesis submission restrictions

APPENDIX F

CHAPTER 8—additional information on contour mapping

ESRI ArcMap 10.1 was used to generate the contour maps, and the extension Geostatistical Analyst was used to process the data to create the final map. Following the methods of Mole (2012), an inverse distance weighted (IDW) interpolation method was used to contour the Hf dataset. One limitation of this method is that some datasets may have several points with the same X, Y coordinates (i.e. inherited zircon grains), and if they represent different values they are considered 'coincident' points. Where there are coincident points that represent analyses from magmatic and inherited zircon from the same sample, preference is given to the magmatic zircon and the inherited analysis manually discarded. If there are coincident points for inherited zircon from the same sample the environment setting 'include all' is used in (Geostatistical Analyst). Another limitation is that although the inherited zircon provide the ability to show the isotopic composition of older crustal events, their spatial location may not reflect the current crustal geometry. For example, the Gascoyne Province was not in its current position until c. 1950 Ma, however, inherited grains are recorded in Gascoyne Province samples as far back as 3500 Ma (T1, Fig 8.5). Magmatic and inherited zircon analyses are indicated clearly on maps (Fig. 8.1, Fig. 8.5) in order to aid in interpretation. Fig. AF.1 shows εHf_t contour mapping timeslices for the Gascoyne Province with additional linear structures.

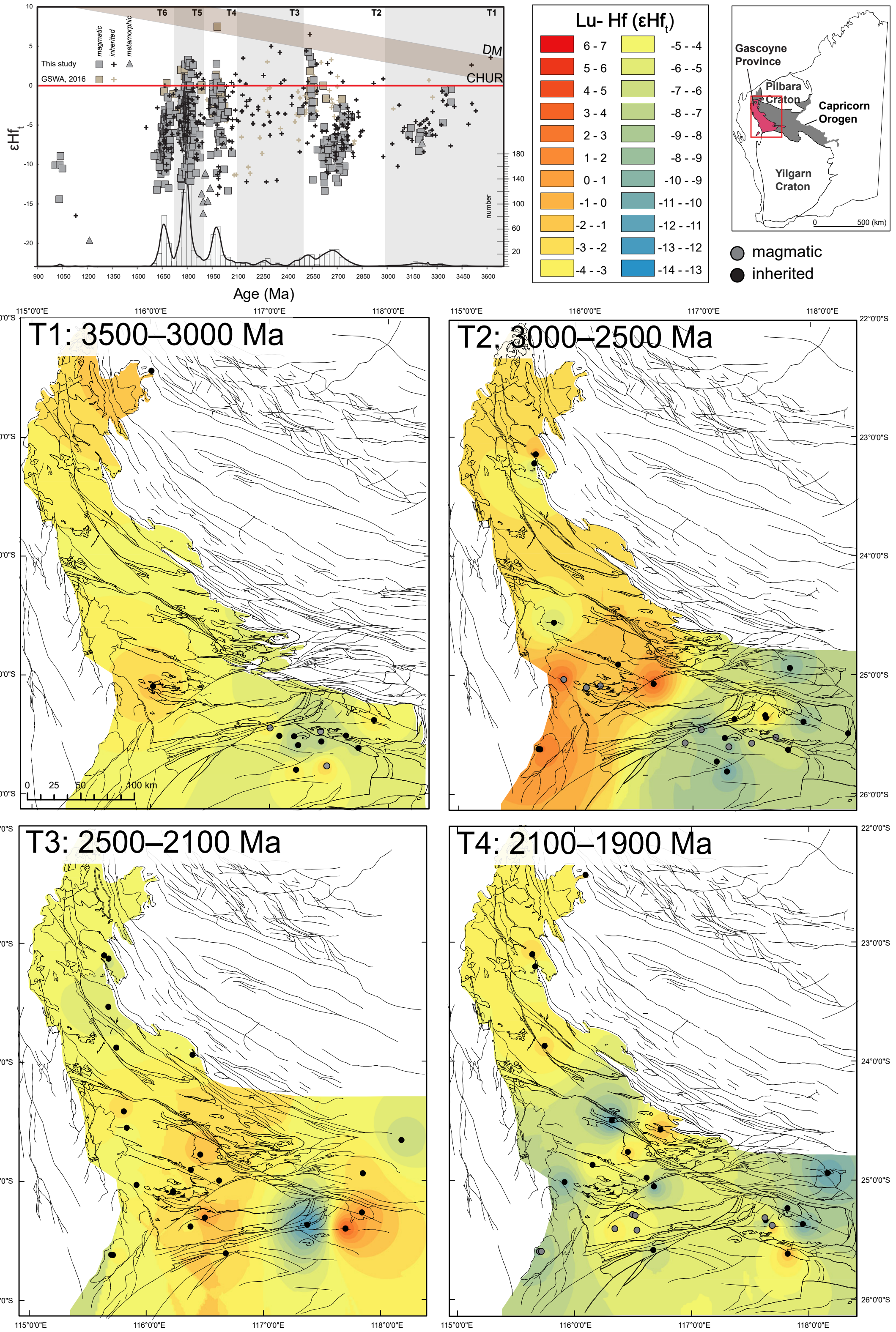

Figure AF.1 continues with caption overleaf

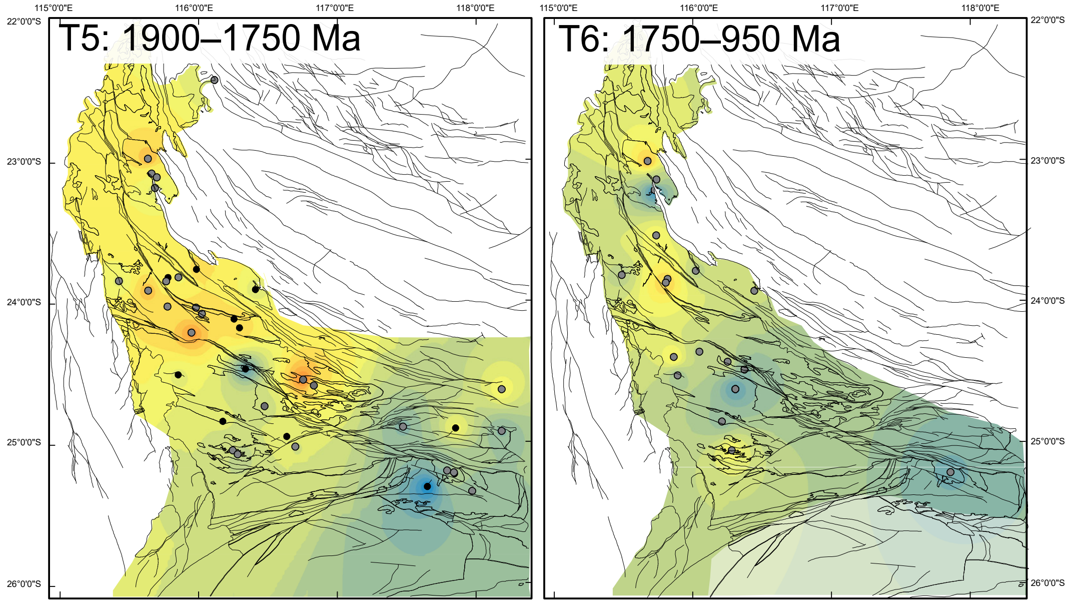

Figure AF.1 εHf$_t$ contour mapping timeslices for the Gascoyne Province (a) εHf$_t$ versus age for all collated data. A total of 74 samples (Chapter 4–7) were combined with data from 14 granitoid samples from GSWA data (Appendix F). Vertical sections indicate timeslice intervals. (b) Timeslices **T1–T6** showing linear structures (present day).

Table AF.1 Collated Lu–Hf isotope data for the Yilgarn Craton (Figure 8.1)

Sample ID	Sample source	Rock Type	Terrane[1]	Domain[2]	Longitude	Latitude
178122	GSWA, 2016	metarhyolite	EGST	Burtville/Yamarna	123.490	-28.046
179435	GSWA, 2016	monzogranite	EGST	Burtville/Yamarna	123.113	-28.082
179448	GSWA, 2016	tonalite	EGST	Burtville/Yamarna	123.372	-27.759
179449	GSWA, 2016	monzogranite	EGST	Burtville/Yamarna	123.425	-27.993
179450	GSWA, 2016	metatonalite	EGST	Burtville/Yamarna	123.877	-28.024
183147	GSWA, 2016	monzogranite	EGST	Burtville/Yamarna	123.646	-28.208
193360	GSWA, 2016	orthogneiss	EGST	Burtville/Yamarna	123.224	-29.334
193410	GSWA, 2016	metagranodiortie	EGST	Burtville/Yamarna	123.318	-29.235
178102	Ivanic et al. 2012	granitic rock	YT	Murchison	118.607	-26.745
178103	Ivanic et al. 2012	granitic rock	YT	Murchison	118.265	-26.735
178105	Ivanic et al. 2012	granitic rock	YT	Murchison	118.489	-26.881
178141	Ivanic et al. 2012	quartz diorite	YT	Murchison	118.299	-27.092
178142	Ivanic et al. 2012	metarhyolite	YT	Murchison	118.384	-27.034
178194	Ivanic et al. 2012	granite orthogneiss	YT	Murchison	117.667	-27.233
178196	Ivanic et al. 2012	granodiorite	YT	Murchison	117.590	-27.120
178197	Ivanic et al. 2012	monzogranite	YT	Murchison	117.591	-27.124
178199	Ivanic et al. 2012	granodiorite	YT	Murchison	117.941	-27.024
185923	Ivanic et al. 2012	dioritic gneiss	YT	Murchison	117.696	-27.412
185929	Ivanic et al. 2012	granitic rock	YT	Murchison	117.974	-26.698
185932	Ivanic et al. 2012	meta-igneous felsic volcanic	YT	Murchison	118.176	-27.341
185933	Ivanic et al. 2012	granodiorite	YT	Murchison	118.163	-27.349
193972	Ivanic et al. 2012	meta-igneous felsic volcanic	YT	Murchison	117.526	-26.972
80434	This study	granodiorite	NT	Narryer	117.484	-25.773
80453	This study	metamonzogranite	NT	Narryer	117.226	-25.806
80459	This study	metgranite	NT	Narryer	117.086	-25.522
152855	This study	granitic rock	EGST	Kalgoorlie	120.433	-25.908
152879	This study	granitic rock	EGST	Kalgoorlie	120.215	-25.643
120644	This study	granitic rock	YT	Goodin Inlier	119.203	-25.968
120678	This study	granitic rock	YT	Goodin Inlier	119.429	-25.793
120696	This study	granitic rock	YT	Goodin Inlier	119.260	-25.891
139282	This study	granitic rock	YT	Goodin Inlier	119.236	-26.056
139286	This study	granitic rock	YT	Goodin Inlier	119.323	-25.752
168947	This study	gneiss	GT	Glenburgh	115.829	-25.034
185955	This study	granitic gneiss	GT	Glenburgh	116.294	-24.909
120601	This study	metasediment	YT	Marymia Inlier	119.002	-25.664
148344	This study	metagranite	YT	Marymia Inlier	120.024	-25.181
206935	This study	granitic gneiss	YT	Marymia Inlier	119.505	-25.175
216141	This study	granitic rock	YT	Marymia Inlier	119.370	-25.496
Jc15 (NV8)	This study	granitic rock	YT	Marymia Inlier	119.465	-25.476
133547	This study	granitic gneiss	YT	Marymia Inlier	117.007	-25.455
139459	This study	monzogranite	YT	Marymia Inlier	116.867	-25.567
142896	This study	monzogranite	YT	Marymia Inlier	117.438	-25.567
142901	This study	gneiss	YT	Marymia Inlier	117.243	-25.599
142914	This study	monzogranite	YT	Marymia Inlier	117.139	-25.723
144464	This study	felsic gneiss	YT	Marymia Inlier	117.210	-25.525
80484	This study	metagranite	NT	YGC	115.626	-25.621
135418	This study	granitic gneiss	NT	YGC	177.889	-25.474
142848	This study	monzogranite	NT	YGC	117.645	-25.521
144376	This study	metagranite	NT	YGC	117.434	-25.484
142988	Johnson et al. 2017a	tonalite	GT	GT	116.021	-25.102
164309	Johnson et al. 2017a	granodiorite	GT	GT	116.142	-25.087
168950	Johnson et al. 2017a	gneiss	GT	GT	115.611	-25.618
188973	Johnson et al. 2017a	meta-igneous felsic	GT	GT	116.917	-24.855

Table AF.1 continued

W29	Kemp et al. 2010	tonalite	NT	Narryer	116.849	-26.204
W34	Kemp et al. 2010	monzogranite	NT	Narryer	117.260	-26.099
W35	Kemp et al. 2010	granodiorite	NT	Narryer	117.114	-26.131
W61	Kemp et al. 2010	granite	NT	Narryer	117.025	-26.174
W62	Kemp et al. 2010	monzogranite	NT	Narryer	117.025	-26.174
W63	Kemp et al. 2010	trondjemite	NT	Narryer	117.309	-26.064
W65	Kemp et al. 2010	trondjemite	NT	Narryer	117.366	-25.932
98260	Mole et al. 2014	monzogranite	EGST	Kalgoorlie	121.074	-30.695
118954	Mole et al. 2014	felsic schist	EGST	Kalgoorlie	120.700	-27.800
142920	Mole et al. 2014	felsic porphyry	YT	Southern Cross	119.331	-29.853
168956	Mole et al. 2014	porphyritic granodiorite	YT	Southern Cross	119.008	-30.319
168959	Mole et al. 2014	porphyritic granophyre	YT	Southern Cross	119.392	-30.222
168960	Mole et al. 2014	meta-ignimbrite	YT	Southern Cross	119.290	-30.177
168961	Mole et al. 2014	welded tuffaceous rhyolite	YT	Southern Cross	119.283	-30.131
168965	Mole et al. 2014	granodiorite	YT	Southern Cross	119.757	-29.482
168970	Mole et al. 2014	syenogranite	YT	Southern Cross	119.263	-29.070
168972	Mole et al. 2014	monzogranite	YT	Southern Cross	119.124	-29.094
168973	Mole et al. 2014	monzogranite	YT	Murchison	118.714	-29.567
168976	Mole et al. 2014	monzogranite	YT	Southern Cross	119.881	-30.180
169064	Mole et al. 2014	Porphyritic monzogranite	YT	Southern Cross	119.804	-29.950
178050	Mole et al. 2014	granodiorite	YT	Southern Cross	119.253	-28.860
92969082	Mole et al. 2014	monzogranite	EGST	Kalgoorlie	120.567	-28.157
97969104	Mole et al. 2014	monzogranite dyke	YT	Southern Cross	119.520	-29.052
99969049	Mole et al. 2014	porphyritic granite dyke	YT	Murchison	118.112	-30.908
95YQ87	Mole et al. 2014	seriate monzogranite	YT	Southern Cross	119.566	-30.915
97969102B	Mole et al. 2014	porphyritic monzogranite	YT	Southern Cross	119.592	-29.024
98967102E	Mole et al. 2014	granodiorite xenolith	YT	Southern Cross	119.309	-30.633
ARC19	Mole et al. 2014	granodiorite	YT	Southern Cross	119.521	-30.886
ARC1A	Mole et al. 2014	syenogranite	YT	Southern Cross	119.188	-30.328
ARC48	Mole et al. 2014	seriate monzogranite	YT	Murchison	118.881	-30.954
LNN1-9794	Mole et al. 2014	rhyolite-dacite	EGST	Kalgoorlie	121.121	-28.337
MKD1-180	Mole et al. 2014	andesite-basaltic andesite	EGST	Kalgoorlie	120.546	-27.230
93901	Wyche et al. 2012	granodiorite	EGST	Kalgoorlie	121.367	-30.250
98255	Wyche et al. 2012	monzogranite	EGST	Kalgoorlie	120.943	-30.220
98256	Wyche et al. 2012	syenogranite	EGST	Kalgoorlie	120.921	-30.228
98258	Wyche et al. 2012	monzogranite	EGST	Kalgoorlie	120.857	-30.350
98267	Wyche et al. 2012	monzogranite	EGST	Kalgoorlie	120.794	-30.295
98268	Wyche et al. 2012	monzogranite	EGST	Kalgoorlie	120.818	-30.218
100710	Wyche et al. 2012	metafelsic volcanic	EGST	Kurnalpi	121.695	-30.558
100726	Wyche et al. 2012	metafelsic volcanic	EGST	Kurnalpi	121.827	-30.779
101348	Wyche et al. 2012	metafelsic volcanic	EGST	Kurnalpi	121.827	-30.779
101381	Wyche et al. 2012	monzogranite	EGST	Kurnalpi	121.973	-29.740
105015	Wyche et al. 2012	granite dyke	YT	Murchison	116.825	-26.494
110710	Wyche et al. 2012	metafelsic volcanic	EGST	Kalgoorlie	121.695	-30.558
112117	Wyche et al. 2012	monzogranite	YT	Southern Cross	120.562	-29.669
142849	Wyche et al. 2012	pegmatitic granite	YT	Murchison	117.604	-25.439
142855	Wyche et al. 2012	monzogranite	YT	Murchison	117.919	-25.333
142905	Wyche et al. 2012	paragneiss	YT	Murchison	117.474	-25.222
142915	Wyche et al. 2012	monzogranite	YT	Southern Cross	119.446	-29.961
142919	Wyche et al. 2012	monzogranite	YT	Southern Cross	119.264	-29.927
142994	Wyche et al. 2012	monzogranite	YT	Southern Cross	120.549	-29.926
168902	Wyche et al. 2012	syenogranite	YT	Southern Cross	120.115	-29.836
168966	Wyche et al. 2012	granitic gneiss	YT	Southern Cross	119.173	-29.383
177932	Wyche et al. 2012	metagranodiortie	YT	Southern Cross	119.601	-27.430
178059	Wyche et al. 2012	monzogranite	YT	Southern Cross	119.930	-27.602
178104	Wyche et al. 2012	granodiorite	YT	Murchison	118.293	-26.794
179239	Wyche et al. 2012	rhyolite	YT	Southern Cross	119.561	-27.386

Table AF.1 continued

183921	Wyche et al. 2012	volcaniclastic rock	YT	Murchison	118.509	-26.821
185928	Wyche et al. 2012	metatonalite	YT	Murchison	117.972	-26.722
104940A	Wyche et al. 2012	metadacite	EGST	Kurnalpi	122.067	-30.967
104948A	Wyche et al. 2012	metadacite	EGST	Kurnalpi	122.400	-30.783

[1] EGST = Eastern Goldfields Superterrane, GT = Glenburgh Terrane, YT = Youanmi Terrane, YGC = Yarlarweeolor Gneiss Complex

[2] Yilgarn Craton terrane/domain structure of Cassidy et al. (2006)

Table AF.2 Collated Lu–Hf isotope data for the Gascoyne Province (Figure 8.5)

Sample ID	Sample source	Rock Type	Unit	Latitude	Longitude
142926	GSWA	tonalite	Dalgaringa Supersuite	-25.31584	116.43657
142928	GSWA	tonalite	Dalgaringa Supersuite	-25.43871	116.45152
142932	GSWA	granodiorite	Dalgaringa Supersuite	-25.42866	116.26163
142933	GSWA	mafic ediorite	Dalgaringa Supersuite	-25.40631	116.21741
142988	GSWA	biotite tonalite	Halfway Gneiss	-25.1018	116.0212
159996	GSWA	biotite monzogranite	Moorarie Supersuite	-25.0961	116.1414
164309	GSWA	granodiorite	Halfway Gneiss	-25.08686	116.14202
168950	GSWA	tonalite gneiss	Dalgaringa Supersuite	-25.61763	115.61143
168952	GSWA	tonalite	Dalgaringa Supersuite	-25.619	115.6279
169087	GSWA	granodiorite	Moorarie Supersuite	-23.11547	115.55032
169088	GSWA	monzogranite	Moorarie Supersuite	-23.14237	115.58802
169089	GSWA	syenogranite	Moorarie Supersuite	-23.21966	115.57568
178029	GSWA	monzogranite	Durlacher Supersuite	-23.80212	115.87818
88405	GSWA	granodiorite	Moorarie Supersuite	-24.21995	116.19144

APPENDIX G

TWO COMPONENT MIXING MODELLING

AG.1 Two component mixing modelling

Chapter 5 (Figure 5.8)

% juvenile component	$\delta^{18}O$ [‰]	εHf (r=0.36)	εHf (r=0.04)	% Halfway Gneiss
0	7.1	-11.8	-11.8	100
10	7	-11	-11.7	90
20	6.9	-10.1	-11.6	80
30	6.7	-9.1	-11.5	70
40	6.6	-7.9	-11.3	60
50	6.5	-6.4	-11.1	50
60	6.4	-4.7	-10.7	40
70	6.3	-2.5	-10.1	30
80	6.1	0.2	-9.1	20
90	6	3.8	-6.6	10
100	5.9	8.6	8.6	0

% juvenile component	$\delta^{18}O$ [‰]	εHf (r=0.36)	εHf (r=0.04)	% Halfway Gneiss
0	7.1	-11.8	-11.8	100
10	6.9	-11	-11.7	90
20	6.7	-10.1	-11.6	80
30	6.6	-9.1	-11.5	70
40	6.4	-7.9	-11.3	60
50	6.2	-6.4	-11.1	50
60	6	-4.7	-10.7	40
70	5.8	-2.5	-10.1	30
80	5.7	0.2	-9.1	20
90	5.5	3.8	-6.6	10
100	5.3	8.6	8.6	0

Chapter 6 (Figure 6.9)

% meta-sediments	$\delta^{18}O$ [‰]	εHf (r=0.36)	εHf (r=0.36)	% Glenburgh Terrane
0	10	-1.3	-1.3	100
10	9.61	-1.9	-1.6	90
20	9.22	-2.6	-1.9	80
30	8.83	-3.5	-2.2	70
40	8.44	-4.5	-2.6	60
50	8.05	-5.6	-3.1	50
60	7.66	-7.0	-3.7	40
70	7.27	-8.8	-4.4	30
80	6.88	-11.0	-5.3	20
90	6.49	-13.8	-6.5	10
100	6.1	-17.7	-8.1	0

% meta-sediments	$\delta^{18}O$ [‰]	εHf (r=0.04)	% depleted mantle
0	10	-1.3	100
10	9.53	-1.3	90
20	9.06	-1.3	80
30	8.59	-1.2	70
40	8.12	-1.2	60
50	7.65	-1.1	50
60	7.18	-1.0	40
70	6.71	-0.9	30
80	6.24	-0.6	20
90	5.77	0.0	10
100	5.3	4.0	0

Chapter 7 (Figure 7.7)

% Moorarie Supersuite	$\delta^{18}O$ [‰]	εHf (r=0.36)	% Halfway Gneiss
0	6.2	-19.7	100
10	6.3	-19.4	90
20	6.3	-19.0	80
30	6.4	-18.5	70
40	6.5	-18.0	60
50	6.6	-17.4	50
60	6.6	-16.7	40
70	6.7	-15.7	30
80	6.8	-14.6	20
90	6.8	-13.1	10
100	6.9	-11.0	0

Chapter 7 (Figure 7.8)

% Durlacher Supersuite	$\delta^{18}O$ [‰]	εHf (r=0.36)	% meta-sediments
0	8.1	-21.1	100
10	8.2	-19.4	90
20	8.3	-17.7	80
30	8.4	-15.9	70
40	8.5	-14.0	60
50	8.6	-12.1	50
60	8.6	-10.1	40
70	8.7	-8.0	30
80	8.8	-5.9	20
90	8.9	-3.6	10
100	9	-1.3	0

Chapter 8

% juvenile component	$\delta^{18}O$ [‰]	εHf (r=0.36)	εHf (r=0.04)	% Halfway Gneiss
0	7.5	-5.0	-5.0	100
10	7.3	-4.5	-4.9	90
20	7.1	-3.9	-4.9	80
30	6.8	-3.3	-4.8	70
40	6.6	-2.5	-4.7	60
50	6.4	-1.6	-4.5	50
60	6.2	-0.5	-4.3	40
70	6	0.9	-3.9	30
80	5.7	2.7	-3.3	20
90	5.5	4.9	-1.7	10
100	5.3	8.0	8.0	0